

*Quantum Electrodynamical Corrections  
in Atoms from Coupled Cluster Theory*

A THESIS

*submitted for the award of Ph.D. degree of*

MOHANLAL SUKHADIA UNIVERSITY

*in the*

*Faculty of Science*

*by*

Siddhartha Chattopadhyay



*Under the Supervision of*

Angom Dilip Kumar Singh

Associate Professor

Theoretical Physics Division

Physical Research Laboratory

Ahmedabad, India

DEPARTMENT OF PHYSICS

MOHANLAL SUKHADIA UNIVERSITY

UDAIPUR

Year of submission: 2013

*To*  
*My family*

## ***DECLARATION***

*I, Mr. Siddhartha Chattopadhyay, S/O Mr. Rabindranath Chattopadhyay, J-118, PRL residences, Navrangpura, Ahmedabad, 380009, hereby declare that the work incorporated in the present thesis entitled, “**Quantum Electrodynamical Corrections in Atoms from Coupled Cluster Theory**” is my own and original. This work (in part or in full) has not been submitted to any University for the award of a Degree or a Diploma. I have properly acknowledged the material collected from secondary sources wherever required. I solely own the responsibility for the originality of the entire content.*

Date :

(Siddhartha Chattopadhyay)

# ***CERTIFICATE***

I feel great pleasure in certifying that the thesis entitled, “**Quantum Electrodynamical Corrections in Atoms from Coupled Cluster Theory**” embodies a record of the results of investigations carried out by Mr. Siddhartha Chattopadhyay under my guidance. He has completed the following requirements as per Ph.D. regulations of the University.

- (a) Course work as per the university rules.
- (b) Residential requirements of the university.
- (c) Regularly submitted six monthly progress reports.
- (c) Presented his work in the departmental committee.
- (d) Published minimum of one research papers in a referred research journal.

I am satisfied with the analysis of data, interpretation of results and conclusions drawn. I recommend the submission of thesis.

Date : August 6, 2013

Dr. Angom Dilip Kumar Singh  
(Thesis Supervisor)  
Associate Professor,  
Physical Research Laboratory,  
Ahmedabad, India

Countersigned by  
Head of the Department

# Acknowledgments

*The time has now finally arrived when I can look back over the journey of last five years in the dream of completion of my PhD. Standing at the extreme-end of this trail, I can admit that this walk would have never been possible without the constant help and support of various people from different disciplines.*

*It has been a great privilege to spend several years in Physical Research Laboratory, a reputed institute, where I was given an academic yet homely atmosphere throughout my entire PhD tenure. All the members of Physical Research Laboratory will always remain very dear to me.*

*First I would like to express my heartfelt gratitude to my supervisor Prof. Angom Dilip Kumar Singh for being so inspirational, supportive and patient with me. I am grateful to him for his thorough and detailed revision of my work. One thing that I highly value is his enormous patience to explain various topics that came up on numerous events of discussions. Apart from being my PhD mentor, I must thank him for the stimulating broad discussion that not only helped me to understand the subject but also enlightened me on the basic values and ethics in scientific activities. In addition, he has always given me great freedom to pursue independent research work. I could not be prouder of my academic roots, and hope that I can in turn pass on the research values and the dreams that he has given to me.*

*I would also like to thank Dr. B. K. Mani for providing encouraging and constructive feedback. I must thank him for patiently teaching me the basic topics of the subject. His thorough help, with his insightful thought on writing a systematic code, is gloriously reflected in the present work.*

*I would like to thank Avijit Sen from IACS, Kolkata and Narendranath Dutta*

from IIT, Kharagpur for exciting discussions. I must also express my sincere gratitude to Mr. Alak Banik for useful discussions. My special thanks to the past group members, Salman Silotri, Sandeep Gautam and the present members, Arko Roy and Kuldeep Suthar for stimulating discussions.

My debt of gratitude also goes to Prof. B. K. Sahoo who provided the vision, encouragement and advise necessary for me to proceed through the doctoral program, and complete my dissertation. The questions and comments that I received from him illuminated my understanding of the subject. I would also like to express my gratitude to other faculty members in the Theoretical Physics division, especially Prof. N. Mahajan, Prof. J. Bhatt, Prof. H. Mishra, Prof. R. Rangarajan, Prof. S. Goswami, Prof. S. Mohanty, Prof. S. Rindani, Prof. U. Sarkar for taking stimulating course works and giving the flavor of doing research. My special thanks goes to the academic committee for thoroughly reviewing my work. Their guidance has served me well and I owe them my heartfelt appreciation.

I also acknowledge the help from PRL computer center. My work has immensely benefited from the high performance computing cluster. I thank all the present and past members of the computer center, especially, Mr. Jigar Raval, Mr. Samuel Johnson and Mr. Mrugesh Gajjar for their sincere support. I am also thankful to all the staff members of PRL library, Administration, Dispensary for their cooperation.

I would like to thank my seniors especially Anjishnu Sarkar for helping me with computational issues. My heartfelt of gratitude goes to Suratna Das, who instilled within me a love of creative pursuits, science and language, all of which finds a place in this thesis. A very special thanks to Abhishek and Tanushree for pouring enormous joy and excitement in my otherwise monotonous life. I thank all my batch-mates, Amrendra, Arun, Chinmay, Koushik, Sunil, Susanta, Vema and Yogita for making my stay at PRL comfortable. They have been like the surrogate family to me, bearing the pain of my frustrations and sharing the moments of success. I also thank my seniors Joydeep, Mala, Paramita, Suman, Subrata, Moumita, Tapas, and juniors Shashi, Fazlul for their help.

I would not have contemplated this road without my family who always stood

*by my side with immense support and encouragement. And last, but not the least, to Kabitri, who shares my passions, thank you for reigniting my dreams.*

# Abstract

The relativistic description is an inevitable choice to study heavy atoms and ions as it is the simplified model within the fundamental description given by quantum electrodynamics (QED). The precision of atomic experiments have reached a stage where it is possible to test the theory of QED precisely in small atomic systems. Recent progress in the study of highly charged ions motivates us to investigate the QED effects in heavy atoms and ions. It is a challenging problem to take into account the QED effects and electron correlation simultaneously. The QED effects are studied in great detail in hydrogen like systems and it is important to mention that the present CODATA recommended value of the fine structure constant originates from such a system.

The simplified description of a many electron atom in the framework of relativistic quantum mechanics is through the Dirac-Coulomb Hamiltonian,  $H^{\text{DC}}$ . G. Breit derived a more appropriate Hamiltonian to incorporate the relativistic corrections to the static Coulomb interaction. For heavy atoms and ions, the Dirac-Coulomb-Breit Hamiltonian ( $H^{\text{DCB}}$ ) is an appropriate choice. However, there are complications associated with the  $H^{\text{DCB}}$ . Brown and Ravenhall showed that the  $H^{\text{DC}}$  as well as  $H^{\text{DCB}}$  are not bounded from below, and these lead to *variational collapse* and *continuum dissolution*. Later, Sucher [1] showed that this catastrophe can be avoided by using projection operators and proposed a no-virtual-pair approximation (NVPA). In this approximation, one projects out the negative energy part of the spectrum. In this way we can treat the Coulomb and Breit interactions on the same footing. According to Lindgren [2], the effects which are not considered in the NVPA approximation are the QED effects. These are the radiative effects and the non-radiative effects. Breit inter-

action is considered as the QED effects as it can be derived from the lowest order one photon exchange between electrons. The radiative effects include vacuum polarization and self-energy corrections, which are known as the Lamb-Shift in many electron atoms. In this thesis we consider the  $H^{\text{DCB}}$  along with the vacuum polarization correction.

The coupled-cluster theory (CCT) [3, 4] which was initially developed to study many body problems in nuclear physics, is a powerful and elegant method to solve the atomic many body problem as well. In the CCT the electron-electron correlation effects are taken to all order. Most of the relativistic coupled-cluster (RCC) calculations take into account the single and double excitations to all order and hence, in literature they are widely known as the RCCSD methods. Due to the complex angular momentum algebra and computational cost, the genuine triple excitations are difficult to incorporate in the RCC calculation. Several groups use the approximate triple excitations to estimate the correction from the triple excitations. In the present thesis we consider the triple excitations up to all order in the RCC theory. In the present work we also develop perturbed relativistic coupled-cluster (PRCC) theory to calculate different atomic properties. The PRCC theory is different from the previous RCC-based theories in a number of ways. The most important one is the representation of the cluster operators in the PRCC theory. The cluster operator can be a rank-1 tensor operator and it has the advantage of incorporating multiple perturbations of different ranks in the electronic sector. With the RCC wave-function which incorporates the vacuum polarization correction and the Breit interaction correction, we examine several important atomic properties. To mention a few, the effect of triple excitation to the correlation energy of closed shell atoms and the removal energies of one valence atoms. We investigate the dipole polarizability of closed shell atoms with the PRCC theory. The influence of Breit interaction and the QED effects in the dipole polarizability is discussed in great detail.

**Keywords** : Vacuum Polarization, Bound state QED, Breit interaction, Coupled-cluster theory, Perturbed relativistic coupled-cluster theory, Triple excitations, Dipole Polarizability.

# List of Publications

1. *Electric dipole polarizability from perturbed relativistic coupled-cluster theory: Application to neon,*  
**S. Chattopadhyay**, B. K. Mani, and D. Angom, Phys. Rev. A, **86**, 022522 (2012).
2. *Perturbed coupled-cluster theory to calculate dipole polarizabilities of closed-shell systems: Application to Ar, Kr, Xe, and Rn,*  
**S. Chattopadhyay**, B. K. Mani, and D. Angom, Phys. Rev. A, **86**, 062508 (2012).
3. *Electric dipole polarizabilities of alkali-metal ions from perturbed relativistic coupled-cluster theory,*  
**S. Chattopadhyay**, B. K. Mani, and D. Angom, Phys. Rev. A, **87**, 042520 (2013).
4. *Electric dipole polarizabilities of doubly ionized alkaline Earth metal ions from perturbed relativistic coupled-cluster theory,*  
**S. Chattopadhyay**, B. K. Mani, and D. Angom, Phys. Rev. A **87** 062504 (2013).

# List of Abbreviations

CCT	Coupled-Cluster Theory
CCSD	Coupled-Cluster Singles and Doubles
CI	Configuration Interaction
DC	Dirac-Coulomb
DCB	Dirac-Coulomb-Breit
DHF	Dirac-Hartree-Fock
DK	Douglas-Kroll
GTO	Gaussian Type Orbital
HF	Hartree Fock
MBPT	Many Body Perturbation Theory
MCDHF	Multi configuration Dirac-Hartree-Fock
PNC	Parity Non-Conservation
PRCC	Perturbed Relativistic Coupled-Cluster
QED	Quantum Electrodynamics
RCC	Relativistic Coupled-Cluster
RCCSD	Relativistic Coupled-Cluster Singles and Doubles
RCCSDT	Relativistic Coupled-Cluster Singles, Doubles and Triples
RCI	Relativistic Configuration Interaction
RMBPT	Relativistic Many Body Perturbation Theory
SCF	Self Consistent Field
SE	Self Energy
VP	Vacuum Polarization

# Contents

<b>Acknowledgments</b>	<b>iv</b>
<b>Abstract</b>	<b>vii</b>
<b>List of Publications</b>	<b>ix</b>
<b>List of Abbreviations</b>	<b>x</b>
<b>List of Tables</b>	<b>xiv</b>
<b>List of Figures</b>	<b>xvii</b>
<b>1 Introduction</b>	<b>1</b>
1.1 Thesis overview . . . . .	7
1.2 Units and notations . . . . .	9
<b>2 Many Body Perturbation Theory with QED effects</b>	<b>10</b>
2.1 Relativistic Hamiltonian for atomic calculation . . . . .	11
2.1.1 Breit interaction . . . . .	11
2.1.2 Vacuum polarization . . . . .	14
2.2 Dirac-Coulomb-Breit Hamiltonian with Uehling potential . . . . .	18
2.3 Dirac-Hartree-Fock theory with QED effects . . . . .	19
2.4 Single particle wave-functions . . . . .	20
2.5 Matrix element of the Breit interaction . . . . .	22
2.6 Atomic MBPT . . . . .	24
2.7 Correlation energy of closed-shell atoms . . . . .	27

---

2.8	Results and discussions . . . . .	28
2.8.1	Basis set . . . . .	29
2.8.2	Breit interaction correction . . . . .	32
2.8.3	Vacuum polarization correction . . . . .	34
2.8.4	Correlation energy with Breit interaction . . . . .	38
<b>3</b>	<b>QED effects in closed-shell atoms using coupled-cluster theory</b>	<b>39</b>
3.1	Relativistic coupled-cluster theory of closed-shell atoms . . . . .	40
3.1.1	Linearized RCC theory with triple excitations . . . . .	42
3.2	Angular momentum representation of $T_3^{(0)}$ . . . . .	44
3.2.1	Angular momentum diagram evaluation with $T_3^{(0)}$ . . . . .	45
3.3	Perturbed relativistic coupled-cluster theory . . . . .	47
3.3.1	Tensor structure of PRCC operator . . . . .	48
3.3.2	PRCC equations . . . . .	49
3.3.3	Nonlinear terms in PRCC . . . . .	51
3.3.4	Intermediate diagrams . . . . .	62
<b>4</b>	<b>QED effects in open-shell atoms using coupled-cluster theory</b>	<b>65</b>
4.1	RCC theory for one valence atoms . . . . .	66
4.2	Electric dipole transition from RCCSDT theory . . . . .	69
4.3	Results and Discussions . . . . .	70
4.3.1	Properties of one valence atoms . . . . .	71
4.3.2	Excitation energies . . . . .	72
4.3.3	Electric dipole transition amplitudes . . . . .	77
<b>5</b>	<b>Some Applications</b>	<b>80</b>
5.1	Theory of dipole polarizability . . . . .	81
5.2	Results and discussions . . . . .	83
5.2.1	Dipole polarizability of Neon from PRCC theory . . . . .	83
5.2.2	Dipole polarizability of Ar, Kr, Xe and Rn . . . . .	88
5.2.3	Dipole Polarizability of Alkali Metal Ions . . . . .	95
5.2.4	Dipole Polarizability of Alkaline-Earth Metal Ions . . . . .	101

---

<b>6 Future Directions and Discussions</b>	<b>109</b>
<b>A Matrix Element of Breit Interaction</b>	<b>111</b>
<b>B Matrix Element of Dipole Operator</b>	<b>115</b>
<b>Bibliography</b>	<b>118</b>
<b>Publications attached with the thesis</b>	<b>125</b>

# List of Tables

2.1	The $\alpha_0$ and $\beta$ parameters of the even tempered GTO basis used in the present calculations. . . . .	29
2.2	Orbital energies of Ne obtained from GRASP92 and GTO (in a.u). . . . .	30
2.3	The $\alpha_0$ and $\beta$ parameters of the even tempered GTO basis used in the present calculations. . . . .	30
2.4	Comparison between GTO and GRASP92 (in a.u). . . . .	31
2.5	The $\alpha_0$ and $\beta$ parameters of the even tempered GTO basis used in for alkali metal ions. . . . .	31
2.6	Core orbital energies of $\text{Cs}^+$ in atomic units. . . . .	32
2.7	The $\alpha_0$ and $\beta$ parameters of the even tempered GTO basis for different ions used in the present calculations. . . . .	33
2.8	Comparison between the ground state SCF energies obtained from the computations with GTO and GRASP92. The energies are in atomic units. . . . .	33
2.9	SCF Energies for noble gas atoms . . . . .	33
2.10	VP Corrections to the orbital energies of $\text{Ca}^{2+}$ . Here [x] represents multiplication by $10^x$ . . . . .	35
2.11	VP Corrections to the orbital energies of $\text{Sr}^{2+}$ . Here [x] represents multiplication by $10^x$ . . . . .	36
2.12	VP Corrections to the orbital energies of $\text{Ba}^{2+}$ . Here [x] represents multiplication by $10^x$ . . . . .	37
2.13	VP Corrections to the orbital energies of $\text{Ra}^{2+}$ . Here [x] represents multiplication by $10^x$ . . . . .	37

---

2.14	Second-order correlation energies of closed shell atoms. . . . .	38
4.1	Removal Energies of several excited states of ${}^7\text{Li}$ in $\text{cm}^{-1}$ . . . . .	73
4.2	Removal Energies of ground and excited states of ${}^{23}\text{Na}$ in $\text{cm}^{-1}$ . . . . .	73
4.3	Contribution to the removal Energies ${}^{23}\text{Na}$ in $\text{cm}^{-1}$ . . . . .	74
4.4	Removal Energies of ground and excited states of ${}^{39}\text{K}$ in $\text{cm}^{-1}$ . . . . .	74
4.5	Contribution to the removal energies ${}^{39}\text{K}$ in $\text{cm}^{-1}$ . . . . .	75
4.6	Removal Energies of ground and excited states of ${}^{85}\text{Rb}$ in $\text{cm}^{-1}$ . . . . .	75
4.7	Contribution to the removal energies ${}^{85}\text{Rb}$ in $\text{cm}^{-1}$ . . . . .	76
4.8	Removal Energies of ground and excited states of ${}^{133}\text{Cs}$ in $\text{cm}^{-1}$ . . . . .	76
4.9	Contribution to the removal energies ${}^{133}\text{Cs}$ in $\text{cm}^{-1}$ . . . . .	77
4.10	Reduced electric dipole matrix element of ${}^7\text{Li}$ in a.u . . . . .	77
4.11	Reduced electric dipole matrix element of ${}^{23}\text{Na}$ in a.u . . . . .	78
4.12	Reduced electric dipole matrix element of ${}^{39}\text{K}$ in a.u . . . . .	78
4.13	Reduced electric dipole matrix element of ${}^{85}\text{Rb}$ in a.u . . . . .	78
4.14	Reduced electric dipole matrix element of ${}^{133}\text{Cs}$ in a.u . . . . .	79
5.1	Convergence pattern of $\alpha$ (Ne) as a function of the basis set size. . . . .	84
5.2	The static dipole polarizability, $\alpha$ , of Ne from linearized PRCC and comparison with previous results. . . . .	85
5.3	Contribution to $\alpha$ of Ne from different terms of the dressed dipole operator in the linearized PRCC theory. . . . .	85
5.4	Contribution to $\alpha$ of Ne from different terms of the dressed dipole operator in the nonlinear PRCC theory. . . . .	86
5.5	Two of the leading order terms in the nonlinear PRCC Theory. . . . .	86
5.6	The contribution to $\alpha$ from the fourth order term in nonlinear PRCC theory. . . . .	87
5.7	Convergence pattern of $\alpha$ (Kr) as a function of the basis set size. . . . .	89
5.8	The static dipole polarizability, $\alpha$ (atomic units), from linearized PRCC and comparison with previous results. . . . .	90
5.9	Contribution to $\alpha$ from different terms of the dressed dipole oper- ator in the linearized PRCC theory . . . . .	91

5.10	Contribution to $\alpha$ from different terms of the dressed dipole operator in the non-linear PRCC theory. . . . .	92
5.11	Core orbital contribution from $\mathbf{T}_1^{(1)\dagger}\mathbf{D}$ to $\alpha$ . . . . .	92
5.12	Core orbitals contribution from $\mathbf{T}_1^{(1)\dagger}\mathbf{DT}_2^{(0)}$ to $\alpha$ of Argon and Krypton. . . . .	93
5.13	Core orbitals contribution from $\mathbf{T}_1^{(1)\dagger}\mathbf{DT}_2^{(0)}$ to $\alpha$ of Xenon and Radon. . . . .	95
5.14	Static dipole polarizability of alkali ions. . . . .	96
5.15	Contribution to $\alpha$ from different terms and their hermitian conjugates in the linearized PRCC theory. . . . .	97
5.16	Contribution to $\alpha$ from different terms and their conjugate in the PRCC theory after including the terms nonlinear in cluster operators. . . . .	98
5.17	Four leading contributions to $\{\mathbf{T}_1^{(1)\dagger}\mathbf{D} + \text{h.c}\}$ to $\alpha$ in terms of the core spin-orbitals. . . . .	99
5.18	Core orbitals contribution from $\mathbf{T}_1^{(1)\dagger}\mathbf{DT}_2^{(0)}$ to $\alpha$ of $\text{Na}^+$ and $\text{K}^+$ . . . . .	99
5.19	Core orbitals contribution from $\mathbf{T}_1^{(1)\dagger}\mathbf{DT}_2^{(0)}$ to $\alpha$ of $\text{Rb}^+$ , $\text{Cs}^+$ and $\text{Fr}^+$ . . . . .	100
5.20	Static dipole polarizability of doubly ionized alkaline-Earth-metal ions and the values are in atomic units. . . . .	102
5.21	Contribution to $\alpha$ from different terms and their hermitian conjugates in the LPRCC and PRCC theory. . . . .	105
5.22	Four leading contributions to $\{\mathbf{T}_1^{(1)\dagger}\mathbf{D} + \text{h.c}\}$ to $\alpha$ in terms of the core spin-orbitals. . . . .	106
5.23	Core orbitals contribution from $\mathbf{T}_1^{(1)\dagger}\mathbf{DT}_2^{(0)}$ to $\alpha$ of $\text{Mg}^{2+}$ and $\text{Ca}^{2+}$ . . . . .	107
5.24	Core orbitals contribution from $\mathbf{T}_1^{(1)\dagger}\mathbf{DT}_2^{(0)}$ to $\alpha$ of $\text{Sr}^{2+}$ , $\text{Ba}^{2+}$ and $\text{Ra}^{2+}$ . . . . .	108

# List of Figures

1.1	Feynman diagram for (a) self-energy and (b) vacuum polarization of bound electron. . . . .	4
2.1	Feynman diagram for lowest order one-photon exchange. . . . .	12
2.2	Feynman diagram for vacuum polarization. . . . .	15
2.3	Feynman diagram for Uehling Potential Correction. . . . .	15
2.4	MBPT diagrams corresponding to the $E_{\text{corr}}^{(2)}$ . . . . .	28
3.1	Diagrammatic representation of $T_1^{(0)}$ , $T_2^{(0)}$ and $T_3^{(0)}$ operators. . .	41
3.2	Diagrams of $T_1^{(0)}$ arising from $\left\{ \overline{H_N T_3^{(0)}} \right\}$ . . . . .	43
3.3	Diagrams of $T_2^{(0)}$ arising from $\left\{ \overline{H_N T_3^{(0)}} \right\}$ . . . . .	43
3.4	Diagrams of $T_3^{(0)}$ arising from $\left\{ \overline{H_N T_2^{(0)}} \right\}$ and $\left\{ \overline{H_N T_3^{(0)}} \right\}$ . . . . .	44
3.5	Angular momentum representation of $T_3^{(0)}$ operator. . . . .	45
3.6	Angular momentum diagram contribute to the $T_1^{(0)}$ excitation amplitude. . . . .	46
3.7	Angular momentum contribute to the $T_2^{(0)}$ excitation amplitude. . .	46
3.8	Angular momentum diagram contribute to the $T_3^{(0)}$ excitation amplitude. . . . .	47
3.9	Diagrammatic representation of $\mathbf{T}_1^{(1)}$ and $\mathbf{T}_2^{(1)}$ . . . . .	48
3.10	Diagrams of $\mathbf{T}_1^{(1)}$ arising from $\overline{H_N T_1^{(0)}} \mathbf{T}_1^{(1)}$ . . . . .	53
3.11	The $\mathbf{T}_1^{(1)}$ diagrams arising from the contraction $\overline{H_N T_1^{(0)}} \mathbf{T}_2^{(1)}$ . . . . .	53
3.12	The $\mathbf{T}_1^{(1)}$ diagrams arising from the contraction $\overline{H_N T_2^{(0)}} \mathbf{T}_1^{(1)}$ . . . . .	54
3.13	The $\mathbf{T}_1^{(1)}$ diagrams arising from the contraction $\overline{H_N T_1^{(0)} T_1^{(0)}} \mathbf{T}_1^{(1)}$ . . .	54
3.14	The $\mathbf{T}_2^{(1)}$ diagrams arising from the contraction $\overline{H_N T_1^{(0)}} \mathbf{T}_1^{(1)}$ . . . . .	55

3.15	The $\mathbf{T}_2^{(1)}$ diagrams arising from the contraction $\overline{H_N T_1^{(0)}} \mathbf{T}_2^{(1)}$ . . . . .	56
3.16	The $\mathbf{T}_2^{(1)}$ diagrams arising from the contraction $\overline{H_N T_2^{(0)}} \mathbf{T}_1^{(1)}$ . . . . .	57
3.17	The $\mathbf{T}_2^{(1)}$ diagrams arising from the contraction $\overline{H_N T_2^{(0)}} \mathbf{T}_2^{(1)}$ . . . . .	58
3.18	Diagrams arising from the contraction $\overline{H_N T_1^{(0)} T_1^{(0)}} \mathbf{T}_1^{(1)}$ . . . . .	59
3.19	Diagrams arising from the contraction $\overline{H_N T_1^{(0)} T_1^{(0)}} \mathbf{T}_2^{(1)}$ . . . . .	59
3.20	Diagrams arising from the contraction $\overline{H_N T_1^{(0)} T_2^{(0)}} \mathbf{T}_1^{(1)}$ . . . . .	60
3.21	Diagrams arising from the contraction $\overline{H_N T_1^{(0)} T_1^{(0)} T_1^{(0)}} \mathbf{T}_1^{(1)}$ . . . . .	60
3.22	Singles diagrams arising from the contraction $\overline{H_{\text{int}} T^{(0)}}$ and $\overline{H_{\text{int}} T^{(0)} T^{(0)}}$ . . . . .	61
3.23	Doubles diagrams arising from the contraction $\overline{H_{\text{int}} T^{(0)}}$ and $\overline{H_{\text{int}} T^{(0)} T^{(0)}}$ . . . . .	61
3.24	Example diagrams of $H_N T_2^{(0)} T_2^{(0)}$ which contribute to the $\mathbf{T}_2^{(1)}$ equations. The portion of the diagrams within the rectangles with rounded corners are examples of the one body (a) and two-body (b) intermediate diagrams. . . . .	63
4.1	Diagrammatic representation of open shell coupled-cluster operator : (a) Single excitation operator, (b) Double excitations operator, (c) Triple excitations operator. . . . .	67
4.2	Attachment energy diagrams arising at the triple excitation level. . . . .	68
4.3	Leading diagrams arising from the contraction $\{\overline{S_2^{(0)\dagger} \mathbf{D} S_3^{(0)}}\}$ contribute to the reduced dipole matrix element. Dashed line represent the dipole operator. . . . .	70
5.1	Diagrams of the $\alpha$ in the PRCC theory. The single excitation operators with a wavy line represent $\mathbf{T}_1^{(1)}$ . Similarly, the double excitation diagrams with an extra vertical line represent $\mathbf{T}_2^{(1)}$ . . . . .	82
5.2	Contributions to the next to leading order terms $\mathbf{T}_1^{(1)\dagger} \mathbf{D} T_2^{(0)}$ + h.c. in terms of the pairs of core spin-orbitals. . . . .	100

# Chapter 1

## Introduction

Quantum electrodynamics describes the interaction between electrons and photons at the fundamental scale. It was mainly developed by Schwinger, Tomonaga, Feynman and Dyson [5–12] in the late 1940s. The theory is one of the most successful one in modern physics. It has been tested to very high precision in the last few decades. An example is the anomalous magnetic moment of the electron and the fine structure constant. To be more precise, the anomalous magnetic moment of the electron is determined both experimentally [13] as well as theoretically [14] with parts-per-trillion accuracy.

The small atomic systems are suitable to study the QED effects because of their simple atomic structure. One special advantage is that in an atom the bound electrons always experience the presence of electric field of the nucleus, and thus atom acts like a small laboratory to precisely determine the QED effects. With the increase in  $Z$ , the average electric field on the bound electrons increases with to factor of  $\approx 10^6$  from  $Z = 1$  to  $Z = 92$  [15]. The electrons at the innermost orbitals experience the strongest electric field. To describe such atomic systems very precisely, one must account for the QED corrections. However, computational complexities limit us to apply the theory to the simple atomic systems. For one electron atom and hydrogen like ions, it is possible to treat the QED effects analytically and presents less computational challenges than many electron atoms and ions.

The enormous success of QED in calculating atomic properties like the tran-

sition energies, is limited to a weak electric field. To elaborate let us take the following example : the electric field strength at the surface of the Uranium nucleus, which has a radius of 7.42 fm is  $\mathbf{E} \approx 2 \times 10^{19}$  V/cm and the magnetic field at the surface of the nucleus of  $^{209}\text{Bi}$  is  $|\mathbf{B}| \approx 10^{12}$  Gauss. Therefore, one of the goals for near future is to describe the properties of such atoms in super strong field. With the advent of powerful Lasers it is experimentally possible to create such strong field in laboratory and test precisely the QED effects. To describe such systems it is necessary to develop non-perturbative techniques in QED. This will not only extend our understanding of the fundamental process at the quantum scale, but also can lead to practical applications.

The theory of QED is well suited for one electron atom, but in the present context we wish to study the QED effects in many electron atoms. The appropriate point to start in relativistic atomic structure calculation is the Dirac-Coulomb Hamiltonian. After the development of relativistic quantum mechanics in the late 1930s, there was an effort to generalize the non-relativistic problems to the relativistic domain. Here it is worth to mention that Dirac pointed out in his pioneering work on quantum mechanics of many electron systems [16] that

*“The general theory of quantum mechanics is now almost complete, the imperfections that still remain being in connection with the exact fitting in of the theory with relativity ideas. These give rise to difficulties only when high-speed particles are involved, and are therefore of no importance in the consideration of atomic and molecular structure and ordinary chemical reactions, in which it is, indeed, usually sufficiently accurate if one neglects relativity variation of mass with velocity and assumes only Coulomb forces between the various electrons and atomic nuclei. The underlying physical laws necessary for the mathematical theory of a large part of physics and the whole of chemistry are thus completely known, and the difficulty is only that the exact application of these equations leads to equations much too complicated to be soluble. It therefore becomes desirable that approximate practical methods of applying quantum mechanics should be developed, which can lead to an explanation of the main features of complex atomic systems without too much computation”.*

After that, however, several developments have taken place in the field of relativistic atomic structure calculations and it is now well established [17, 18] that one needs the relativistic quantum mechanics for an appropriate description of the multi-electron atoms. As we know the solution of the Dirac equation leads to the positive and negative energy states, Dirac pointed out the existence of negative energy solutions and proposed the idea of electron sea to prevent the transition from the positive energy state to the negative energy state. This has an important implications on the stability of atoms and molecules.

The Dirac Hamiltonian with the two electron Coulomb interaction is the natural choice to describe the many electron atoms. Later G. Breit [19] pointed out the relativistic correction to the two electron Coulomb interaction. The Dirac Hamiltonian is Lorentz invariant. So, the description of free electron in the framework of Dirac equation is also appropriate. But when we use the two electron Coulomb interaction along with the Dirac Hamiltonian, then it is not Lorentz invariant. As Grant [20] pointed out that it has significant impact while calculating the radiative transitions in atoms and it is appropriate to use the Dirac-Coulomb-Breit Hamiltonian for a proper relativistic description. The negative energy states in the Dirac Hamiltonian motivated the development of a fundamental theory which consider an indefinite number of particles. The coupling between the electron-positron field with the photon field is the basic ingredient of QED. It correctly describes the radiative processes and collision processes by using Feynman diagrams. The fundamental process that we consider as the QED corrections in atoms are the vacuum polarization correction and self-energy correction [15]. These radiative corrections are shown in Fig. 1.1. Where the double lines represents the bound electrons. The Fig. 1.1 (a) represents the self energy part of the QED corrections in which a bound electron emits a photon and after it reabsorbed after sometime. This self energy correction is the dominant QED correction for hydrogen atom and hydrogen like ions because of small mass of the electrons. Fig. 1.1 (b) is the vacuum polarization part of the QED corrections. In this process the photon, which mediates the interaction between the nucleus and the bound electron, creates virtual electron-positron pair. For heavy atoms

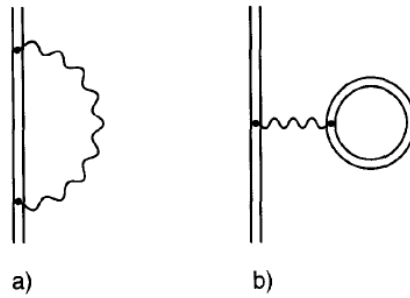


Figure 1.1: Feynman diagram for (a) self-energy and (b) vacuum polarization of bound electron.

and ions the vacuum polarization contribution to the orbital energies is significant and is comparable to the self energy process. For example, in hydrogen like uranium, the combined contribution from the vacuum polarization and the self energy to the K-shell electron energy shift is 266 eV. It is comparable to the total 1S binding energy which is 132 KeV. The two above mentioned radiative processes have ultraviolet divergence and requires special renormalization technique. However, we consider only the vacuum polarization process in the present thesis work. The above discussion implies that the QED corrections in heavy atoms and ions is important to study and have many practical consequences.

The QED corrections are considered in the perturbation expansion of the fine structure constant,  $\alpha \approx 1/137$ . Since the nuclear charge  $Z$  is important for heavy atoms and ions, the QED perturbation expansion is considered in  $Z\alpha$  [21].

The radiative correction in atoms was studied by Uehling [22] in his calculation of lowest order vacuum polarization correction in hydrogen like ions. After Lamb and Retherford discovered the splitting of  $2s_{1/2}$  and  $2p_{1/2}$  states in hydrogen atoms [23], it is clear that the Dirac one electron theory is insufficient for a proper description of atoms and ions. This is because according to Dirac theory the  $2s_{1/2}$  and  $2p_{1/2}$  states are degenerate, but Lamb and Retherford observed that those two states are non degenerate and the energy difference is  $\approx 1057$  MHz. This ground breaking measurement paved the way to construct a fundamental theory to describe the interaction between electrons and photons.

The objective of the present thesis is to study the QED effects in many elec-

tron atoms. To be precise the initial development in QED takes up the issue of single electron atoms and ions where the electron-electron correlation is completely absent. To take the electronic correlation it is important to start with the Dirac-Hartree-Fock self consistent field theory. The relativistic self-consistent field method was used by Swirles [24] in her remarkable work in the early days of relativistic quantum mechanics. The pioneering work by Grant [25] and Desclaux [26] on the multiconfiguration Dirac-Fock method is the basis of relativistic atomic structure calculations. The advantage of the MCDF method is that it can take into account some part of the many body contributions like the correlation energy which is neglected at the relativistic SCF method. As first pointed out by Brown and Ravenhall [27], the use of Dirac-Hartree-Fock Hamiltonian implies the inclusion of the negative energy solutions and it leads to the *variational collapse* and *continuum dissolution*. Later, J. Sucher [1] showed that the problem can be solved theoretically by using the projection operators technique and it can be used to project out the negative energy solutions. The construction of the projection operator is purely theoretical as one needs to know the complete set of eigenstates to construct the projection operator. However, in practical calculations it is not possible to construct the complete set of eigenstates a priori. In numerical computation with the finite basis sets, we use the kinetic balance condition [28, 29] between the large and the small components of the four component radial wave-function to avoid *variational collapse* and *continuum dissolution*.

Principally two techniques are used to incorporate the correlation along with the QED effects in many electron atoms. In one approach one uses the perturbation expansion in  $\alpha$  and  $Z\alpha$  with Hylleraas [30] type relativistic wave-function. The advantage is that the correlation is built in the wave-function and we can directly calculate the QED effects. This method is suitable for low- $Z$  atoms and ions, and has been used extensively by Drake *et al.* [31, 32] and Pachucki *et al.* [33, 34]. In this kind of calculations the electronic correlation is taken accurately but can not be applied to heavy atoms and ions. The second approach is based on the finite basis set expansion of single particle relativistic wave-functions. This is used in the present thesis. This approach is used extensively in atomic as well as

molecular physics calculations. To mention a few by Grant *et al.* [35], Johnson *et al.* [36] and Das *et al.* [37]. Here, the advantage is that as  $Z$  increases the inner electrons are relativistic and are well described by the single particle Dirac equation. However, the effects of correlation is missing in this kind of calculation. We can take the QED effects precisely within the description of single particle wave function by incorporating the QED Hamiltonian along with the Dirac-Coulomb-Breit model. To incorporate the correlation effects it is important to go beyond the Dirac-Hartree-Fock model.

In the post Hartree-Fock period several many body methods were developed to incorporate the electron correlation precisely. The many body perturbation theory (MBPT) is one of the earliest approach to take into account the electron correlation in atomic physics calculations [38]. The relativistic version of time independent MBPT treat electron correlation to arbitrary order. But, with the increase in the order of perturbation the complicacy of the diagrams increases and after third order it is difficult to consider all the terms.

The coupled-cluster theory (CCT) [3, 4] is one of the most elegant many body theory which incorporates the electron correlation to all order. The details of the CCT and different variants are described in a recent review [39]. The theory has been widely used for atomic [40–43], molecular [44], nuclear [45] and condensed matter physics [46] calculations. As pointed out by Lindgren [47], we can directly incorporate the QED effects in the wave-function and leads to a covariant formulation. It is also important to mention that appropriate starting point to incorporate the QED effects is to start with the S-matrix formalism as described by Mohr *et al.* [15]. There are other techniques in the literature to consider the QED corrections like the two times Green's function by Shabaev [48] and the covariant evolution operator technique by Lindgren *et al.* [49]. The latter two techniques are appropriate choice for many electron systems because it can treat the quasi degeneracy systematically. These techniques are relativistically covariant and use Feynman gauge, and can handle more than one photon exchange effects. In the present work we only focus on the leading order one photon exchange corrections to the Coulomb interaction. The QED effects at the

lowest order of perturbation theory consist of the vacuum polarization correction and the self energy effects. It is important to mention that vacuum polarization and the self energy effects are most important for QED correction after Breit interaction.

In the present thesis we incorporate the vacuum polarization effect and the Breit interaction correction to the wave-function in DHF theory. We use these DHF wave-function as the reference state wave-function for the RCC theory. Then Breit interaction correction is then incorporated in the two electron integrals in the RCC theory. Along with this we consider the triple excitations in the RCC theory to estimate the contribution from it to the different atomic properties. We introduce perturbed relativistic coupled-cluster theory (PRCC) [50, 51] to incorporate multiple perturbations in a many electron atom. The PRCC theory has the potential to take into account different kind of perturbation in a systematic way. We demonstrate the power of PRCC theory by evaluating the static dipole polarizability of closed shell atoms and ions.

## 1.1 Thesis overview

In chapter 2, we discuss about atomic MBPT with QED effects. We introduce the relativistic Dirac-Coulomb Hamiltonian and discuss the importance of Breit interaction. In this chapter we derived the general expression of Breit interaction from the one photon exchange process in QED. We then derive the form of Uehling potential which is the leading order correction in vacuum polarization. We follow the convention of natural units to derive the expression. We then, introduce the MBPT and describe how we consider the QED effects in the framework of MBPT. We introduce the Gaussian type finite basis set which we consider for the numerical calculation. We then explain, about the optimization of the basis set by comparing our values of the SCF energy and the orbital energies from the GRASP92 code [52]. We present our results of the correction due to Breit interaction and vacuum polarization to the orbital energies and SCF energy in subsequent part. We end the chapter with a discussion on the Breit

interaction contribution to the correlation energy of noble gas atoms.

In chapter 3, QED effects in closed shell atoms is investigated with relativistic coupled-cluster theory. In this chapter we introduce the triple excitations in the RCC theory and the diagrammatic representation of triple excitations to calculate angular momentum diagrams. We then, discuss about the RCC amplitude equations with triple excitations in great detail. Next we introduce the perturbed relativistic coupled-cluster theory to incorporate external or internal perturbations in atomic system. For example, we discuss about the static electric field as the external perturbation in many electron atoms in the present context. We derive the PRCC amplitude equations and presented the details of the non-linear PRCC diagrams. The general PRCC theory is discussed extensively in this chapter.

In chapter 4, QED effects in open shell atoms with RCC theory is studied. The triple excitations contribution to the removal energies of ground state and low lying excited states are discussed. We also study the electric dipole transition amplitudes by using the RCCSDT wave-function.

In chapter 5, the static dipole polarizability of closed shell atoms and ions is discussed. We introduce the static dipole polarizability from the time independent perturbation theory and derive the equivalent expression in RCC theory. We apply the PRCC theory to calculate the static dipole polarizability with Dirac-Coulomb-Breit Hamiltonian. We begin with Neon, as it is one of the noble gas atoms with small  $Z$ . We investigate the term wise contribution from non-linear PRCC theory to the dipole polarizability of Neon. Next we study the other heavy noble gas atoms and discuss about the importance of Breit interaction in heavy atoms. We also calculate the static dipole polarizability of alkali-metal ions and doubly ionized alkaline Earth metal ions using PRCC theory. We demonstrate the core polarization and pair-correlation effects. We end the chapter with a discussion on the theoretical uncertainty in our calculations.

Chapter 6 covers the conclusions and future direction of the present work.

## 1.2 Units and notations

In relativistic quantum mechanics and quantum field theory, it is convenient to use natural unit system. In this system the action, which is energy times time is measured in  $\hbar$  and velocity is defined in units of  $c$ . In natural units the permittivity of vacuum,  $\epsilon_0$  is unity, so the permeability of the vacuum,  $\mu_0$  is also unity. Therefore, in natural units  $\hbar = c = \epsilon_0 = \mu_0 = 1$ . The fine structure constant,  $\alpha$  is

$$\alpha = \frac{e^2}{4\pi}. \quad (1.1)$$

The natural units are convenient to use while deriving the expression of Uehling potential and Breit interaction. However, for the numerical computation we use the atomic units. In this unit system,  $m_e = e = \hbar = 4\pi\epsilon_0 = 1$ . Here,  $m_e$  is the mass of the electron. Therefore the fine structure constant in atomic unit is simply the inverse of the velocity of light. For which we use the latest value recommended by CODATA in numerical calculation and it is  $\alpha^{-1} = 137.035\,999\,074$  [53].

For the relativistic calculation we use the following notation of metric tensor

$$g_{\mu\nu} = \begin{pmatrix} 1 & 0 & 0 & 0 \\ 0 & -1 & 0 & 0 \\ 0 & 0 & -1 & 0 \\ 0 & 0 & 0 & -1 \end{pmatrix} \quad (1.2)$$

In this thesis the Greek indices ( $\mu, \nu = 0, 1, 2, 3$ ) are used to represent the component four vectors and Latin indices ( $i, j, k = 1, 2, 3$ ) are used to represent the component of three vectors.

# Chapter 2

## Many Body Perturbation Theory with QED effects

The QED effects in many electron atoms and ions are possible to test experimentally with high accuracy. In many electron atoms and ions along with QED effects, the electron correlation correction is very important. MBPT has proven to be successful to a certain level to take into account the electron correlation in a systematic way. The electron correlation effects in MBPT are treated perturbatively in order by order. For a closed shell atom the model space in MBPT is constructed using a single Slater determinant. So the closed shell atoms and ions are the ideal testing grounds of QED. Since the complicacy of QED calculation increases very rapidly with the order of perturbation, we treat the QED correction in lowest order of perturbation theory, i.e, lowest order in  $Z\alpha$  in the framework of relativistic MBPT.

The chapter is organized as follows: In section 2, we introduce the Dirac-Coulomb Hamiltonian and its importance in the relativistic atomic structure calculation. In the next part, we discuss about the Breit interaction in the framework of QED. The VP correction to the many electron atom is described in great detail in section 2.1. The Dirac-Coulomb-Breit Hamiltonian together with the QED corrections to the nuclear potential is the starting point of the MBPT for closed and open shell atoms in the present work. In section 2.4, we introduce the single particle wave-functions for the SCF calculation. The matrix element

of Breit interaction is discussed in section 2.5. Section 2.6 contains the detailed description of the generalized Bloch equation with the relativistic Hamiltonian in atomic MBPT. We introduce the diagrammatic MBPT to calculate the correlation energy of closed shell atoms in section 2.7. In subsequent part we discuss in great detail the results from Breit and QED correction to the orbital energy in the SCF method. We also demonstrate the importance of considering the Breit interaction in the calculation of correlation energy of closed shell atoms. Based on the above mentioned results, we end the chapter with subsequent conclusion.

## 2.1 Relativistic Hamiltonian for atomic calculation

In the relativistic atomic structure calculations it is important to consider the relativistic as well as the correlation effects simultaneously. As a starting point Dirac Hamiltonian with the Coulomb potential, referred to as the Dirac-Coulomb Hamiltonian,  $H^{\text{DC}}$ , is an appropriate choice. For a N-electron atom or ion [18]

$$H^{\text{DC}} = \sum_{i=1}^N [c\boldsymbol{\alpha}_i \cdot \mathbf{p}_i + (\beta_i - 1)c^2 - V_Z(r_i)] + \sum_{i<j} \frac{1}{r_{ij}}, \quad (2.1)$$

where,  $\boldsymbol{\alpha}_i$  and the  $\beta_i$  are the Dirac matrices,  $V_Z(r_i)$  is the nuclear potential,  $Z$  ( $Z \geq N$ ) is the nuclear charge and the last term represents the electron-electron Coulomb interaction. The Hamiltonian,  $H^{\text{DC}}$  is not gauge invariant. A fully gauge invariant electron-electron interaction should be ideal as it is important for radiative transitions in atoms. To circumvent the problem partially we consider the Breit interaction term in the atomic Hamiltonian. The full Dirac-Coulomb-Breit Hamiltonian will be then an appropriate choice for atomic structure calculations.

### 2.1.1 Breit interaction

The interaction between two Dirac particles for the one photon exchange process can be represented using the Feynman diagram [54] in Fig. 2.1. The S-matrix

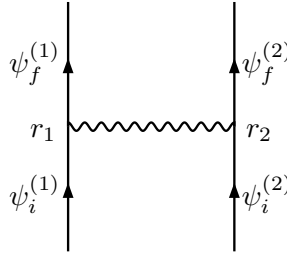


Figure 2.1: Feynman diagram for lowest order one-photon exchange.

element of this process is

$$S_{fi} = -i \int d^4 r_1 \int d^4 r_2 \quad j_{fi}^{(2)}(r_2) D_F(r_1 - r_2) j_{fi}^{(1)}(r_1). \quad (2.2)$$

Here  $D_F(r_1 - r_2)$  is the photon propagator and  $j_{fi}^{(n)}$  represents the transition currents

$$j_{fi}^{(n)}(r) = \bar{\psi}_f^{(n)}(r) \gamma^\mu \psi_i^{(n)}(r) = j_{fi}^{(n)}(\mathbf{r}) e^{i\omega_{fi}^{(n)} t}. \quad (2.3)$$

We get this after separating the time dependent part in  $j_{fi}^{(n)}(r)$  and  $\omega_{fi}^{(n)} = E_f^{(n)} - E_i^{(n)}$  is the transition frequency. Using the form of momentum space photon propagator in Feynman gauge, the S-matrix element can be written as

$$S_{fi} = -i \int d^4 r_1 \int d^4 r_2 \int \frac{d^4 k}{(2\pi)^4} \quad j_{fi}^{(2)}(\mathbf{r}_2) e^{i\omega_{fi}^{(2)} t_2} \frac{-4\pi}{k^2 + i\epsilon} e^{-ik \cdot (r_1 - r_2)} j_{fi}^{(1)}(\mathbf{r}_1) e^{i\omega_{fi}^{(1)} t_1} \quad (2.4)$$

We separate the  $t_1$  dependent part in the transition current and integrate it. So the integral reduces to three dimensional integral and for the  $k$ - space integration, we choose the spherical coordinates. After solving the integral using the techniques of complex analysis we obtain

$$S_{fi} = -i \int d^3 r_2 \int dt \quad j_{fi}^{(2)}(\mathbf{r}_2, t) \underbrace{\int d^3 r_1 \quad j_{fi}^{(1)}(\mathbf{r}_1) \frac{e^{i\omega_{fi}^{(1)}(t - |\mathbf{r}_1 - \mathbf{r}_2|)}}{|\mathbf{r}_1 - \mathbf{r}_2|}}_{A_{fi}^{(1)}(\mathbf{r}_2, t)}. \quad (2.5)$$

So the transition current  $j_{fi}^{(2)}(\mathbf{r}_2, t)$  interacts with the electromagnetic potential  $A_{fi}^{(1)}(\mathbf{r}_2, t)$  arising from the other particle at an earlier time. And the time difference is  $|\mathbf{r}_1 - \mathbf{r}_2| \equiv |\mathbf{r}_1 - \mathbf{r}_2|/c$ . So, the potential can be written as the retarded

potential and for small velocity i.e.  $v \ll c$  we can write the S-matrix element as

$$S_{fi} \approx -2\pi i \delta(\omega_{fi}^{(1)} + \omega_{fi}^{(2)}) \int d^3 r_2 \int d^3 r_1 \psi_f^{(2)\dagger}(\mathbf{r}_2) \psi_f^{(1)\dagger}(\mathbf{r}_1) (\mathbb{1} \cdot \mathbb{1} - \boldsymbol{\alpha}_1 \cdot \boldsymbol{\alpha}_2) \left( \frac{1}{|\mathbf{r}_1 - \mathbf{r}_2|} + i \frac{\omega_{fi}}{c} - \frac{1}{2c^2} \omega_{fi}^2 |\mathbf{r}_1 - \mathbf{r}_2| \right) \psi_i^{(2)}(\mathbf{r}_2) \psi_i^{(1)}(\mathbf{r}_1). \quad (2.6)$$

Here we consider only the lowest order term in the Taylor series expansion of frequency dependent part.

The initial and final state wave-functions are assumed to be the stationary eigenstate of the Dirac Hamiltonian.

$$H^{(1)} = c\boldsymbol{\alpha}^{(1)} \cdot \mathbf{p}^{(1)} + \beta^{(1)}c^2 + H_{\text{ext}}^{(1)}, \quad (2.7)$$

$H_{\text{ext}}^{(1)}$  is the external potential present in the system. So we can write

$$\begin{aligned} H^{(1)}\psi_i^{(1)}(\mathbf{r}_1) &= E_i^{(1)}\psi_i^{(1)}(\mathbf{r}_1), \\ H^{(1)}\psi_f^{(1)}(\mathbf{r}_1) &= E_f^{(1)}\psi_f^{(1)}(\mathbf{r}_1). \end{aligned} \quad (2.8)$$

Similarly, there is an equivalent expression for  $H^{(2)}$ . Now with the assumption  $\omega_{fi}^{(1)} = -\omega_{fi}^{(2)}$  we can get the following identity in terms of the Dirac Hamiltonian.

$$-\omega_{fi}^2 |\mathbf{r}_1 - \mathbf{r}_2| = \left[ H^{(1)}, [H^{(2)}, |\mathbf{r}_1 - \mathbf{r}_2|] \right]. \quad (2.9)$$

The momentum operator does not commute with  $|\mathbf{r}_1 - \mathbf{r}_2|$ . Using  $[\mathbf{p}, f(\mathbf{x})] = -i\nabla f(\mathbf{x})$ , we can rewrite

$$-\omega_{fi}^2 |\mathbf{r}_1 - \mathbf{r}_2| = c^2 \left[ \frac{\boldsymbol{\alpha}^{(1)} \cdot \boldsymbol{\alpha}^{(2)}}{|\mathbf{r}_1 - \mathbf{r}_2|} - \frac{\{\boldsymbol{\alpha}^{(1)} \cdot \mathbf{r}_1 - \mathbf{r}_2\} \{\boldsymbol{\alpha}^{(2)} \cdot \mathbf{r}_1 - \mathbf{r}_2\}}{|\mathbf{r}_1 - \mathbf{r}_2|^3} \right]. \quad (2.10)$$

Combining the above result, the S-matrix element can be written as

$$S_{fi} = -2\pi i \delta(\omega_{fi}^{(1)} + \omega_{fi}^{(2)}) \int d^3 r_2 \int d^3 r_1 \psi_f^{(2)\dagger}(\mathbf{r}_2) \psi_f^{(1)\dagger}(\mathbf{r}_1) \left\{ \frac{\mathbb{1} \cdot \mathbb{1}}{|\mathbf{r}_1 - \mathbf{r}_2|} - \frac{\boldsymbol{\alpha}_1 \cdot \boldsymbol{\alpha}_2 + \{\boldsymbol{\alpha}_1 \cdot \hat{\mathbf{n}}\} \{\boldsymbol{\alpha}_2 \cdot \hat{\mathbf{n}}\}}{2|\mathbf{r}_1 - \mathbf{r}_2|} \right\} \psi_i^{(2)}(\mathbf{r}_2) \psi_i^{(1)}(\mathbf{r}_1). \quad (2.11)$$

Here  $\hat{\mathbf{n}} = (\mathbf{r}_1 - \mathbf{r}_2)/|\mathbf{r}_1 - \mathbf{r}_2|$  is the direction vector. The Eq. (2.11) represents the interaction of two particles through an effective interaction  $U(\mathbf{x} - \mathbf{y})$ , which is of the form

$$\begin{aligned} U(\mathbf{r}_1 - \mathbf{r}_2) &= \frac{1}{|\mathbf{r}_1 - \mathbf{r}_2|} - \frac{\boldsymbol{\alpha}_1 \cdot \boldsymbol{\alpha}_2 + \{\boldsymbol{\alpha}_1 \cdot \hat{\mathbf{n}}\} \{\boldsymbol{\alpha}_2 \cdot \hat{\mathbf{n}}\}}{2|\mathbf{r}_1 - \mathbf{r}_2|}, \\ &= U_C(\mathbf{r}_1 - \mathbf{r}_2) + U_{\text{Br}}(\mathbf{r}_1 - \mathbf{r}_2). \end{aligned} \quad (2.12)$$

The first term in the above equation is the Coulomb interaction between two particles and along with that we get a correction term  $U_{\text{Br}}$ ; which is known as the Breit interaction. This correction term to the electron-electron interaction represents the magnetic interaction and the retardation. With the inclusion of the  $U_{\text{Br}}$ , the Hamiltonian includes the lowest order one photon exchange process. In Dirac theory the velocity operator is  $\mathbf{v}_i = c\boldsymbol{\alpha}_i$ , so  $U_{\text{Br}}$  is quadratic in velocity. In classical electrodynamics this correction to the Coulomb potential is known as the Darwin term [55].

With the Breit interaction the total atomic Hamiltonian is

$$H^{\text{DCB}} = \sum_{i=1}^N [c\boldsymbol{\alpha}_i \cdot \mathbf{p}_i + (\beta_i - 1)c^2 - V_N(r_i)] + \sum_{i<j}^N \left[ \frac{1}{r_{ij}} + g^{\text{B}}(r_{ij}) \right], \quad (2.13)$$

Where the last two terms,  $1/r_{ij}$  and  $g^{\text{B}}(r_{ij})$ , are the Coulomb and Breit interactions, respectively. We can rewrite the Breit interaction as

$$g^{\text{B}}(r_{12}) = -\frac{1}{2r_{12}} \left[ \boldsymbol{\alpha}_1 \cdot \boldsymbol{\alpha}_2 + \frac{(\boldsymbol{\alpha}_1 \cdot \mathbf{r}_{12})(\boldsymbol{\alpha}_2 \cdot \mathbf{r}_{12})}{r_{12}^2} \right]. \quad (2.14)$$

The Hamiltonian,  $H^{\text{DCB}}$  is the starting point of our relativistic atomic calculations and we shall discuss about the matrix element of Breit interaction and its implementation in section 2.5.

### 2.1.2 Vacuum polarization

The photon which mediates the interaction between the bound electrons and the nucleus in an atom can generate virtual electron-positron pairs. This polarizes the vacuum and the effect is known as the vacuum polarization. In the lowest order of coupling constant  $Z\alpha$ , the photon propagates freely, but the creation of  $e^-e^+$  pair modifies the Coulomb field and effectively shifts the orbital energy levels of many electron atoms. The Feynman diagram corresponding to the first-order vacuum polarization process is shown in Fig. 2.2. The lowest order non-vanishing contribution in VP correction comes from the Uehling potential [22]. The Feynman diagram of the Uehling potential correction [56] is shown in Fig. 2.3. To derive the functional form of Uehling potential we start with a point

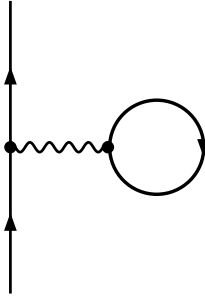


Figure 2.2: Feynman diagram for vacuum polarization.

charge  $-Ze$ . The charge density is

$$j_{\mu}(r) = -Ze\delta^3(\mathbf{r})\delta_{\mu 0}. \quad (2.15)$$

Fig. 2.3 represents the modified photon propagator by

$$\begin{aligned} \frac{-ig_{\mu\nu}}{q^2 + i\varepsilon} &\rightarrow \left[ \frac{-i}{q^2 + i\varepsilon} \right]^2 \int \frac{d^4k}{(2\pi)^4} \text{Tr} \left[ (-ie\gamma_{\mu}) \frac{i}{\not{k} - m + i\varepsilon} (-ie\gamma_{\nu}) \frac{i}{\not{k} - \not{q} - m + i\varepsilon} \right], \\ &= \left[ \frac{-i}{q^2 + i\varepsilon} \right] \Pi_{\mu\nu}(q) \left[ \frac{-i}{q^2 + i\varepsilon} \right]. \end{aligned} \quad (2.16)$$

Here  $\Pi_{\mu\nu}(q)$  is the polarization tensor and  $\not{k}, \not{q}$  represents the four momentum.

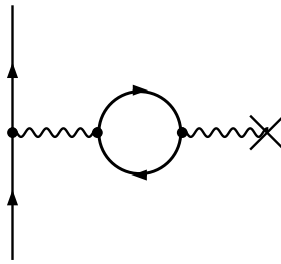


Figure 2.3: Feynman diagram for Uehling Potential Correction.

The momentum integral has two electron propagators which contains two  $k$  in the denominator and therefore it diverges quadratically in  $k$ . Since the gauge transformation does not physically shift the energy levels, one can write

$$q^{\mu} \Pi_{\mu\nu} = 0. \quad (2.17)$$

Using the Pauli-Villars regularization [57], the regularized polarization tensor,  $\bar{\Pi}_{\mu\nu}$  is written as

$$\bar{\Pi}_{\mu\nu}(q, m^2) = \Pi_{\mu\nu}(q, m^2) + \sum_i C_i(M_i^2)\Pi_{\mu\nu}(q, M_i^2), \quad (2.18)$$

The use of the regularized polarization tensor,  $\bar{\Pi}_{\mu\nu}$  avoids the divergence. Here  $C_i$  and  $M_i$  are the auxiliary functions chosen such that the integral converge. We follow the treatment of ref.[54] to evaluate the VP potential. To calculate the functional form of the potential we start with the modified photon propagator  $D'_F$ . The potential in the momentum space assumes the form

$$A'_\mu(r) = \int \frac{d^4q}{(2\pi)^4} e^{-iq \cdot r} D'_{F\mu\nu}(q) j^\nu(q). \quad (2.19)$$

After renormalization the polarization function is

$$\bar{\Pi}(q^2) \equiv -\frac{e^2}{3\pi} \ln \frac{\Lambda^2}{m^2} + \Pi^R(q^2). \quad (2.20)$$

Here  $\Lambda$  is the cut-off momentum. The first term in the above regularized vacuum polarization tensor consists of a constant term and a momentum dependent part  $\Pi^R(q^2)$ . Using the renormalized vacuum polarization function, the modified photon propagator is

$$D'_{F\mu\nu}(q) = \frac{-4\pi g_{\mu\nu}}{q^2} [1 + \Pi^R(q^2)]. \quad (2.21)$$

and the momentum dependent regularized polarization tensor is of following form

$$\Pi^R(q^2) = \frac{2\alpha}{\pi} \int_0^1 d\beta \beta(1-\beta) \ln \left[ 1 + \frac{q^2}{m^2} \beta(1-\beta) \right]. \quad (2.22)$$

Therefore the modified potential of Eq. (2.19) is

$$A'_\mu(r) = \int \frac{d^4q}{(2\pi)^4} e^{-iq \cdot r} [1 + \Pi^R(q^2)] A_\mu(q). \quad (2.23)$$

In the momentum space, the unmodified potential can be written as,  $A_\mu(q) = D_{F\mu\nu} j^\nu(q)$ . As mentioned earlier, we consider stationary charge in the present case, thus  $j_\mu(r) = j_\mu(\mathbf{r})$ . So the modified potential becomes

$$A'_0(\mathbf{r}) = \int \frac{d^3q}{(2\pi)^3} e^{i\mathbf{q} \cdot \mathbf{r}} [1 + \Pi^R(-\mathbf{q}^2)] A_0(\mathbf{q}). \quad (2.24)$$

With the renormalized photon polarization function

$$A'_0(\mathbf{r}) = \int \frac{d^3q}{(2\pi)^3} e^{i\mathbf{q}\cdot\mathbf{r}} \frac{4\pi}{\mathbf{q}^2} \left\{ 1 + \frac{2\alpha}{\pi} \int_0^1 d\beta \beta(1-\beta) \ln \left[ 1 + \frac{\mathbf{q}^2}{m^2} \beta(1-\beta) \right] \right\}. \quad (2.25)$$

The Fourier transform of the first term gives the ordinary Coulomb potential. Along with the Coulomb potential we have the correction term. We eliminate the logarithm using the techniques of partial integration and with the substitution of  $v = 2\beta - 1$ , the photon polarization function is

$$\Pi^R(-\mathbf{q}^2) = \frac{\alpha}{\pi} \frac{\mathbf{q}^2}{4m^2} \int_0^1 dv \frac{v^2(1 - \frac{1}{3}v^2)}{1 + \frac{\mathbf{q}^2}{4m^2}(1 - v^2)} \quad (2.26)$$

Using the techniques of complex analysis the potential is

$$A'_0(\mathbf{r}) = \frac{-Ze}{r} \left[ 1 + \frac{\alpha}{\pi} \int_0^1 dv \frac{v^2(1 - \frac{1}{3}v^2)}{1 - v^2} e^{(-\frac{2m}{\sqrt{1-v^2}})r} \right]. \quad (2.27)$$

With a transformation  $t = \sqrt{(1 - v^2)}$  the modified potential is

$$A'_0(\mathbf{r}) = \frac{-Ze}{r} \left[ 1 + \frac{2\alpha}{3\pi} \int_1^\infty dt \left( 1 + \frac{1}{2t^2} \right) \frac{\sqrt{t^2 - 1}}{t^2} e^{-2mtr} \right]. \quad (2.28)$$

The first term in Eq. (2.28) is the Coulomb potential and the second term is the correction to the Coulomb potential. It is known as the Uehling potential and this form of potential is suitable for numerical integration. So far we have used the natural system of units, where  $\hbar = c = 1$ . For atomic calculations we converted the above system of units to atomic units, i.e,  $m_e = \hbar = e = 4\pi\epsilon_0 = 1$ . So for atomic calculations the Uehling potential is

$$V_{\text{Ue}}(r) = -\frac{2\alpha Z}{3\pi r} \int_1^\infty dt \sqrt{t^2 - 1} \left( \frac{1}{t^2} + \frac{1}{2t^4} \right) \exp \left[ -\frac{2rt}{\alpha} \right]. \quad (2.29)$$

The Eq. (2.29) represents the leading order VP correction to the electron nucleus interaction for a point like nucleus. For heavy atoms nuclei are often modeled as spherical distribution of charge. So, a finite size Fermi charge distribution model of the nucleus is more appropriate [58] and it is defined as

$$\rho_{\text{nuc}}(r) = \frac{\rho_0}{1 + e^{(r-c)/a}}, \quad (2.30)$$

here  $a = t4 \ln(3)$ . The parameter  $c$  is the half charge radius so that  $\rho_{\text{nuc}}(c) = \rho_0/2$  and  $t$  is the skin thickness. For a consistent treatment of the nucleus-electron

interaction,  $V_{\text{Ue}}(r)$  must be modified to account for the finite nuclear size. This can be achieved by folding  $V_{\text{Ue}}(r)$  with the  $\rho_{\text{nuc}}(r)$  [59]. Then the modified form of the Uehling potential is [60]

$$V_{\text{Ue}}(r) = -\frac{2\alpha^2}{3r} \int_0^\infty dx x \rho(x) \int_1^\infty dt \sqrt{t^2 - 1} \left( \frac{1}{t^3} + \frac{1}{2t^5} \right) (e^{-2ct|(r-x)|} - e^{-2ct(r+x)}). \quad (2.31)$$

We implement Eq. (2.31) in the SCF calculation while generating the electron orbitals.

## 2.2 Dirac-Coulomb-Breit Hamiltonian with Uehling potential

Along with the  $V_{\text{Ue}}(r)$ , the total atomic Hamiltonian of a many electron atom is

$$H^{\text{DCB}} = \sum_{i=1}^N \left[ c\boldsymbol{\alpha}_i \cdot \mathbf{p}_i + (\beta_i - 1)c^2 - V'_N(r_i) \right] + \sum_{i<j}^N \left[ \frac{1}{r_{ij}} + g^{\text{B}}(r_{ij}) \right]. \quad (2.32)$$

The first part of the  $H^{\text{DCB}}$  consists of one-body operators. The  $V'_N(r_i)$  is the modified nuclear potential due to VP correction. The modified nuclear potential has the form

$$V'_N(r_i) = V_Z(r_i) + V_{\text{Ue}}(r_i). \quad (2.33)$$

The second term in Eq. (2.32) consists of the two body operators which includes the Breit interaction. The  $H^{\text{DCB}}$  is an ideal starting point of relativistic atomic structure and properties calculations. However, there are complications associated with  $H^{\text{DCB}}$ . Brown and Ravenhall [27] have shown that the  $H^{\text{DC}}$  as well as  $H^{\text{DCB}}$  are not bounded from below and these lead to *variational collapse* and *continuum dissolution*. Later, Sucher [1] showed that this catastrophe can be avoided by using projection operators. Sucher proposed a no-virtual-pair approximation (NVPA) Hamiltonian. In the NVPA approximation the total Hamiltonian is

$$H^{\text{DCB}} = \Lambda_{++} \left\{ \sum_{i=1}^N \left[ c\boldsymbol{\alpha}_i \cdot \mathbf{p}_i + (\beta_i - 1)c^2 - V'_N(r_i) \right] + \sum_{i<j} \left[ \frac{1}{r_{ij}} + g^{\text{B}}(r_{ij}) \right] \right\} \Lambda_{++}. \quad (2.34)$$

Where  $\Lambda_{++}$  is an operator which projects to the positive energy solutions. Projecting the Hamiltonian with  $\Lambda_{++}$  ensures that the effects of the negative energy continuum states are neglected in the calculations. The NVPA Hamiltonian incorporates the Breit interaction and represents the first order relativistic correction to the electron-electron interaction. In a other words, the NVPA Hamiltonian incorporate the magnetic interactions and the retardation effects to the Coulomb interaction. From the QED point of view the Breit interaction takes into account all the effects of order  $\alpha^2$  and it is valid in the Coulomb gauge. On the other hand the VP correction, which is a part of the Lamb shift incorporates the effects of  $\alpha^3$  in QED perturbation theory.

## 2.3 Dirac-Hartree-Fock theory with QED effects

For many electron atoms and ions the eigen-value equation with the  $H^{\text{DCB}}$  is

$$H^{\text{DCB}}|\Psi_i\rangle = E_i|\Psi_i\rangle. \quad (2.35)$$

The two body part in  $H^{\text{DCB}}$  consists of the electron-electron interaction and because of this term the above eigenvalue equation is not exactly solvable. To solve the eigen-value equation, the independent particle with central field approximation is a good starting point. In this model, the total wave-function of many electron atoms is constructed from the anti-symmetrized single particle wave-functions. This is the simplest model to describe many electron atoms [18, 61]. In this model we separate the  $H^{\text{DCB}}$  in to two parts, one is the solvable part or zeroth order,  $H_{\text{DHF}}$  and the residual interaction part,  $V_{\text{res}}$ .

$$\begin{aligned} H^{\text{DCB}} &= \left\{ \sum_{i=1}^N [c\boldsymbol{\alpha}_i \cdot \mathbf{p}_i + (\beta_i - 1)c^2 - V_N(r_i) + U_{\text{DHF}}(r_i)] \right\} + \\ &\quad \left\{ \sum_{i<j}^N \left[ \frac{1}{r_{ij}} + g^{\text{B}}(r_{ij}) \right] - \sum_{i=1}^N U_{\text{DHF}}(r_i) \right\}, \\ &= H_{\text{DHF}} + V_{\text{res}}. \end{aligned} \quad (2.36)$$

Here,  $U_{\text{DHF}}(r_i)$  is the Dirac-Hartree-Fock (DHF) potential,

$$U_{\text{DHF}}(r_i) = \sum_a^{\text{occ}} \left[ \langle a | g(r_{ij}) | ia \rangle - \langle a | g(r_{ij}) | ai \rangle \right]. \quad (2.37)$$

Here,  $g(r_{ij}) = \frac{1}{r_{ij}} + g^B(r_{ij})$  is the two body part of  $H^{\text{DCB}}$ .  $a$  represents core orbital and  $i$  represents any orbital (core, valence or virtual). The  $H_{\text{DHF}}$  is the solvable part of the Hamiltonian and this is further expressed as the sum of  $N$  single particle operators.

$$H_{\text{DHF}} = \sum_{i=1}^N h_{\text{DHF}}(r_i). \quad (2.38)$$

The single particle DHF Hamiltonian is

$$h_{\text{DHF}}(r_i) = c\boldsymbol{\alpha}_i \cdot \mathbf{p}_i + (\beta_i - 1)c^2 - \frac{z}{r_i} - V_{\text{Ue}}(r_i) + u_{\text{DHF}}(r_i) \quad (2.39)$$

In this model the residual interaction part of the Hamiltonian is ignored at the first step of calculation. Different many body methods like MBPT, CI, CCT have been developed to account this term as accurately as possible.

## 2.4 Single particle wave-functions

The eigen-value equation with the single particle Hamiltonian,  $h_{\text{DHF}}(r_i)$  is

$$h_{\text{DHF}}(r_i)|\psi_i\rangle = \epsilon_i|\psi_i\rangle. \quad (2.40)$$

Here  $|\psi_i\rangle$  is the single particle wave-function and  $\epsilon_i$  is the single particle energy. To begin the calculation in the frame work of Dirac theory, the relativistic orbitals are described by Dirac bi-spinors and in the central field model it is [62]

$$\psi_{n\kappa m}(\mathbf{r}) = \frac{1}{r} \begin{pmatrix} P_{n\kappa}(r)\chi_{\kappa m}(\hat{\mathbf{r}}) \\ iQ_{n\kappa}(r)\chi_{-\kappa m}(\hat{\mathbf{r}}) \end{pmatrix} \quad (2.41)$$

where,  $P_{n\kappa}$  and  $Q_{n\kappa}$  are the large and small components of the radial wave-function. The  $\chi_{\kappa m}(\hat{\mathbf{r}})$  is the Dirac spinor and it can be expanded in terms of spherical harmonics,

$$\chi_{\kappa m}(\hat{\mathbf{r}}) = \sum_{\sigma=\pm\frac{1}{2}} \langle lm - \sigma, \frac{1}{2}\sigma | jm \rangle Y_l^{m-\sigma}(\theta, \phi) \phi^\sigma. \quad (2.42)$$

Where  $\langle lm - \sigma, \frac{1}{2}\sigma | jm \rangle$  is the Clebsch-Gordan coefficient,  $Y_l^m(\theta, \phi)$  is the spherical harmonics and  $\phi^\sigma$  is the two-component spinor. An approximate method which

can avoid the negative energy is the finite basis set and we consider the GTO's where radial part of the wave-function is defined as the linear combination terms of Gaussian type functions [37, 63].

$$\begin{aligned} P_{n\kappa}(r) &= \sum_p C_{\kappa p}^L g_{\kappa p}^L(r), \\ Q_{n\kappa}(r) &= \sum_p C_{\kappa p}^S g_{\kappa p}^S(r). \end{aligned} \quad (2.43)$$

Where  $C_{\kappa p}^L$  and  $C_{\kappa p}^S$  are the coefficients of the expansion, the index  $p$  runs over the number of basis functions considered for each symmetry. The large component of the Gaussian type functions is

$$g_{\kappa p}^L(r) = N_{\kappa p}^L r^{n_\kappa} e^{-\alpha_p r^2}, \quad (2.44)$$

where

$$\begin{aligned} n_\kappa &= \kappa + 1 \text{ for } \kappa > 0; \\ &= -\kappa \text{ for } \kappa < 0. \end{aligned} \quad (2.45)$$

The Gaussian type functions of the small components are defined through the kinetic balance condition [28].

$$g_{\kappa p}^S(r) = N_{\kappa p}^S \left( \frac{d}{dr} + \frac{\kappa}{r} \right) g_{\kappa p}^L(r), \quad (2.46)$$

Where  $N_{\kappa p}^L$  and  $N_{\kappa p}^S$  are the normalization factor for large and small component of the radial wave-function. The exponents  $\alpha_p$  depends on two parameters  $\alpha_0$  and  $\beta$ .

$$\alpha_p = \alpha_0 \beta^{p-1}, \quad p = 1, \dots, N, \quad (2.47)$$

where the parameters  $\alpha_0$  and  $\beta$  depend on the nuclear charge  $Z$  and number of electrons  $N$ . We will discuss in detail how to choose these two parameters for different atoms.

The finite basis approach to solve DHF equations numerically is well established technique [37] and widely used for heavy atoms. Though we initially discussed about the projection operator to circumvent the problem of negative energy continuum, in reality it is only a theoretical and formal construction

motivated from field theory. The use of kinetic balance condition [28, 29] between the large and the small components of the radial wave-function with the proper boundary condition in the basis set is the essential ingredient of finite basis calculation. In this thesis we use the GTO finite basis set method for all computations.

## 2.5 Matrix element of the Breit interaction

To solve the DHF equation self-consistently we need to construct the matrix element of the Breit interaction. There are two different approaches reported in previous works to calculate the matrix element of Breit interaction,  $g^B(r_{12})$ . The first approach [64] couples the angular parts of the orbitals with Dirac matrices to give a linear combination of vector spherical harmonics. This is then combined with the angular part of the orbitals. In the second approach [65, 66],  $g^B(r_{12})$  is expanded as a linear combination of irreducible tensor operators. In the present work we use the latter and employ the expressions given in Ref. [63] to incorporate  $g^B(r_{12})$  in the GTO calculations.

Coulomb and Breit interactions are scalar operators. These operators can be written as the product of two tensor operators [18]

$$g(r_1, r_2) = \sum_k g_k(r_1, r_2) \mathbf{T}^k(\hat{r}_1) \cdot \mathbf{T}^k(\hat{r}_2), \quad (2.48)$$

Where  $g_k(r_1, r_2)$  depends only on the radial coordinates and the tensor operator  $\mathbf{T}^k(\hat{r})$  acts on the angular part. To calculate the matrix element of  $g(r_1, r_2)$  we use the Wigner-Eckart theorem

$$\langle ab | g(r_1, r_2) | cd \rangle = \sum_{k,q} \begin{pmatrix} j_a & k & j_c \\ m_a & q & m_c \end{pmatrix} \begin{pmatrix} j_b & k & j_d \\ m_b & q & m_d \end{pmatrix} X^k(abcd), \quad (2.49)$$

where  $X^k(abcd)$  is the effective interaction strength. For the frequency indepen-

dent Breit interaction the effective interaction strength is defined as

$$\begin{aligned}
X_{\text{Br}}^k(abcd) &= (-1)^k \langle j_a || \mathbf{C}^k || j_c \rangle \langle j_b || \mathbf{C}^k || j_d \rangle \left\{ \begin{matrix} j_a & j_c & k \\ j_b & j_d & k \end{matrix} \right\} \\
&\times \left[ \sum_{k=\nu-1}^{\nu+1} \pi^o(\kappa_a, \kappa_c, k) \pi^o(\kappa_b, \kappa_d, k) \sum_{\mu=1}^4 r_{\mu}^{k\nu}(abcd) R_{\mu}^k(abcd) \right. \\
&\quad \left. + \pi^o(\kappa_a, \kappa_c, k-1) \pi^o(\kappa_b, \kappa_d, k-1) \sum_{\mu=1}^8 s_{\mu}^k(abcd) S_{\mu}^k(abcd) \right] \quad (2.50)
\end{aligned}$$

The interaction strength for  $g^B(r_{12})$  is expressed in terms of the parity and angular momentum selection rule and the reduced matrix elements of the  $\mathbf{C}$  tensor operators along with the radial integrals. The parity selection rule  $\pi^o$  shows that it is odd parity. The reduced matrix element is

$$\langle j_a || \mathbf{C}^k || j_c \rangle = (-1)^{j_a+1/2} [j_a, j_c]^{1/2} \begin{pmatrix} j_a & k & j_c \\ 1/2 & 0 & -1/2 \end{pmatrix}. \quad (2.51)$$

The radial integrals  $R_{\mu}^k(abcd)$  and  $S_{\mu}^k(abcd)$  are

$$R^k(abcd) = \int_0^{\infty} dr_2 \int_0^{\infty} dr_1 \rho_{ac}(r_1) U_k(r_1, r_2) \rho_{bd}(r_2) \quad (2.52)$$

$$S^k(abcd) = \int_0^{\infty} dr_2 \int_0^{\infty} dr_1 \rho_{ac}(r_1) W_k(r_1, r_2) \rho_{bd}(r_2). \quad (2.53)$$

In the above equation  $\rho_{ab}(r) = P_a(r)Q_b(r)$ ,

$$W_k(r_1, r_2) = -\frac{1}{2}[k] \left\{ \bar{U}_{k-1}(r_1, r_2) - \bar{U}_{k+1}(r_1, r_2) \right\}. \quad (2.54)$$

The  $\bar{U}_k$  is defined as

$$\bar{U}_k(r_1, r_2) = \begin{cases} r_1^k / r_2^{k+1} & \text{if } r_1 < r_2; \\ 0 & \text{if } r_1 > r_2. \end{cases} \quad (2.55)$$

So we can write

$$U_k(r_1, r_2) = \bar{U}_k(r_1, r_2) + \bar{U}_k(r_2, r_1). \quad (2.56)$$

The coefficients  $r_{\mu}^{k\nu}$  and  $s_{\mu}^k$  are given in ref. [18, 66]. These coefficients are further combined to calculate the matrix element of Breit interaction in the DHF theory. We give the details of the Breit integrals in appendix A.

The model space of a closed shell atom consist of a single Slater determinant. For a closed shell atom the SCF energy is

$$E_{\text{DHF}} = \sum_{a=1}^{\text{occ}} \left\{ \langle a | h_{\text{DHF}} | a \rangle + \frac{1}{2} \sum_b [\langle ab | g | ab \rangle - \langle ba | g | ab \rangle] \right\}, \quad (2.57)$$

Where the first term is the matrix element of the one-body part of the DHF Hamiltonian. The second term is the matrix element of the two-body operators. In the present work we will concentrate on the matrix element of the Breit operator which is a two body operator.

## 2.6 Atomic MBPT

Various many body methods have been developed to incorporate the residual part of  $H^{\text{DCB}}$ . The many body perturbation theory (MBPT) systematically incorporates the  $V_{\text{res}}$  to higher orders. In the DHF theory we solve the the  $H_{\text{DHF}}$  self-consistently to obtain the single particle state  $|\phi_i\rangle$ . With the  $H^{\text{DCB}}$  we consider the eigenvalue equation

$$H^{\text{DCB}}\Psi^a = E^a\Psi_a, \quad (2.58)$$

where  $a = 1, 2, \dots, d$ , forms a subspace of the total Hilbert space constructed from the  $H^{\text{DCB}}$ . Let us assume that for each of the  $d$  solutions there exist a corresponding zeroth order or model function  $\Psi_0^a$ . This model space is spanned by the solutions of  $H_{\text{DHF}}$ . In this process, we split up the total Hilbert space into two parts, the model space and the orthogonal space and we define the projection operators for the model space and the complementary space as

$$P = \sum_{\alpha} |\phi_{\alpha}\rangle\langle\phi_{\alpha}|, Q = \sum_{\beta \neq \alpha} |\phi_{\beta}\rangle\langle\phi_{\beta}|, \quad (2.59)$$

where  $P + Q = 1$ . The zeroth-order wave functions are the projections of the exact eigenfunctions on the model space, that is

$$\Psi_0^a = P\Psi^a. \quad (2.60)$$

We define a wave operator,  $\Omega$  which plays the key role in MBPT. It transforms the model space wave functions,  $\Psi_0^a$  into the corresponding exact eigenfunctions,

$$\Psi^a = \Omega\Psi_0^a. \quad (2.61)$$

The wave operator can be determined from the Brillouin-Wigner perturbation theory (BWPT) or Rayleigh-Schrödinger perturbation theory (RSPT). Ref. [61, 67] give a detailed overview of these perturbation techniques. We will follow the latter approach to calculate the wave operator. To find an equation for the wave operator we operate  $P$  from the left on Eq. (2.58),

$$\begin{aligned} PH\Psi^a &= E^a\Psi_0^a, \\ PH\Omega\Psi_0^a &= E^a\Psi_0^a. \end{aligned} \quad (2.62)$$

This can be rewritten as

$$H_{\text{eff}}\Psi_0^a = E^a\Psi_0^a, \quad (2.63)$$

where,  $H_{\text{eff}} = PH\Omega P$  is the effective atomic Hamiltonian. The above equation implies that when  $H_{\text{eff}}$  operate on zeroth order wave function, it produces the exact energy eigenstates. Now if we operate  $\Omega$  on Eq. (2.63) from left then we obtain

$$\Omega PH\Omega\Psi_0^a = E^a\Psi_0^a = E^a\Psi^a = H\Omega\Psi_0^a. \quad (2.64)$$

From the expression of  $H_{\text{eff}}$ , we get

$$\Omega H_{\text{eff}} = H\Omega. \quad (2.65)$$

This is an important expression in terms of operators which does not depend on energy explicitly. Since the zeroth order Hamiltonian,  $H_0$ , commutes with the  $P$  operator. Here by zeroth order Hamiltonian we mean the solvable part of the atomic Hamiltonian and in our case it is  $H_{\text{DHF}}$ . Then we can rewrite

$$[\Omega, H_0]P = (V\Omega - \Omega PV\Omega)P. \quad (2.66)$$

This is the generalized Bloch equation and was first formulated by Lindgren [68]. In perturbation theory we expand the wave operator as

$$\Omega = \Omega^{(0)} + \Omega^{(1)} + \Omega^{(2)} + \dots \quad (2.67)$$

With this, the generalized Bloch equation can be written as

$$[\Omega^{(n)}, H_0]P = (V\Omega - \Omega V_{\text{eff}})^{(n)}P. \quad (2.68)$$

Where  $V_{\text{eff}} = PV\Omega$ . The above equation generates the Rayleigh-Schrödinger perturbation expansion. This expansion contains unlinked diagrams. Based on the linked cluster expansion, the unlinked diagrams are eliminated in the Bruekner-Goldstone diagrammatic expansion [61, 69]. Therefore the generalized Bloch equation takes the form

$$[\Omega^{(n)}, H_0]P = (V\Omega - \Omega V_{\text{eff}})_{\text{linked}}^{(n)}P. \quad (2.69)$$

This is an order by order expansion and the diagrammatic approach is simpler to handle the perturbation theory. More conveniently Eq. (2.69) can be written as

$$[\Omega, H_0]P = (V\Omega - \Omega V_{\text{eff}})_{\text{linked}}P. \quad (2.70)$$

The last term in Eq. (2.70) corresponds to the folded diagram that arise only in open-shell atoms. For closed-shell atom the generalized Bloch equation is

$$[\Omega^{(n)}, H_0]P = [V\Omega^{(n-1)}]_{\text{linked}}P. \quad (2.71)$$

In the perturbative expansion of  $\Omega$ , we write it as one-, two-, three, ... body terms by using the second quantization method. For this we explicitly write the first order Eq. (2.71) as

$$[\Omega^{(1)}, H_0] = [V]_{\text{linked}} = V_1 + V_2. \quad (2.72)$$

Here  $[V]_{\text{linked}} = V_1 + V_2$  consists of only one and two body terms, as the atomic Hamiltonian consists of only one and two body terms. In the second quantized form, the operators are expressed as

$$\begin{aligned} V_1 &= \sum_{ij} a_i^\dagger a_j \langle i|v_1|j\rangle, \\ V_2 &= \sum_{ijkl} a_i^\dagger a_j^\dagger a_l a_k \langle ij|v_2|kl\rangle. \end{aligned} \quad (2.73)$$

Where  $a_i^\dagger(a)$  are the particle-hole creation (annihilation) operators. In the DHF theory  $v_1 = u_{\text{DHF}}$  which is defined in Eq. (2.39). The first order wave operator, can be separated in two parts, one consists of the one body part and the other is the two body part, that is

$$\Omega^{(1)} = \Omega_1^{(1)} + \Omega_2^{(2)}. \quad (2.74)$$

Using the time independent Wick's theorem we evaluate the commutator in Eq. (2.72) and the wave operators are

$$\begin{aligned}\Omega_1^{(1)} &= \sum_{ap} a_p^\dagger a_a \frac{\langle p|v|a\rangle}{\epsilon_a - \epsilon_p}, \\ \Omega_2^{(2)} &= \sum_{abpq} a_p^\dagger a_q^\dagger a_b a_a \frac{\langle pq|v|ab\rangle}{\epsilon_a + \epsilon_b - \epsilon_p - \epsilon_q}.\end{aligned}\quad (2.75)$$

The indices,  $a, b, \dots (p, q, \dots)$  represent the core (virtual) orbitals. Since we are using the DHF orbital as our reference state,  $v$  represents the two electron interaction part and this gives the most dominant contribution to the correlation energy of atoms.

## 2.7 Correlation energy of closed-shell atoms

In this section, we calculate the correlation energy of closed-shell atom using MBPT. With  $H^{\text{DCB}}$  the eigen-value equation is

$$H^{\text{DCB}}|\Psi_i\rangle = E_i|\Psi_i\rangle. \quad (2.76)$$

Here  $|\Psi_i\rangle$  are the exact eigenstates of the  $H^{\text{DCB}}$ . In terms of  $\Omega$  in MBPT

$$H^{\text{DCB}}\Omega|\Phi_i\rangle = E_i\Omega|\Phi_i\rangle. \quad (2.77)$$

Here the eigenstates,  $|\Phi_i\rangle$ 's are the reference states and as discussed in the earlier section it is equivalent to  $|\Psi_0^a\rangle$ , which belong to the model space. For a closed shell atom it consist of a single Slater determinant and  $|\Psi_0^a\rangle \equiv |\Phi_i\rangle$ . In the model space Eq. (2.77) is written as

$$H_{\text{eff}}|\Phi_i\rangle = E_i|\Phi_i\rangle. \quad (2.78)$$

Recall  $H_{\text{eff}} = PH_0P + PV\Omega P$ , is the effective Hamiltonian. The construction of the  $H_{\text{eff}}$  is very important and depends on the  $\Omega$ .  $H_{\text{eff}}$  acts on the reference state of the system and gives the exact energy eigenvalue of the many electron atom. So, we can write

$$\begin{aligned}E_i &= \langle \Phi_i | H_{\text{eff}} | \Phi_i \rangle. \\ &= \langle \Phi_i | PH_0P + PV\Omega P | \Phi_i \rangle.\end{aligned}\quad (2.79)$$

The first term in Eq. (2.79) refers to the self-consistent field (SCF) energy of the atom. The second term gives the correction due to  $V_{\text{res}}$  and it is known as the correlation energy of the atom. In terms of wave operator the  $n$ -th order energy correction is

$$E_i^{(n)} = \langle \Phi_i | \{ \overline{V_{\text{res}}} \Omega^{(n-1)} \} | \Phi_i \rangle. \quad (2.80)$$

Accordingly, the second order correlation energy correction

$$E_{\text{corr}}^{(2)} = \langle \Phi_i | \overline{V_{\text{res}}} \Omega^{(1)} | \Phi_i \rangle. \quad (2.81)$$

Separating the perturbation and the wave-operator in one and two body terms, the correlation energy becomes

$$E_{\text{corr}}^{(2)} = \langle \Phi_i | \overline{V_2} \Omega_2^{(1)} | \Phi_i \rangle. \quad (2.82)$$

Here the one body term does not contribute to the second order correlation energy. The contraction between the two body interaction,  $V_2$  and  $\Omega_2^{(1)}$  gives two closed diagrams which are shown in Fig. 2.4. Here the dotted line represents  $V_2$ .

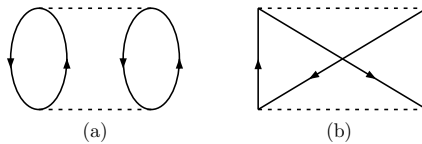


Figure 2.4: MBPT diagrams corresponding to the  $E_{\text{corr}}^{(2)}$ .

To evaluate the diagrams we use the Coulomb as well as Breit interaction in our calculations for  $E_{\text{corr}}^{(2)}$  of closed shell atoms.

## 2.8 Results and discussions

In this section we discuss the results of the Breit interaction correction to the orbital energies of the noble gas atoms. Then we discuss the VP correction to the orbital energies of the doubly ionized alkaline Earth-metal ions.

### 2.8.1 Basis set

The first step of any atomic theory calculations is to generate an orbital basis set. For the present work, we use the Dirac-Hartree-Fock Hamiltonian and even-tempered Gaussian type orbitals (GTOs) [29]. As we mention earlier, the radial part of the spin-orbitals are linear combinations of the Gaussian type functions. The small components of the spin-orbitals are linear combination of  $g_{\kappa p}^S(r)$ , which are generated from  $g_{\kappa p}^L(r)$  through the kinetic balance condition [28]. We calculate the GTOs on a grid [37] and optimize the values of  $\alpha_0$  and  $\beta$  for individual atoms to match the spin-orbital energies and self consistent field (SCF) energy obtained from GRASP92 code [52], which numerically solves the Dirac-Hartree-Fock integro-differential equations.

#### Noble gas atoms

Among the noble gas atoms Ne is the ideal candidate to start the DHF calculations. Since it is a low- $Z$  atom, it is appropriate to consider the  $H^{\text{DC}}$  to generate the orbital basis set. The values of  $\alpha_0$  and  $\beta$  for Ne are unique for each symmetry of spin-orbitals. The symmetry-wise values of the optimized parameters are listed in Table. 2.1. Here we have listed the parameters for the virtual orbital

Symmetry	$s_{1/2}$	$p_{1/2}$	$p_{3/2}$	$d_{3/2}$	$d_{5/2}$	$f_{5/2}$
$\alpha_0$	0.0925	0.1951	0.1917	0.0070	0.0070	0.0069
$\beta$	1.45	2.71	2.71	2.70	2.70	2.69
Symmetry	$f_{7/2}$	$g_{7/2}$	$g_{9/2}$			
$\alpha_0$	0.0069	0.0069	0.0069			
$\beta$	2.69	2.69	2.69			

Table 2.1: The  $\alpha_0$  and  $\beta$  parameters of the even tempered GTO basis used in the present calculations.

along with the core orbitals for Ne. Although, in principle, a complete set of orbitals are required, it is nearly impossible to go beyond a few hundred GTO's. Even at a few hundred, the computational requirements are very high. Another

practical consideration is, with further increase of the basis set size the gain in accuracy is marginal or non-existent after the basis set converges. The basis parameters are optimized such that the core orbital energies are in good agreement with the results of GRASP92 code. For information, the orbital energies are listed in Table. 2.2. With GTO, we are able to reproduce the numerical results of the orbital energies very well. The largest difference is observed in  $1s_{1/2}$ , for which the GTO orbital energy is lower by 0.0032 a.u.

Orbital	$1s_{1/2}$	$2s_{1/2}$	$2p_{1/2}$	$2p_{3/2}$
GTO	-32.8177	-1.9357	-0.8526	-0.8480
GRASP92	-32.8145	-1.9387	-0.8528	-0.8482

Table 2.2: Orbital energies of Ne obtained from GRASP92 and GTO (in a.u.).

For Ar, Kr, Xe and Rn the symmetry-wise values of the optimized  $\alpha_0$  and  $\beta$  are listed in Table. 2.3. In the table we have listed the core orbital parameters for

Atom	$s$		$p$		$d$	
	$\alpha_0$	$\beta$	$\alpha_0$	$\beta$	$\alpha_0$	$\beta$
Ar	0.00055	1.620	0.00515	2.405	0.00570	2.850
Kr	0.00015	2.015	0.00945	2.975	0.00635	2.845
Xe	0.00012	2.215	0.00495	2.995	0.00745	2.460
Rn	0.00010	2.280	0.00671	2.980	0.00715	2.720

Table 2.3: The  $\alpha_0$  and  $\beta$  parameters of the even tempered GTO basis used in the present calculations.

the noble gas atoms. The comparison of the SCF energies are given in Table. 2.4. Except for Rn, there is excellent agreement between the SCF energies obtained from GTO and GRASP92.

Atom	GTO	GRASP92
Ar	-528.6837	-528.6837
Kr	-2789.8605	-2788.8605
Xe	-7446.8976	-7446.8976
Rn	-23602.0202	-23602.0232

Table 2.4: Comparison between GTO and GRASP92 (in a.u.).

### Alkali metal ions

For the alkali metal ions we use the  $V_{N-1}$  nuclear potential. So for a singly charged ion of  $N$  electrons the atomic Hamiltonian is

$$H^{\text{DCB}} = \Lambda_{++} \sum_{i=1}^N [c\boldsymbol{\alpha}_i \cdot \mathbf{p}_i + (\beta_i - 1)c^2 - V_{N+1}(r_i)] + \sum_{i<j} \left[ \frac{1}{r_{ij}} + g^{\text{B}}(r_{ij}) \right] \Lambda_{++}. \quad (2.83)$$

$V_{N+1}(r_i)$  is the electrostatic potential arising from the  $Z = (N + 1)$  nucleus. For the alkali ions the optimized value of  $\alpha_0$  and  $\beta$  are listed in Table. 2.5.

Atom	$s$		$p$		$d$	
	$\alpha_0$	$\beta$	$\alpha_0$	$\beta$	$\alpha_0$	$\beta$
Na <sup>+</sup>	0.0025	2.210	0.00955	2.125	0.00700	2.750
K <sup>+</sup>	0.0055	2.250	0.00995	2.155	0.00690	2.550
Rb <sup>+</sup>	0.0052	2.300	0.00855	2.205	0.00750	2.145
Cs <sup>+</sup>	0.0097	2.050	0.00975	2.005	0.00995	1.705
Fr <sup>+</sup>	0.0068	2.110	0.00645	2.050	0.00985	1.915

Table 2.5: The  $\alpha_0$  and  $\beta$  parameters of the even tempered GTO basis used in for alkali metal ions.

For comparison, the spin-orbital energies of Cs<sup>+</sup> obtained from the GTO and GRASP92 are listed in Table 2.6. In the table, the deviation of the GTO results from the GRASP92 is  $\sim 10^{-3}$ , which is quite small. We obtain similar level of deviations for the other alkali metal ions as well.

Orbital	DC	GRASP92 [52]	Orbital	DC	GRASP92 [52]
$1s_{1/2}$	-1330.1173	-1330.1129	$4s_{1/2}$	-9.5128	-9.5106
$2s_{1/2}$	-212.5643	-212.5673	$4p_{1/2}$	-7.4463	-7.4437
$2p_{1/2}$	-199.4294	-199.4288	$4p_{3/2}$	-6.9209	-6.9188
$2p_{3/2}$	-186.4366	-186.4358	$4d_{3/2}$	-3.4856	-3.4921
$3s_{1/2}$	-45.9697	-45.9695	$4d_{5/2}$	-3.3969	-3.4038
$3p_{1/2}$	-40.4483	-40.4455	$5s_{1/2}$	-1.4898	-1.4933
$3p_{3/2}$	-37.8943	-37.8917	$5p_{1/2}$	-0.9079	-0.9139
$3d_{3/2}$	-28.3096	-28.3030	$5p_{3/2}$	-0.8403	-0.8459

Table 2.6: Core orbital energies of  $\text{Cs}^+$  in atomic units.

### Alkaline Earth-metal ions

For doubly ionized alkaline earth-metal atoms, we use the  $V_{N-2}$  nuclear potential. Here the atomic Hamiltonian is

$$H^{\text{DCB}} = \Lambda_{++} \sum_{i=1}^N [c\alpha_i \cdot \mathbf{p}_i + (\beta_i - 1)c^2 - V_{N+2}(r_i)] + \sum_{i<j}^N \left[ \frac{1}{r_{ij}} + g^{\text{B}}(r_{ij}) \right] \Lambda_{++}. \quad (2.84)$$

Where  $V_{N+2}(r_i)$  is the nuclear potential arising from the  $Z = (N + 2)$  nucleus. The symmetry wise values of the optimized  $\alpha_0$  and  $\beta$  for doubly ionized alkaline earth-metal atoms are listed in Table. 2.7 The comparison of the SCF energies for the doubly ionized alkaline atoms are given in Table. 2.8.

### 2.8.2 Breit interaction correction

To assess the relative importance of Breit interaction, we calculate the first order energy correction

$$\langle H^{\text{B}} \rangle_{\text{DF}} = \langle \Phi_0 | \sum_{i<j} g^{\text{B}}(r_{ij}) | \Phi_0 \rangle, \quad (2.85)$$

where,  $|\Phi_0\rangle$  is the ground state reference function generated from the Dirac-Hartree-Fock spin-orbitals and  $H^{\text{B}} = \sum_{i<j} g^{\text{B}}(r_{ij})$  represents the many-electron form of the Breit interaction. The  $\langle H^{\text{B}} \rangle_{\text{DF}}$  of the rare gas atoms Ar, Kr, Xe and

Atom	$s$		$p$		$d$	
	$\alpha_0$	$\beta$	$\alpha_0$	$\beta$	$\alpha_0$	$\beta$
Mg <sup>2+</sup>	0.00825	2.310	0.00715	2.365	0.00700	2.700
Ca <sup>2+</sup>	0.00895	2.110	0.00815	2.150	0.00750	2.500
Sr <sup>2+</sup>	0.00975	2.100	0.00915	2.010	0.00900	2.030
Ba <sup>2+</sup>	0.00985	2.150	0.00975	2.070	0.00995	2.010
Ra <sup>2+</sup>	0.00995	2.110	0.00925	2.090	0.00850	2.010

Table 2.7: The  $\alpha_0$  and  $\beta$  parameters of the even tempered GTO basis for different ions used in the present calculations.

Atom	GTO	GRASP92
Mg <sup>2+</sup>	-199.1500	-199.1501
Ca <sup>2+</sup>	-679.1038	-679.1038
Sr <sup>2+</sup>	-3177.5211	-3177.5218
Ba <sup>2+</sup>	-8135.1404	-8135.1421
Ra <sup>2+</sup>	-26027.5632	-26027.5634

Table 2.8: Comparison between the ground state SCF energies obtained from the computations with GTO and GRASP92. The energies are in atomic units.

Rn are listed in Table. 2.9. For each atom we calculated the SCF energy with

Atom	$E_{\text{SCF}}^{\text{DC}}$	$E_{\text{SCF}}^{\text{DCB}}$	$\langle H^{\text{B}} \rangle_{\text{DF}}$	Ref. [70]
Ar	-528.6837	-528.5511	0.1326	0.1324
Kr	-2788.8605	-2787.4310	1.4295	1.4268
Xe	-7446.8976	-7441.1248	5.7728	5.7753
Rn	-23602.0202	-23572.8480	29.1722	29.3968

Table 2.9: SCF Energies for noble gas atoms

$H^{\text{DC}}$  and  $H^{\text{DCB}}$ . Here

$$E_{\text{SCF}}^{\text{DC}} = \langle \Phi_0 | H^{\text{DC}} | \Phi_0 \rangle \quad (2.86)$$

and

$$E_{\text{SCF}}^{\text{DCB}} = \langle \Phi_0 | H^{\text{DCB}} | \Phi_0 \rangle. \quad (2.87)$$

Here,  $H^{\text{DC}} = H^{\text{DCB}} - H^{\text{B}}$ , is the atomic Hamiltonian without the Breit interaction. From the table, it is evident that our results are in very good agreement with the previous results [70]. The largest deviation from the previous results is observed in Rn, our result of  $\langle H^{\text{B}} \rangle_{\text{DF}}$  is 0.8% lower than the previous result. However, as the Breit interaction contribution to  $E_{\text{SCF}}^{\text{DCB}}$  is a mere 0.12% in Rn, in absolute terms, the deviation is  $\approx 0.001\%$ . Our results are also in good agreement with the results of another previous study [71].

### 2.8.3 Vacuum polarization correction

We calculated the vacuum polarization (VP) correction to the orbital energies of doubly ionized alkaline Earth-metal ions. To study the VP corrections arising from  $V_{\text{Ue}}$ , we compute the orbital energy corrections in the self consistent field (SCF) calculations. We also compute the first order correction using the many-body perturbation theory. In the former case, SCF calculations, the VP potential is considered along with the DHF potential,  $U_{\text{DHF}}$ . The single particle eigen-value equation is then

$$[h_0 + V_{\text{Ue}}(r) + U_{\text{DHF}}(r)] |\psi'_i\rangle = \epsilon'_i |\psi'_i\rangle,$$

where,  $h_0 = c\boldsymbol{\alpha} \cdot \mathbf{p} + (\beta - 1)c^2 - V_{\text{N-2}}(r)$  is the single particle part of  $H^{\text{DCB}}$ ,  $U_{\text{DHF}}(r)$  is the Dirac-Hartree-Fock potential,  $|\psi'_i\rangle$  is a four component orbital and  $\epsilon'_i$  is the corresponding eigenvalue. Similarly, we use *unprimed* states,  $|\psi_i\rangle$ , to represent orbitals which are eigenfunctions of the DHF Hamiltonian, that is

$$[h_0 + U_{\text{DHF}}(r)] |\psi_i\rangle = \epsilon_i |\psi_i\rangle,$$

where  $\epsilon_i$  is the DHF energy of the orbital. To quantify the VP effect we define

$$\Delta\epsilon_i = \epsilon'_i - \epsilon_i, \quad (2.88)$$

as the change in the orbital energy due to  $V_{\text{Ue}}(r)$ . Following the time-independent many-body perturbation theory, the first order energy correction associated with

$V_{Ue}(r)$  is

$$\langle V_{Ue} \rangle_i = \langle \psi_i | V_{Ue}(r) | \psi_i \rangle.$$

Since the VP potential is attractive and short range in nature, it has larger effect on the orbitals which have finite probability density within the nucleus. So, at the first order  $\langle V_{Ue} \rangle$  is negative for orbitals, but only the  $s_{1/2}$  orbitals have negative  $\Delta\epsilon$  for all the ions. A similar pattern is reported in ref. [72] for the orbitals energies of  $Cs^+$ . For the  $Ra^{2+}$  ion, in addition to  $s_{1/2}$  the  $p_{1/2}$  orbitals also have negative  $\Delta\epsilon$ . More details of the  $\Delta\epsilon_i$  and  $\langle V_{Ue} \rangle_i$  for the core orbitals of the  $Ca^{2+}$ ,  $Sr^{2+}$ ,  $Ba^{2+}$  and  $Ra^{2+}$ , and are discussed in the following paras.

$Ca^{2+}$

We calculate the VP correction to the orbital energy with a series of SCF calculations and results are listed in Table. 2.10. As to be expected, the first order correction  $\langle V_{Ue} \rangle$  is negative for all the core orbitals. But the values of  $\Delta\epsilon$  are negative only for the  $s_{1/2}$  orbitals. Another important observation is, for  $s_{1/2}$  orbitals  $\langle V_{Ue} \rangle_i$  and  $\Delta\epsilon_i$  are similar in value. But, for the other orbitals, besides the change in sign, the values of  $\langle V_{Ue} \rangle_i$  and  $\Delta\epsilon_i$  are different by several orders of magnitude.

Orbital	$\Delta\epsilon$	$\langle V_{Ue} \rangle$
$1s_{1/2}$	$-4.204[-3]$	$-4.435[-3]$
$2s_{1/2}$	$-3.531[-4]$	$-3.790[-4]$
$2p_{1/2}$	$4.884[-5]$	$-1.511[-6]$
$2p_{3/2}$	$4.938[-5]$	$-2.732[-7]$
$3s_{1/2}$	$-4.391[-5]$	$-4.500[-5]$
$3p_{1/2}$	$6.817[-6]$	$-1.619[-7]$
$3p_{3/2}$	$6.880[-6]$	$-2.931[-8]$

Table 2.10: VP Corrections to the orbital energies of  $Ca^{2+}$ . Here [x] represents multiplication by  $10^x$ .

$\text{Sr}^{2+}$

The VP corrections to the orbital energies arising from  $V_{\text{Ue}}(r)$  are listed in Table 2.11. From the table it is evident that  $\Delta\epsilon_{1s_{1/2}}$  is an order of magnitude larger than in  $\text{Ca}^{2+}$ . In addition, we also observe a four orders of magnitude difference between the  $\langle V_{\text{Ue}} \rangle_i$  and  $\Delta\epsilon_i$  of the  $3d$  orbitals. This is not surprising as the short range  $V_{\text{Ue}}(r)$  have little effect on the electrons in the higher angular momentum orbitals like  $d$ .

Orbital	$\Delta\epsilon$	$\langle V_{\text{Ue}} \rangle$
$1s_{1/2}$	-5.721[-2]	-5.904[-2]
$2s_{1/2}$	-5.968[-3]	-6.231[-3]
$2p_{1/2}$	3.604[-4]	-1.144[-4]
$2p_{3/2}$	4.354[-4]	-1.636[-5]
$3s_{1/2}$	-1.003[-3]	-1.045[-3]
$3p_{1/2}$	8.281[-5]	-1.995[-5]
$3p_{3/2}$	9.664[-5]	-2.865[-6]
$3d_{3/2}$	8.145[-5]	-4.341[-9]
$3d_{5/2}$	8.048[-5]	-1.123[-9]
$4s_{1/2}$	-1.301[-4]	-1.320[-4]
$4p_{1/2}$	1.592[-5]	-2.086[-6]
$4p_{3/2}$	1.747[-5]	-2.984[-7]

Table 2.11: VP Corrections to the orbital energies of  $\text{Sr}^{2+}$ . Here [x] represents multiplication by  $10^x$ .

$\text{Ba}^{2+}$

In  $\text{Ba}^{2+}$ , the orbital energy corrections arising from the VP are listed in Table 2.12 and here we find an important change in the pattern of  $\Delta\epsilon$ . The  $\Delta\epsilon$  of  $p_{1/2}$  and  $p_{3/2}$  continue to be positive, but  $\Delta\epsilon_{2p_{1/2}}$  is  $\approx 72\%$  smaller than  $\Delta\epsilon_{2p_{3/2}}$ . For the remaining  $np_{1/2}$  and  $np_{3/2}$ , although the difference is not so dramatic, the differences are still large.

Orbital	$\Delta\epsilon$	$\langle V_{Ue} \rangle$	Orbital	$\Delta\epsilon$	$\langle V_{Ue} \rangle$
$1s_{1/2}$	-2.952[-1]	-3.025[-1]	$4s_{1/2}$	-1.531[-3]	-1.599[-3]
$2s_{1/2}$	-3.493[-2]	-3.623[-2]	$4p_{1/2}$	8.513[-5]	-7.689[-5]
$2p_{1/2}$	5.074[-4]	-1.669[-3]	$4p_{3/2}$	1.476[-4]	-8.242[-6]
$2p_{3/2}$	1.786[-3]	-1.748[-4]	$4d_{3/2}$	1.272[-4]	-4.004[-8]
$3s_{1/2}$	-7.084[-3]	-7.391[-3]	$4d_{5/2}$	1.245[-4]	-9.185[-8]
$3p_{1/2}$	1.984[-4]	-3.725[-4]	$5s_{1/2}$	-2.449[-4]	-2.473[-4]
$3p_{3/2}$	4.926[-4]	-3.981[-5]	$5p_{1/2}$	2.295[-5]	-1.071[-5]
$3d_{3/2}$	4.856[-4]	-2.047[-7]	$5p_{3/2}$	3.230[-5]	-1.066[-6]
$3d_{5/2}$	4.737[-4]	-4.712[-8]			

Table 2.12: VP Corrections to the orbital energies of  $Ba^{2+}$ . Here [x] represents multiplication by  $10^x$ .

$Ra^{2+}$

Orbital	$\Delta\epsilon$	$\langle V_{Ue} \rangle$	Orbital	$\Delta\epsilon$	$\langle V_{Ue} \rangle$
$1s_{1/2}$	-2.560	-2.614	$4d_{3/2}$	1.350[-3]	-3.943[-6]
$2s_{1/2}$	-3.881[-1]	-3.999[-1]	$4d_{5/2}$	1.282[-3]	-7.062[-7]
$2p_{1/2}$	-3.802[-2]	-5.753[-2]	$4f_{5/2}$	1.015[-3]	-1.647[-9]
$2p_{3/2}$	1.211[-2]	-2.707[-3]	$4f_{7/2}$	9.928[-4]	-4.229[-10]
$3s_{1/2}$	-8.999[-2]	-9.315[-2]	$5s_{1/2}$	-5.378[-3]	-5.633[-3]
$3p_{1/2}$	-9.620[-3]	-1.504[-2]	$5p_{3/2}$	4.845[-4]	-4.200[-5]
$3p_{3/2}$	3.728[-3]	-7.545[-4]	$5d_{3/2}$	4.074[-4]	-6.735[-7]
$3d_{3/2}$	4.213[-3]	-1.330[-5]	$5d_{5/2}$	3.859[-4]	-1.187[-7]
$3d_{5/2}$	3.953[-3]	-2.385[-6]	$6s_{1/2}$	-9.883[-4]	-9.951[-4]
$4s_{1/2}$	-2.362[-2]	-2.451[-2]	$6p_{1/2}$	-1.613[-5]	-1.290[-4]
$4p_{1/2}$	-2.238[-3]	-3.938[-3]	$6p_{3/2}$	1.211[-4]	-5.949[-6]
$4p_{3/2}$	1.315[-3]	-1.999[-4]			

Table 2.13: VP Corrections to the orbital energies of  $Ra^{2+}$ . Here [x] represents multiplication by  $10^x$ .

Coming to the orbital energy correction arising from VP, listed in Table. 2.13, there is a key difference from the other ions. The values of  $\Delta\epsilon_{np_{1/2}}$ , in addition

to  $\Delta\epsilon_{ns_{1/2}}$  are negative.

### 2.8.4 Correlation energy with Breit interaction

To investigate in detail we calculate the Breit interaction correction to the correlation energy of some closed shell atoms using MBPT. Here we include up to  $i$ -symmetry to calculate the correlation energy. The calculation of  $E_{\text{corr}}^{(2)}$  from MBPT is discussed in great detail by Mani *et al.* [40, 73]. In the present work we incorporated the Breit interaction to the residual part of the atomic Hamiltonian. Our results are in good agreement with Ishikawa *et al.* [74].

Atom	$E_{\text{corr}}^{(2)}$	$\Delta E_{\text{Br}}^{(2)}$	Other Work[74]
Ne	-0.3843	-0.0013	-0.3853
Ar	-0.7004	-0.0051	-0.7060
Kr	-1.8696	-0.0270	-1.8879
Xe	-3.0504	-0.0737	-3.0674

Table 2.14: Second-order correlation energies of closed shell atoms.

Here we list the total  $E_{\text{corr}}^{(2)}$  as defined in Eq. (2.82) including the Breit part in the first column. Our results for Ne is very close to the previous result after taking into account the Breit interaction. For Ne the contribution from the Breit interaction is  $\approx 0.3\%$ . For Ar, Kr and Xe we found a similar pattern. As the atomic number  $Z$  increases the contribution from the Breit interaction to the correlation energy increases. For Ar, Kr and Xe the Breit interaction contribution is  $\approx 0.7\%, 1.5\%, 2.5\%$  to the  $E_{\text{corr}}^{(2)}$ . For Ne, Ar, Kr and Xe, our result are on the lower side than ref. [74]. Here we must emphasize that the previous result is also with  $H^{\text{DCB}}$  Hamiltonian.

# Chapter 3

## QED effects in closed-shell atoms using coupled-cluster theory

The coupled-cluster theory is proved to be one of the most powerful and reliable many body theories. In the previous chapter we discussed about the MBPT, which is the starting point of coupled-cluster theory. The relativistic coupled cluster theory is the relativistic version of the well known coupled-cluster theory. In the present work, the  $H^{\text{DCB}}$  is used as the starting point of our calculations. We introduce the triple excitation in the RCC theory as it is important to go beyond coupled-cluster single and double (CCSD) approximation. This is because the CCSD approximation misses several important many body diagrams starting from second order of MBPT. The triple excitations at the linearized RCC theory will pave the way for high precision results for atomic structure calculations. Because of computational cost and other complications associated with angular integration, selection rules, cluster storage scheme etc. most of the physicist use approximate triple excitations in RCC theory in the past. But with the advent of powerful computational facilities, we can incorporate the triple excitations in the RCC theory. This chapter deals with the formulation of RCCSDT theory. Along with this we develop perturbed relativistic coupled-cluster (PRCC) theory. PRCC theory can be used to incorporate multiple perturbations in many electron atoms. The formulation of the PRCC operator is general and we use CCSD approximation in this context. It means that the PRCC operators can

take into account external perturbations like static electric field or internal perturbations like hyperfine interaction etc. It is important to mention that it can also be used to study nuclear spin-dependent parity non-conservation effects in atoms.

The chapter is organized as follows: we discuss about the closed-shell RCC theory in section 3.1. Here we introduce the triple excitation cluster operator in the RCC theory. We also discuss about the linearized RCCSDT amplitude equations in this part. We end the section with a discussion on the angular momentum diagram representation and evaluation of triple excitation operator. In section 3.2 we introduce the PRCC theory. We then, discuss about the tensor structure of PRCC operators. We discuss in detail about the PRCC amplitude equations. In addition we discuss about all the single and double excitation diagrams in PRCC theory in detail. We end the chapter with a discussion on the intermediate diagrams. Here we focus on how to reduce the computational cost using the intermediate diagrams.

### 3.1 Relativistic coupled-cluster theory of closed-shell atoms

For a closed-shell atom the eigen-value equation with the Dirac-Coulomb-Breit Hamiltonian is

$$H^{\text{DCB}}|\Psi_0\rangle = E_0|\Psi_0\rangle, \quad (3.1)$$

Where  $|\Psi_0\rangle$  is the exact eigen function and  $E_0$  is the corresponding exact eigenvalue. In coupled-cluster theory (CCT) we write the exact ground state of many electron atom as

$$|\Psi_0\rangle = e^{T^{(0)}}|\Phi_0\rangle, \quad (3.2)$$

Where  $T^{(0)}$  is the cluster operator and  $|\Phi_0\rangle$  is the reference state wave-function. For  $N$ -electron atom the cluster operator consists of  $N$ - number of excitation

operators and it is written as

$$T^{(0)} = \sum_{i=1}^N T_i^{(0)}. \quad (3.3)$$

Here the superscript (0) is introduced to distinguish between the residual Coulomb interaction,  $V_{\text{res}}$  and an additional perturbation in atoms. The CCSD approximation provides a good starting point for atomic many body calculations, And it is described in great detail by Mani *et al.* [40, 73]. As mentioned earlier, we shall concentrate on the salient features of triple excitations in the present work. In the CCSDT approximation the cluster operator for a closed-shell atom is

$$T^{(0)} = T_1^{(0)} + T_2^{(0)} + T_3^{(0)}. \quad (3.4)$$

In the second quantized form the excitation operators are written as

$$\begin{aligned} T_1^{(0)} &= \sum_a^p t_a^p a_p^\dagger a_a, \\ T_2^{(0)} &= \frac{1}{4} \sum_{ab}^{pq} t_{ab}^{pq} a_p^\dagger a_q^\dagger a_b a_a, \\ T_3^{(0)} &= \frac{1}{12} \sum_{abc}^{pqr} t_{abc}^{pqr} a_p^\dagger a_q^\dagger a_r^\dagger a_c a_b a_a. \end{aligned} \quad (3.5)$$

The indices  $a, b, c, \dots (p, q, r, \dots)$  represent core (virtual) orbitals. In the CCSDT approximation, we fully incorporate the effects of single, double and triple excitations to all order.

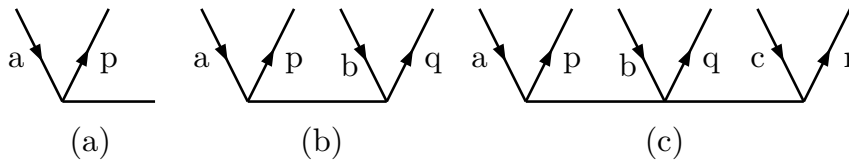


Figure 3.1: Diagrammatic representation of  $T_1^{(0)}$ ,  $T_2^{(0)}$  and  $T_3^{(0)}$  operators.

With the coupled-cluster wave-function, the eigenvalue Eq. (3.2) assumes the form

$$H^{\text{DCB}} e^{T^{(0)}} |\Phi_0\rangle = E_0 e^{T^{(0)}} |\Phi_0\rangle. \quad (3.6)$$

Using the normal ordered form of the Hamiltonian,  $H_N = H^{\text{DCB}} - \langle \Phi_0 | H^{\text{DCB}} | \Phi_0 \rangle$ , one can write

$$H_N |e^{T^{(0)}} | \Phi_0 \rangle = \Delta E e^{T^{(0)}} | \Phi_0 \rangle, \quad (3.7)$$

Where  $\Delta E$  is the correlation energy of the closed-shell atom. Operating  $e^{-T^{(0)}}$  from the left side on the above equation and projecting on the single excited,  $|\Phi_a^p\rangle$ , double excited,  $|\Phi_{ab}^{pq}\rangle$  and triple excited,  $|\Phi_{abc}^{pqr}\rangle$ , we obtain the coupled-cluster amplitude equations in the RCCSDT theory.

$$\langle \Phi_a^p | \bar{H}_N | \Phi_0 \rangle = 0, \quad (3.8a)$$

$$\langle \Phi_{ab}^{pq} | \bar{H}_N | \Phi_0 \rangle = 0, \quad (3.8b)$$

$$\langle \Phi_{abc}^{pqr} | \bar{H}_N | \Phi_0 \rangle = 0. \quad (3.8c)$$

Here  $\bar{H}_N = e^{-T^{(0)}} H_N e^{T^{(0)}}$  is the similarity transformed Hamiltonian. Using the time independent Wick's theorem for the product of operators and the fact that the  $H_N$  contains at most two body operators, we can write

$$\begin{aligned} \bar{H}_N = & H_N + \left\{ \overline{H_N T^{(0)}} \right\} + \frac{1}{2!} \left\{ \overline{\overline{H_N T^{(0)}} T^{(0)}} \right\} + \frac{1}{3!} \left\{ \overline{\overline{\overline{H_N T^{(0)}} T^{(0)}} T^{(0)}} \right\} + \\ & \frac{1}{4!} \left\{ \overline{\overline{\overline{\overline{H_N T^{(0)}} T^{(0)}} T^{(0)}} T^{(0)}} \right\}. \end{aligned} \quad (3.9)$$

Thus,  $\bar{H}_N$  can at the most be quartic in  $T^{(0)}$ . However, the most dominant term is  $\left\{ \overline{H_N T^{(0)}} \right\}$  and it subsumes all the important many body effects.

### 3.1.1 Linearized RCC theory with triple excitations

As a starting point we choose the linearized RCC theory with triple excitations. In this linearized RCCSDT theory the coupled-cluster amplitude equations are

$$\langle \Phi_a^p | \left\{ \overline{H_N T_1^{(0)}} \right\} + \left\{ \overline{H_N T_2^{(0)}} \right\} + \left\{ \overline{H_N T_3^{(0)}} \right\} | \Phi_0 \rangle = -\langle \Phi_a^p | H_N | \Phi_0 \rangle, \quad (3.10a)$$

$$\langle \Phi_{ab}^{pq} | \left\{ \overline{H_N T_1^{(0)}} \right\} + \left\{ \overline{H_N T_2^{(0)}} \right\} + \left\{ \overline{H_N T_3^{(0)}} \right\} | \Phi_0 \rangle = -\langle \Phi_{ab}^{pq} | H_N | \Phi_0 \rangle, \quad (3.10b)$$

$$\langle \Phi_{abc}^{pqr} | \left\{ \overline{H_N T_1^{(0)}} \right\} + \left\{ \overline{H_N T_2^{(0)}} \right\} + \left\{ \overline{H_N T_3^{(0)}} \right\} | \Phi_0 \rangle = 0. \quad (3.10c)$$

The above set of equation forms the single, double and triple excitation amplitude equations. Here we notice,  $\langle \Phi_{abc}^{pqr} | H_N | \Phi_0 \rangle$  is zero as  $H_N$  consists of one and

two body operators. The details of linearized RCCSD diagrams are discussed in ref. [73]. Here we will focus mainly on the  $T_3^{(0)}$  part of the RCC theory. After incorporating the  $T_3^{(0)}$  in the RCCSDT theory, the main challenge is the evaluation of the diagrams arising from contracting  $H_N$  with the  $T_3^{(0)}$  operator. Here, we must emphasize that along with the single and double diagrams from the RCCSD approximation we also have single and double excitation diagram from the  $T_3^{(0)}$  operator. To be more precise, we obtain two single excitation diagrams from the contraction between the  $H_N$  and  $T_3^{(0)}$  and they contribute to Eq. (3.10a). The corresponding diagrams are shown in Fig. 3.2. There are total

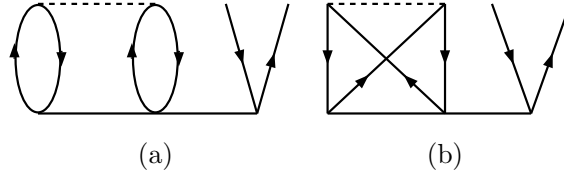


Figure 3.2: Diagrams of  $T_1^{(0)}$  arising from  $\{\overline{H_N T_3^{(0)}}\}$ .

four  $T_2^{(0)}$  diagrams which arise from the contraction of  $H_N$  with  $T_3^{(0)}$  and they contribute to Eq. (3.10b). The  $T_2^{(0)}$  diagrams are shown in Fig. 3.3. The  $T_3^{(0)}$

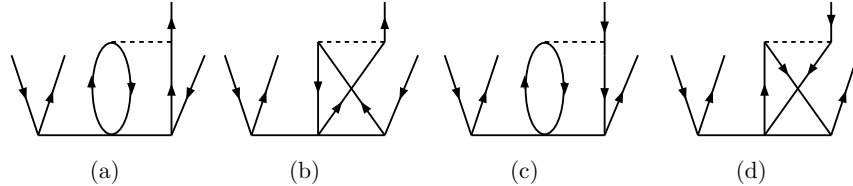


Figure 3.3: Diagrams of  $T_2^{(0)}$  arising from  $\{\overline{H_N T_3^{(0)}}\}$ .

diagrams which contribute to Eq. (3.10c) are shown in Fig. 3.4. Among the eight diagrams in Fig. 3.4, diagram (a) and (b) arise from  $\{\overline{H_N T_2^{(0)}}\}$  and the remaining six diagrams arise  $\{\overline{H_N T_3^{(0)}}\}$ . In order to solve the set of RCCSDT Eq. (3.10a), (3.10b) and (3.10c), we write these in the matrix form

$$\begin{pmatrix} H_{11} & H_{12} & H_{13} \\ H_{21} & H_{22} & H_{23} \\ H_{31} & H_{32} & H_{33} \end{pmatrix} \begin{pmatrix} t_a^p \\ t_{ab}^{pq} \\ t_{abc}^{pqr} \end{pmatrix} = - \begin{pmatrix} B_1 \\ B_2 \\ 0 \end{pmatrix}. \quad (3.11)$$

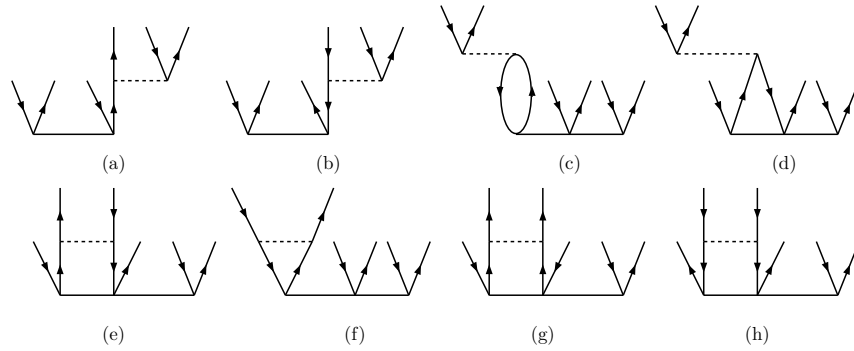
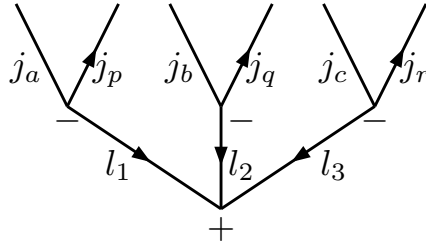


Figure 3.4: Diagrams of  $T_3^{(0)}$  arising from  $\{\overline{H_N T_2^{(0)}}\}$  and  $\{\overline{H_N T_3^{(0)}}\}$ .

The above equations form a set of coupled linear algebraic equations and it is solved using the Jacobi method as it is easy to parallelize.

### 3.2 Angular momentum representation of $T_3^{(0)}$

In the previous section we presented the coupled-cluster amplitude equations including  $T_3^{(0)}$  and the technique to solve the RCCSDT equations. To solve the RCCSDT equations a basic step is to map  $T_3^{(0)}$  diagram to an angular momentum diagram which is inevitable to solve the angular part of the matrix elements. Now the basic rules of angular momentum algebra can not be applied directly to the diagrams involving  $T_3^{(0)}$ . The reason is, the diagrammatic representation of  $T_3^{(0)}$  has four lines associated with one of the vertices. This does not have an equivalent angular momentum diagram. So to apply the rules of angular momentum algebra we construct the simplest possible representation of  $T_3^{(0)}$  and it is shown in Fig. 3.5. Here  $j_a, j_b, j_c(j_p, j_q, j_r)$  are the total angular momentum of core (virtual) orbitals. While drawing the diagrams and arrows, we follow the sign and arrow convention of Lindgren and Morrison [61]. In this angular momentum representation, we obtain a multipole line by coupling two angular momentum lines. For example, the coupling between  $j_a$  and  $j_p$  gives the multipole  $l_1$ . The three multipoles,  $l_1, l_2$ , and  $l_3$  should further follow the triangular condition. Along with the triangular conditions, the orbitals must follow parity selection

Figure 3.5: Angular momentum representation of  $T_3^{(0)}$  operator.

rule. Since the parity of the excited state  $|\Phi_{abc}^{pqr}\rangle = T_3^{(0)}|\Phi_0\rangle$  must be same as  $|\Phi_0\rangle$ ,  $(-1)^{(l_a+l_p+l_b+l_q+l_c+l_r)} = 1$ . Here,  $l_a, l_b, l_c(l_p, l_q, l_r)$  are the orbital angular momentum of core (virtual) orbitals. So, the orbitals and the multipoles must satisfy the following triangular and parity selection rules

$$\begin{aligned}
 |j_a - j_p| &\leq l_1 \leq (j_a + j_p), \\
 |j_b - j_q| &\leq l_2 \leq (j_b + j_q), \\
 |j_c - j_r| &\leq l_3 \leq (j_c + j_r), \\
 |l_1 - l_2| &\leq l_3 \leq (l_1 + l_2), \\
 (-1)^{(l_a+l_p+l_b+l_q+l_c+l_r)} &= 1.
 \end{aligned} \tag{3.12}$$

### 3.2.1 Angular momentum diagram evaluation with $T_3^{(0)}$

In this section we give the details of evaluating the angular momentum diagrams associated with  $T_3^{(0)}$ . The diagrams that will arise after considering the  $T_3^{(0)}$  operator are shown in Fig. 3.2, 3.3 and 3.4. Let us consider the diagram in Fig. 3.2(a). The corresponding angular momentum diagram is shown in Fig. 3.6, where  $j_a, j_b, j_c(j_p, j_q, j_r)$  are the total angular momentum of core (virtual) orbitals and  $k_1$  corresponds to the multipole line of two body interaction term and  $l_i$  are the multipole lines. To evaluate the above angular momentum diagram we use the JLV theorems [61] as these give a diagrammatic treatment to represent the tensor operator product of the coupled angular momentum states. Finally

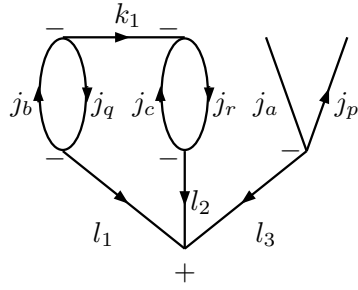


Figure 3.6: Angular momentum diagram contribute to the  $T_1^{(0)}$  excitation amplitude.

we obtain the following result after evaluating the diagram in Fig. 3.6.

$$= \delta(l_1, 0) \frac{\delta(k_1, l_3)}{[k_1]} \frac{\delta(l_2, l_3)}{\sqrt{[l_1]}} (-1)^{(j_b+j_q+j_c+j_r)} \times \begin{array}{c} j_a \quad j_p \\ \diagdown \quad \diagup \\ \hline \end{array}$$

As we can see the final form contains Kronecker delta function, phase factor and the free part corresponds to the angular momentum diagram of  $T_1^{(0)}$  operator. Similarly, angular momentum diagram corresponding to the diagram in Fig. 3.3(a) is shown in Fig. 3.7. Here also the we apply the JLV theorems to evaluate

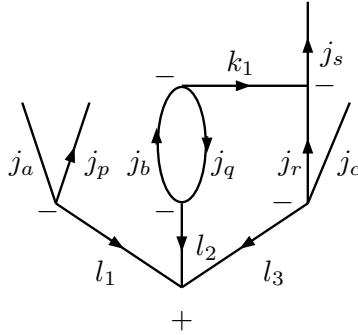


Figure 3.7: Angular momentum diagram contribute to the  $T_2^{(0)}$  excitation amplitude.

the diagram. The final expression after evaluation is

$$= \delta(l, l_1) \frac{\delta(k_1, l_2)}{[k_1]} (-1)^{(-j_b+j_q+j_c+j_s)} \left\{ \begin{array}{ccc} j_c & j_r & l_3 \\ l_2 & l_1 & j_s \end{array} \right\} \times \begin{array}{c} j_a \quad j_p \quad j_b \quad j_q \\ \diagdown \quad \diagup \quad \diagdown \quad \diagup \\ \hline l_1 \end{array}$$

Similar to  $T_1^{(0)}$ , the angular part consist of the the Kronecker delta function, phase factor. Along with this we have a 6- $j$  symbol and the free part corresponds

to angular momentum diagram of  $T_2^{(0)}$  operator. The  $T_3^{(0)}$  diagram arising from  $T_2^{(0)}$  and  $T_3^{(0)}$  operator are shown in Fig. 3.4. The angular momentum diagram of diagram in Fig. 3.4(c) is shown in Fig. 3.8.

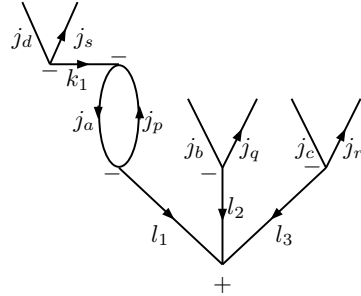


Figure 3.8: Angular momentum diagram contribute to the  $T_3^{(0)}$  excitation amplitude.

After applying JLV theorems in the above diagrams we obtain the following form

$$= \frac{\delta(k_1, l_1)}{[k_1]} (-1)^{(-j_d + j_s + k_1)} \times$$

In this case along with the phase factor we have the free part which corresponds to the  $T_3^{(0)}$  operator. Here we presented three simplest coupled-cluster diagram and their angular factor evaluation. In a systematic way we calculate all the angular factor corresponding to the diagrams which arises after incorporating  $T_3^{(0)}$  excitations. So to conclude this section, we consider the full triple excitation in the linearized RCC theory. The coupled-cluster wave-function generated in the RCCSDT theory is further used to calculate atomic properties.

### 3.3 Perturbed relativistic coupled-cluster theory

To incorporate an additional perturbation Hamiltonian  $H_{\text{int}}$ , we introduce the perturbed coupled-cluster operator  $\mathbf{T}^{(1)}$ . This implies,  $H_{\text{int}}$  is applied once and

$V_{\text{res}}$  to all order in all possible sequences. In general,  $\mathbf{T}^{(1)}$  is a tensor operator and the multipole structure depends on the properties of  $H_{\text{int}}$ . With the perturbation, the modified eigenvalue equation is

$$(H^{\text{DCB}} + \lambda H_{\text{int}})|\tilde{\Psi}_0\rangle = \tilde{E}|\tilde{\Psi}_0\rangle, \quad (3.13)$$

where,  $\lambda$  is the perturbation parameter. Consider the case where  $H_{\text{int}}$  represents the interaction with an external static electric field  $\mathbf{E}$ . The interaction Hamiltonian is then  $H_{\text{int}} = -\sum_i \mathbf{r}_i \cdot \mathbf{E} = \mathbf{D} \cdot \mathbf{E}$ , where  $\mathbf{D}$  is the many electron electric dipole operator. The perturbed atomic state in PRCC theory is

$$|\tilde{\Psi}_i\rangle = e^{T^{(0)} + \lambda \mathbf{T}^{(1)} \cdot \mathbf{E}} |\Phi_0\rangle = e^{T^{(0)}} [1 + \lambda \mathbf{T}^{(1)} \cdot \mathbf{E}] |\Phi_0\rangle. \quad (3.14)$$

This approach has the advantage of taking into account the effect of multiple perturbations systematically. Other than  $\mathbf{E}$ ,  $H_{\text{int}}$  could be one of the interactions internal to the atom like Breit interaction, hyperfine interaction, etc. For the

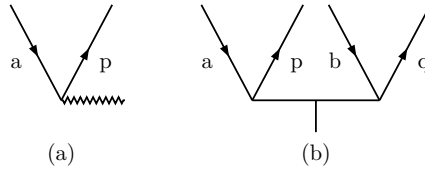


Figure 3.9: Diagrammatic representation of  $\mathbf{T}_1^{(1)}$  and  $\mathbf{T}_2^{(1)}$ .

present work, we examine  $\mathbf{T}^{(1)}$  arising from  $\mathbf{E}$  which is a odd parity vector operator in the electronic space. The perturbed wave-function can be used in the properties calculation and using it we can avoid the sum over complete set of intermediate states.

### 3.3.1 Tensor structure of PRCC operator

For the present case,  $\mathbf{E}$  as the perturbation, we can write the perturbed single excitation cluster operator as

$$\mathbf{T}_1^{(1)} = \sum_{a,p} \tau_a^p \mathbf{C}_1(\hat{r}) a_p^\dagger a_a. \quad (3.15)$$

Here,  $\mathbf{T}_1^{(1)}$  is a vector operator in the electronic space and the  $\mathbf{C}$ -tensor,  $\mathbf{C}_1(\hat{r})$  represents the vector nature of  $\mathbf{T}^{(1)}$ . The key difference between  $\mathbf{T}_1^{(1)}$  and  $T^{(0)}$  is the parity condition, For  $T^{(0)}$  the total orbital parity must be odd, in other words  $(-1)^{l_a+l_p} = -1$ . Diagrammatically, the  $\mathbf{T}_1^{(1)}$  operator is represented as shown in Fig. 3.9(a). It is similar to the conventional representation of  $T_1^{(0)}$  but the interaction line is replaced by a wavy line.

The tensor structure of  $\mathbf{T}_2^{(1)}$ , on the other hand, has additional complications as it consists of two vertices. After due consideration of the  $H_{\text{int}}$  and  $T^{(0)}$  multipole structure, it is represented as

$$\mathbf{T}_2^{(1)} = \sum_{a,b,p,q} \sum_{l,k} \tau_{ab}^{pq}(l,k) \{ \mathbf{C}_l(\hat{r}_1) \mathbf{C}_k(\hat{r}_2) \}^1 a_p^\dagger a_q^\dagger a_b a_a. \quad (3.16)$$

Like in  $\mathbf{T}_1^{(1)}$ ,  $\mathbf{C}_k$  are the  $\mathbf{C}$ -tensor operators and, two  $\mathbf{C}$ -tensor operators of rank  $l$  and  $k$  are coupled to a rank one tensor operator,  $\mathbf{T}_2^{(1)}$ . At the two vertices, the orbital angular momenta must satisfy the triangular conditions  $|j_a - j_p| \leq l \leq (j_a + j_p)$  and  $|j_b - j_q| \leq k \leq (j_b + j_q)$ . In addition, the two tensor operators must be such that  $|l - k| \leq 1 \leq (l + k)$ . These selection rules arise from the triangular conditions at the vertices. The other selection rule follows from the parity condition, as  $H_{\text{int}}$  is parity odd, the orbitals must satisfy the condition  $(-1)^{(l_a+l_p)} = -(-1)^{(l_b+l_q)}$ . The diagrammatic representation of  $\mathbf{T}_2^{(1)}$  is shown in Fig. 3.9(b), where the vertical line on the interaction line is to represent the rank of the operator. Further more, this representation, at a later stage, simplifies the angular integration using diagrammatic technique.

### 3.3.2 PRCC equations

The ground state eigenvalue equation with  $H_{\text{int}}$  is

$$(H^{\text{DCB}} + \lambda H_{\text{int}}) e^{[T^{(0)} + \lambda \mathbf{T}^{(1)} \cdot \mathbf{E}]} |\Phi_0\rangle = \tilde{E}_0 e^{[T^{(0)} + \lambda \mathbf{T}^{(1)} \cdot \mathbf{E}]} |\Phi_0\rangle. \quad (3.17)$$

When  $H_{\text{int}}$  is parity odd, like in the present case, there is no first order perturbative correction to energy, so  $\tilde{E}_0 = E_0$ . In the CCSD approximation we define the perturbed cluster operator  $\mathbf{T}^{(1)}$  as

$$\mathbf{T}^{(1)} = \mathbf{T}_1^{(1)} + \mathbf{T}_2^{(1)}. \quad (3.18)$$

In this approximation the PRCC equations are derived from Eq. (3.17). As we mentioned earlier, the derivation associated with coupled-cluster theory involves several operator contractions and these are more transparent with the normal ordered Hamiltonian  $H_N = H^{\text{DCB}} - \langle \Phi_i | H^{\text{DCB}} | \Phi_i \rangle$ . The eigenvalue equation then has the form

$$[H_N + \lambda H_{\text{int}}] |\tilde{\Psi}_0\rangle = [E_0 - \langle \Phi_0 | H^{\text{DCB}} | \Phi_0 \rangle] |\tilde{\Psi}_0\rangle. \quad (3.19)$$

A more convenient form of the eigenvalue equation is

$$(H_N + \lambda H_{\text{int}}) |\tilde{\Psi}_0\rangle = \Delta E_0 |\tilde{\Psi}_0\rangle, \quad (3.20)$$

where,  $\Delta E_0 = E_0 - \langle \Phi_0 | H^{\text{DCB}} | \Phi_0 \rangle$  is the ground state correlation energy. Following the definition in Eq. (3.18), the PRCC eigen-value equation is

$$(H_N + \lambda H_{\text{int}}) e^{T^{(0)} + \lambda \mathbf{T}^{(1)} \cdot \mathbf{E}} |\Phi_0\rangle = \Delta E_0 e^{T^{(0)} + \lambda \mathbf{T}^{(1)} \cdot \mathbf{E}} |\Phi_0\rangle. \quad (3.21)$$

Applying  $e^{-T^{(0)}}$  from the left, we get

$$[\bar{H}_N + \lambda \bar{H}_{\text{int}}] e^{\lambda \mathbf{T}^{(1)} \cdot \mathbf{E}} |\Phi_0\rangle = \Delta E_0 e^{\lambda \mathbf{T}^{(1)} \cdot \mathbf{E}} |\Phi_0\rangle, \quad (3.22)$$

where,  $\bar{H} = e^{-T^{(0)}} H e^{T^{(0)}}$  is the similarity transformed Hamiltonian. Multiply Eq. (3.22) from left by  $e^{-\lambda \mathbf{T}^{(1)}}$  and consider terms linear in  $\lambda$ , we get the PRCC equation

$$[\bar{H}_N, \mathbf{T}^{(1)}] \cdot \mathbf{E} + \bar{H}_{\text{int}} |\Phi_0\rangle = 0. \quad (3.23)$$

Here, the similarity transformed interaction Hamiltonian  $\bar{H}_{\text{int}}$  terminates at second order as  $H_{\text{int}}$  is a one-body interaction Hamiltonian. Expanding  $\bar{H}_{\text{int}}$ , the PRCC equation takes the form

$$\left\{ [\bar{H}_N^{\text{DCB}}, \mathbf{T}^{(1)}] + \dots \right\} \cdot \mathbf{E} |\Phi_0\rangle = \left\{ \mathbf{D} + [\mathbf{D}, T^{(0)}] + \frac{1}{2} [[\mathbf{D}, T^{(0)}], T^{(0)}] \right\} \cdot \mathbf{E} |\Phi_0\rangle. \quad (3.24)$$

Here after, for simplicity, we drop  $\mathbf{E}$  from the equations and for compact notation. The cluster equations of  $\mathbf{T}_1^{(1)}$  are obtained after projecting the equation on singly excited states  $\langle \Phi_a^p |$ . These excited states, however, must be opposite in parity to  $|\Phi_0\rangle$ . Similarly, the  $\mathbf{T}_2^{(1)}$  equations are obtained after projecting on the doubly

excited states  $\langle \Phi_{ab}^{pq} |$ . After the application of Wick's theorem, the  $\mathbf{T}^{(1)}$  equations are

$$\begin{aligned} \langle \Phi_a^p | \left[ H_N + \overline{H_N \mathbf{T}^{(1)}} + \overline{H_N T^{(0)} \mathbf{T}^{(1)}} + \frac{1}{2!} \overline{H_N T^{(0)} T^{(0)} \mathbf{T}^{(1)}} \right] | \Phi_0 \rangle = \\ \langle \Phi_a^p | \left[ \overline{\mathbf{D} T^{(0)}} + \frac{1}{2!} \overline{\mathbf{D} T^{(0)} T^{(0)}} \right] | \Phi_0 \rangle, \end{aligned} \quad (3.25a)$$

$$\begin{aligned} \langle \Phi_{ab}^{pq} | \left[ H_N + \overline{H_N \mathbf{T}^{(1)}} + \overline{H_N T^{(0)} \mathbf{T}^{(1)}} + \frac{1}{2!} \overline{H_N T^{(0)} T^{(0)} \mathbf{T}^{(1)}} + \dots \right] | \Phi_0 \rangle \\ = \langle \Phi_{ab}^{pq} | \left[ \overline{\mathbf{D} T^{(0)}} + \frac{1}{2!} \overline{\mathbf{D} T^{(0)} T^{(0)}} \right] | \Phi_0 \rangle, \end{aligned} \quad (3.25b)$$

where  $\overline{AB}$  represents all possible contractions between the two operators  $A$  and  $B$ . The Eq. (3.25a) and (3.25b) form a set of coupled nonlinear algebraic equations. However,  $T^{(0)}$  are solved first as these are independent of  $\mathbf{T}^{(1)}$ , the PRCC equations are then reduced to coupled linear algebraic equations. An approximation which incorporates all the important many-body effects like random phase approximation (RPA) is the linearized PRCC (LPRCC) theory. In this approximation, only the terms linear in  $T$ , equivalent to retaining only  $\overline{H_N \mathbf{T}^{(1)}}$  and  $\overline{\mathbf{D} T^{(0)}}$  in Eq. (3.25a) and (3.25b), are considered.

### 3.3.3 Nonlinear terms in PRCC

The calculations with the LPRCC approximation involves ten single excitation and ten double excitation many-body diagrams, and it is computationally less complex and hence faster. In our calculations, the LPRCC equations are solved first and we use the solutions as the initial guess to solve the full PRCC equations. To describe the PRCC equations in detail, we examine each of the nonlinear terms in Eq. (3.25a) and (3.25b). These involve more contractions and are larger in number than the linear terms. To begin with consider the second term on the left hand side of Eq. (3.25a) and (3.25b), second order in  $T$ , in CCSD approximation it expands to

$$\overline{H_N T^{(0)} \mathbf{T}^{(1)}} = \overline{H_N T_1^{(0)} \mathbf{T}_1^{(1)}} + \overline{H_N T_1^{(0)} \mathbf{T}_2^{(1)}} + \overline{H_N T_2^{(0)} \mathbf{T}_1^{(1)}} + \overline{H_N T_2^{(0)} \mathbf{T}_2^{(1)}}. \quad (3.26)$$

All the terms contribute to both  $\mathbf{T}_1^{(1)}$  and  $\mathbf{T}_2^{(1)}$ . Similarly, the third term on the left hand side of Eq. (3.25a) and (3.25b), third order in  $T$ , expands to

$$\overline{\overline{H_N T^{(0)} T^{(0)}} \mathbf{T}^{(1)}} = \overline{\overline{H_N T_1^{(0)} T_1^{(0)}} \mathbf{T}_1^{(1)}} + \overline{\overline{H_N T_1^{(0)} T_2^{(0)}} \mathbf{T}_1^{(1)}} + \overline{\overline{H_N T_1^{(0)} T_1^{(0)}} \mathbf{T}_2^{(1)}} + \overline{\overline{H_N T_1^{(0)} T_2^{(0)}} \mathbf{T}_2^{(1)}}. \quad (3.27)$$

In this equation, out of the four terms, only the first one contributes to  $\mathbf{T}_1^{(1)}$ , but, all the terms contribute to  $\mathbf{T}_2^{(1)}$ . At the fourth order there is only one term and it contributes to only  $\mathbf{T}_2^{(1)}$ . The terms on the right hand side of Eq. (3.25a) and (3.25b) expand to

$$\overline{\mathbf{D}T^{(0)}} = \overline{\mathbf{D}T_1^{(0)}} + \overline{\mathbf{D}T_2^{(0)}}, \quad (3.28a)$$

$$\overline{\mathbf{D}T^{(0)} T^{(0)}} = \overline{\mathbf{D}T_1^{(0)} T_1^{(0)}} + \overline{\mathbf{D}T_1^{(0)} T_2^{(0)}}. \quad (3.28b)$$

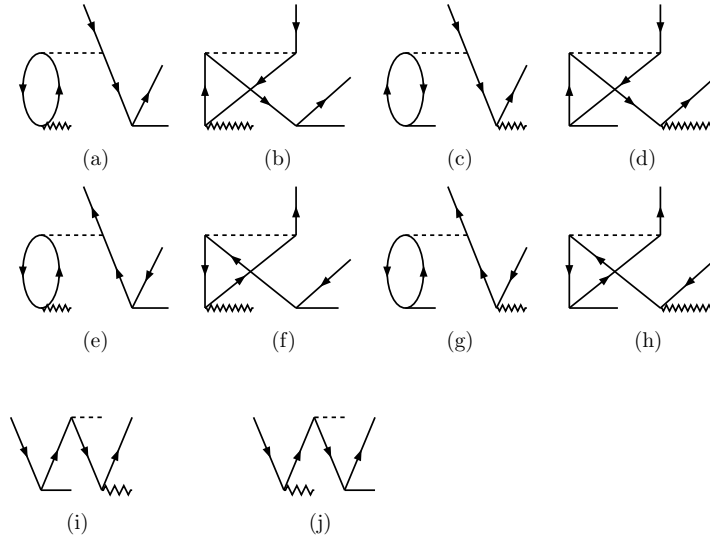
Here,  $\overline{\mathbf{D}T_1^{(0)}}$  and  $\overline{\mathbf{D}T_1^{(0)} T_2^{(0)}}$  are nonzero only for  $\mathbf{T}_1^{(1)}$  and  $\mathbf{T}_2^{(1)}$ , respectively. Each of the terms, after contraction, generate several topologically unique Goldstone diagrams. The diagrammatic treatment is preferred for further analysis as it simplifies the calculations and is well suited to represent contractions between the operators. In the next few sub-sections we discuss the  $\mathbf{T}_1^{(1)}$  and  $\mathbf{T}_2^{(1)}$  diagrams and their algebraic expressions.

### $\mathbf{T}_1^{(1)}$ diagrams

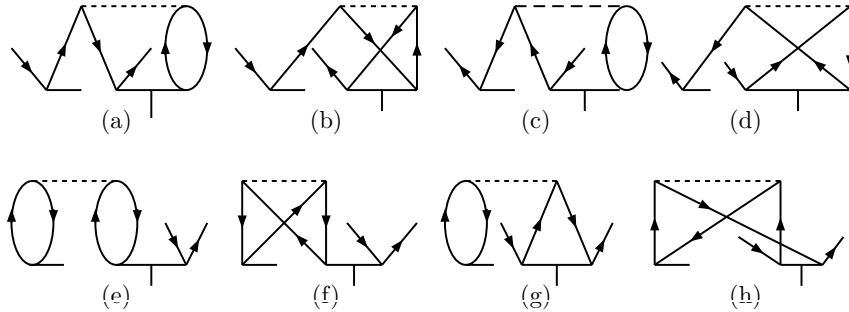
In this sub-section we describe the  $\mathbf{T}_1^{(1)}$  diagrams arising from the non-linear terms. The many-body diagrams or the Goldstone diagrams are drawn and evaluated as described in ref. [61]. Consider the first term on the right hand side of Eq. (3.26),  $\overline{\overline{H_N T_1^{(0)}} \mathbf{T}_1^{(1)}}$ , it is equivalent to ten diagrams and these are shown in Fig. 3.10. Algebraically, we can write it as

$$\langle \overline{\overline{H_N T_1^{(0)}} \mathbf{T}_1^{(1)}} \rangle_a^p = \sum_{bcqa} \tilde{g}_{bcqa} (t_c^p \tau_b^q + t_b^q \tau_c^p) + \sum_{bpqr} \tilde{g}_{bpqr} (t_a^r \tau_b^q + t_b^q \tau_a^r). \quad (3.29)$$

where  $g_{ijkl} = \langle ij|1/r_{12} + g^B(r_{12})|kl\rangle$  is the matrix element of the electron-electron interactions and  $\tilde{g}_{ijkl} = g_{ijkl} - g_{ijlk}$  is the antisymmetrized matrix element. We have used  $\langle \dots \rangle_a^p$  to represent the matrix element  $\langle \Phi_a^p | \dots | \Phi_0 \rangle$ . The diagrams


 Figure 3.10: Diagrams of  $\mathbf{T}_1^{(1)}$  arising from  $\overline{H_N T_1^{(0)}} \mathbf{T}_1^{(1)}$ .

in Fig. 3.10(i-j), arising from the one-body part of  $H_N$ , evaluate to zero when orbitals are calculated with Dirac-Hartree-Fock-Breit potential. The next term in Eq. (3.26),  $\overline{H_N T_1^{(0)}} \mathbf{T}_2^{(1)}$ , generates eight diagrams and these are shown in Fig. 3.11. It is to be noted here, the contractions with only  $g_{abpq}$  type of two-body


 Figure 3.11: The  $\mathbf{T}_1^{(1)}$  diagrams arising from the contraction  $\overline{H_N T_1^{(0)}} \mathbf{T}_2^{(1)}$ .

interaction are non-zero. The algebraic expression of the diagrams is

$$\langle \overline{H_N T_1^{(0)}} \mathbf{T}_2^{(1)} \rangle_a^p = \sum_{bcqr} \tilde{g}_{cbrq} (t_a^r \tau_{pq}^{cb} + t_c^p \tau_{ab}^{rq} + t_c^r \tau_{ba}^{qp} + t_b^q \tau_{ac}^{rp}).$$

We next consider the term  $\overline{H_N T_2^{(0)}} \mathbf{T}_1^{(1)}$  in Eq. (3.26), this is the last term among the second order terms. Like the previous term, after contraction it generates

eight diagrams and these are shown in Fig. 3.12. The topological structure of

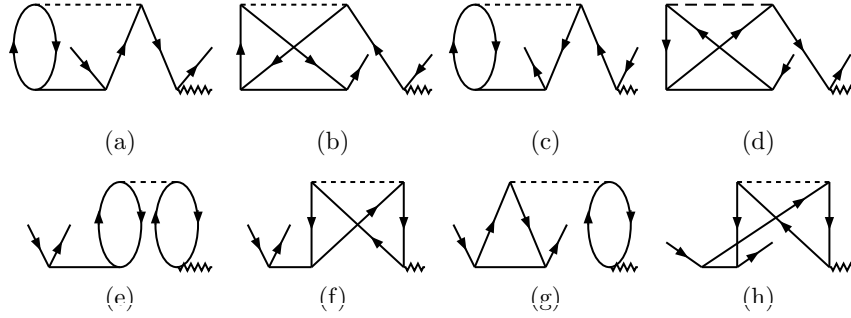


Figure 3.12: The  $\mathbf{T}_1^{(1)}$  diagrams arising from the contraction  $\overline{H_N T_2^{(0)} T_1^{(1)}}$ .

the diagrams are very similar to those of Fig. 3.11 and the algebraic expression of the diagrams is

$$\langle \overline{H_N T_2^{(0)} T_1^{(1)}} \rangle_a^p = \sum_{bcqr} \tilde{g}_{bcqr} (t_{ba}^{qr} \tau_p^c + t_{bc}^{qp} \tau_a^r + t_{ab}^{pq} \tau_c^r + t_{ac}^{rp} \tau_b^q). \quad (3.30)$$

At the third order, as mentioned earlier, only  $\overline{H_N T_1^{(0)} T_1^{(0)} T_1^{(1)}}$  contributes to the  $\mathbf{T}_1^{(1)}$  diagrams. This term generates six Goldstone diagrams and these are shown in Fig. 3.13. The algebraic expression of the diagrams is

$$\langle \overline{H_N T_1^{(0)} T_1^{(0)} T_1^{(1)}} \rangle_a^p = \sum_{bcqr} \tilde{g}_{bcqr} (t_a^r t_c^p \tau_q^b + t_b^q t_a^r \tau_c^p + t_b^q t_c^p \tau_a^r).$$

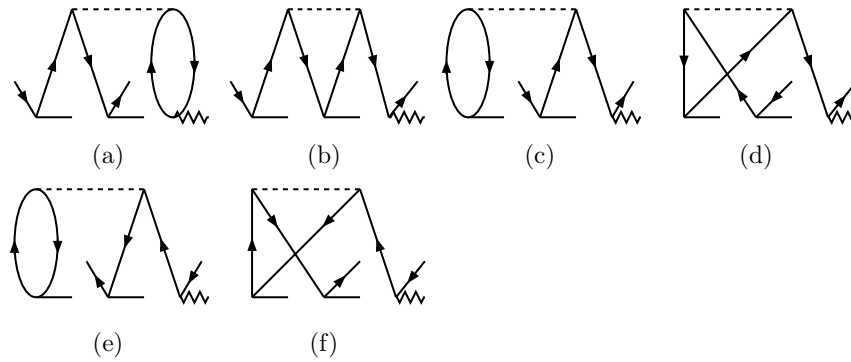


Figure 3.13: The  $\mathbf{T}_1^{(1)}$  diagrams arising from the contraction  $\overline{H_N T_1^{(0)} T_1^{(0)} T_1^{(1)}}$ .

In total, the nonlinear terms in the  $\mathbf{T}_1^{(1)}$  equation generate 30 Goldstone diagrams. Considering that  $T_2^{(0)}$  and  $\mathbf{T}_1^{(1)}$  are the dominant cluster operators, in

terms of amplitudes, in the unperturbed RCC and PRCC, respectively, we can expect the magnitude of  $\overline{H_N T_2^{(0)}} \mathbf{T}_1^{(1)}$  to be the largest.

### $\mathbf{T}_2^{(1)}$ diagrams

In this sub-section we discuss the Goldstone diagrams of  $\mathbf{T}_2^{(1)}$  arising from the non-linear terms on the left hand side of Eq. (3.25b). Consider the second order term, after expansion there are four terms as given in Eq. (3.26) and all have nonzero contribution to  $\mathbf{T}_2^{(1)}$ . The first term,  $\overline{H_N T_1^{(0)}} \mathbf{T}_1^{(1)}$ , has six diagrams and

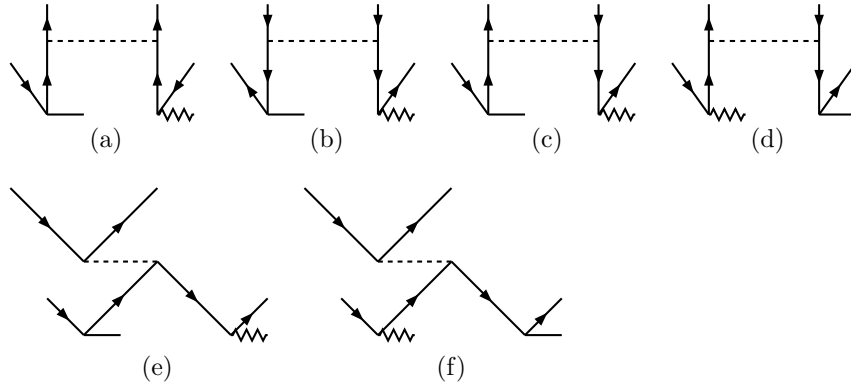


Figure 3.14: The  $\mathbf{T}_2^{(1)}$  diagrams arising from the contraction  $\overline{H_N T_1^{(0)}} \mathbf{T}_1^{(1)}$ .

these are shown in Fig. 3.14. The equivalent algebraic expression is

$$\begin{aligned} \langle \overline{H_N T_1^{(0)}} \mathbf{T}_1^{(1)} \rangle_{ab}^{pq} &= \sum_{rs} g_{pqrs} t_a^r \tau_b^s + \sum_{cd} g_{cdab} t_c^p \tau_d^q - \\ &\sum_{cr} g_{pcrb} [(t_a^r + t_b^r) \tau_c^q - t_c^q (\tau_a^r + \tau_b^r)]. \end{aligned} \quad (3.31)$$

where, we have used  $\langle \dots \rangle_{ab}^{pq}$  to represent the matrix element  $\langle \Phi_{ab}^{pq} | \dots | \Phi_0 \rangle$ . The next term in Eq. (3.26),  $\overline{H_N T_1^{(0)}} \mathbf{T}_2^{(1)}$ , has sixteen diagrams and these are shown in Fig. 3.15. However, the last two diagrams in Fig. 3.15(o-p) are zero, like in the present work, Dirac-Hartree-Fock-Breit orbitals are used. The equivalent algebraic expression is

$$\begin{aligned} \langle \overline{H_N T_1^{(0)}} \mathbf{T}_2^{(1)} \rangle_{ab}^{pq} &= \sum_{crs} g_{cqrs} (t_c^r \tau_{ba}^{sp} - t_c^s \tau_{ba}^{rp} + t_b^s \tilde{\tau}_{ca}^{rp} - t_b^r \tau_{ca}^{sp} - t_a^r \tau_{cb}^{ps} - t_c^p \tau_{ab}^{rs}) + \\ &\sum_{cdr} g_{cdrb} (-t_c^r \tau_{da}^{qp} + t_d^r \tau_{ca}^{qp} - t_d^q \tilde{\tau}_{ca}^{rp} + t_c^p \tau_{ad}^{rq} + t_a^r \tau_{cd}^{pq}). \end{aligned} \quad (3.32)$$

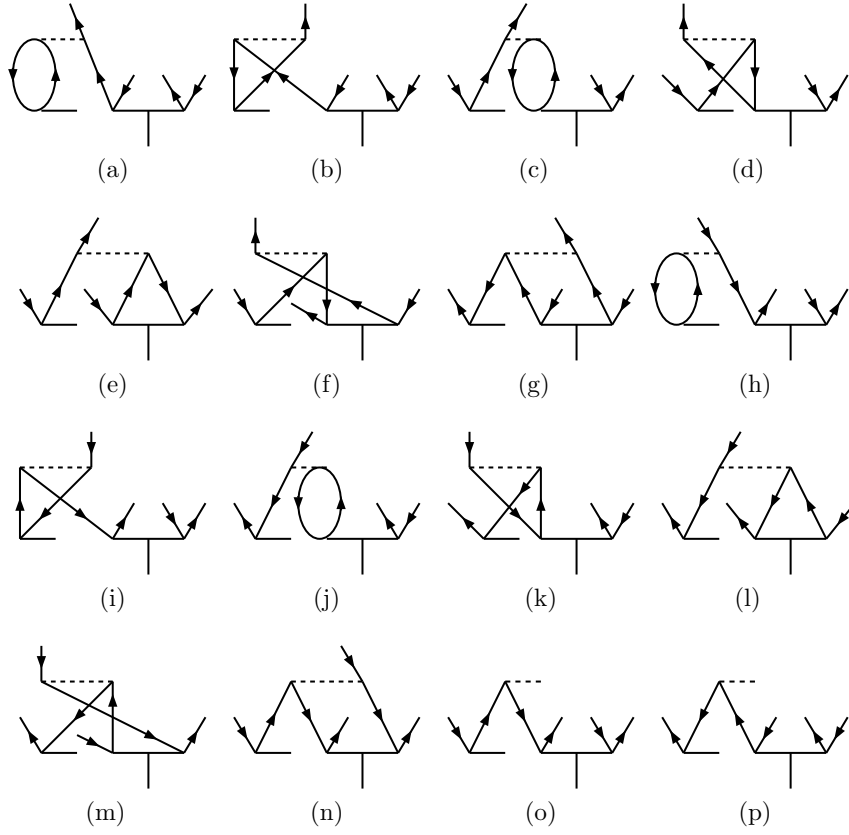


Figure 3.15: The  $\mathbf{T}_2^{(1)}$  diagrams arising from the contraction  $\overline{H_N T_1^{(0)}} \mathbf{T}_2^{(1)}$ .

where,  $\tilde{\tau}_{ca}^{rp} = \tau_{ca}^{rp} - \tau_{ac}^{rp}$  is the antisymmetrised amplitude of  $\mathbf{T}_2^{(1)}$ . Interchanging the order of excitations of the cluster operators, we get the next term  $\overline{H_N T_2^{(0)}} \mathbf{T}_1^{(1)}$ . As in the previous term there are sixteen diagrams and these are shown in Fig. 3.16. The equivalent algebraic expression is

$$\begin{aligned} \langle \overline{H_N T_2^{(0)}} \mathbf{T}_1^{(1)} \rangle_{ab}^{pq} &= \sum_{crs} g_{cgrs} (\tilde{t}_{ac}^{pr} \tau_b^s - t_{ac}^{ps} \tau_b^r - t_{bc}^{sp} \tau_a^r + t_{ab}^{ps} \tau_c^r - t_{ab}^{pr} \tau_c^s - t_{ab}^{rs} \tau_c^p) + \\ &\quad \sum_{cdr} g_{cdrb} (\tilde{t}_{ca}^{pr} \tau_d^q - t_{ad}^{pr} \tau_c^q + t_{da}^{qr} \tau_c^p - t_{ad}^{pq} \tau_c^r + t_{ac}^{pq} \tau_d^r + t_{cd}^{pq} \tau_a^r) \end{aligned} \quad (3.33)$$

where,  $\tilde{t}_{ac}^{pr} = t_{ac}^{pr} - t_{ca}^{rp}$  is the antisymmetrised amplitude of  $T_2^{(0)}$ . The last second order term is  $\overline{H_N T_2^{(0)}} \mathbf{T}_2^{(1)}$  in Eq. (3.26). we have a large number of diagrams as both of the cluster operators are double excitation. There are eighteen diagrams

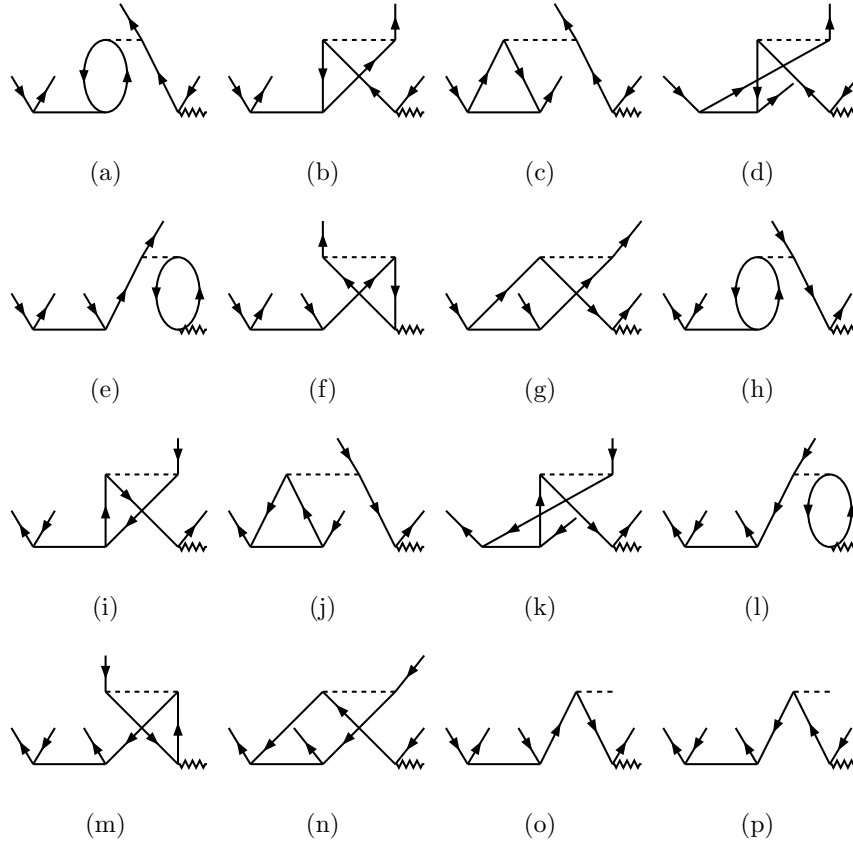


Figure 3.16: The  $\mathbf{T}_2^{(1)}$  diagrams arising from the contraction  $\overline{H_N T_2^{(0)}} \mathbf{T}_1^{(1)}$ .

and these are shown in Fig. 3.17. The algebraic expression for the diagrams is

$$\begin{aligned} \langle \overline{H_N T_2^{(0)}} \mathbf{T}_2^{(1)} \rangle_{ab}^{pq} = & \sum_{cdrs} g_{cdrs} (\tilde{t}_{ac}^{pr} \tilde{\tau}_{db}^{sq} - \tilde{t}_{ac}^{ps} \tau_{db}^{rq} + t_{ac}^{ps} \tau_{db}^{qr} + t_{ac}^{sq} \tau_{db}^{pr} - \tilde{t}_{ca}^{rs} \tau_{db}^{pq} - \tilde{t}_{cd}^{rp} \tau_{ab}^{sq} \\ & - t_{ab}^{ps} \tau_{dc}^{qr} + t_{ab}^{pr} \tau_{dc}^{qs} - t_{ac}^{pq} \tilde{\tau}_{bd}^{rs} + t_{ab}^{rs} \tau_{cd}^{pq} + t_{cd}^{pq} \tau_{ab}^{rs}). \end{aligned} \quad (3.34)$$

Collecting all the diagrams which are second order in  $\mathbf{T}^{(1)}$ , there are 56 Goldstone diagrams in the  $\mathbf{T}_2^{(1)}$  equation after contraction of the cluster operators with  $H_N$ .

At the third order, all the terms in Eq. (3.27) have non-zero contributions to  $\mathbf{T}_2^{(1)}$ . There are six Goldstone diagrams from the first term  $\overline{H_N T_1^{(0)}} T_1^{(0)} \mathbf{T}_1^{(1)}$  and these are shown in Fig. 3.18. The equivalent algebraic expression of the

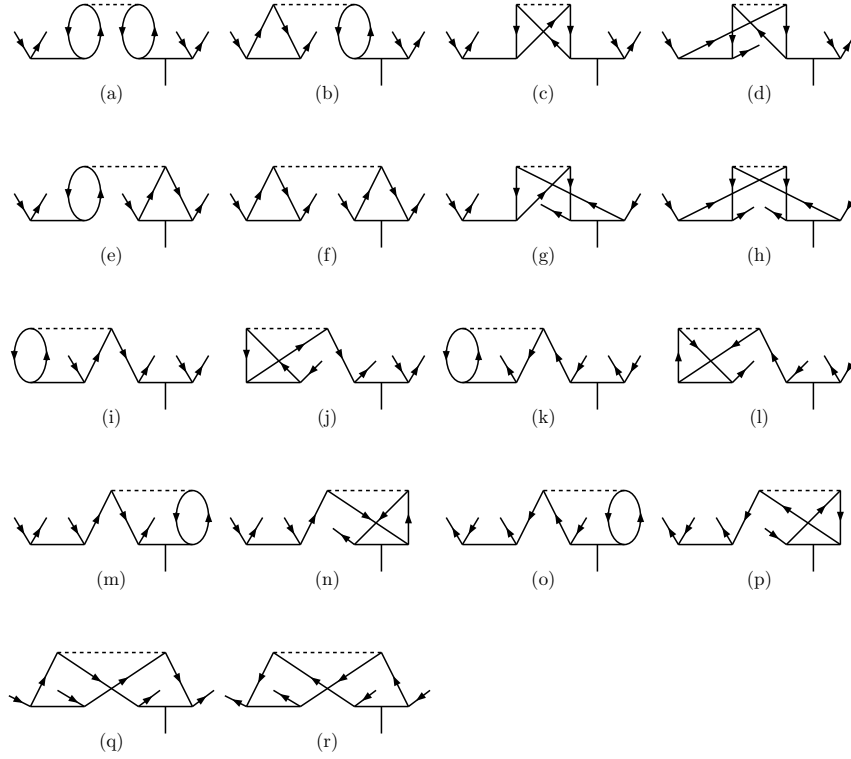


Figure 3.17: The  $\mathbf{T}_2^{(1)}$  diagrams arising from the contraction  $\overline{\overline{H_N T_2^{(0)}}} \mathbf{T}_2^{(1)}$ .

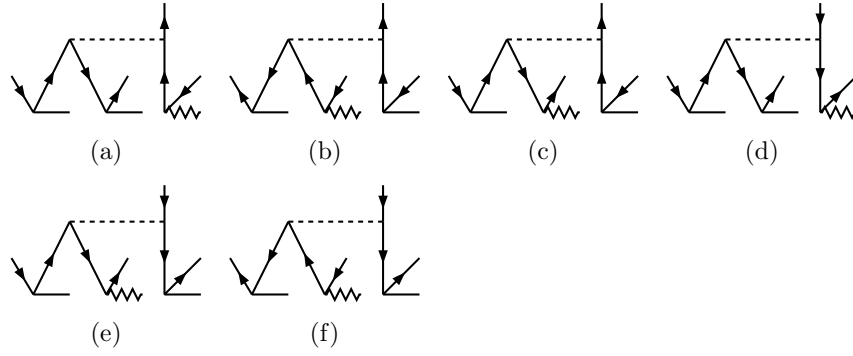
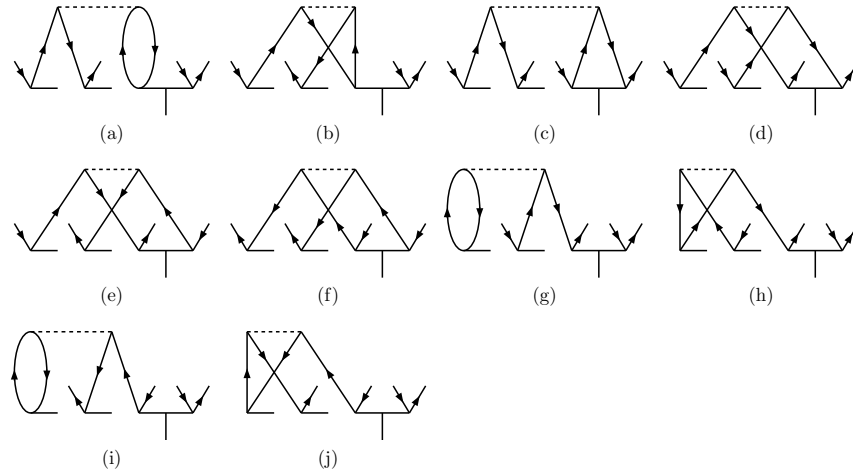
diagrams is

$$\begin{aligned} \langle \overline{\overline{H_N T_1^{(0)}}} \overline{\overline{T_1^{(0)}}} \mathbf{T}_1^{(1)} \rangle_{ab}^{pq} &= \sum_{crs} g_{cqr} [-t_a^r t_c^p \tau_b^s - (t_c^p \tau_a^r - t_a^r \tau_c^p) t_b^s] \\ &+ \sum_{cdr} g_{cdr} [t_a^r (t_c^p \tau_d^q + \tau_c^p t_d^q) + t_c^p \tau_a^r t_d^q]. \end{aligned} \quad (3.35)$$

The overall contribution from these diagrams is expected to be small as these are quadratic in  $T_1^{(0)}$ . The next term in Eq. (3.27),  $\overline{\overline{H_N T_1^{(0)}}} \overline{\overline{T_1^{(0)}}} \mathbf{T}_2^{(1)}$ , has ten Goldstone diagrams and these are shown in Fig. 3.19. and the equivalent algebraic expression of the diagrams is

$$\begin{aligned} \langle \overline{\overline{H_N T_1^{(0)}}} \overline{\overline{T_1^{(0)}}} \mathbf{T}_2^{(1)} \rangle_{ab}^{pq} &= \sum_{cdrs} g_{cdrs} [t_a^r t_c^p \tau_{bd}^{sq} + t_a^r t_d^p \tau_{cb}^{sq} + t_a^r t_b^s \tau_{cd}^{pq} + t_d^q (t_a^r \tau_{cb}^{ps} + t_c^p \tau_{ab}^{rs}) \\ &- (t_c^r t_a^s - t_c^s t_a^r) \tau_{db}^{pq} - (t_c^r t_d^p - t_d^r t_c^p) \tau_{ab}^{sq}]. \end{aligned} \quad (3.36)$$

Contributions from these diagrams will be lower than  $\overline{\overline{H_N T_1^{(0)}}} \overline{\overline{T_1^{(0)}}} \mathbf{T}_1^{(1)}$  as these depend on  $\mathbf{T}_2^{(1)}$ , which is smaller in magnitude than  $\mathbf{T}_1^{(1)}$ . The contributions from the two terms are expected to be small as these are second order in  $T_1^{(0)}$ . The last

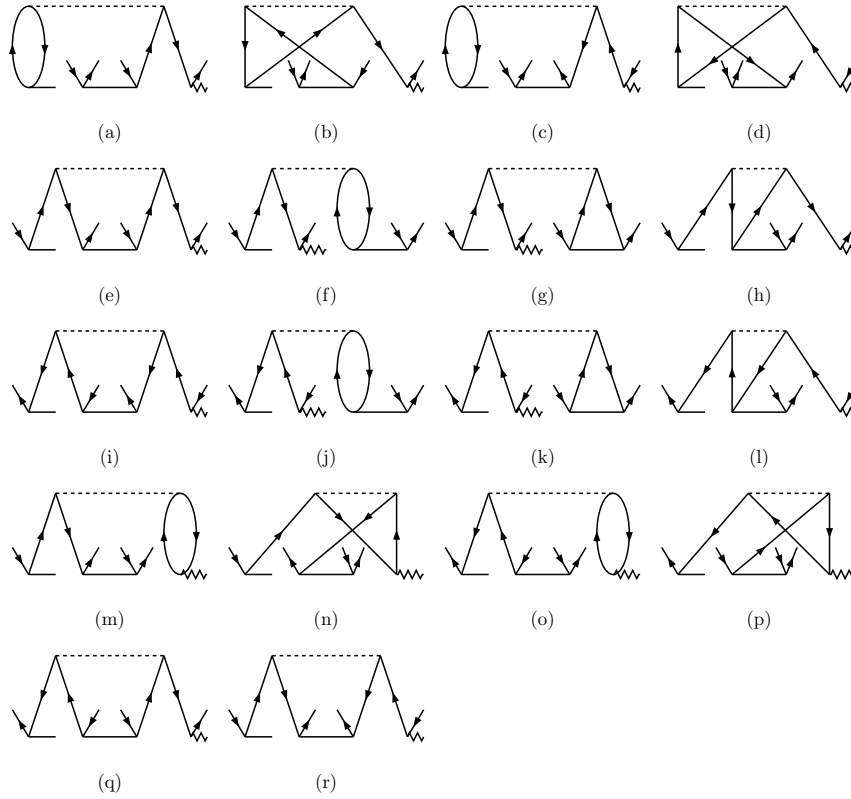

 Figure 3.18: Diagrams arising from the contraction  $\overline{\overline{H_N T_1^{(0)} T_1^{(0)}}} \mathbf{T}_1^{(1)}$ .

 Figure 3.19: Diagrams arising from the contraction  $\overline{\overline{H_N T_1^{(0)} T_1^{(0)}}} \mathbf{T}_2^{(1)}$ .

third order term,  $\overline{\overline{H_N T_1^{(0)} T_2^{(0)}}} \mathbf{T}_1^{(1)}$ , has eighteen diagrams and these are shown in

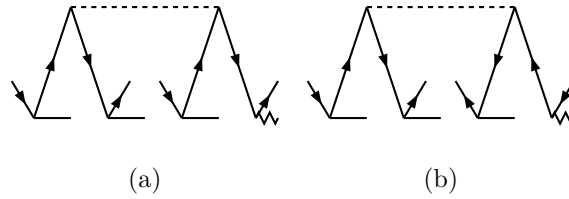
Fig. 3.20. The algebraic equivalent of these diagrams is

$$\begin{aligned} \langle \overline{\overline{H_N T_1^{(0)} T_2^{(0)}}} \mathbf{T}_1^{(1)} \rangle_{ab}^{pq} = & \sum_{cdrs} g_{cdrs} [(t_c^s t_{ab}^{pr} - t_c^r t_{ab}^{ps}) \tau_d^q - (t_c^r t_{ad}^{pq} - t_d^r t_{ac}^{pq}) \tau_b^s + t_a^r (t_{cb}^{ps} \tau_d^q - \tilde{t}_{db}^{sq} \tau_c^p + t_{cb}^{sq} \tau_d^p \\ & - t_{cb}^{pq} \tau_d^s + t_{db}^{pq} \tau_c^s + t_{cd}^{pq} \tau_b^s) + t_c^p (t_{ad}^{rq} \tau_b^s - \tilde{t}_{db}^{sq} \tau_a^r + t_{db}^{rq} \tau_a^s - t_{ab}^{rq} \tau_d^s + t_{ab}^{sq} \tau_d^r + t_{ab}^{rs} \tau_d^q)]. \end{aligned} \quad (3.37)$$

Among the third order terms in the  $\mathbf{T}_2^{(1)}$  equation this will be the leading order term as it depends on  $T_2^{(0)}$  and  $\mathbf{T}_1^{(1)}$ , the dominant cluster operators among the unperturbed and perturbed cluster operators, respectively. There are two Goldstone diagrams from the fourth order term and these are shown in Fig. 3.21


 Figure 3.20: Diagrams arising from the contraction  $\overline{\overline{\overline{H_N T_1^{(0)} T_2^{(0)} T_1^{(1)}}}}$ .

and the algebraic expression is


 Figure 3.21: Diagrams arising from the contraction  $\overline{\overline{\overline{H_N T_1^{(0)} T_1^{(0)} T_1^{(0)} T_1^{(1)}}}}$ .

$$\langle \overline{\overline{\overline{H_N T_1^{(0)} T_1^{(0)} T_1^{(0)} T_1^{(1)}}}} \rangle_{ab}^{pq} = \sum_{cdrs} g_{cdrs} t_a^r t_c^p (t_b^s t_d^q + t_d^q t_b^s).$$

Among all the diagrams considered so far these two diagrams will have the lowest contributions as these are third order in  $T_1^{(0)}$ . However, for completeness we include these in the calculations.

$\overline{\mathbf{D}}T^{(0)}$  and  $\overline{\mathbf{D}}T^{(0)}T^{(0)}$  diagrams

Another group of PRCC diagrams arise from the contraction of  $\mathbf{D}$  and  $T^{(0)}$ , these contribute to the right hand side of Eq. (3.25a) and (3.25b). In this group, there are five Goldstone diagrams of  $\mathbf{T}^{(1)}$  and these are shown in Fig. 3.22. Among

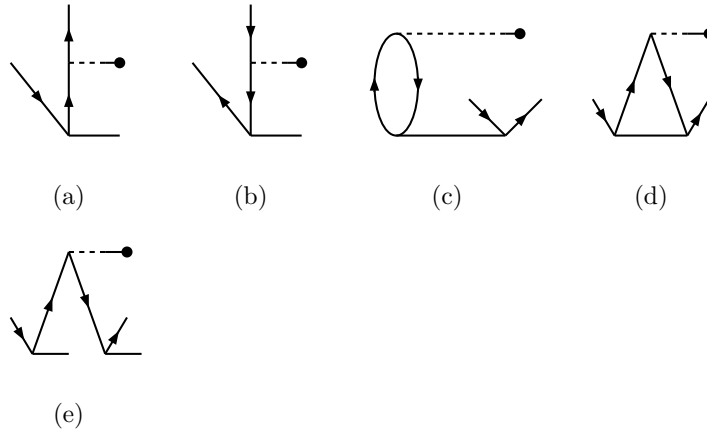


Figure 3.22: Singles diagrams arising from the contraction  $\overline{H_{\text{int}}T^{(0)}}$  and  $\overline{H_{\text{int}}T^{(0)}T^{(0)}}$ .

the diagrams only the last one is nonlinear in  $T^{(0)}$ . The algebraic expression of the diagrams is

$$\langle \overline{\mathbf{D}}T^{(0)} \rangle_a^p + \langle \overline{\mathbf{D}}T^{(0)}T^{(0)} \rangle_a^p = \sum_q \mathbf{r}_{pq} t_a^q - \sum_c \mathbf{r}_{ca} t_c^p + \sum_{bq} \mathbf{r}_{bq} (t_{ba}^{qp} - t_{ab}^{qp} - t_a^q t_b^q) \quad (3.38)$$

where,  $\mathbf{r}_{ij} = \langle i|\mathbf{r}|j \rangle$  is the electronic part of the single particle matrix element. For  $\mathbf{T}_2^{(1)}$ , there are four diagrams and these are shown in Fig. 3.23 and last two are nonlinear in  $T^{(0)}$ . The algebraic expression of the diagrams is

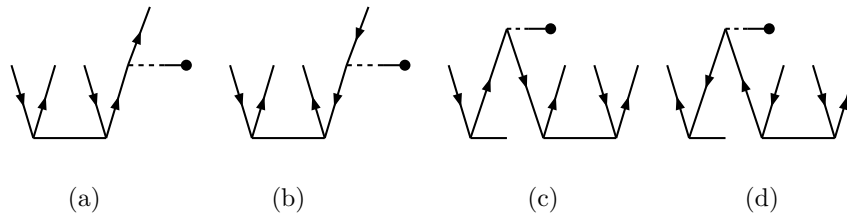


Figure 3.23: Doubles diagrams arising from the contraction  $\overline{H_{\text{int}}T^{(0)}}$  and  $\overline{H_{\text{int}}T^{(0)}T^{(0)}}$ .

$$\langle \overline{\mathbf{D}\mathbf{T}}^{(0)} \rangle_{ab}^{pq} + \langle \overline{\mathbf{D}\mathbf{T}}^{(0)} \mathbf{T}^{(0)} \rangle_{ab}^{pq} = \sum_r \mathbf{r}_{qr} t_{ab}^{pr} - \sum_c \mathbf{r}_{cb} t_{ac}^{pq} + \sum_{cr} \mathbf{r}_{cr} (-t_a^r t_{cb}^{pq} - t_c^p t_{ab}^{rq}) \quad (3.39)$$

This completes the diagrammatic and algebraic analysis of the nonlinear terms in the  $\mathbf{T}^{(1)}$  equations. To obtain the linear algebraic equations of the cluster amplitudes, each of the diagrams or terms in the algebraic expression requires further simplification to radial and angular components. The angular part is evaluated diagrammatically, however the diagrams are different from the Goldstone diagrams.

### 3.3.4 Intermediate diagrams

The PRCC diagrams corresponding to the nonlinear terms are numerous and topologically complex. Further more, in these diagrams, the number of the spin-orbitals involved is large and in general, the diagrams with the largest number of spin-orbitals are associated with the terms  $H_N T_2^{(0)} \mathbf{T}_2^{(1)}$ ,  $H_N T_1^{(0)} T_1^{(0)} \mathbf{T}_2^{(1)}$  and  $H_N T_1^{(0)} T_1^{(0)} T_1^{(0)} \mathbf{T}_1^{(1)}$ . All of these terms have a common feature: the presence of the two electron integral  $\langle ab|g(r_{12})|pq\rangle$ . Returning to the number of spin-orbitals, the  $T_2^{(0)}$  diagrams arising from any of the three terms mentioned earlier consist of four core and virtual spin-orbitals each. Accordingly, the number of times a diagram is evaluated,  $N_d$ , scales as  $n_o^4 n_v^4$  and this sets the scale of computational requirements. Here,  $n_o$  and  $n_v$  are the number of core and virtual spin-orbitals, respectively. In the present work, for lighter atoms and moderate sized basis sets  $n_o \sim 10$  and  $n_v \sim 100$ , even then  $N_d \sim 10^{12}$ . This is a large number and puts a huge constraint on the computational resources.

To mitigate the computational constraints arising from the  $n_o^4 n_v^4$  scaling, we separate the diagrams into two parts. One of the parts scales at the most  $n_o^2 n_v^4$  and the total diagram is equivalent to the product of the parts. The part of the diagram which is calculated first is referred to as the intermediate diagram. During computations, all the intermediate diagrams are calculated first and stored. Later, these are combined with the remaining part of the PRCC diagram and the total diagram is calculated. The scaling still remains at  $n_o^2 n_v^4$  and compared to the  $n_o^4 n_v^4$  scaling, this improves the performance by several orders of magnitudes.

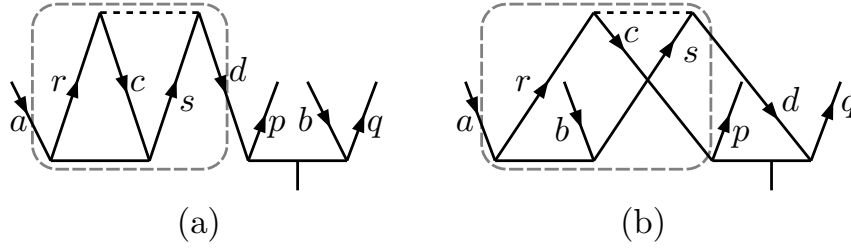


Figure 3.24: Example diagrams of  $H_N T_2^{(0)} T_2^{(0)}$  which contribute to the  $\mathbf{T}_2^{(1)}$  equations. The portion of the diagrams within the rectangles with rounded corners are examples of the one body (a) and two-body (b) intermediate diagrams.

To examine in more detail, consider the term  $H_N T_2^{(0)} \mathbf{T}_2^{(1)}$ , the algebraic expression for one of the terms contributing to the  $\mathbf{T}_2^{(0)}$  is

$$(\tau_{ab}^{pq})_{3.24a} a_p^\dagger a_q^\dagger a_b a_a = \sum_{rcsd} t_{ac}^{rs} v_{rs}^{cd} \tau_{db}^{pq} a_p^\dagger a_q^\dagger a_b a_a, \quad (3.40)$$

and it is diagrammatically equivalent to Fig. 3.24(a). However, while evaluating the diagram, the part within the dashed round rectangle or the intermediate diagram can be separated and computed first. Eq. (3.40) can then be written as

$$(\tau_{ab}^{pq})_{3.24a} a_p^\dagger a_q^\dagger a_b a_a = \sum_d \left( \eta_a^d a_d^\dagger a_a \right) \left( \tau_{db}^{pq} a_p^\dagger a_q^\dagger a_b a_d \right), \quad (3.41)$$

where  $\eta_a^d = \sum_{rcs} t_{ac}^{rs} v_{rs}^{cd}$  is the amplitude of the effective one-body operator corresponding to the intermediate diagram. The computation of  $\eta_a^d$  scales as  $n_o^3 n_v^2$  and when contracted with  $\mathbf{T}_2^{(1)}$ , the computation still scales as  $n_o^3 n_v^2$ . This is much less than the  $n_o^4 n_v^4$  scaling. Consider another term

$$(\tau_{ab}^{pq})_{3.24b} a_p^\dagger a_q^\dagger a_b a_a = \sum_{rcsd} t_{ab}^{rs} v_{rs}^{cd} \tau_{cd}^{pq} a_p^\dagger a_q^\dagger a_b a_a, \quad (3.42)$$

and it is diagrammatically equivalent to Fig. 3.24(b). Like in the previous case, the intermediate diagram ( part within the dashed round-rectangle ) can be calculated first and the equation can be rewritten as

$$(\tau_{ab}^{pq})_{3.24b} a_p^\dagger a_q^\dagger a_b a_a = \sum_{cd} \left( \eta_{ab}^{cd} a_c^\dagger a_d^\dagger a_b a_a \right) \left( \tau_{cd}^{pq} a_p^\dagger a_q^\dagger a_d a_c \right). \quad (3.43)$$

Here, the intermediate diagram corresponds to a two-body effective operator with amplitude  $\eta_{ab}^{cd} = \sum_{rs} t_{ab}^{rs} v_{rs}^{cd}$  and scales as  $n_o^4 n_v^2$ . The scaling remains the

same when the total diagram is evaluated. Extending the method to other diagrams, there are other forms of one-body and two-body intermediate diagrams depending on the topology.

In conclusion, this chapter deals with the theoretical foundation of RCCSDT and PRCC theory for closed shell atoms. We introduce the angular momentum representation of the triple excitation operator and this representation is convenient to calculate complicated angular momentum diagrams that arise after considering the  $T_3^{(0)}$  in the RCC theory. In the next part we introduce PRCC theory. This takes into account multiple perturbations in many electron atoms. We formulated the theory and introduce the tensor structure of the PRCC operators. While evaluating the topologically complex diagrams we introduce intermediate diagrams. It simplifies the Goldstone diagrams and reduce the computational cost. Most importantly these,  $T_3^{(0)}$  and PRCC theory, when combined with the vacuum polarization potential and Breit interaction provides a test of QED corrections in closed-shell atoms and ions.

# Chapter 4

## QED effects in open-shell atoms using coupled-cluster theory

One valence atoms and ions are ideal testing ground for different many body techniques because of the simple electronic structure. It has one electron in the valence shell and it is essentially the simplest atomic system to study core-valence correlation effects. Different atomic many body theories have been used to study one valence atom and ions. However, these techniques are essentially an extension of closed shell many body theories. We will particularly focus on the QED effects on one valence properties using coupled-cluster theory. As we mentioned earlier, in many electron atoms, along with the electron-electron correlation it is important to take into account the QED effects. Though the highly charged ions like hydrogen like ions are ideal to test QED effects precisely, QED effects are also important to precisely determine properties like the nuclear spin-dependent PNC effects in atoms. In the present work we employ coupled-cluster theory of one valence atoms with the  $H^{\text{DCB}}$ . Here we emphasize that to determine the electronic correlations precisely we Incorporated the  $T_3^{(0)}$  at the linearized RCC theory. The RCC theory with  $T_3^{(0)}$  and QED corrections is the ideal platform to study the interplay of electronic correlation and QED effects in many electron atoms and ions.

The chapter is organized as follows: we first introduce the RCC theory for one valence atoms in section 4.1. Here we will introduce the triple excitation in

the RCC theory and the RCCSDT amplitude equations for one valence atoms. In section 4.2 we discuss the electric dipole transition amplitudes in one valence atoms. In the results and discussions part we focus on the excitation energy and the electric dipole transitions of several states in one valence atoms.

## 4.1 RCC theory for one valence atoms

For one valence atom the eigenvalue equation is

$$H^{\text{DCB}}|\Psi_v\rangle = E_v|\Psi_v\rangle. \quad (4.1)$$

Here  $|\Psi_v\rangle$  is the eigen state and  $E_v$  is the corresponding eigen value for one valence atom or ion. For these system we have an additional complication. Along with the core and virtual orbitals we have a valence sector. As Lindgren [61] pointed out, that a valence orbital can be treated both as core and virtual, and we can then apply the general formalism of particle-hole states for the valence sector. For one valence atom or ion we introduce another set of cluster operator  $S^{(0)}$  along with the  $T^{(0)}$  operator. This separation between the two sets of cluster operators simplify the problem of solving the eigen-value equation. Essentially, we first solve the closed-shell part of the system to obtain the  $T^{(0)}$  amplitudes, and then we solve for the valence part to obtain the  $S^{(0)}$  amplitudes.

In RCC theory the ground state wave-function of a one valence atom is defined as

$$|\Psi_v\rangle = e^{T^{(0)}+S^{(0)}}|\Phi_v\rangle. \quad (4.2)$$

Here  $|\Phi_v\rangle$  is the reference state wave-function of the one valence atom and it is obtained as  $|\Phi_v\rangle = a_v^\dagger|\Phi_0\rangle$ . Here  $|\Phi_0\rangle$  is the reference state wave function of the closed-shell part of the one valence system. For a one valence system,

$$e^{S^{(0)}} = 1 + S^{(0)}. \quad (4.3)$$

This is because, we can excite at most one electron from the valence orbital to the virtual. So, the contribution from the higher order terms in  $S^{(0)}$  are zero. With this definition we can write the ground state wave function of a one valence

system as

$$|\Psi_v\rangle = e^{T^{(0)}}(1 + S^{(0)})|\Phi_v\rangle. \quad (4.4)$$

Using the above definition of ground state wave-function the eigen-value equation, Eq. (4.1) is

$$H^{\text{DCB}}e^{T^{(0)}}(1 + S^{(0)})|\Phi_v\rangle = E_v e^{T^{(0)}}(1 + S^{(0)})|\Phi_v\rangle. \quad (4.5)$$

In the CCSDT approximation along with the closed-shell cluster operator, the open shell cluster operator are expanded as

$$\begin{aligned} T^{(0)} &= T_1^{(0)} + T_2^{(0)} + T_3^{(0)}, \\ S^{(0)} &= S_1^{(0)} + S_2^{(0)} + S_3^{(0)}. \end{aligned} \quad (4.6)$$

Like the  $T^{(0)}$  operators the  $S^{(0)}$  operators can be diagrammatically represented as shown in Fig. 4.1. In the figure  $a, b, c, \dots (p, q, r, \dots)$  represents the core

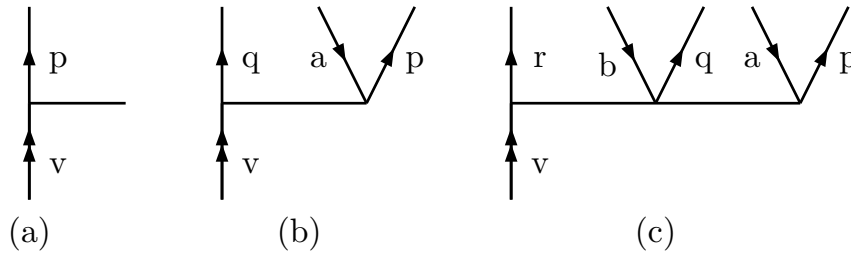


Figure 4.1: Diagrammatic representation of open shell coupled-cluster operator : (a) Single excitation operator, (b) Double excitations operator, (c) Triple excitations operator.

(virtual) orbitals and  $v$  denotes the valence orbital. Using the normal ordered Hamiltonian,  $H_N$  we can rewrite the eigen-value equation as

$$H_N|\Psi_v\rangle = \Delta E_v|\Phi_v\rangle, \quad (4.7)$$

Where  $\Delta E_v$  is the correlation energy of the one valence system. Now to obtain the coupled-cluster amplitude equations we operate by  $e^{-T^{(0)}}$  from left and project it on the single, double and triple excited determinants. The RCCSDT amplitude equations for one valence system are

$$\langle \Phi_v^p | \bar{H}_N + \bar{H}_N S_1^{(0)} + \bar{H}_N S_2^{(0)} + \bar{H}_N S_3^{(0)} | \Phi_v \rangle = \Delta E_v \langle \Phi_v^p | S_1^{(0)} | \Phi_v \rangle, \quad (4.8a)$$

$$\langle \Phi_{va}^{pq} | \bar{H}_N + \bar{H}_N S_1^{(0)} + \bar{H}_N S_2^{(0)} + \bar{H}_N S_3^{(0)} | \Phi_v \rangle = \Delta E_v \langle \Phi_{va}^{pq} | S_2^{(0)} | \Phi_v \rangle, \quad (4.8b)$$

$$\langle \Phi_{vab}^{pqr} | \bar{H}_N + \bar{H}_N S_1^{(0)} + \bar{H}_N S_2^{(0)} + \bar{H}_N S_3^{(0)} | \Phi_v \rangle = \Delta E_v \langle \Phi_{vab}^{pqr} | S_3^{(0)} | \Phi_v \rangle. \quad (4.8c)$$

In these equations  $\bar{H}_N = e^{-T^{(0)}} H_N e^{T^{(0)}}$  is the dressed Hamiltonian. The RCCSDT amplitude equations are obtained using the orthogonality condition of ground and excited state determinants. After applying the Wick's theorem for the product of operators we obtain the cluster amplitude equations.

$$\langle \Phi_v^p | \bar{H}_N + \{ \overline{H_N S_1^{(0)}} \} + \{ \overline{H_N S_2^{(0)}} \} + \{ \overline{H_N S_3^{(0)}} \} | \Phi_0 \rangle = E_v^{\text{att}} \langle \Phi_v^p | S_1^{(0)} | \Phi_0 \rangle, \quad (4.9a)$$

$$\langle \Phi_{va}^{pq} | \bar{H}_N + \{ \overline{H_N S_1^{(0)}} \} + \{ \overline{H_N S_2^{(0)}} \} + \{ \overline{H_N S_3^{(0)}} \} | \Phi_0 \rangle = E_v^{\text{att}} \langle \Phi_{va}^{pq} | S_2^{(0)} | \Phi_0 \rangle, \quad (4.9b)$$

$$\langle \Phi_{vab}^{pqr} | \bar{H}_N + \{ \overline{H_N S_1^{(0)}} \} + \{ \overline{H_N S_2^{(0)}} \} + \{ \overline{H_N S_3^{(0)}} \} | \Phi_0 \rangle = E_v^{\text{att}} \langle \Phi_{vab}^{pqr} | S_3^{(0)} | \Phi_0 \rangle. \quad (4.9c)$$

Here  $E_v^{\text{att}}$  represents the attachment energy of the valence electron. It means we need  $E_v^{\text{att}}$  to remove the valence electron from a neutral atom. In the present work we will emphasize about the theoretical details of attachment energy from triple excitation. The attachment energy from RCCSD theory is discussed in great detail by B. K. Mani [73]. The attachment energy diagrams that will arise after incorporating the triple excitation is shown in Fig. 4.2. Along with the

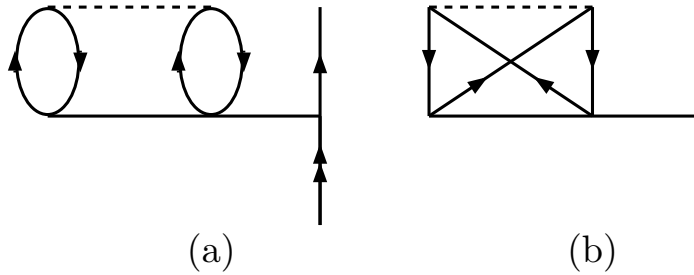


Figure 4.2: Attachment energy diagrams arising at the triple excitation level.

diagrams that arise at the RCCSD theory we incorporate two diagrams which are shown in Fig. 4.2 to estimate the contribution from triple excitations to  $E_v^{\text{att}}$ .

## 4.2 Electric dipole transition from RCCSDT theory

The main objective of developing different many body theories is to calculate different atomic properties. It is also important to mention that the precision of experimental data have improved in past few decades and this implies the need for better theoretical methods. The wave-function generated in the RCCSDT theory can be used to calculate different atomic properties and one of the very basic properties is to evaluate the electric dipole transition matrix element. Here we shall discuss calculation of the electric dipole matrix element in the framework of RCC theory. A radiative transition occurs when a photon is absorbed or emitted by the atom. The dominant contributions to the radiative transitions comes from the electric dipole transition. In order to derive the expression of dipole matrix element, we start with the reduced matrix element of the dipole operator between initial state  $|\Psi_i\rangle$  and final state  $|\Psi_f\rangle$ . The form of the reduced matrix element is

$$D_{fi} = \frac{\langle\Psi_f||\mathbf{D}||\Psi_i\rangle}{\sqrt{\langle\Psi_f|\Psi_f\rangle\langle\Psi_i|\Psi_i\rangle}}. \quad (4.10)$$

Since the dipole operator,  $\mathbf{D}$  is an odd parity operator, for a nonzero contribution the parity of the  $|\Psi_i\rangle$  and  $|\Psi_f\rangle$  should be opposite. The details of the matrix element of the dipole operator is discussed in appendix B. To calculate  $D_{fi}$  from CCT, we substitute the CC wave-function in Eq. (4.10), then

$$\begin{aligned} D_{fi} = & \langle\Phi_w||\mathbf{D} + T^{(0)\dagger}\mathbf{D} + \mathbf{D}T^{(0)} + T^{(0)\dagger}\mathbf{D}T^{(0)} + S^{(0)\dagger}\mathbf{D} + \mathbf{D}S^{(0)} \\ & + S^{(0)\dagger}\mathbf{D}S^{(0)}||\Phi_v\rangle. \end{aligned} \quad (4.11)$$

Here, we consider only the terms up to to second orders in cluster amplitudes. The non-terminating series,  $e^{T^{(0)\dagger}}\mathbf{D}e^{T^{(0)}}$  is a major constraint in RCC theory. But based on earlier calculation [75], which studied an all order method to evaluate the reduced dipole matrix elements of singly ionized group II elements, we can safely neglect the the higher order terms which has three or more cluster operators. The diagrams are topologically same as the diagrams to evaluate

hyperfine interaction in ref. [73]. Here we focus on the diagrams which arise from incorporating the  $T_3^{(0)}$  at the properties level. Since the contribution from the closed-shell cluster operator is negligible, we concentrate on the properties diagram that arise after due consideration of the  $S^{(0)}$  operator. At minimum we need two cluster operators to start with. Following the rule of level of excitation (l.o.e) we can construct the properties diagram from  $S_2^{(0)\dagger} \mathbf{D} S_3^{(0)}$  contraction. The diagrams arising from  $\{\overline{S_2^{(0)\dagger} \mathbf{D} S_3^{(0)}}\}$  are shown in Fig. 4.3.

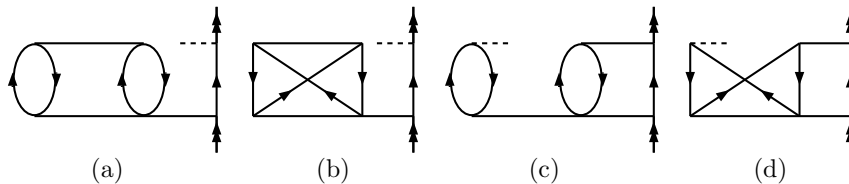


Figure 4.3: Leading diagrams arising from the contraction  $\{\overline{S_2^{(0)\dagger} \mathbf{D} S_3^{(0)}}\}$  contribute to the reduced dipole matrix element. Dashed line represent the dipole operator.

### 4.3 Results and Discussions

In this section we discuss in detail the properties of one valence atoms. As we mentioned earlier, we particularly focus on the  $E_v^{\text{att}}$  of one valence atoms after incorporating the  $T_3^{(0)}$  and  $S_3^{(0)}$  in the RCC theory. Along with this we also discuss about the results of  $D_{fi}$  for one valence atoms. Like in the closed-shell atoms, we first introduce the basis set parameters for the one valence atoms. We first compare DHF SCF energy and orbital energy obtained from GRASP [52]. Here again we use GTOs with even tempered basis set parameters. Before starting the discussion on the properties of one valence atom, we must mention that we use the same basis set parameters as we have use to calculate the Breit correction and VP correction in the second chapter. This is because, with the  $V^{N-1}$  potential we can construct a complete set of basis for the neutral atom. It must be mentioned that it is true for a general basis set like the GTO's as well as B-spline basis sets.

### 4.3.1 Properties of one valence atoms

In this subsection we discuss about the excitation energy, and  $D_{fi}$  of one valence atoms and compare these with the previous theoretical and experimental values. The present numerical calculations are based on the RCCSDT code and triple excitations is considered at the wave-function level. For the  $D_{fi}$  calculation and for excitation energy we consider  $(T_3^{(0)} + S_3^{(0)})$  at the wave-function as well as at the properties level. The main difficulty in computations with the triple excitations is the number of triples amplitude. It is very large compare to the single and double excitation cluster amplitudes. For example, in the case of Li, the number of single excitation amplitude  $\approx 10^2$  and double excitation amplitude  $\approx 10^4$ , but the number of triple excitation amplitude is  $\approx 10^8$ . So to calculate triple excitations we truncate the number of core and virtual orbitals in the RCC computation. Now in the numerical implementation of the triple excitation we choose the cut off energy such that at the initial guess value from MBPT is not very small. To do this we consider the energy denominator part of the approximate triples. The energy denominator is

$$\Delta E = \frac{1}{(\varepsilon_p + \varepsilon_q + \varepsilon_r - \varepsilon_a - \varepsilon_b - \varepsilon_c)}. \quad (4.12)$$

This is very important while considering the triple excitation. The  $\Delta E$  for different combination of core and virtual orbitals should never be very small. Otherwise it is very difficult to obtain converged RCC wave-function. So, we introduce a cut-off to the core and virtual orbital energies. There is one important consideration associated with the triple excitations in RCC theory. In the  $s_{1/2}$  and  $p_{1/2}$  orbitals we can have at the most two electrons, however, the triples cluster amplitude takes into account all possible triple excitations. So we have to put constraints for  $s_{1/2}$  and  $p_{1/2}$  orbitals. Following the Pauli's exclusion principle we set the cluster amplitudes to zero when more than two core or virtual orbital belong to the same  $s_{1/2}$  or  $p_{1/2}$  symmetry. Another issue related to numerical implementation of the triples amplitude is to consider only unique cluster amplitudes. To do that we impose the condition  $p > q > r$  and  $a > b > c$ . This plays an important role while storing the amplitudes during computations.

### 4.3.2 Excitation energies

The excitation energy and the ionization potential (I.P) of the group I elements are discussed here. The energies of the different excited states are evaluated in the RCC theory, and compared with the previous theoretical value and the NIST recommended value. The results for  ${}^7\text{Li}$  are listed in Table. 4.1. In the literature it is also referred to as the removal energy. We follow these nomenclature and our results of the removal energies of  $2s_{1/2}$  to  $4d_{5/2}$  are listed in Table. 4.1. As we can see, the result of  $2s_{1/2}$  state deviated by from the NIST recommended value by  $5.5 \text{ cm}^{-1}$ . This could be due to several reasons. As pointed out by Johnson *et al.* [76] in his remarkable work on several atomic properties of  ${}^7\text{Li}$ , the recoil correction contribution to the removal energy is  $3.59 \text{ cm}^{-1}$ . However, the recoil correction which is due to reduced mass correction and mass polarization, are not considered in the present work. The other contribution is the Lamb shift correction, which is not completely accounted in the present work. Here we consider only the vacuum polarization correction to the orbital energies. In the present calculation of I.P and excitation energies we consider only up to  $h$  symmetry. But it has been pointed out in ref. [76] that the contribution from  $i$  and  $j$  symmetry is  $\approx 1 \text{ cm}^{-1}$ .

Coming to the highly excited states, our results are in very good agreement with the NIST recommended values. This is because the highly excited states, which are far from the nucleus, are less affected by recoil correction. The same pattern was observed by Johnson and his coworkers in ref. [76]. So to sum up, if we add all these corrections to the present work in the framework of RCC theory the result is within 0.1% of the NIST recommended value.

For Na we calculate the removal energies of  $3s_{1/2}$ ,  $3p_{1/2}$  and  $3p_{3/2}$  orbitals. The results for Na are listed in Table 4.2.

Orbital	This Work	$E_{\text{NIST}}$ [77]	Previous Work[76]
$2s_{1/2}$	-43481.7	-43487.2	-43487.5
$2p_{1/2}$	-28570.5	-28583.5	-28581.9
$2p_{3/2}$	-28570.1	-28583.2	-28581.5
$3s_{1/2}$	-16256.1	-16281.0	-16281.0
$3p_{1/2}$	-12548.5	-12561.8	-12561.2
$3p_{3/2}$	-12548.3	-12561.8	-12561.0
$3d_{3/2}$	-12203.6	-12204.1	-12204.0
$3d_{5/2}$	-12203.6	-12204.0	-12204.0
$4s_{1/2}$	-8152.9	-8475.1	-8475.1
$4p_{1/2}$	-7011.9	-7017.6	-7017.2
$4p_{3/2}$	-7011.8	-7017.6	-7017.2
$4d_{3/2}$	-6863.6	-6863.8	-6863.8
$4d_{5/2}$	-6863.5	-6863.8	-6863.8

Table 4.1: Removal Energies of several excited states of  ${}^7\text{Li}$  in  $\text{cm}^{-1}$ .

Orbital	This Work	$E_{\text{NIST}}$ [77]	Previous Work[42]
$3s_{1/2}$	-41373	-41449	-41376
$3p_{1/2}$	-24469	-24493	-24472
$3p_{3/2}$	-24437	-24476	-24453

Table 4.2: Removal Energies of ground and excited states of  ${}^{23}\text{Na}$  in  $\text{cm}^{-1}$ .

The results show good agreement with the NIST recommended values as well as with previous RCCSD [42] results. Here again we observe the same trend like Li, our values are on the lower side from that of the NIST recommended values. The discrepancy may be due to choice of basis set as well as neglecting the recoil correction in the present work. In Table. 4.3 we listed the contribution from different terms to the removal energy.

Orbital	DHF	RCCSD	RCCSDT	Total
$3s_{1/2}$	-39944	-1428	-1429	-41373
$3p_{1/2}$	-24032	-438	-437	-24469
$3p_{3/2}$	-24010	-428	-427	-24437

Table 4.3: Contribution to the removal Energies  $^{23}\text{Na}$  in  $\text{cm}^{-1}$ .

As expected the DHF contribution, the first column in Table. 4.3, gives the dominant contribution. The column labeled RCCSDT gives the contribution to the removal energy after incorporating the triple excitations in RCC theory. The inclusion of the triples improve the result of the ground state,  $3s_{1/2}$ . On the other hand, for  $3p_{1/2}$  and  $3p_{3/2}$  excited state the inclusion of triples deteriorates the result. There is one important point to be noticed, the contribution from the triple excitations is very small and it is  $\approx 1\text{cm}^{-1}$  for ground as well as excited states.

For K the result of removal energies are listed in Table. 4.4.

Orbital	This Work	$E_{\text{NIST}}$ [77]	Previous Work[42]
$4s_{1/2}$	-35117	-35010	-35080
$4p_{1/2}$	-22047	-22025	-22044
$4p_{3/2}$	-21988	-21967	-21984

Table 4.4: Removal Energies of ground and excited states of  $^{39}\text{K}$  in  $\text{cm}^{-1}$ .

Here the values of removal energies exhibit a trend opposite to Li and Na. In this case our results are higher than the NIST recommended value. However, our results follows the same pattern as that of the previous RCCSD work [42]. The term wise contribution to the removal energy is listed in Table. 4.5.

Orbital	DHF	RCCSD	RCCSDT	Total
$4s_{1/2}$	-32372	-2743	-2745	-35117
$4p_{1/2}$	-21003	-1031	-1044	-22047
$4p_{3/2}$	-20959	-1009	-1029	-21988

Table 4.5: Contribution to the removal energies  $^{39}\text{K}$  in  $\text{cm}^{-1}$ .

One interesting point is the contribution from triples to the removal energies. Although the contribution to the ground state,  $4s_{1/2}$ , is small, for the excited states it is significant. For  $4p_{1/2}$  and  $4p_{3/2}$ , the contributions from triple excitations are  $13 \text{ cm}^{-1}$  and  $20 \text{ cm}^{-1}$  respectively.

The results for removal energies of ground state and excited states of Rb are listed in Table 4.6.

Orbital	This Work	$E_{\text{NIST}}$ [77]	Previous Work[42]
$5s_{1/2}$	-33777	-33691	-33762
$5p_{1/2}$	-21123	-21112	-21130
$5p_{3/2}$	-20883	-20874	-20888

Table 4.6: Removal Energies of ground and excited states of  $^{85}\text{Rb}$  in  $\text{cm}^{-1}$ .

In case of Rb the trend is very similar to K, our results are higher than the NIST recommended values. Here, we must mention that as we go to the high- $Z$  atoms the deviations from the NIST recommended values increases. This could be due to several reasons. One major reason is the contribution from higher symmetry, like  $i, j$  are neglected in the present work. Along with this the nuclear recoil correction may be important. Our result for the  $4s_{1/2}$  state deviates from NIST value by an amount of  $86 \text{ cm}^{-1}$ , which is  $\approx 0.3\%$ . The different contributions to the removal energies are listed in Table. 4.7.

Orbital	DHF	RCCSD	RCCSDT	Total
$5s_{1/2}$	-30572	-3230	-3205	-33777
$5p_{1/2}$	-19928	-1199	-1195	-21123
$5p_{3/2}$	-19730	-1134	-1153	-20883

Table 4.7: Contribution to the removal energies  $^{85}\text{Rb}$  in  $\text{cm}^{-1}$ .

The dominant contribution arises from the DHF term. But, there is a different trend in the contributions from the triple excitations. The third column of Table 4.7 shows that there is a negative contribution from the triple excitations. The same pattern is observed in both the ground as well as excited states. Here the contribution to the ground state,  $5s_{1/2}$ , from the triple excitation is  $25 \text{ cm}^{-1}$ .

Cs is an important atom to study. In this case as well we calculate the removal energies for ground state and excited states, and compared it with the previous results. The results of Cs are listed in Table 4.8.

Orbital	This Work	$E_{\text{NIST}}$ [77]	Previous Work[42]
$6s_{1/2}$	-31539	-31407	-31529
$6p_{1/2}$	-20209	-20228	-20258
$6p_{3/2}$	-19675	-19674	-19695

Table 4.8: Removal Energies of ground and excited states of  $^{133}\text{Cs}$  in  $\text{cm}^{-1}$ .

The ground state removal energy deviates from NIST value by  $132 \text{ cm}^{-1}$ , but it is in good agreement with the previous theoretical value. Our result for the other two low lying excited states shows a reverse trend. The result for  $6p_{1/2}$  is lower than the NIST recommended value but for the  $6p_{3/2}$  state it is larger by  $1 \text{ cm}^{-1}$ . In Table 4.9 we listed the DHF, RCCSD and RCCSDT contributions to the removal energy.

Orbital	DHF	RCCSD	RCCSDT	Total
$6s_{1/2}$	-27961	-3585	-3578	-31539
$6p_{1/2}$	-18787	-1449	-1422	-20209
$6p_{3/2}$	-18391	-1280	-1284	-19675

Table 4.9: Contribution to the removal energies  $^{133}\text{Cs}$  in  $\text{cm}^{-1}$ .

It is important to mention that the inclusion of the triple excitations improves the result. Although our result for ground state deviates by 0.4% from NIST value, overall it is in good agreement with the previous work based on RCC theory.

### 4.3.3 Electric dipole transition amplitudes

We evaluate the  $D_{fi}$  of various allowed transitions for one valence atoms. This is calculated using the CC wave-function with triple excitations. The results for Li are listed in Table 4.10

	This Work	Expt.[78]	RCCSD[42]
$2s_{1/2} - 2p_{1/2}$	3.3175	3.317(4)	3.3173
$2s_{1/2} - 2p_{3/2}$	4.6918	4.689(5)	4.6914

Table 4.10: Reduced electric dipole matrix element of  $^7\text{Li}$  in a.u

and our results are excellent. The values are within the uncertainty limit of the experimental value. Our results for the  $2s_{1/2} - 2p_{1/2}$  transition as well as  $2s_{1/2} - 2p_{3/2}$  agrees well with the previous RCCSD work by Pal *et al.* [42]. Here we incorporate the triple excitations in the CC wave-function and find that the contribution is negligible, it is  $\approx 10^{-6}$  a.u. For Na we presented the result of electric dipole transition in Table 4.11

	This Work	Expt.[78]	RCCSD[42]
$3s_{1/2} - 3p_{1/2}$	3.5358	3.5246(23)	3.5380
$3s_{1/2} - 3p_{3/2}$	5.0003	4.9838(34)	5.0030

Table 4.11: Reduced electric dipole matrix element of  $^{23}\text{Na}$  in a.u

and are in good agreement with the previous RCCSD values. Our value deviates from the experimental value by 0.3% for  $3s_{1/2} - 3p_{1/2}$  transition and  $3s_{1/2} - 3p_{3/2}$  transition. One important point to notice is, the results from our as well as from the previous work are higher than the experimental value. The result of  $D_{fi}$  for K are listed in Table 4.12.

	This Work	Expt.[78]	RCCSD[42]
$4s_{1/2} - 4p_{1/2}$	4.0839	4.102(5)	4.1274
$4s_{1/2} - 4p_{3/2}$	5.7840	5.800(8)	5.8314

Table 4.12: Reduced electric dipole matrix element of  $^{39}\text{K}$  in a.u

Our result for  $4s_{1/2} - 4p_{1/2}$  transition deviates from the experimental value by 0.4% and for  $4s_{1/2} - 4p_{3/2}$  transition it is 0.3%. Here we observe an opposite trend while comparing our results with the previous RCCSD work. The previous RCCSD result is higher than the experimental value.

The results for Rb are listed in Table 4.13.

	This Work	Expt.[78]	RCCSD[42]
$5s_{1/2} - 5p_{1/2}$	4.2133	4.231(3)	4.2611
$5s_{1/2} - 5p_{3/2}$	5.9617	5.977(4)	6.0132

Table 4.13: Reduced electric dipole matrix element of  $^{85}\text{Rb}$  in a.u

In this case our result is 0.4% lower than the experimental value for  $5s_{1/2} - 5p_{1/2}$  transition and it is 0.3% for  $5s_{1/2} - 5p_{3/2}$  transition. On the other hand we observe a similar pattern while comparing with previous RCCSD work: the previous RCCSD results are 0.7% and 0.6% higher than the experimental value

of  $5s_{1/2} - 5p_{1/2}$  and  $5s_{1/2} - 5p_{3/2}$  experimental data, respectively. For Cs we list our results of  $D_{fi}$  in Table 4.14.

	This Work	Expt.[78]	RCCSD[42]
$6s_{1/2} - 6p_{1/2}$	4.4520	4.4890(65)	4.5443
$6s_{1/2} - 6p_{3/2}$	6.2953	6.3238(73)	6.3919

Table 4.14: Reduced electric dipole matrix element of  $^{133}\text{Cs}$  in a.u

And our result of  $6s_{1/2} - 6p_{1/2}$  transition is 0.8% lower than the experimental data. For the  $6s_{1/2} - 6p_{3/2}$  transition our result is 0.5% lower than the experimental data. The previous RCCSD result is on the higher side, and for the  $6s_{1/2} - 6p_{1/2}$  transition it is 1.2% higher than the experimental value. For the  $6s_{1/2} - 6p_{3/2}$  transition also the previous RCCSD value is 1% higher than the experimental value. So we observe that, overall our results are within 1% of the experimental data.

To conclude this chapter, we discussed the issue of including the triple excitations in the framework of RCC theory. We derived the RCC amplitude equations and define the RCC wave-functions including the triple excitations. After which we discussed the calculation of removal energy and  $D_{fi}$  with the RCC wave-function. We presented our result for the removal energies of ground and excited states of Li, Na, K, Rb and Cs. Overall our results are in very good agreement with the NIST recommended values. We then discussed the results of  $D_{fi}$  for Li, Na, K, Rb and Cs. It is also important to mention that the precise value of  $D_{fi}$  encourages us to calculate the scalar and tensor polarizability with high precision.

# Chapter 5

## Some Applications

The electric dipole polarizability,  $\alpha$ , is the lowest order linear response property relevant to a wide range of physical phenomena related to microscopic and macroscopic properties. Among the macroscopic properties, the dielectric constant and refractive index of gas are the important ones. In the case of microscopic properties, the parity non-conservation in atoms [79], optical atomic clocks [80, 81] and physics with the condensates of dilute atomic gases [82–84] are of current interest. For accurate theoretical calculation of  $\alpha$ , a precise treatment of the electron correlation effects is very important. In the past, a wide variety of atomic many body theories were used to calculate  $\alpha$ . The recent review by Mitroy *et al.* [85] gives a detailed overview of the atomic and ionic polarizabilities. We apply the PRCC theory to calculate  $\alpha$  of closed-shell atoms and ions.

The chapter is organized as follows : we introduce the expression of the static  $\alpha$  in the frame work of time independent perturbation theory. The expression of  $\alpha$  in PRCC theory is then discussed. We then discuss the dipole polarizability diagrams in the PRCC theory. In section 5.2 we discuss about the  $\alpha$  of Ne from PRCC theory in great detail. To test the power of PRCC theory we investigated the term wise contribution to  $\alpha$ . In section 5.4 we provide the detailed description of the  $\alpha$  of noble gas atoms. We also discuss about the core polarization effects and pair correlation effects. Similarly, we study  $\alpha$  of alkali metal ions using PRCC theory in section 5.5. In section 5.6 we discuss the  $\alpha$  of alkaline-Earth metal ions. For both, alkali metal ions and alkaline-Earth metal ions, we investigate the core

polarization pair correlation effects. Then we end the chapter with conclusion.

## 5.1 Theory of dipole polarizability

From the second order time-independent perturbation theory, the ground state dipole polarizability of a closed-shell atom is

$$\alpha = -2 \sum_I \frac{\langle \Psi_0 | \mathbf{D} | \Psi_I \rangle \langle \Psi_I | \mathbf{D} | \Psi_0 \rangle}{E_0 - E_I}, \quad (5.1)$$

where  $|\Psi_I\rangle$  are the intermediate atomic states and  $E_I$  is the energy of the atomic state. As  $\mathbf{D}$  is an odd parity operator,  $|\Psi_I\rangle$  must be opposite in parity to  $|\Psi_0\rangle$ . In the PRCC theory we can write

$$\alpha = - \frac{\langle \tilde{\Psi}_0 | \mathbf{D} | \tilde{\Psi}_0 \rangle}{\langle \tilde{\Psi}_0 | \tilde{\Psi}_0 \rangle}. \quad (5.2)$$

From the definition of  $|\tilde{\Psi}_0\rangle$  in Eq. (3.14) and based on the parity selection rules, only the terms linear in  $\lambda$  are nonzero. That is,

$$\alpha = - \frac{\langle \Phi_0 | \mathbf{T}^{(1)\dagger} \bar{\mathbf{D}} + \bar{\mathbf{D}} \mathbf{T}^{(1)} | \Phi_0 \rangle}{\langle \Psi_0 | \Psi_0 \rangle}, \quad (5.3)$$

where,  $\bar{\mathbf{D}} = e^{T^{(0)\dagger}} \mathbf{D} e^{T^{(0)}}$ , represents the unitary transformed electric dipole operator and  $\langle \Psi_0 | \Psi_0 \rangle$  is the normalization factor. From here on, it is implicit that expressions with more than one operator involves contraction and for compact notation, we drop the notation to represent operator contractions. Retaining the the leading order terms, we obtain

$$\begin{aligned} \alpha \approx & \frac{1}{\mathcal{N}} \langle \Phi_0 | \mathbf{T}_1^{(1)\dagger} \mathbf{D} + \mathbf{D} \mathbf{T}_1^{(1)} + \mathbf{T}_1^{(1)\dagger} \mathbf{D} T_1^{(0)} + T_1^{(0)\dagger} \mathbf{D} \mathbf{T}_1^{(1)} + \mathbf{T}_2^{(1)\dagger} \mathbf{D} T_1^{(0)} \\ & + T_1^{(0)\dagger} \mathbf{D} \mathbf{T}_2^{(1)} + \mathbf{T}_1^{(1)\dagger} \mathbf{D} T_2^{(0)} + T_2^{(0)\dagger} \mathbf{D} \mathbf{T}_1^{(1)} + \mathbf{T}_2^{(1)\dagger} \mathbf{D} T_2^{(0)} + T_2^{(0)\dagger} \mathbf{D} \mathbf{T}_2^{(1)} | \Phi_0 \rangle, \end{aligned} \quad (5.4)$$

where  $\mathcal{N} = \langle \Phi_0 | \exp[T^{(0)\dagger}] \exp[T^{(0)}] | \Phi_0 \rangle$  is the normalization factor, which involves a non-terminating series of contractions between  $T^{(0)\dagger}$  and  $T^{(0)}$ . However, in the present work we use  $\mathcal{N} \approx \langle \Phi_0 | T_1^{(0)\dagger} T_1^{(0)} + T_2^{(0)\dagger} T_2^{(0)} | \Phi_0 \rangle$ . From the above expression of  $\alpha$ , an evident advantage of calculation using PRCC theory is the absence of summation over  $|\Psi_I\rangle$ . The summation is subsumed in the evaluation

of the  $\mathbf{T}^{(1)}$  in a natural way. This is one of the key advantage of using PRCC theory.

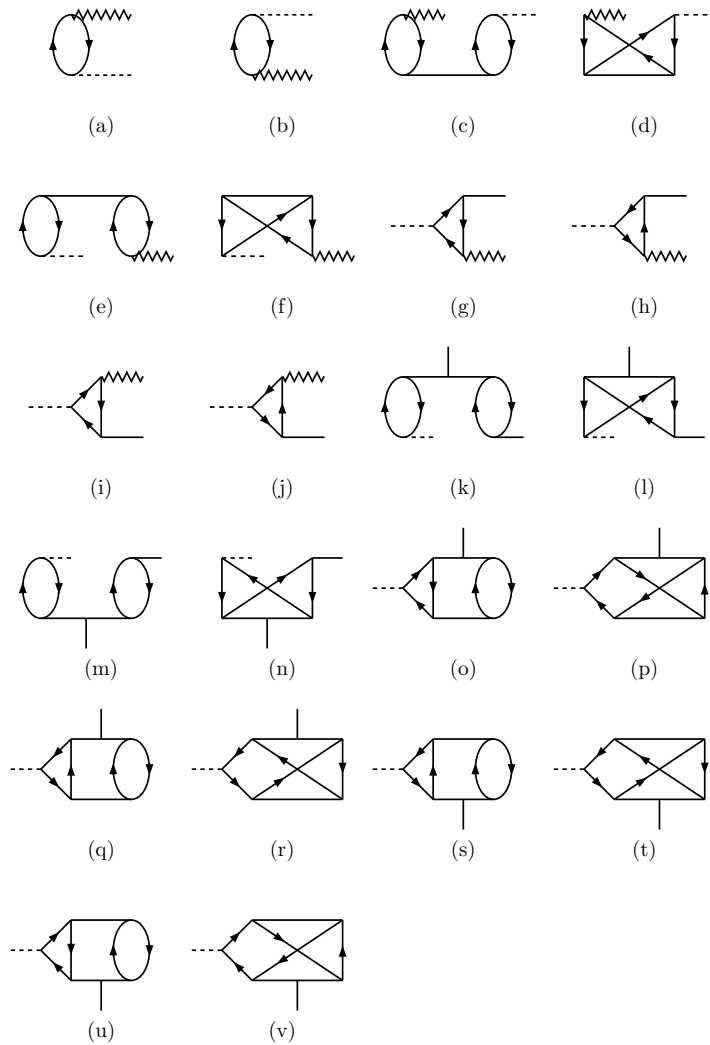


Figure 5.1: Diagrams of the  $\alpha$  in the PRCC theory. The single excitation operators with a wavy line represent  $\mathbf{T}_1^{(1)}$ . Similarly, the double excitation diagrams with an extra vertical line represent  $\mathbf{T}_2^{(1)}$ .

For further analysis and evaluation of the different terms in Eq. (5.4), we use many-body diagrams or Goldstone diagrams. To evaluate the diagrams we follow the notations and conventions given in ref. [61]. However, as described in the previous chapters, there is an additional feature in the diagrams of  $\alpha$ , we employ a wavy interaction line to represent the diagrams of  $\mathbf{T}_1^{(1)}$ , so that it is different from the diagrams of  $T_1^{(0)}$ . Similarly, to represent  $\mathbf{T}_2^{(1)}$  we introduce a

vertical line to the interaction line. After due consideration of the equivalent diagrams, the terms in Eq. (5.4) correspond to 22 unique Goldstone diagrams and these are shown in Fig. 5.1. The equivalent algebraic expression is

$$\begin{aligned}
\alpha = & \sum_{ap} (\tau_a^{p*} d_{ap} + d_{ap}^* \tau_a^p) + \sum_{abpq} [(\tau_a^{p*} d_{bq}^* + \tau_a^{q*} d_{bp}^*) t_{ab}^{pq} + \tilde{t}_{ab}^{pq*} d_{ap} \tau_b^q] + \\
& \sum_{apq} (t_a^{q*} d_{pq} \tau_a^p + \tau_a^{q*} d_{pq} t_a^p) - \sum_{abp} (t_b^{p*} d_{ab} \tau_a^p + \tau_b^{p*} d_{ab} t_a^p) + \sum_{abpq} (\tilde{\tau}_{ab}^{pq*} d_{bq} t_b^q + d_{bq}^* t_b^{q*} \tilde{\tau}_{ab}^{pq}) + \\
& \sum_{abpqr} (\tilde{\tau}_{ab}^{rq*} d_{pr} t_{ab}^{pq} + \tilde{t}_{ab}^{rq*} d_{pr} \tau_{ab}^{pq}) + \sum_{abcpq} (\tilde{\tau}_{cb}^{pq*} d_{ca} t_{ab}^{pq} + \tilde{t}_{cb}^{pq*} d_{ca} \tau_{ab}^{pq}), \tag{5.5}
\end{aligned}$$

where  $d_{ab} = \langle a|d|b\rangle$ , and  $\tilde{\tau}_{ab}^{pq} = \tau_{ab}^{pq} - \tau_{ab}^{qp}$  and  $\tilde{t}_{ab}^{pq} = t_{ab}^{pq} - t_{ab}^{qp}$  are the antisymmetrised cluster amplitudes. In the figure, the first two diagrams, Fig. 5.1(a) and 5.1(b), are the most important ones. These represent  $\mathbf{T}_1^{(1)\dagger} \mathbf{D}$  and  $\mathbf{D} \mathbf{T}_1^{(1)}$ , respectively, and subsume DF and the effects of random phase approximation (RPA). The next two diagrams in the figure, Fig.5.1(c-d), arise from the term  $\mathbf{T}_1^{(1)\dagger} \mathbf{D} \mathbf{T}_2^{(0)}$ , and the diagrams in Fig.5.1(e-f) correspond to the hermitian conjugate,  $T_2^{(0)\dagger} \mathbf{D} \mathbf{T}_1^{(1)}$ . These are the two leading order terms among the second order contributions, in terms of the cluster amplitudes, to  $\alpha$ . The reason is, both the terms consist of dominant RCC and PRCC amplitudes,  $T_2^{(0)}$  and  $\mathbf{T}_1^{(1)}$ , respectively.

Among the second order contributions, the next to leading order terms are  $\mathbf{T}_2^{(1)\dagger} \mathbf{D} \mathbf{T}_2^{(0)}$  and  $T_2^{(0)\dagger} \mathbf{D} \mathbf{T}_2^{(1)}$ . Each of these terms generate four diagrams, Fig.5.1(o-r) and Fig.5.1(s-v) correspond to  $\mathbf{T}_2^{(1)\dagger} \mathbf{D} \mathbf{T}_2^{(0)}$  and  $T_2^{(0)\dagger} \mathbf{D} \mathbf{T}_2^{(1)}$ , respectively. The remaining second order terms,  $\mathbf{T}_1^{(1)\dagger} \mathbf{D} \mathbf{T}_1^{(0)}$ ,  $\mathbf{T}_2^{(1)\dagger} \mathbf{D} \mathbf{T}_1^{(0)}$  and their hermitian conjugates, have marginal contributions to  $\alpha$ . However, for completeness, these are included in the computations.

## 5.2 Results and discussions

### 5.2.1 Dipole polarizability of Neon from PRCC theory

To study PRCC we first consider the linearized version, which we refer to as the linearized PRCC (LPRCC). In this case, there are then 10 diagrams each

in  $\mathbf{T}_1^{(1)}$  and  $\mathbf{T}_2^{(1)}$  cluster equations. However, only 6 of the  $\mathbf{T}_1^{(1)}$  diagrams but all the  $\mathbf{T}_2^{(1)}$  diagrams contribute when Dirac-Hartree-Fock orbitals are used. A detailed descriptions of the diagrammatic calculations are given in ref. [86]. After examining the results from the LPRCC we systematically incorporate other terms, nonlinear in cluster amplitudes, in the PRCC calculations. To optimize the basis set chosen for the calculations, we examine the convergence of  $\alpha$  with the size of basis set. Consider the case of Ne, we start with a basis set of 50 GTOs and do a series of calculations by increasing the basis size in steps. The value of  $\alpha$  converges to 2.6695 when the basis set size is 124. However, for confirmation we increase the basis set size upto 171 and the results are listed in Table. 5.1.

No. of orbitals	Basis size	$\alpha$
50	(10s, 6p, 6d, 4f, 4g)	2.7279
60	(12s, 7p, 7d, 5f, 5g)	2.7087
75	(13s, 9p, 9d, 7f, 6g)	2.6849
91	(15s, 11p, 11d, 8f, 8g)	2.6712
108	(20s, 13p, 11d, 11f, 9g)	2.6696
124	(22s, 14p, 14d, 13f, 10g)	2.6695
145	(27s, 17p, 16d, 14f, 12g)	2.6695
163	(29s, 21p, 17d, 16f, 13g)	2.6695
171	(31s, 23p, 18d, 16f, 13g)	2.6695

Table 5.1: Convergence pattern of  $\alpha$  (Ne) as a function of the basis set size.

In the properties calculations the CC expression of the  $\alpha$ ,  $e^{\mathbf{T}^{(1)\dagger}} \mathbf{D} e^{T^{(0)}} + e^{T^{(0)\dagger}} \mathbf{D} e^{\mathbf{T}^{(1)}}$ , is a non-terminating series. However, as described earlier, in the present calculations we consider upto second order in  $T$ . The contributions from the higher order terms, based on previous studies with an iterative all order method [75], is negligible. The result from the LPRCC theory, along with previous and experimental values, are given in Table. 5.2. It shows that our results agrees very well with the experimental data and indicates that the PRCC theory, even at the linear level, gives accurate results for a single reference system

This work	CCSDT[87]	RCCSDT[88]	MBPT[89]	Expt.[90]
2.6695	2.6648	2.697	2.665	2.670(5)

Table 5.2: The static dipole polarizability,  $\alpha$ , of Ne from linearized PRCC and comparison with previous results.

like Ne. The contributions from different terms in Eq. (5.4) are listed in Table. 5.3. As evident from the table, the dominant contribution arises from  $\{\overline{\mathbf{T}}_1^{(1)\dagger}\mathbf{D}\}$

Contributions from	$\alpha$
$\{\overline{\mathbf{T}}_1^{(1)\dagger}\mathbf{D}\} + \text{h.c.}$	2.6610
$\{\overline{\mathbf{T}}_1^{(1)\dagger}\mathbf{D}T_2^{(0)}\} + \text{h.c.}$	-0.0478
$\{\overline{\mathbf{T}}_1^{(1)\dagger}\mathbf{D}T_1^{(0)}\} + \text{h.c.}$	0.0644
$\{\overline{\mathbf{T}}_2^{(1)\dagger}\mathbf{D}T_1^{(0)}\} + \text{h.c.}$	-0.0062
$\{\overline{\mathbf{T}}_2^{(1)\dagger}\mathbf{D}T_2^{(0)}\} + \text{h.c.}$	0.0961
Normalization	1.0367
Total	2.6695

Table 5.3: Contribution to  $\alpha$  of Ne from different terms of the dressed dipole operator in the linearized PRCC theory.

and its hermitian conjugate. This is not surprising as these terms subsume the DF contribution and core-polarization effects. The general trend is, for closed-shell atoms, the DF and core-polarization effects are the leading order and next to leading order, respectively. Coming to the pair correlation effects, the leading contribution arise from  $\{\overline{\mathbf{T}}_2^{(1)\dagger}\mathbf{D}T_2^{(0)}\}$  and its hermitian conjugate. This is along the expected lines as the  $T_2^{(0)}$  amplitude is larger, compared to  $T_1^{(0)}$ , on account of pair-correlations. The contributions from the remaining terms are small and cancellations reduce the combined contribution even further.

The next level of calculation is to consider all the terms in the non-linear PRCC theory. The term wise contributions are listed in Table. 5.4 and the net result of 2.7383 is 2.6% larger than the LPRCC result. As evident from the table, most of the change is attributed to  $\{\overline{\mathbf{T}}_1^{(1)\dagger}\mathbf{D}\}$  and hermitian conjugate.

CC terms	$\alpha$
$\{\overline{\mathbf{T}_1^{(1)\dagger} \mathbf{D}}\} + \text{h.c.}$	2.7344
$\{\overline{\mathbf{T}_1^{(1)\dagger} \mathbf{D} T_2^{(0)}}\} + \text{h.c.}$	-0.0492
$\{\overline{\mathbf{T}_1^{(1)\dagger} \mathbf{D} T_1^{(0)}}\} + \text{h.c.}$	0.0670
$\{\overline{\mathbf{T}_2^{(1)\dagger} \mathbf{D} T_1^{(0)}}\} + \text{h.c.}$	-0.0058
$\{\overline{\mathbf{T}_2^{(1)\dagger} \mathbf{D} T_2^{(0)}}\} + \text{h.c.}$	0.0924
Normalization	1.0367
Total	2.7383

Table 5.4: Contribution to  $\alpha$  of Ne from different terms of the dressed dipole operator in the nonlinear PRCC theory.

Contribution from this term is 2.7% larger in the nonlinear PRCC, which is comparable to the change in the value of  $\alpha$ . This is one of the case where higher order calculations does not translate to improved accuracy. A similar situation, but in a different context, was observed in a detailed analysis of contributions from nonlinear terms in the CCSD and dressing to calculate the magnetic dipole hyperfine constant of Li [91]. As mentioned in the work referred, the contributions from higher order cluster operators,  $T_3^{(0)}$  and  $T_4^{(0)}$ , could be of different phase and bring  $\alpha$  closer to experimental data.

Contributions	$\{\overline{H_N T_2^{(0)} \mathbf{T}_1^{(1)}}\}$	$\{\overline{H_N T_1^{(0)} T_1^{(0)} \mathbf{T}_2^{(1)}}\}$
$\{\overline{\mathbf{T}_1^{(1)\dagger} \mathbf{D}}\} + \text{h.c.}$	2.7456	2.6628
$\{\overline{\mathbf{T}_1^{(1)\dagger} \mathbf{D} T_2^{(0)}}\} + \text{h.c.}$	-0.0492	-0.0478
$\{\overline{\mathbf{T}_1^{(1)\dagger} \mathbf{D} T_1^{(0)}}\} + \text{h.c.}$	0.0674	0.0642
$\{\overline{\mathbf{T}_2^{(1)\dagger} \mathbf{D} T_1^{(0)}}\} + \text{h.c.}$	-0.0058	-0.0058
$\{\overline{\mathbf{T}_2^{(1)\dagger} \mathbf{D} T_2^{(0)}}\} + \text{h.c.}$	0.0933	0.0922
Normalization	1.0367	1.0367
Total	2.7503	2.6677

Table 5.5: Two of the leading order terms in the nonlinear PRCC Theory.

Through a series of rigorous calculations, we examine the changes in  $\alpha$ , and

associate it with a nonlinear term in PRCC theory. At the second order, there is an anomalously large contribution from  $\{\overline{H_N T_2^{(0)}} \mathbf{T}_1^{(1)}\}$ , it induces a change of 0.0808 a.u. to the net result of  $\alpha$ . This term accounts for the large change of  $\alpha$  in the nonlinear PRCC calculations. Compared to this term, the contribution from the other terms at this order are marginal. The next largest contribution arises from  $\{\overline{H_N T_1^{(0)}} \mathbf{T}_2^{(1)}\}$ , it contributes 0.0086 a.u. The other contributions are 0.0004 and 0.0034 a.u. from  $\{\overline{H_N T_1^{(0)}} \mathbf{T}_1^{(1)}\}$  and  $\{\overline{H_N T_2^{(0)}} \mathbf{T}_2^{(1)}\}$ , respectively.

At the third order  $\{\overline{H_N T_1^{(0)} T_1^{(0)}} \mathbf{T}_1^{(1)}\}$  and  $\{\overline{H_N T_1^{(0)} T_2^{(0)}} \mathbf{T}_2^{(1)}\}$  contribute equally, 0.0077 a.u. each. The contribution from the last term at this order,  $\{\overline{H_N T_1^{(0)} T_1^{(0)} T_2^{(0)}} \mathbf{T}_2^{(1)}\}$ , is  $-0.0018$  a.u. To illustrate the relative changes arising from the third order terms, we list the contributions from the leading order terms in the second and third order in Table. 5.5. It is evident from the table that the difference between the second and third order contributions arises from the  $\{\overline{\mathbf{T}_1^{(1)\dagger} \mathbf{D}}\}$  and its hermitian conjugate.

At the fourth order there is only one term  $\{\overline{H_N T_1^{(0)} T_1^{(0)} T_1^{(0)} T_1^{(0)}} \mathbf{T}_1^{(1)}\}$  and contributes 0.0077 a.u. This detailed study implies that the higher order terms in the PRCC equations, third and fourth order, have negligible effect on  $\alpha$ . Since the effect of the higher terms are tightly coupled to the electron correlation effects, a similar trend may occur in other properties as well. To estimate the

Contributions From	$\{\overline{H_N T_1^{(0)} T_1^{(0)} T_1^{(0)} T_1^{(0)}} \mathbf{T}_1^{(1)}\}$
$\{\overline{\mathbf{T}_1^{(1)\dagger} \mathbf{D}}\} + \text{h.c.}$	2.6688
$\{\overline{\mathbf{T}_1^{(1)\dagger} \mathbf{D} T_2^{(0)}}\} + \text{h.c.}$	-0.0478
$\{\overline{\mathbf{T}_1^{(1)\dagger} \mathbf{D} T_1^{(0)}}\} + \text{h.c.}$	0.0645
$\{\overline{\mathbf{T}_2^{(1)\dagger} \mathbf{D} T_1^{(0)}}\} + \text{h.c.}$	-0.0062
$\{\overline{\mathbf{T}_2^{(1)\dagger} \mathbf{D} T_2^{(0)}}\} + \text{h.c.}$	0.0962
Normalization	1.0367
Total	2.6772

Table 5.6: The contribution to  $\alpha$  from the fourth order term in nonlinear PRCC theory.

uncertainty in our calculations, we have identified two sources in the calculations using PRCC with CCSD approximation. First type of error is associated with the orbital basis set truncation and the termination of iteration while solving the  $\mathbf{T}_1^{(1)}$  and  $\mathbf{T}_2^{(1)}$  equations. Based on the basis set convergence, as described earlier, the uncertainty from the basis set truncation is negligible. Similarly, the uncertainty from the termination of cluster amplitude calculation is negligible as we set  $10^{-7}$  as the convergence criterion. The second type of error arises from the truncation of the CC theory at  $T_2^{(0)}$  and the truncation of  $e^{\mathbf{T}^{(1)\dagger}} \mathbf{D} e^{T^{(0)}} + e^{T^{(0)\dagger}} \mathbf{D} e^{\mathbf{T}^{(1)}}$ . Based on other detailed studies, the contributions from the triples and quadruple excitations could be in the range of  $\approx -2.6\%$ . So that it balances the larger error arising from the inclusion of the nonlinear terms in the PRCC theory. Based our earlier studies with iterative method [75], to incorporate higher order terms in the properties calculations with CC theory, the contributions from the third or higher order in  $e^{\mathbf{T}^{(1)\dagger}} \mathbf{D} e^{T^{(0)}} + e^{T^{(0)\dagger}} \mathbf{D} e^{\mathbf{T}^{(1)}}$  is negligibly small. The contribution from Breit and QED corrections could be another source of error. However, as  $Z\alpha \ll 1$  for Ne, the uncertainty from excluding Breit and QED correction could easily be  $\approx 0.01\%$ . Here,  $\alpha$  is the fine structure constant and is not to be confused with the dipole polarizability. The estimated uncertainty is consistent with the estimates of the contribution from the Breit interaction to correlation energy [74]. Combining all the sources of error, the uncertainty for the calculations with nonlinear PRCC is  $\approx 2.6\%$ . But the uncertainty with linearized PRCC calculations is below  $0.1\%$ . The lower uncertainty associated with the linearized theory is due to the different trends in the contributions from higher order terms.

### 5.2.2 Dipole polarizability of Ar, Kr, Xe and Rn

The  $\alpha$  of the Ar, Kr, Xe and Rn is discussed in this section. To optimize the basis set size, we examine the convergence of  $\alpha$  using the LPRCC theory. We start with a basis set of 50 GTOs and increase the basis set size in steps through a series of calculations. As an example the results for the case of Kr is listed in Table. 5.7. The value of  $\alpha$  changes by only  $7 \times 10^{-4}$  when the number of basis states is increased from 117 to 131. So, we can use the former for our calculations

without compromising the desired accuracy.

No. of orbitals	Basis size	$\alpha$
79	(15s, 9p, 9d, 7f, 7g)	16.8759
97	(17s, 11p, 11d, 9f, 9g)	16.7507
117	(21s, 13p, 13d, 11f, 11g)	16.7403
131	(25s, 15p, 14d, 13f, 11g)	16.7396
139	(25s, 16p, 15d, 13f, 13g)	16.7394
155	(29s, 17p, 16d, 15f, 15g)	16.7394

Table 5.7: Convergence pattern of  $\alpha$  (Kr) as a function of the basis set size.

In this set of calculations we use  $H^{\text{DCB}}$ . With the introduction of the Breit interaction in the total atomic Hamiltonian, the number of two electron integrals becomes large and we need large memory to store these integrals. At the first order MBPT, which we use as the initial guess, there is an important change with the inclusion of  $H^{\text{B}}$ . With only the Coulomb interaction, at the first order MBPT, the wave operator follows the Coulomb parity selection rule and only selected multipoles of the Coulomb interaction contributes. However, with  $H^{\text{B}}$ , which has opposite parity selection rule compared to Coulomb interaction, all multipoles of the two-electron interaction which satisfy the triangular conditions are allowed. In Table 5.8, we list the values of  $\alpha$  calculated using the LPRCC theory. For comparison we have also included the results from previous theoretical studies and experimental data. There are no discernible trends in the previous theoretical results and present work. For Kr and Xe, the results from the many-body perturbation theory (MBPT) [89] is higher than the experimental data, but with RCCSD triples (RCCSDT) approximations [88], Ar and Kr have higher values. For Ar our result is 1% higher than the experimental data and this is consistent with the RCCSDT result reported in a previous work. It must, however, be mentioned that the previous work is based on third-order Douglas-Kroll [92] method. Our result for Kr is in excellent agreement with the experimental data. This could be a coincidence arising from well chosen basis

set parameters and inherent property of PRCC to incorporate correlation effects more completely within a basis set. In the case of Xe our result is 3.4% lower

Method	Ar	Kr	Xe	Rn
RCCSDT[88]	11.22	16.80	27.06	33.18
CCSDT [87]	11.084	16.839	27.293	34.43
MBPT[89]	11.062	17.214	28.223	
This work	11.213	16.736	26.432	35.391
Expt.[93]	11.091	16.740	27.340	
Expt.[94]	11.081(5)	16.766(8)		

Table 5.8: The static dipole polarizability,  $\alpha$  (atomic units), from linearized PRCC and comparison with previous results.

than the experimental data and 2.4 % lower than the RCCSDT result. The later, difference from the the RCCSDT result, can be partly attributed to the triple excitations. There is no experimental data of  $\alpha$  for Rn, the highest  $Z$  atom among the noble gases. In ref. [88], the  $\alpha$  of Rn is computed using RCCSDT and their result is 6.2% lower than our result.

To estimate the importance of Breit interaction, we exclude  $H^B$  in the PRCC calculations and then calculate  $\alpha$ . The results are 11.202, 16.728, 26.404, 35.266 a.u. for Ar, Kr, Xe and Rn respectively. These represent a decrease of 0.010, 0.012, 0.021 and 0.133 a.u. from the results with the inclusion of  $H^B$ . Except for Rn, the change in  $\alpha$  is below 0.1%. This implies that to obtain accurate results for Rn, it is desirable to include Breit interaction in the calculations.

To examine the results in more detail, the contributions from the terms in the expression of  $\alpha$  given in Eq. (5.4) are listed in Table 5.9. It is evident that  $\mathbf{T}_1^{(1)\dagger}\mathbf{D}$  and its hermitian conjugate are the leading order terms. This is to be expected as these terms include the Dirac-Hartree-Fock-Breit contribution and RPA effects, which have the dominant contributions. In all the cases, the result from  $\mathbf{T}_1^{(1)\dagger}\mathbf{D}$  is larger than the total value of  $\alpha$  and shows dependence on  $Z$ : the results of Ar, Kr, Xe and Rn from this term are 8.7%, 11.2%, 16.7% and 17.7%

Contributions from	Ar	Kr	Xe	Rn
$\mathbf{T}_1^{(1)\dagger}\mathbf{D} + \text{h.c.}$	12.191	18.613	30.855	41.641
$\mathbf{T}_1^{(1)\dagger}\mathbf{D}T_2^{(0)} + \text{h.c.}$	-0.545	-0.888	-1.677	-2.328
$\mathbf{T}_2^{(1)\dagger}\mathbf{D}T_2^{(0)} + \text{h.c.}$	0.510	0.748	1.352	1.862
$\mathbf{T}_1^{(1)\dagger}\mathbf{D}T_1^{(0)} + \text{h.c.}$	-0.057	-0.118	-0.357	-0.301
$\mathbf{T}_2^{(1)\dagger}\mathbf{D}T_1^{(0)} + \text{h.c.}$	0.022	0.038	0.092	0.073
Normalization	1.081	1.099	1.145	1.157
Total	11.213	16.736	26.432	35.391

Table 5.9: Contribution to  $\alpha$  from different terms of the dressed dipole operator in the linearized PRCC theory

higher than the total values of  $\alpha$ , respectively. The next to leading order terms are  $\mathbf{T}_1^{(1)\dagger}\mathbf{D}T_2^{(0)}$  and its hermitian conjugate. Contributions from these terms are, approximately, a factor of twenty smaller than the leading order terms and opposite in phase. On a closer inspection, it is natural that  $\mathbf{T}_1^{(1)\dagger}\mathbf{D}T_2^{(0)}$  and its hermitian conjugate are the next to leading order terms. At the second order, these are the terms which have  $\mathbf{T}_1^{(1)}$  and  $T_2^{(0)}$ , the dominant cluster amplitudes in the perturbed and unperturbed relativistic coupled-cluster theories. The results from  $\mathbf{T}_1^{(1)\dagger}\mathbf{D}T_2^{(0)}$  have large cancellations with the term  $\mathbf{T}_2^{(1)\dagger}\mathbf{D}T_2^{(0)}$ , which is almost the same in magnitude but opposite in sign. Interestingly, a similar pattern occurs with the  $\mathbf{T}^{(1)\dagger}\mathbf{D}T_2^{(0)}$  terms. Namely, the results from  $\mathbf{T}_1^{(1)\dagger}\mathbf{D}T_2^{(0)}$  are negative and opposite in sign to  $\mathbf{T}_2^{(1)\dagger}\mathbf{D}T_2^{(0)}$ .

The results from the full PRCC, including the terms nonlinear in cluster amplitudes are given in table 5.10. From the table, it is clear that the nonlinear terms tend to increase the deviations from the experimental data. For Ar, the non-linear PRCC theory result is 5.4% larger than the result from linearized PRCC and it is 6.5% larger than the experimental result. Similarly, for Xe the nonlinear PRCC result is 6.3% larger than the linearized PRCC result. On the other hand for Kr, the non-linear PRCC results are marginally larger than the linearized PRCC results. The larger values of  $\alpha$  in the non-linear PRCC

Contributions from	Ar	Kr	Xe
$\mathbf{T}_1^{(1)\dagger}\mathbf{D} + \text{h.c.}$	12.950	18.622	33.108
$\mathbf{T}_1^{(1)\dagger}\mathbf{D}T_2^{(0)} + \text{h.c.}$	-0.579	-0.899	-1.7964
$\mathbf{T}_2^{(1)\dagger}\mathbf{D}T_2^{(0)}\} + \text{h.c.}$	0.488	0.769	1.278
$\mathbf{T}_1^{(1)\dagger}\mathbf{D}T_1^{(0)} + \text{h.c.}$	-0.061	-0.096	-0.392
$\mathbf{T}_2^{(1)\dagger}\mathbf{D}T_1^{(0)} + \text{h.c.}$	0.022	0.035	0.095
Normalization	1.081	1.099	1.145
Total	11.859	16.771	28.203

Table 5.10: Contribution to  $\alpha$  from different terms of the dressed dipole operator in the non-linear PRCC theory.

can almost entirely be attributed to higher value of  $\mathbf{T}_1^{(1)\dagger}\mathbf{D}$  and its hermitian conjugate. It means that the non-linear terms tend to increase the RPA effects. This is an example where inclusion of higher order terms enhance the uncertainty. It is possible that triple excitations, higher order excitation not considered in the present work, may balance the deviations and bring the results closer to the experimental data.

Ar	Kr	Xe	Rn
8.152 ( $3p_{3/2}$ )	12.872 ( $4p_{3/2}$ )	22.292 ( $5p_{3/2}$ )	34.524 ( $6p_{3/2}$ )
3.914 ( $3p_{1/2}$ )	5.572 ( $4p_{1/2}$ )	8.120 ( $5p_{1/2}$ )	6.502 ( $6p_{1/2}$ )
0.100 ( $3s_{1/2}$ )	0.058 ( $4s_{1/2}$ )	0.222 ( $4d_{5/2}$ )	0.382 ( $5d_{5/2}$ )
0.012 ( $2p_{3/2}$ )	0.056 ( $3d_{5/2}$ )	0.140 ( $4d_{3/2}$ )	0.214 ( $5d_{3/2}$ )

Table 5.11: Core orbital contribution from  $\mathbf{T}_1^{(1)\dagger}\mathbf{D}$  to  $\alpha$ .

For a more detailed analysis of the contributions from the RPA effects, we consider contributions from each of the core orbitals in  $\mathbf{T}_1^{(1)\dagger}\mathbf{D}$ . In terms of orbital indices the expression is

$$\mathbf{T}_1^{(1)\dagger}\mathbf{D} + \text{H.c.} = \sum_{ap} (\mathbf{r}_{ap}\tau_a^p + \tau_a^{p*}\mathbf{r}_{pa}), \quad (5.6)$$

where,  $\mathbf{r}$  is the single particle electric dipole operator. The values of the four

leading core orbitals ( $a$ ) for each of the atoms are listed in Table. 5.11. In all the cases, the result from the outermost  $np_{3/2}$  valence orbitals are the largest. This is not surprising as these are the orbitals which have the largest spatial extent. In addition, as the matrix elements in the expression of  $\alpha$  has a quadratic dependence on radial distance, orbitals with larger radial extent have higher contributions. The next largest values arise from the  $np_{1/2}$  valence orbitals. Here we notice an interesting pattern in the results, with higher  $Z$  the ratio of the contribution from  $np_{3/2}$  to  $np_{1/2}$  increases. For Ar, Kr and Xe the ratios are 2.1, 2.3 and 2.7, respectively. However, the ratio for Rn is much larger, it is 5.3. The reason for the trend in the ratios is the contraction of the  $np_{1/2}$  core orbitals due to relativistic corrections. Hence, the  $np_{1/2}$  valence orbitals of higher  $Z$  atoms show larger contraction and accounts for the higher ratio. The third largest contributions in Ar and Kr arise from the  $3s_{1/2}$  and  $4s_{1/2}$  orbitals, respectively. This is expected as these are the orbitals which are energetically just below the  $np$  orbitals and spatially as well. On the contrary, for Xe and Rn, the third largest contributions must be from the  $5s_{1/2}$  and  $6s_{1/2}$  orbitals, respectively, but this is not case as these orbitals are contracted because of relativistic corrections. So, the diffused  $nd_{5/2}$  orbitals have the third largest values. From the trends in the results of the RPA effects, it is obvious that the relativistic corrections are important for Xe and Rn.

Ar		Kr	
-0.124	$(3p_{3/2}, 3p_{1/2})$	-0.205	$(4p_{3/2}, 4p_{1/2})$
-0.118	$(3p_{3/2}, 3p_{3/2})$	-0.193	$(4p_{3/2}, 4p_{3/2})$
-0.027	$(3p_{1/2}, 3p_{1/2})$	-0.038	$(4p_{1/2}, 4p_{1/2})$
-0.006	$(3p_{3/2}, 3s_{1/2})$	-0.008	$(4p_{3/2}, 3d_{5/2})$

Table 5.12: Core orbitals contribution from  $\mathbf{T}_1^{(1)\dagger}\mathbf{DT}_2^{(0)}$  to  $\alpha$  of Argon and Krypton.

Next, we examine the pair-correlation effects, which manifest through the next to leading order terms,  $\mathbf{T}_1^{(1)\dagger}\mathbf{DT}_2^{(0)}$  and its hermitian conjugate. In terms

of orbital indices

$$\mathbf{T}_1^{(1)\dagger} \mathbf{D} T_2^{(0)} + \text{H.c.} = \sum_{abpq} [(\tau_a^{p*} \mathbf{r}_{bq} - \tau_a^{q*} \mathbf{r}_{bp}) t_{ab}^{pq} + t_{ab}^{pq*} (\tau_a^p \mathbf{r}_{qb} - \tau_a^q \mathbf{r}_{pb})]. \quad (5.7)$$

The values of the four leading terms, listed in terms of the pairs of the core orbitals ( $ab$ ), for Ar and Kr are given in Table. 5.12. From the table we can identify  $(np_{3/2}, np_{1/2})$  as the most dominant pairing of the core-orbitals among the double excitations. Considering that the pairing is between different orbitals, the number of cluster amplitudes is large and this explains the large contribution. The second and third dominant contributions, from the  $(np_{3/2}, np_{3/2})$  and  $(np_{1/2}, np_{1/2})$  pairs, are also on account of number of cluster amplitudes. Since  $np_{3/2}$  and  $np_{1/2}$  each accommodate four and two electrons each, respectively, the former has a larger number of cluster amplitudes. There is a small but important change in the results of Xe and Rn listed in Table. 5.13. The most dominant pair for these atoms is  $(np_{3/2}, np_{3/2})$  and the next dominant pair is  $(np_{3/2}, np_{1/2})$ . This is in contrast to the sequence observed in Ar and Kr. The reason is, although the later pair has more cluster amplitudes, the  $np_{1/2}$  is contracted due to relativistic corrections. So, the contributions to  $\alpha$  from  $T_2^{(0)}$  involving  $np_{1/2}$  is smaller. The difference between the results from the two pairs is even more dramatic in Rn. There are other changes in the case of Rn. The  $(6p_{3/2}, 5d_{5/2})$  pair, involving the diffused  $5d_{5/2}$ , is now the third largest contribution. And the  $(6p_{1/2}, 6p_{1/2})$ , which has the contracted  $6p_{1/2}$  orbital, is the fourth largest contribution. This difference in the sequence of leading contributions for Rn arises from the larger relativistic corrections. Here also we estimate the uncertainty in the calculation of  $\alpha$ . As mentioned in the uncertainty estimation of Ne, here also we have identified few important sources of uncertainty. The first one is the truncation of orbital basis sets. Although we start with 9 symmetry for all the calculations, we increase the number of symmetries upto 13 in steps. The basis set chosen for the results given are after the value of  $\alpha$  converges to  $10^{-4}$ . So, the uncertainty from the basis set truncation is negligible. The second source of uncertainty is the truncation of CC theory at the single and double excitation for both the unperturbed and perturbed RCC theory. Based on earlier studies, the

Xe		Rn	
-0.361	(5p <sub>3/2</sub> , 5p <sub>3/2</sub> )	-0.591	(6p <sub>3/2</sub> , 6p <sub>3/2</sub> )
-0.359	(5p <sub>3/2</sub> , 5p <sub>1/2</sub> )	-0.387	(6p <sub>3/2</sub> , 6p <sub>1/2</sub> )
-0.054	(5p <sub>1/2</sub> , 5p <sub>1/2</sub> )	-0.071	(6p <sub>3/2</sub> , 5d <sub>5/2</sub> )
-0.035	(5p <sub>3/2</sub> , 4d <sub>5/2</sub> )	-0.036	(6p <sub>1/2</sub> , 6p <sub>1/2</sub> )

Table 5.13: Core orbitals contribution from  $\mathbf{T}_1^{(1)\dagger}\mathbf{DT}_2^{(0)}$  to  $\alpha$  of Xenon and Radon.

contributions from the triples and quadruple excitations could be at the most  $\approx 3.3\%$ . This is also consistent with the deviations from the experimental data. Finally, the truncation of  $e^{\mathbf{T}^{(1)\dagger}}\mathbf{D}e^{\mathbf{T}^{(0)}} + e^{\mathbf{T}^{(0)\dagger}}\mathbf{D}e^{\mathbf{T}^{(1)}}$  is another source of uncertainty. From our earlier studies with iterative method [75] to incorporate higher order terms in the properties calculations with CC theory, the contributions from the third or higher order is negligibly small. Quantum electrodynamical (QED) corrections in this set of calculations is another source of uncertainty. However, it is expected to be smaller than the correction from the Breit interaction. As the largest Breit correction, in the case of Rn, is 0.1%, we can assume the corrections from QED effects to be at the most 0.1%. So, adding this, the maximum uncertainty in our calculations is 3.4%. However, it must be emphasized that, for Ar and Kr, the uncertainty is much smaller than this bound.

### 5.2.3 Dipole Polarizability of Alkali Metal Ions

For the case of alkali metal ions, we consider terms up to second order in the cluster operators. We have, however, studied terms which are third order in cluster operators and examined the contributions from the leading order terms. But the contributions are negligible and this validates our choice of considering terms only up to second order in cluster operators. To begin with, we compute  $\alpha$  using the cluster amplitude obtained from the LPRCC and results are presented in Table 5.14. In the table we have listed, for systematic comparison, the experimental data and results from previous theoretical computations.

Atom	LPRCC + Breit	RCCSDT	RRPA [95]	Expt.
Na <sup>+</sup>	1.009	1.00(4)[96]	0.9457	0.9980(33) [97]
K <sup>+</sup>	5.521	5.52(4)[96]	5.457	5.47(5) [98]
Rb <sup>+</sup>	8.986	9.11(4)[96] 9.11(4)[100]	9.076	9.0 [99]
Cs <sup>+</sup>	14.924	15.8(1)[96]	15.81	15.644(5) [101]
Fr <sup>+</sup>	19.506	20.4(2)[96]		

Table 5.14: Static dipole polarizability of alkali ions.

For Na<sup>+</sup> and K<sup>+</sup>, our values of  $\alpha$  are higher than the experimental values by 1% and 0.9%, respectively. However, for Rb<sup>+</sup> and Cs<sup>+</sup> our results are lower than the experimental values by 0.15% and 4.8%, respectively. In comparison to the previous theoretical results, our results of Na<sup>+</sup> and K<sup>+</sup> are in excellent agreement with the previous work which used the RCCSDT method for computation. But, for Rb<sup>+</sup> and Cs<sup>+</sup>, like in the experimental data, our results are lower than the RCCSDT results. One possible reason for the deviations in the heavier ions could be the exclusion of triple excitation cluster operators in the present work. Our result of Fr<sup>+</sup> seems to bear out this reasoning as the same trend (our result is 4.4% lower than the RCCSDT result) is observed in this case as well. However, in absence of experimental data for Fr<sup>+</sup>, it is difficult to arrive at a definite conclusion.

To investigate the importance of Breit interaction,  $H_B$ , in computing  $\alpha$  of the alkali ions, we exclude  $H_B$  in the Hamiltonian and do a set of systematic calculations. Our results for the values of  $\alpha$  are then 1.008, 5.514, 8.973 and 14.908 for Na<sup>+</sup>, K<sup>+</sup>, Rb<sup>+</sup> and Cs<sup>+</sup>, respectively. These values are 0.001, 0.007, 0.013 and 0.016 a.u lower than the results computed using the Dirac-Coulomb-Breit Hamiltonian. This indicates that the correction from the Breit interaction is larger in heavier ions and this is as expected since the stronger nuclear potential in heavier ions translates to larger Breit correction. However, the largest change is  $\sim 0.001\%$  and shows that the contribution from Breit interaction to  $\alpha$  can be

neglected.

For a more detailed study, we examine the contributions from each of the terms in the Eq. (5.4) and these are listed in Table. 5.21. The leading order

Terms + h.c.	Na <sup>+</sup>	K <sup>+</sup>	Rb <sup>+</sup>	Cs <sup>+</sup>	Fr <sup>+</sup>
$\mathbf{T}_1^{(1)\dagger}\mathbf{D}$	1.018	6.043	10.029	17.472	22.926
$\mathbf{T}_1^{(1)\dagger}\mathbf{D}T_2^{(0)}$	-0.018	-0.299	-0.519	-1.023	-1.326
$\mathbf{T}_1^{(1)\dagger}\mathbf{D}T_1^{(0)}$	0.012	-0.038	-0.072	-0.188	-0.126
$\mathbf{T}_2^{(1)\dagger}\mathbf{D}T_1^{(0)}$	-0.001	0.008	0.016	0.039	0.026
$\mathbf{T}_2^{(1)\dagger}\mathbf{D}T_2^{(0)}$	0.023	0.204	0.332	0.654	0.834
Normalization	1.025	1.072	1.089	1.136	1.145
Total	1.009	5.521	8.986	14.924	19.506

Table 5.15: Contribution to  $\alpha$  from different terms and their hermitian conjugates in the linearized PRCC theory.

contribution arises from  $\mathbf{T}_1^{(1)\dagger}\mathbf{D} + \text{h.c}$  and diagrammatically, it corresponds to the first two diagrams in Fig. 5.1. These are also the lowest order terms and are the dominant terms since these subsume the contributions from the Dirac-Fock and RPA effects. For all the ions, the results from the dominant terms exceeds the final results and similar trend is observed in the results of noble gas atoms as well [50, 51]. The next to leading order (NLO) contributions arise from the  $\mathbf{T}_1^{(1)\dagger}\mathbf{D}T_2^{(0)} + \text{h.c}$ . The contributions from these terms are an order of magnitude smaller than  $\mathbf{T}_1^{(1)\dagger}\mathbf{D} + \text{h.c}$  but more importantly, the contributions are opposite in phase. Interestingly, the next important terms  $\mathbf{T}_2^{(1)\dagger}\mathbf{D}T_2^{(0)} + \text{h.c}$  have contributions which nearly cancels the NLO contributions. Continuing further, among the second order terms, the smallest contribution arise from  $\mathbf{T}_2^{(1)\dagger}\mathbf{D}T_1^{(0)} + \text{h.c}$ ., which is perhaps not surprising since  $\mathbf{T}_2^{(1)\dagger}$  and  $T_1^{(0)}$  are the cluster operators with smaller amplitudes in PRCC and RCC theories, respectively. Collecting the results, the net contributions from the second order terms are 0.016, -0.117, -0.223, -0.456 and -0.517 for Na<sup>+</sup>, K<sup>+</sup>, Rb<sup>+</sup>, Cs<sup>+</sup> and Fr<sup>+</sup>, respectively.

Next, we consider all the terms in the PRCC theory, including the terms which are non-linear in cluster operators. The results of  $\alpha$  are presented in the Table 5.16.

Terms + h.c.	Na <sup>+</sup>	K <sup>+</sup>	Rb <sup>+</sup>	Cs <sup>+</sup>
$\mathbf{T}_1^{(1)\dagger}\mathbf{D}$	1.034	6.302	10.438	18.376
$\mathbf{T}_1^{(1)\dagger}\mathbf{D}\mathbf{T}_2^{(0)}$	-0.018	-0.316	-0.544	-1.084
$\mathbf{T}_1^{(1)\dagger}\mathbf{D}\mathbf{T}_1^{(0)}$	0.012	-0.040	-0.076	-0.198
$\mathbf{T}_2^{(1)\dagger}\mathbf{D}\mathbf{T}_1^{(0)}$	-0.0008	0.008	0.016	0.038
$\mathbf{T}_2^{(1)\dagger}\mathbf{D}\mathbf{T}_2^{(0)}$	0.024	0.194	0.308	0.596
Normalization	1.026	1.072	1.090	1.136
Total	1.025	5.735	9.305	15.606

Table 5.16: Contribution to  $\alpha$  from different terms and their conjugate in the PRCC theory after including the terms nonlinear in cluster operators.

For Na<sup>+</sup> the result of  $\alpha$  is 2.6% higher than the experimental value. Similarly, for K<sup>+</sup> and Rb<sup>+</sup> the results are 4.6% and 3.3% higher than the experimental values. For Cs<sup>+</sup> the nonlinear PRCC theory gives a much improved result than the LPRCC results and the deviation from the experimental value is reduced to 0.24%. On a closer examination, most of the change associated with the nonlinear PRCC can be attributed to the increased contribution from  $\mathbf{T}_1^{(1)\dagger}\mathbf{D}$  + h.c. As these terms subsume RPA effects, the increased contributions indicate that RPA effects are larger in the nonlinear PRCC.

To investigate the RPA effects in detail, we isolate the contributions from each of the core spin-orbitals to  $\mathbf{T}_1^{(1)\dagger}\mathbf{D}$  + h.c. and The dominant contributions are presented in Table. 5.22.

It is to be noted that  $\alpha$  has a quadratic dependence on the radial distance, so the orbitals with larger spatial extent contribute dominantly. The effect of this is discernible in the results, for all the alkali ions the leading contribution to  $\alpha$  arises from the outermost  $np_{3/2}$  orbital, which is the occupied orbital with largest radial extent. The next leading contribution arise from the  $np_{1/2}$  orbital.

Na <sup>+</sup>	K <sup>+</sup>	Rb <sup>+</sup>	Cs <sup>+</sup>	Fr <sup>+</sup>
0.652 (2p <sub>3/2</sub> )	4.016 (3p <sub>3/2</sub> )	6.858 (4p <sub>3/2</sub> )	12.375 (5p <sub>3/2</sub> )	18.287 (6p <sub>3/2</sub> )
0.322 (2p <sub>1/2</sub> )	1.938 (3p <sub>1/2</sub> )	3.038 (4p <sub>1/2</sub> )	4.735 (5p <sub>1/2</sub> )	4.073 (6p <sub>1/2</sub> )
0.044 (2s <sub>1/2</sub> )	0.076 (3s <sub>1/2</sub> )	0.058 (4s <sub>1/2</sub> )	0.192 (4d <sub>5/2</sub> )	0.376 (5d <sub>5/2</sub> )
0.0004 (1s <sub>1/2</sub> )	0.008 (2p <sub>3/2</sub> )	0.044 (3d <sub>5/2</sub> )	0.121 (4d <sub>3/2</sub> )	0.211 (5d <sub>3/2</sub> )

Table 5.17: Four leading contributions to  $\{\mathbf{T}_1^{(1)\dagger}\mathbf{D} + \text{h.c.}\}$  to  $\alpha$  in terms of the core spin-orbitals.

An important observation is, as we proceed from from lower  $Z$  to higher  $Z$ , the ratio of contribution of  $np_{3/2}$  to the  $np_{1/2}$  increases. It is 1.8, 2.1, 2.3, 2.6 and 4.5 for Na<sup>+</sup>, K<sup>+</sup>, Rb<sup>+</sup>, Cs<sup>+</sup> and Fr<sup>+</sup> respectively. The ratio is much larger in the case Fr<sup>+</sup> and without any ambiguity it can be attributed to the relativistic contraction of the  $np_{1/2}$  orbital. The third leading contribution for Na<sup>+</sup>, K<sup>+</sup>, Rb<sup>+</sup> arise from the 2s<sub>1/2</sub>, 3s<sub>1/2</sub> and 4s<sub>1/2</sub> orbital respectively. But, for Cs<sup>+</sup> and Fr<sup>+</sup> the third leading contribution arise from 4d<sub>5/2</sub> and 5d<sub>5/2</sub> orbital respectively. This is because the 5s<sub>1/2</sub> and 6s<sub>1/2</sub> orbital are contracted due to large relativistic effects. From the above analysis of RPA effects, the trend in the contributions demonstrates the importance of relativistic corrections in Cs<sup>+</sup> and Fr<sup>+</sup>.

Na <sup>+</sup>		K <sup>+</sup>	
-0.0040	(2p <sub>3/2</sub> , 2p <sub>3/2</sub> )	-0.0646	(3p <sub>3/2</sub> , 3p <sub>3/2</sub> )
-0.0021	(2p <sub>3/2</sub> , 2p <sub>1/2</sub> )	-0.0367	(3p <sub>3/2</sub> , 3p <sub>1/2</sub> )
-0.0021	(2p <sub>1/2</sub> , 2p <sub>3/2</sub> )	-0.0360	(3p <sub>1/2</sub> , 3p <sub>3/2</sub> )
-0.0010	(2p <sub>1/2</sub> , 2p <sub>1/2</sub> )	-0.0148	(3p <sub>1/2</sub> , 3p <sub>1/2</sub> )

Table 5.18: Core orbitals contribution from  $\mathbf{T}_1^{(1)\dagger}\mathbf{DT}_2^{(0)}$  to  $\alpha$  of Na<sup>+</sup> and K<sup>+</sup>.

To study the pair-correlation effects, we identify the pairs of core spin-orbitals in the next leading order terms  $\mathbf{T}_1^{(1)\dagger}\mathbf{DT}_2^{(0)} + \text{h.c.}$  The four leading order pairs for Na<sup>+</sup> and K<sup>+</sup>, and Rb<sup>+</sup>, Cs<sup>+</sup> and Fr<sup>+</sup> are listed in table 5.18 and 5.19 respectively. The dominant contribution, for all the ions, arise from the combination ( $np_{3/2}, np_{3/2}$ ) orbital pairing. To illustrate the relative values, the contributions

from the pairs of the five outermost core spin-orbitals of  $\text{Rb}^+$  is shown as a barchart in Fig. 5.2.

$\text{Rb}^+$		$\text{Cs}^+$		$\text{Fr}^+$	
-0.1113	$(4p_{3/2}, 4p_{3/2})$	-0.2126	$(5p_{3/2}, 5p_{3/2})$	-0.3078	$(6p_{3/2}, 6p_{3/2})$
-0.0601	$(4p_{3/2}, 4p_{1/2})$	-0.1073	$(5p_{3/2}, 5p_{1/2})$	-0.1266	$(6p_{3/2}, 6p_{1/2})$
-0.0565	$(4p_{1/2}, 4p_{3/2})$	-0.0930	$(5p_{1/2}, 5p_{3/2})$	-0.0828	$(6p_{1/2}, 6p_{3/2})$
-0.0223	$(4p_{1/2}, 4p_{1/2})$	-0.0347	$(5p_{1/2}, 5p_{1/2})$	-0.0489	$(6p_{3/2}, 5d_{5/2})$

Table 5.19: Core orbitals contribution from  $\mathbf{T}_1^{(1)\dagger}\mathbf{DT}_2^{(0)}$  to  $\alpha$  of  $\text{Rb}^+$ ,  $\text{Cs}^+$  and  $\text{Fr}^+$ .

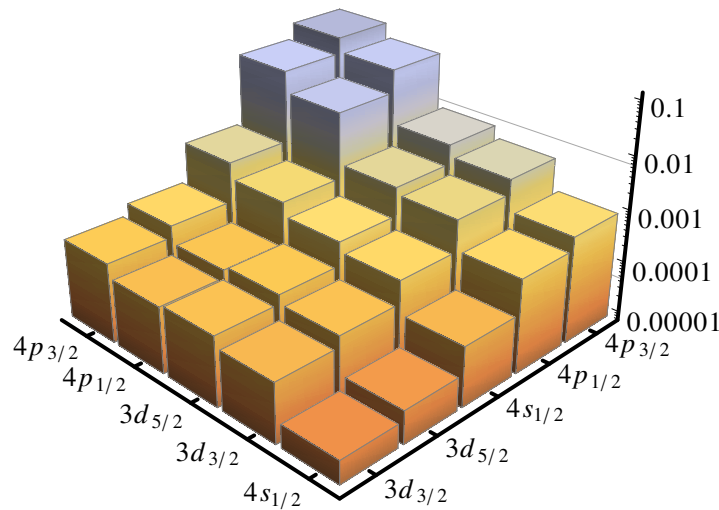


Figure 5.2: Contributions to the next to leading order terms  $\mathbf{T}_1^{(1)\dagger}\mathbf{DT}_2^{(0)} + \text{h.c.}$  in terms of the pairs of core spin-orbitals.

Comparing the results of all the ions, there is a major difference in the results of  $\text{Fr}^+$ . For  $\text{Fr}^+$  the fourth largest contribution is from the  $(6p_{3/2}, 5d_{5/2})$  pair, whereas for the other ions it is  $(np_{1/2}, np_{1/2})$ . This is again a consequence of the contraction of the  $6s_{1/2}$  spin-orbital in  $\text{Fr}^+$  due to relativistic effects.

Coming to the uncertainty estimates of the results of alkali ions, we have identified the following important sources and based on these we calculate the uncertainty in our results. The truncation of the spin-orbital basis sets is one of

the possible source. For all the ions we start the computations with 9 symmetries and increase up to 13 symmetries. Along with it, we also vary the number of the spin-orbitals till  $\alpha$  converges to  $\approx 10^{-4}$ . So, we can safely neglect this uncertainty for our calculations. Another source of uncertainty is the truncation of the CC theory at the single and double excitation for both unperturbed and the perturbed RCC theories. The truncation of  $e^{\mathbf{T}^{(1)\dagger}} \mathbf{D} e^{\mathbf{T}^{(0)}} + e^{\mathbf{T}^{(0)\dagger}} \mathbf{D} e^{\mathbf{T}^{(1)}}$  at the second order in cluster operator is also a source of uncertainty. However, from our earlier studies [75] and our studies on the contribution from third order terms, the contribution from higher orders is negligibly small. The quantum electrodynamical(QED) corrections is another source of uncertainty in our calculations and based on our previous studies, we estimate it at 0.1%. In total, we estimate the maximum uncertainty in our results as  $\approx 3.4\%$ . For lighter ions, the uncertainty is much lower.

#### 5.2.4 Dipole Polarizability of Alkaline-Earth Metal Ions

As mentioned earlier, for the case of alkaline-Earth metal ions also we consider up to second order in cluster amplitudes. However, considering that the cluster operators  $T_2^{(0)}$  and  $\mathbf{T}_1^{(1)}$  accounts for more than 95% of the many-body effects in RCC and PRCC, the terms considered in Eq. (5.4) give very accurate results. To verify, we have examined the leading terms which are third order in cluster amplitudes and find the contributions are  $\sim 10^{-4}$ . So, for the present work, as we consider  $\alpha$  upto third decimal place, it is appropriate to neglect the contributions from terms which are third and higher order in cluster operators.

In table 5.20 we list the  $\alpha$  of alkaline-Earth metal ions  $\text{Mg}^{2+}$ ,  $\text{Ca}^{2+}$ ,  $\text{Sr}^{2+}$ ,  $\text{Ba}^{2+}$  and  $\text{Ra}^{2+}$  computed using Eq. (5.4). The results are based on two sets of calculations: one is based on the cluster amplitudes obtained from LPRCC and the other is based on PRCC. For a systematic comparison we also list the previous theoretical and experimental results. The results of  $\alpha$  along with the orbital energy corrections arising from  $V_{\text{Ue}}(r)$  for each of the ions are discussed in the subsequent sections.

Atom	This Work	Method	Previous Works	Method
$\text{Mg}^{2+}$	0.489	(LPRCC)	0.469 <sup>1</sup>	RRPA
	0.495	(PRCC)	0.489(5) <sup>2</sup>	Expt.
$\text{Ca}^{2+}$	3.284	(LPRCC)	3.262 <sup>3</sup>	RCCSDT
	3.387	(PRCC)	3.254 <sup>1</sup>	RRPA
			3.26(3) <sup>2</sup>	Expt.
$\text{Sr}^{2+}$	5.748	(LPRCC)	5.792 <sup>3</sup>	RCCSDT
	5.913	(PRCC)	5.813 <sup>1</sup>	RRPA
$\text{Ba}^{2+}$	10.043	(LPRCC)	10.491 <sup>3</sup>	RCCSDT
	10.426	(PRCC)	10.61 <sup>1</sup>	RRPA
$\text{Ra}^{2+}$	12.908	(LPRCC)	13.361 <sup>3</sup>	RCCSDT
	13.402	(PRCC)		

Table 5.20: Static dipole polarizability of doubly ionized alkaline-Earth-metal ions and the values are in atomic units.

### $\text{Mg}^{2+}$

The  $\alpha$  of  $\text{Mg}^{2+}$  computed with LPRCC is in excellent agreement with the experimental data. However, the PRCC result is 1.2% higher than the LPRCC result and experimental data. This may be due to a part of the additional many-body effects arising from the nonlinear terms in the cluster amplitude equations, but which may ultimately cancel with the contributions from the cluster amplitudes of higher excitations like  $T_3^{(0)}$  and  $\mathbf{T}_3^{(1)}$ . The RRPA result is 4.1% lower than the experimental data and it is also lower than both the LPRCC and PRCC results. It must be added that a similar trend is observed for the  $\text{Na}^+$  ion [103], which is isoelectronic with  $\text{Mg}^{2+}$ , the RRPA result of  $\alpha$  is lower than the experimental data [95]. This trend may be on account of the inherent strength and limitation

of RRPA, the potential to incorporate core-polarization effects very accurately and weakness to account for pair correlation effects. To estimate the contribution from the Breit interaction we consider the Dirac-Coulomb Hamiltonian with the VP potential. The contribution from the Breit interaction can be safely neglected for this ion as the contribution is less than 0.02%.

### Ca<sup>2+</sup>

For Ca<sup>2+</sup>, the LPRCC result of  $\alpha$  is within the experimental uncertainty and it is in good agreement with the result from a previous work, which is based on the RCCSDT theory. The PRCC result is 3.1% larger than the LPRCC result and deviates from the experimental data by 3.7%. On the other hand, the result from the RRPA [95], like in Mg<sup>2+</sup>, is lower than the experimental data. Based on another set of calculations with the Dirac-Coulomb Hamiltonian, the contribution from the Breit interaction is estimated to be 0.004, which is a mere  $\approx 0.1\%$  of the total value.

### Sr<sup>2+</sup>

For Sr<sup>2+</sup> it is important to have accurate theoretical results as there are no experimental data of  $\alpha$ . From the Table 5.20 the LPRCC result of 5.748 is in very good agreement with the previous work using RCCSDT. And, like in the previous cases, the PRCC result of 5.913 is larger than the LPRCC result. Comparing the results from different theoretical methods, we observe the emergence of two important changes in the relative patterns when compared with the results results of Mg<sup>2+</sup> and Ca<sup>2+</sup>. First, the RRPA result is higher than both the LPRCC and RCCSDT results, and second, the RCCSDT result is larger than the LPRCC result. This may be on account of the filled  $3d$  shell in Sr<sup>2+</sup>. As it is of higher angular momentum, it has larger polarization effects as well as pair correlation effects. A method like RRPA incorporates the core-polarization effects very accurately but could potentially under estimate the pair correlation effects. Not surprisingly, the same trends are observed in the heavier ions Ba<sup>2+</sup> and Ra<sup>2+</sup> with filled  $d$  and  $f$  shells. Based on a comparison with the calculations using the

Dirac-Coulomb Hamiltonian, we estimate the Breit contribution as 0.005. This is negligibly small and similar in magnitude to the case of  $\text{Ca}^{2+}$ .

### $\text{Ba}^{2+}$

Like in  $\text{Sr}^{2+}$ , there are no experimental data of  $\alpha$  for  $\text{Ba}^{2+}$ . Hence, it is important to have accurate theoretical results and in this regard, it is pertinent to calculate  $\alpha$  with a reliable method like RCC. Here, computing with the relativistic version coupled-cluster is essential as the high  $Z$  implies that the relativistic corrections are important. From Table. 5.20, it is evident that our LPRCC result of 10.043 is 4.3% lower than the RCCSDT result. However, our PRCC result is in very good agreement with the RCCSDT result, it is just 0.6% less. Examining the results discussed so far, there is a discernible trend when we compare the PRCC and RCCSDT results. The difference between the two results narrows with increasing  $Z$ . This may be due to the the basic property of the CCT, the inclusion of selected electron correlation effects to all order. So, with higher  $Z$  the importance of the correlation effects grows and the two coupled-cluster based methods incorporate the correlation effects to similar accuracy. The other theoretical result from the RRPA theory is larger than the other results. Following the computations described earlier, we estimate the Breit contribution as 0.007, which is similar to the previous cases.

### $\text{Ra}^{2+}$

Our PRCC result of  $\alpha$  for  $\text{Ra}^{2+}$  is  $\approx 3.7\%$  larger than the LPRCC result. This trend is similar to the case of  $\text{Ba}^{2+}$  and may be attributed to better accounting of correlation effects in PRCC. To be more precise, the importance of the correlation effects grows with increasing number of electrons, but, LPRCC theory is insufficient to incorporate the correlation effects as it considers only the linear terms. The PRCC theory, which includes the nonlinear terms, provides a better description of the electron correlations. This is borne by the fact that the PRCC results are in good agreement with the RCCSDT results, the difference between the two results is just  $\approx 0.3\%$ . Like in the previous cases, the contribution from

the Breit interaction is small and the value is 0.008.

Terms + h.c.	Mg <sup>2+</sup>	Ca <sup>2+</sup>	Sr <sup>2+</sup>	Ba <sup>2+</sup>	Ra <sup>2+</sup>
LPRCC results					
$\mathbf{T}_1^{(1)\dagger}\mathbf{D}$	0.496	3.594	6.400	11.708	15.160
$\mathbf{T}_1^{(1)\dagger}\mathbf{D}\mathbf{T}_2^{(0)}$	-0.008	-0.180	-0.330	-0.676	-0.864
$\mathbf{T}_1^{(1)\dagger}\mathbf{D}\mathbf{T}_1^{(0)}$	0.001	-0.022	-0.044	-0.114	-0.108
$\mathbf{T}_2^{(1)\dagger}\mathbf{D}\mathbf{T}_1^{(0)}$	-0.0001	0.004	0.008	0.020	0.018
$\mathbf{T}_2^{(1)\dagger}\mathbf{D}\mathbf{T}_2^{(0)}$	0.008	0.098	0.174	0.370	0.470
Normalization	1.019	1.064	1.080	1.126	1.137
Total	0.489	3.284	5.748	10.043	12.908
PRCC results					
$\mathbf{T}_1^{(1)\dagger}\mathbf{D}$	0.502	3.718	6.606	12.214	15.820
$\mathbf{T}_1^{(1)\dagger}\mathbf{D}\mathbf{T}_2^{(0)}$	-0.008	-0.188	-0.344	-0.710	-0.908
$\mathbf{T}_2^{(1)\dagger}\mathbf{D}\mathbf{T}_2^{(0)}$	0.002	-0.022	-0.046	-0.120	-0.114
$\mathbf{T}_1^{(1)\dagger}\mathbf{D}\mathbf{T}_1^{(0)}$	-0.0001	-0.004	0.008	0.018	0.016
$\mathbf{T}_2^{(1)\dagger}\mathbf{D}\mathbf{T}_1^{(0)}$	0.008	0.092	0.162	0.338	0.424
Normalization	1.019	1.064	1.080	1.126	1.137
Total	0.495	3.387	5.913	10.426	13.402

Table 5.21: Contribution to  $\alpha$  from different terms and their hermitian conjugates in the LPRCC and PRCC theory.

### Core-polarization and pair correlation effects

In the previous sections we discussed the comparison between the results from different theories, general trends and orbital energy corrections from VP. To examine and investigate the contributions from various many-body effects, which are encapsulated in different terms of LPRCC and PRCC, we isolate the contributions from different terms through a series of computations. The results are listed in Table. 5.21. From the table it is evident that the leading term in the LPRCC as well as PRCC theory is  $\{\mathbf{T}_1^{(1)\dagger}\mathbf{D} + \text{h.c.}\}$ . This is not surprising as it

is the term which subsumes the DF contribution and the RPA effects. Now to understand and quantify the RPA effects in these systems, we separate the core orbital contribution to  $\alpha$ .

Mg <sup>2+</sup>	Ca <sup>2+</sup>	Sr <sup>2+</sup>
0.312 (2p <sub>3/2</sub> )	2.378 (3p <sub>3/2</sub> )	4.344 (4p <sub>3/2</sub> )
0.154 (2p <sub>1/2</sub> )	1.148 (3p <sub>1/2</sub> )	1.940 (4p <sub>1/2</sub> )
0.028 (2s <sub>1/2</sub> )	0.056 (3s <sub>1/2</sub> )	0.048 (4s <sub>1/2</sub> )
0.0002(1s <sub>1/2</sub> )	0.006 (2p <sub>3/2</sub> )	0.034 (3d <sub>5/2</sub> )
Ba <sup>2+</sup>	Ra <sup>2+</sup>	
8.182 (5p <sub>3/2</sub> )	11.766 (6p <sub>3/2</sub> )	
3.188 (5p <sub>1/2</sub> )	2.822 (6p <sub>1/2</sub> )	
0.162 (4d <sub>5/2</sub> )	0.338 (5d <sub>5/2</sub> )	
0.102 (4d <sub>3/2</sub> )	0.192 (5d <sub>3/2</sub> )	

Table 5.22: Four leading contributions to  $\{\mathbf{T}_1^{(1)\dagger}\mathbf{D} + \text{h.c.}\}$  to  $\alpha$  in terms of the core spin-orbitals.

The four dominant contributions from the core orbitals to  $\{\mathbf{T}_1^{(1)\dagger}\mathbf{D} + \text{h.c.}\}$  are listed in table 5.22. For all the ions, the outermost  $p_{3/2}$  orbital is the most dominant and this because of the larger radial extent of the  $p_{3/2}$  orbitals. The next important contribution arises from the outermost  $p_{1/2}$ . A prominent feature that we observe in the results is the ratio between the contribution from the outermost  $p_{3/2}$  to the  $p_{1/2}$  orbitals. The ratio are 2.03, 2.07, 2.24, 2.57 and 4.17 for Mg<sup>2+</sup>, Ca<sup>2+</sup>, Sr<sup>2+</sup>, Ba<sup>2+</sup> and Ra<sup>2+</sup>, respectively. The ratio increase with increasing  $Z$  but for Ra<sup>2+</sup> it is 1.6 times higher than the Ba<sup>2+</sup>. This is an important feature arising from the contraction of  $p_{1/2}$  orbitals due to the relativistic effects, which is more prominent in the heavier atoms and ions. The third largest contribution arise from  $ns_{1/2}$  orbital in the case of Mg<sup>2+</sup>, Ca<sup>2+</sup> and Sr<sup>2+</sup>. This is because the  $ns_{1/2}$  orbital is energetically lower than the  $np_{1/2}$  and relativistic corrections are not large. However, for Ba<sup>2+</sup> and Ra<sup>2+</sup>, due to the relativistic contraction, the contribution from the outermost  $ns_{1/2}$  is suppressed.

And, the third largest contribution arises from the more diffused outer  $nd_{5/2}$  orbital.

The next leading contribution arises from  $\{\mathbf{T}_1^{(1)\dagger}\mathbf{D}T_2^{(0)} + \text{h.c.}\}$ . The contribution from this term is much smaller and opposite in phase to the leading order term. A similar trend is observed in case of the noble gas atoms and was reported in one of our previous works [51]. Among the various terms the  $\{\mathbf{T}_1^{(1)\dagger}\mathbf{D}T_1^{(0)} + \text{h.c.}\}$  has the smallest contribution. This is because of the fact that  $T_1^{(0)}$  and  $\mathbf{T}_2^{(1)}$  have smaller amplitudes in the RCC and PRCC theories, respectively. As can be seen from the table 5.21, the overall contribution from the second order terms are 0.0009, -0.100, -0.192, -0.400, -0.484 for  $\text{Mg}^{2+}$ ,  $\text{Ca}^{2+}$ ,  $\text{Sr}^{2+}$ ,  $\text{Ba}^{2+}$  and  $\text{Ra}^{2+}$ , respectively. Except for  $\text{Mg}^{2+}$ , the higher order terms gives a negative contribution to the  $\alpha$ .

To study the pair-correlation effects we examine the next to leading order term,  $\mathbf{T}_1^{(1)\dagger}\mathbf{D}T_2^{(0)}$  in more detail. In Table 5.23, 5.24 we list the four leading order core-orbital pairs which contribute to  $\alpha$ . The  $(np_{3/2}, np_{3/2})$  orbital pairing gives the most dominant contribution. The next leading order contribution arises from the  $(np_{3/2}, np_{1/2})$  orbital pairing. The same pattern is observed for all the doubly charged ions. For  $\text{Ra}^{2+}$  the fourth largest contribution arise from  $(6p_{3/2}, 5d_{5/2})$  orbital pairing, but for other ions it is from  $(np_{1/2}, np_{1/2})$  orbital pairing. This is because of the relativistic effects, which contracts the outer  $s_{1/2}$  orbital in  $\text{Ra}^{2+}$  more than the other ions. One important point to notice here is the higher order terms does not translate to higher accuracy as observed in the case of  $\text{Mg}^{2+}$  and  $\text{Ca}^{2+}$ .

$\text{Mg}^{2+}$		$\text{Ca}^{2+}$	
-0.002	$(2p_{3/2}, 2p_{3/2})$	-0.038	$(3p_{3/2}, 3p_{3/2})$
-0.001	$(2p_{3/2}, 2p_{1/2})$	-0.022	$(3p_{3/2}, 3p_{1/2})$
-0.001	$(2p_{1/2}, 2p_{3/2})$	-0.022	$(3p_{1/2}, 3p_{3/2})$
-0.0004	$(2p_{1/2}, 2p_{1/2})$	-0.009	$(3p_{1/2}, 3p_{1/2})$

Table 5.23: Core orbitals contribution from  $\mathbf{T}_1^{(1)\dagger}\mathbf{D}T_2^{(0)}$  to  $\alpha$  of  $\text{Mg}^{2+}$  and  $\text{Ca}^{2+}$ .

Sr <sup>2+</sup>		Ba <sup>2+</sup>		Ra <sup>2+</sup>	
-0.069	(4p <sub>3/2</sub> , 4p <sub>3/2</sub> )	-0.132	(5p <sub>3/2</sub> , 5p <sub>3/2</sub> )	-0.186	(6p <sub>3/2</sub> , 6p <sub>3/2</sub> )
-0.038	(4p <sub>3/2</sub> , 4p <sub>1/2</sub> )	-0.070	(5p <sub>3/2</sub> , 5p <sub>1/2</sub> )	-0.077	(6p <sub>3/2</sub> , 6p <sub>1/2</sub> )
-0.036	(4p <sub>1/2</sub> , 4p <sub>3/2</sub> )	-0.061	(5p <sub>1/2</sub> , 5p <sub>3/2</sub> )	-0.052	(6p <sub>1/2</sub> , 6p <sub>3/2</sub> )
-0.014	(4p <sub>1/2</sub> , 4p <sub>1/2</sub> )	-0.022	(5p <sub>1/2</sub> , 5p <sub>1/2</sub> )	-0.039	(6p <sub>3/2</sub> , 5d <sub>5/2</sub> )

Table 5.24: Core orbitals contribution from  $\mathbf{T}_1^{(1)\dagger}\mathbf{DT}_2^{(0)}$  to  $\alpha$  of Sr<sup>2+</sup>, Ba<sup>2+</sup> and Ra<sup>2+</sup>.

### Theoretical Uncertainty

The sources of uncertainty are similar to the earlier cases. Based on a series of test calculations, we estimate the contribution from triple excited cluster amplitudes to less than 0.2% of the total value. So, we can consider the upper bound on the uncertainty from the truncation of the RCC and PRCC theories as 0.4% for the heavier ions Sr<sup>2+</sup>, Ba<sup>2+</sup> and Ra<sup>2+</sup>. Examining the trend in the results of Mg<sup>2+</sup> and Ca<sup>2+</sup>, the uncertainty is likely to be higher for the PRCC results of these ions. But, the LPRCC results could have an uncertainty less than  $\approx 0.4\%$ . The other source of error is the truncation of the non-terminating series of  $\alpha$ . We terminate  $e^{\mathbf{T}^{(1)\dagger}}\mathbf{D}e^{T^{(0)}} + e^{T^{(0)\dagger}}\mathbf{D}e^{\mathbf{T}^{(1)}}$  at the second order in cluster operator. However, based on our earlier study [75], where we reported an iterative technique to calculate properties to all order, the contribution from the third and higher order terms is negligible. So, the uncertainty arising from the truncation in the expression of  $\alpha$  can be neglected. Quantum electrodynamic (QED) corrections is another source of uncertainty in the present calculation. We include the VP potential in the present work but the self-energy part of the radiative corrections is neglected. The self-energy correction is important for the heavy atoms [15]. We can, however, safely neglect it from the error estimates as the contribution is less than the correction from Breit interaction, which accounts for at the most 0.1% of the total value. So, considering all the sources, the upper bound on the uncertainty of the present calculations is  $\approx 0.4\%$  for the LPRCC results of Mg<sup>2+</sup> and Ca<sup>2+</sup>, and PRCC results of Sr<sup>2+</sup>, Ba<sup>2+</sup> and Ra<sup>2+</sup> ions.

# Chapter 6

## Future Directions and Discussions

The present thesis examines the QED corrections in atoms and ions. In this work we develop the RCCSDT theory with  $H^{\text{DCB}}$  as the atomic Hamiltonian. Along with this we consider the vacuum polarization correction to the orbital energies. This approach provides a platform to study the relativistic, correlation and QED effects in heavy atoms. To test the effect of  $T_3^{(0)}$  we study the correlation and excitation energies, electric dipole transition amplitudes. Our results are compatible with the previous RCCSD works. We must emphasize that there is scope to improve on the present work. As we mentioned earlier, we have only considered the vacuum polarization part of the QED corrections in the present work. In future we will focus on incorporating the self energy and the vertex correction to obtain a lowest order QED corrections in atoms.

There is tremendous progress in the field of highly charged ions in the past decades [104]. It is worth to mention that RCC theory can be used to verify the precision experimental results of highly charged ions. It has been pointed out that atomic clocks with exceptional high accuracy can be build using the highly charged ions [105]. For this it is important to develop high precision atomic many body methods and essentially, coupled-cluster theory is one of the leading candidate to test it.

The PRCC theory is a general extension of the RCC method to incorporate an

additional perturbation. The present thesis demonstrates that it is suitable for properties calculations for closed-shell atoms and ions. Although, in the present thesis we have used PRCC theory to calculate electric dipole polarizability, the method can be extended to calculate other atomic properties as well. The nuclear spin dependent parity non-conservation (NSD PNC), which provides an important window to test the physics beyond standard model, can be studied using the PRCC theory [86, 106]. In future we would like to incorporate the QED effects to study the NSD PNC in atoms.

Time dependent coupled-cluster theory is another emerging field that can be studied in future. It is always important to study the dynamics of electrons in many electron atoms. Now with the advent of high power Lasers, experimentally it is possible to study the dynamics of electrons. There is certainly a scope to go beyond the time dependent Hartree-Fock theory to incorporate the correlation effects precisely using the time dependent CCT. The time dependent CCT is studied in the nuclear physics [107] as well as in quantum chemistry [108]. A future possibility is to study the dynamics of the electrons in the framework of time dependent coupled-cluster theory.

# Appendix A

## Matrix Element of Breit Interaction

The matrix element of the Breit interaction is necessary to consider the Breit Hamiltonian at the DHF SCF method as well as in the RCC theory. Here we will follow the treatment of Grant and his coworkers [18, 63, 65, 66].

The interaction strength for the Breit interaction is

$$\begin{aligned}
 X_{\text{Br}}^k(abcd) = & (-1)^k \langle j_a || C^k || j_c \rangle \langle j_b || C^k || j_d \rangle \{j_a j_c k\} \{j_b j_d k\} \times \\
 & \left( \sum_{\nu=k-1}^{k+1} \Pi(\kappa_a, \kappa_c, \nu) \Pi(\kappa_b, \kappa_d, \nu) \sum_{\mu=1}^4 \gamma_{\mu}^{\nu, k}(a, b, c, d) R_{\mu}^{\nu}(a, b, c, d) + \right. \\
 & \left. \underbrace{\Pi(\kappa_a, \kappa_c, k-1) \Pi(\kappa_b, \kappa_d, k-1) \sum_{\mu=1}^8 s_{\mu}^k(a, b, c, d) S_{\mu}^k(a, b, c, d)} \right). \tag{A.1}
 \end{aligned}$$

Let us consider the first term in Eq. (A.1). So for  $\nu = k - 1$  it is

$$\begin{aligned}
 [X_{\text{Br}}^k(abcd)]_{\nu=k-1} = & (-1)^k \langle j_a || C^k || j_c \rangle \langle j_b || C^k || j_d \rangle \{j_a j_c k\} \{j_b j_d k\} \times \\
 & \Pi(\kappa_a, \kappa_c, k-1) \Pi(\kappa_b, \kappa_d, k-1) \left\{ \underbrace{r_1^{k-1, k}(a, b, c, d) R_1^{k-1}(a, b, c, d)} + \right. \\
 & r_2^{k-1, k}(a, b, c, d) R_2^{k-1}(a, b, c, d) + r_3^{k-1, k}(a, b, c, d) R_3^{k-1}(a, b, c, d) + \\
 & \left. r_4^{k-1, k}(a, b, c, d) R_4^{k-1}(a, b, c, d) \right\} \tag{A.2}
 \end{aligned}$$

Let us consider the term in the under-brace, i.e.  $r_1^{k-1, k}(a, b, c, d) R_1^{k-1}(a, b, c, d)$ .

Using the coefficients from Grant's work [18] we can write the term as follows :

$$r_1^{k-1,k}(a, b, c, d)R_1^{k-1}(a, b, c, d) = \{(\kappa_c - \kappa_a) + k\}\{(\kappa_d - \kappa_b) + k\} \left\{ \frac{k+1}{k(2k-1)(2k+1)} \right\} \times \int_0^\infty dr_2 \int_0^\infty dr_1 P_a(r_1)Q_c(r_1)U_{k-1}(r_1, r_2)P_b(r_2)Q_d(r_2).$$

Similarly the other terms can be expressed in terms of the large and small components of the radial wave-function. For completeness we give here all the integrals with the coefficients.

$$\begin{aligned} r_2^{k-1,k}(a, b, c, d)R_2^{k-1}(a, b, c, d) &= \{(\kappa_c - \kappa_a) - k\}\{(\kappa_d - \kappa_b) - k\} \left\{ \frac{k+1}{k(2k-1)(2k+1)} \right\} \times \\ &\quad \int_0^\infty dr_2 \int_0^\infty dr_1 Q_a(r_1)P_c(r_1)U_{k-1}(r_1, r_2)Q_b(r_2)P_d(r_2), \\ r_3^{k-1,k}(a, b, c, d)R_3^{k-1}(a, b, c, d) &= \{(\kappa_c - \kappa_a) + k\}\{(\kappa_d - \kappa_b) - k\} \left\{ \frac{k+1}{k(2k-1)(2k+1)} \right\} \times \\ &\quad \int_0^\infty dr_2 \int_0^\infty dr_1 P_a(r_1)Q_c(r_1)U_{k-1}(r_1, r_2)Q_b(r_2)P_d(r_2), \\ r_4^{k-1,k}(a, b, c, d)R_4^{k-1}(a, b, c, d) &= \{(\kappa_c - \kappa_a) - k\}\{(\kappa_d - \kappa_b) + k\} \left\{ \frac{k+1}{k(2k-1)(2k+1)} \right\} \times \\ &\quad \int_0^\infty dr_2 \int_0^\infty dr_1 Q_a(r_1)P_c(r_1)U_{k-1}(r_1, r_2)P_b(r_2)Q_d(r_2). \end{aligned}$$

For  $\nu = k$  the integrals and the coefficients have the following form :

$$\begin{aligned} r_1^{k,k}(a, b, c, d)R_1^k(a, b, c, d) &= \left\{ \frac{(\kappa_c + \kappa_a)(\kappa_d + \kappa_b)}{k(k+1)} \right\} \times \\ &\quad \int_0^\infty dr_2 \int_0^\infty dr_1 P_a(r_1)Q_c(r_1)U_k(r_1, r_2)P_b(r_2)Q_d(r_2), \\ r_2^{k,k}(a, b, c, d)R_2^k(a, b, c, d) &= \left\{ \frac{(\kappa_c + \kappa_a)(\kappa_d + \kappa_b)}{k(k+1)} \right\} \times \\ &\quad \int_0^\infty dr_2 \int_0^\infty dr_1 Q_a(r_1)P_c(r_1)U_k(r_1, r_2)Q_b(r_2)P_d(r_2), \\ r_3^{k,k}(a, b, c, d)R_3^k(a, b, c, d) &= \left\{ \frac{(\kappa_c + \kappa_a)(\kappa_d + \kappa_b)}{k(k+1)} \right\} \times \\ &\quad \int_0^\infty dr_2 \int_0^\infty dr_1 P_a(r_1)Q_c(r_1)U_k(r_1, r_2)Q_b(r_2)P_d(r_2), \\ r_4^{k,k}(a, b, c, d)R_4^k(a, b, c, d) &= \left\{ \frac{(\kappa_c + \kappa_a)(\kappa_d + \kappa_b)}{k(k+1)} \right\} \times \\ &\quad \int_0^\infty dr_2 \int_0^\infty dr_1 Q_a(r_1)P_c(r_1)U_k(r_1, r_2)P_b(r_2)Q_d(r_2). \end{aligned}$$

For  $\nu = k + 1$  the integrals and the coefficients are

$$\begin{aligned}
r_1^{k+1,k}(a, b, c, d)R_1^{k+1}(a, b, c, d) &= \{(\kappa_c - \kappa_a) - (k + 1)\}\{(\kappa_d - \kappa_b) - (k + 1)\} \times \\
&\quad \left\{ \frac{k}{(k + 1)(2k + 1)(2k + 3)} \right\} \times \\
&\quad \int_0^\infty dr_2 \int_0^\infty dr_1 P_a(r_1) Q_c(r_1) U_{k+1}(r_1, r_2) P_b(r_2) Q_d(r_2), \\
r_2^{k+1,k}(a, b, c, d)R_2^{k+1}(a, b, c, d) &= \{(\kappa_c - \kappa_a) + (k + 1)\}\{(\kappa_d - \kappa_b) + (k + 1)\} \times \\
&\quad \left\{ \frac{k}{(k + 1)(2k + 1)(2k + 3)} \right\} \times \\
&\quad \int_0^\infty dr_2 \int_0^\infty dr_1 Q_a(r_1) P_c(r_1) U_{k+1}(r_1, r_2) Q_b(r_2) P_d(r_2), \\
r_3^{k+1,k}(a, b, c, d)R_3^{k+1}(a, b, c, d) &= \{(\kappa_c - \kappa_a) - (k + 1)\}\{(\kappa_d - \kappa_b) + (k + 1)\} \times \\
&\quad \left\{ \frac{k}{(k + 1)(2k + 1)(2k + 3)} \right\} \times \\
&\quad \int_0^\infty dr_2 \int_0^\infty dr_1 P_a(r_1) Q_c(r_1) U_{k+1}(r_1, r_2) Q_b(r_2) P_d(r_2), \\
r_4^{k+1,k}(a, b, c, d)R_4^{k+1}(a, b, c, d) &= \{(\kappa_c - \kappa_a) + (k + 1)\}\{(\kappa_d - \kappa_b) - (k + 1)\} \times \\
&\quad \left\{ \frac{k}{(k + 1)(2k + 1)(2k + 3)} \right\} \times \\
&\quad \int_0^\infty dr_2 \int_0^\infty dr_1 Q_a(r_1) P_c(r_1) U_{k+1}(r_1, r_2) P_b(r_2) Q_d(r_2).
\end{aligned}$$

Now coming to the under braced term in Eq. (A.1). After expanding it is

$$\begin{aligned}
&\Pi(\kappa_a, \kappa_c, k - 1)\Pi(\kappa_b, \kappa_d, k - 1) \sum_{\mu=1}^8 s_\mu^k(a, b, c, d) S_\mu^k(a, b, c, d) = \\
&\Pi(\kappa_a, \kappa_c, k - 1)\Pi(\kappa_b, \kappa_d, k - 1) \times \left\{ s_1^k(a, b, c, d) S_1^k(a, b, c, d) + \dots + \right. \\
&\left. s_8^k(a, b, c, d) S_8^k(a, b, c, d) \right\}.
\end{aligned}$$

Here we give the details of the integrals and the coefficients in the above expression that we use in our code.

$$\begin{aligned}
s_1^k(a, b, c, d)S_1^k(a, b, c, d) &= -\frac{1}{2(2k + 1)}\{(\kappa_c - \kappa_a) + k\}\{(\kappa_d - \kappa_b) - (k + 1)\} \times \\
&\quad \left[ \int_0^\infty dr_2 \int_0^\infty dr_1 P_a(r_1) Q_c(r_1) \bar{U}_{k-1}(r_1, r_2) P_b(r_2) Q_d(r_2) - \right. \\
&\quad \left. \int_0^\infty dr_2 \int_0^\infty dr_1 P_a(r_1) Q_c(r_1) \bar{U}_{k+1}(r_1, r_2) P_b(r_2) Q_d(r_2) \right],
\end{aligned}$$

$$\begin{aligned}
s_2^k(a, b, c, d)S_2^k(a, b, c, d) &= -\frac{1}{2(2k+1)}\{(\kappa_c - \kappa_a) - (k+1)\}\{(\kappa_d - \kappa_b) + k\} \times \\
&\quad \left[ \int_0^\infty dr_2 \int_0^\infty dr_1 P_b(r_1)Q_d(r_1)\bar{U}_{k-1}(r_1, r_2)P_a(r_2)Q_c(r_2) - \right. \\
&\quad \left. \int_0^\infty dr_2 \int_0^\infty dr_1 P_b(r_1)Q_d(r_1)\bar{U}_{k+1}(r_1, r_2)P_a(r_2)Q_c(r_2) \right], \\
s_3^k(a, b, c, d)S_3^k(a, b, c, d) &= -\frac{1}{2(2k+1)}\{(\kappa_c - \kappa_a) - k\}\{(\kappa_d - \kappa_b) + (k+1)\} \times \\
&\quad \left[ \int_0^\infty dr_2 \int_0^\infty dr_1 Q_a(r_1)P_c(r_1)\bar{U}_{k-1}(r_1, r_2)Q_b(r_2)P_d(r_2) - \right. \\
&\quad \left. \int_0^\infty dr_2 \int_0^\infty dr_1 Q_a(r_1)P_c(r_1)\bar{U}_{k+1}(r_1, r_2)Q_b(r_2)P_d(r_2) \right], \\
s_4^k(a, b, c, d)S_4^k(a, b, c, d) &= -\frac{1}{2(2k+1)}\{(\kappa_c - \kappa_a) + (k+1)\}\{(\kappa_d - \kappa_b) - k\} \times \\
&\quad \left[ \int_0^\infty dr_2 \int_0^\infty dr_1 Q_b(r_1)P_d(r_1)\bar{U}_{k-1}(r_1, r_2)Q_a(r_2)P_c(r_2) - \right. \\
&\quad \left. \int_0^\infty dr_2 \int_0^\infty dr_1 Q_b(r_1)P_d(r_1)\bar{U}_{k+1}(r_1, r_2)Q_a(r_2)P_c(r_2) \right], \\
s_5^k(a, b, c, d)S_5^k(a, b, c, d) &= -\frac{1}{2(2k+1)}\{(\kappa_c - \kappa_a) + k\}\{(\kappa_d - \kappa_b) + (k+1)\} \times \\
&\quad \left[ \int_0^\infty dr_2 \int_0^\infty dr_1 P_a(r_1)Q_c(r_1)\bar{U}_{k-1}(r_1, r_2)Q_b(r_2)P_d(r_2) - \right. \\
&\quad \left. \int_0^\infty dr_2 \int_0^\infty dr_1 P_a(r_1)Q_c(r_1)\bar{U}_{k+1}(r_1, r_2)Q_b(r_2)P_d(r_2) \right], \\
s_6^k(a, b, c, d)S_6^k(a, b, c, d) &= -\frac{1}{2(2k+1)}\{(\kappa_c - \kappa_a) - (k+1)\}\{(\kappa_d - \kappa_b) - k\} \times \\
&\quad \left[ \int_0^\infty dr_2 \int_0^\infty dr_1 Q_b(r_1)P_d(r_1)\bar{U}_{k-1}(r_1, r_2)P_a(r_2)Q_c(r_2) - \right. \\
&\quad \left. \int_0^\infty dr_2 \int_0^\infty dr_1 Q_b(r_1)P_d(r_1)\bar{U}_{k+1}(r_1, r_2)P_a(r_2)Q_c(r_2) \right], \\
s_7^k(a, b, c, d)S_7^k(a, b, c, d) &= -\frac{1}{2(2k+1)}\{(\kappa_c - \kappa_a) - k\}\{(\kappa_d - \kappa_b) - (k+1)\} \times \\
&\quad \left[ \int_0^\infty dr_2 \int_0^\infty dr_1 Q_a(r_1)P_c(r_1)\bar{U}_{k-1}(r_1, r_2)P_b(r_2)Q_d(r_2) - \right. \\
&\quad \left. \int_0^\infty dr_2 \int_0^\infty dr_1 Q_a(r_1)P_c(r_1)\bar{U}_{k+1}(r_1, r_2)P_b(r_2)Q_d(r_2) \right], \\
s_8^k(a, b, c, d)S_8^k(a, b, c, d) &= -\frac{1}{2(2k+1)}\{(\kappa_c - \kappa_a) + (k+1)\}\{(\kappa_d - \kappa_b) + k\} \times \\
&\quad \left[ \int_0^\infty dr_2 \int_0^\infty dr_1 P_b(r_1)Q_d(r_1)\bar{U}_{k-1}(r_1, r_2)Q_a(r_2)P_c(r_2) - \right. \\
&\quad \left. \int_0^\infty dr_2 \int_0^\infty dr_1 P_b(r_1)Q_d(r_1)\bar{U}_{k+1}(r_1, r_2)Q_a(r_2)P_c(r_2) \right].
\end{aligned}$$

# Appendix B

## Matrix Element of Dipole Operator

The matrix element of the dipole operator is extremely useful to calculate the electric dipole transition amplitude as well as for static dipole polarizability calculation. Here we will briefly discuss about the matrix element of the dipole operator.

Using Wigner-Eckart theorem the matrix element of the dipole operator between two configuration state function can be written as

$$\begin{aligned}
 \langle \Psi_i | \mathbf{D} | \Psi_j \rangle &= \langle \gamma(JI)PFM_F | \mathbf{D} | \gamma'(J'I')PF'M'_F \rangle \\
 &= (-1)^{(F-M_F)} \begin{pmatrix} F & 1 & F' \\ -M_F & q & M'_F \end{pmatrix} \langle \gamma(JI)F | \mathbf{D} | \gamma'(J'I')F' \rangle \\
 &= (-1)^{(F-M_F)} (-1)^{J+I+F'+1} \delta(I, I') [F, F'] \begin{pmatrix} F & 1 & F' \\ -M_F & q & M'_F \end{pmatrix} \times \\
 &\quad \left\{ \begin{matrix} F & 1 & F' \\ J' & I & J \end{matrix} \right\} \langle \gamma J || \mathbf{D} || \gamma' J' \rangle. \tag{B.1}
 \end{aligned}$$

In terms of spin-orbital decomposition the reduced matrix element is written as

$$\langle \gamma J || \mathbf{D} || \gamma' J' \rangle = d_k^{ab}(J, J') \langle \gamma J_a || \mathbf{d} || \gamma' J_b \rangle. \tag{B.2}$$

Here  $d_k^{ab}$  are the angular factors. Therefore the reduced matrix elements of the

dipole operator in terms of Dirac spin-orbital can be written as

$$\begin{aligned}
\langle \gamma(l_a, s_a)j_a || \mathbf{d} || \gamma'(l_b, s_b)j_b \rangle &= - \int d^3r \psi_a^\dagger(\mathbf{r}) \mathbf{r} \psi_b(\mathbf{r}), \\
&= - \int_0^\infty dr \int d\Omega \begin{pmatrix} P_a \chi_{\kappa_a m_a}(\hat{r}) \\ iQ_a \chi_{-\kappa_a m_a}(\hat{r}) \end{pmatrix}^\dagger \begin{pmatrix} \mathbf{r} & 0 \\ 0 & \mathbf{r} \end{pmatrix} \times \\
&\quad \begin{pmatrix} P_b \chi_{\kappa_b m_b}(\hat{r}) \\ iQ_b \chi_{-\kappa_b m_b}(\hat{r}) \end{pmatrix} \tag{B.3}
\end{aligned}$$

If z-axis is the axis of quantization, then the component of the dipole operator  $\mathbf{d}$  along the axis of quantization is  $d_z \cos \theta$ . Therefore the reduced matrix element is

$$\langle \gamma(l_a, s_a)j_a || d_z || \gamma'(l_b, s_b)j_b \rangle = - \int_0^\infty dr r (P_a^* P_b + Q_a^* Q_b) \int d\Omega \chi_{\kappa_a m_a}^*(\hat{r}) \cos \theta \chi_{\kappa_b m_b}(\hat{r}). \tag{B.4}$$

Here we use the relations  $\sigma \cdot \hat{\mathbf{r}} \chi_{-\kappa_b m_b} = \chi_{\kappa_b m_b}$  and  $(\sigma \cdot \hat{\mathbf{r}})^2 = 1$ . For convenient we express the dipole operator in terms of the  $\mathbf{C}$  tensor operator. Then the expression is

$$\mathbf{d} = r \mathbf{C}^1. \tag{B.5}$$

The components of the  $\mathbf{C}$  tensor operators are

$$C_q^k(\theta, \phi) = \sqrt{\frac{4\pi}{2k+1}} Y_q^k(\theta, \phi). \tag{B.6}$$

Thus the reduced matrix element of the dipole operator in terms of  $\mathbf{C}$  tensor can be written as

$$\langle \gamma(l_a, s_a)j_a || d_z || \gamma'(l_b, s_b)j_b \rangle = - \int_0^\infty dr r (P_a^* P_b + Q_a^* Q_b) \langle \kappa_a || \mathbf{C}^1 || \kappa_b \rangle. \tag{B.7}$$

Here the last term in the reduced matrix element is

$$\langle \kappa_a || \mathbf{C}^1 || \kappa_b \rangle = (-1)^{j_a+1/2} \sqrt{(2j_a+1)(2j_b+1)} \begin{pmatrix} j_a & j_b & 1 \\ -1/2 & 1/2 & 0 \end{pmatrix} \Pi(l_a + l_b + 1). \tag{B.8}$$

Here the parity condition is

$$\Pi(l_a + l_b + 1) = \begin{cases} 1 & \text{if } l_a + l_b + 1 \text{ is even;} \\ 0 & \text{otherwise.} \end{cases} \tag{B.9}$$

In the present work we consistently use the expression [B.8](#) to evaluate the reduced matrix element of the dipole operator.

# Bibliography

- [1] J. Sucher, [Phys. Rev. A \*\*22\*\*, 348 \(1980\)](#).
- [2] I. Lindgren, [Mol. Phys. \*\*94\*\*, 19 \(1998\)](#).
- [3] F. Coester, [Nucl. Phys. \*\*7\*\*, 421 \(1958\)](#).
- [4] F. Coester and H. Kümmel, [Nucl. Phys. \*\*17\*\*, 477 \(1960\)](#).
- [5] J. Schwinger, [Phys. Rev. \*\*74\*\*, 1439 \(1948\)](#).
- [6] J. Schwinger, [Phys. Rev. \*\*75\*\*, 651 \(1949\)](#).
- [7] J. Schwinger, [Phys. Rev. \*\*76\*\*, 790 \(1949\)](#).
- [8] R. P. Feynman, [Phys. Rev. \*\*76\*\*, 749 \(1949\)](#).
- [9] R. P. Feynman, [Phys. Rev. \*\*76\*\*, 769 \(1949\)](#).
- [10] F. J. Dyson, [Phys. Rev. \*\*75\*\*, 486 \(1949\)](#).
- [11] F. J. Dyson, [Phys. Rev. \*\*75\*\*, 1736 \(1949\)](#).
- [12] S. Schweber, *QED and the Men Who Made It : Dyson, Feynman, Schwinger, and Tomonaga* (Princeton University Press, New Jersey, 1994).
- [13] D. Hanneke, S. Fogwell, and G. Gabrielse, [Phys. Rev. Lett. \*\*100\*\*, 120801 \(2008\)](#).
- [14] T. Kinoshita and M. Nio, [Phys. Rev. D \*\*73\*\*, 013003 \(2006\)](#).
- [15] P. J. Mohr, G. Plunien, and G. Soff, [Phys. Rep \*\*293\*\*, 227 \(1998\)](#).

- 
- [16] P. A. M. Dirac, Proceedings of the Royal Society of London, Series A **123**, 714 (1929).
- [17] W. Johnson, *Atomic Structure Theory: Lectures on Atomic Physics* (Springer, Berlin, 2007).
- [18] I. P. Grant, *Relativistic Quantum Theory of Atoms and Molecules: Theory and Computation* (Springer, New York, 2010).
- [19] G. Breit, *Phys. Rev.* **34**, 553 (1929).
- [20] I. Grant, in *Springer Handbook of Atomic, Molecular, and Optical Physics*, edited by G. Drake (Springer, New York, 2006) pp. 325–357.
- [21] H. Bethe and E. Salpeter, *Quantum Mechanics of One- and Two-Electron Atoms* (Dover Publications, 2008).
- [22] E. A. Uehling, *Phys. Rev.* **48**, 55 (1935).
- [23] W. E. Lamb and R. C. Retherford, *Phys. Rev.* **72**, 241 (1947).
- [24] B. Swirles, Proceedings of the Royal Society of London, Series A **152**, 625 (1935).
- [25] I. P. Grant, *Adv. Phys.* **19**, 747 (1970).
- [26] J. Desclaux, *Comp. Phys. Comm.* **9**, 31 (1975).
- [27] G. E. Brown and D. G. Ravenhall, *Proceedings of the Royal Society of London. Series A. Mathematical and Physical Sciences* **208**, 552 (1951).
- [28] R. E. Stanton and S. Havriliak, *J. Chem. Phys.* **81**, 1910 (1984).
- [29] A. K. Mohanty and E. Clementi, *J. Chem. Phys.* **93**, 1829 (1990).
- [30] E. A. Hylleraas, *Zeitschrift für Physik* **54**, 347 (1929).
- [31] G. W. F. Drake, *Phys. Rev. A* **19**, 1387 (1979).

- 
- [32] T. Zhang, Z.-C. Yan, and G. W. F. Drake, *Phys. Rev. Lett.* **77**, 1715 (1996).
- [33] K. Pachucki and V. A. Yerokhin, *Phys. Rev. A* **79**, 062516 (2009).
- [34] K. Pachucki and V. A. Yerokhin, *Phys. Rev. Lett.* **104**, 070403 (2010).
- [35] I. P. Grant, *J. Phys. B* **42**, 055002 (2009).
- [36] W. R. Johnson, S. A. Blundell, and J. Sapirstein, *Phys. Rev. A* **37**, 307 (1988).
- [37] R. K. Chaudhuri, P. K. Panda, and B. P. Das, *Phys. Rev. A* **59**, 1187 (1999).
- [38] H. P. Kelly, *Phys. Rev.* **136**, B896 (1964).
- [39] R. J. Bartlett and M. Musiał, *Rev. Mod. Phys.* **79**, 291 (2007).
- [40] B. K. Mani, K. V. P. Latha, and D. Angom, *Phys. Rev. A* **80**, 062505 (2009).
- [41] H. S. Nataraj, B. K. Sahoo, B. P. Das, and D. Mukherjee, *Phys. Rev. Lett.* **101**, 033002 (2008).
- [42] R. Pal, M. S. Safronova, W. R. Johnson, A. Derevianko, and S. G. Porsev, *Phys. Rev. A* **75**, 042515 (2007).
- [43] G. Gopakumar, H. Merlitz, S. Majumder, R. K. Chaudhuri, B. P. Das, U. S. Mahapatra, and D. Mukherjee, *Phys. Rev. A* **64**, 032502 (2001).
- [44] T. A. Isaev, A. N. Petrov, N. S. Mosyagin, A. V. Titov, E. Eliav, and U. Kaldor, *Phys. Rev. A* **69**, 030501 (2004).
- [45] G. Hagen, T. Papenbrock, D. J. Dean, and M. Hjorth-Jensen, *Phys. Rev. Lett.* **101**, 092502 (2008).
- [46] R. F. Bishop, P. H. Y. Li, D. J. J. Farnell, and C. E. Campbell, *Phys. Rev. B* **79**, 174405 (2009).

- [47] I. Lindgren, S. Salomonson, and D. Hedendahl, in *Recent Progress in Coupled Cluster Methods*, Vol. 11 (Springer Netherlands, 2010) pp. 357–374.
- [48] V. Shabaev, *Phys. Rep.* **356**, 119 (2002).
- [49] I. Lindgren, S. Salomonson, and B. Åsén, *Phys. Rep.* **389**, 161 (2004).
- [50] S. Chattopadhyay, B. K. Mani, and D. Angom, *Phys. Rev. A* **86**, 022522 (2012).
- [51] S. Chattopadhyay, B. K. Mani, and D. Angom, *Phys. Rev. A* **86**, 062508 (2012).
- [52] F. A. Parpia, C. Froese Fischer, and I. P. Grant, *Comp. Phys. Comm.* **94**, 249 (1996).
- [53] P. J. Mohr, B. N. Taylor, and D. B. Newell, *Rev. Mod. Phys.* **84**, 1527 (2012).
- [54] W. Greiner and J. Reinhardt, *Quantum Electrodynamics* (Springer, Heidelberg, 2009).
- [55] J. D. Jackson, *Classical Electrodynamics* (Wiley, New York, 1999).
- [56] I. Lindgren, *Relativistic Many-Body Theory: A New Field-Theoretical Approach* (Springer, New York, 2011).
- [57] W. Pauli and F. Villars, *Rev. Mod. Phys.* **21**, 434 (1949).
- [58] F. A. Parpia and A. K. Mohanty, *Phys. Rev. A* **46**, 3735 (1992).
- [59] L. W. Fullerton and G. A. Rinker, *Phys. Rev. A* **13**, 1283 (1976).
- [60] W. R. Johnson, I. Bednyakov, and G. Soff, *Phys. Rev. Lett.* **87**, 233001 (2001).
- [61] I. Lindgren and J. Morrison, *Atomic Many-Body Theory* (Springer, Berlin, 2nd Edition, 1986).

- [62] W. Greiner, *Relativistic Quantum Mechanics : Wave Equations* (Springer, Berlin, 2000).
- [63] A. K. Mohanty, F. A. Parpia, and E. Clementi, in *Modern Techniques in Computational Chemistry: MOTECC-91*, edited by E. Clementi (ESCOM, 1991).
- [64] J. B. Mann and W. R. Johnson, *Phys. Rev. A* **4**, 41 (1971).
- [65] I. P. Grant and N. C. Pyper, *J. Phys. B* **9**, 761 (1976).
- [66] I. P. Grant and B. J. McKenzie, *J. Phys. B* **13**, 2671 (1980).
- [67] A. Szabó and N. Ostlund, *Modern Quantum Chemistry: Introduction to Advanced Electronic Structure Theory* (Dover Publications, 1996).
- [68] I. Lindgren, *J. Phys. B* **7**, 2441 (1974).
- [69] I. Lindgren, *Phys. Rep.* **242**, 269 (1994).
- [70] F. A. Parpia, A. K. Mohanty, and E. Clementi, *J. Phys. B* **25**, 1 (1992).
- [71] Y. Ishikawa, H. M. Quiney, and G. L. Malli, *Phys. Rev. A* **43**, 3270 (1991).
- [72] A. Derevianko, B. Ravaine, and W. R. Johnson, *Phys. Rev. A* **69**, 054502 (2004).
- [73] B. K. Mani, *Studies on the Consequences of Discrete Symmetry Violations in Atoms*, Ph.D. thesis, Mohanlal Sukhadia University, Udaipur (2011).
- [74] Y. Ishikawa and K. Koc, *Phys. Rev. A* **50**, 4733 (1994).
- [75] B. K. Mani and D. Angom, *Phys. Rev. A* **81**, 042514 (2010).
- [76] W. R. Johnson, U. I. Safronova, A. Derevianko, and M. S. Safronova, *Phys. Rev. A* **77**, 022510 (2008).
- [77] C. E. Moore, *Atomic Energy Levels* (National Bureau of Standards, Washington D.C, 1971).

- [78] U. Volz and H. Schmoranzner, *Phys. Scr.* **1996**, 48 (1996).
- [79] I. Khriplovich, *Parity Nonconservation in Atomic Phenomena* (Gordon and Breach Science Publishers, Philadelphia, 1991).
- [80] T. Udem, R. Holzwarth, and T. W. Hansch, *Nature* **416**, 233 (2002).
- [81] S. A. Diddams, J. C. Bergquist, S. R. Jefferts, and C. W. Oates, *Science* **306**, 1318 (2004).
- [82] M. H. Anderson, J. R. Ensher, M. R. Matthews, C. E. Wieman, and E. A. Cornell, *Science* **269**, 198 (1995).
- [83] C. C. Bradley, C. A. Sackett, J. J. Tollett, and R. G. Hulet, *Phys. Rev. Lett.* **75**, 1687 (1995).
- [84] K. B. Davis, M. O. Mewes, M. R. Andrews, N. J. van Druten, D. S. Durfee, D. M. Kurn, and W. Ketterle, *Phys. Rev. Lett.* **75**, 3969 (1995).
- [85] J. Mitroy, M. S. Safronova, and C. W. Clark, *J. Phys. B* **43**, 202001 (2010).
- [86] B. K. Mani and D. Angom, ArXiv e-prints (2011), [1105.3447](https://arxiv.org/abs/1105.3447).
- [87] P. Soldan, E. P. F. Lee, and T. G. Wright, *Phys. Chem. Chem. Phys.* **3**, 4661 (2001).
- [88] T. Nakajima and K. Hirao, *Chem. Lett.* **30**, 766 (2001).
- [89] A. J. Thakkar, H. Hettema, and P. E. S. Wormer, *J. Chem. Phys.* **97**, 3252 (1992).
- [90] U. Hohm and K. Kerl, *Mol. Phys.* **69**, 803 (1990).
- [91] A. Derevianko, S. G. Porsev, and K. Beloy, *Phys. Rev. A* **78**, 010503(R) (2008).
- [92] T. Nakajima and K. Hirao, *J. Chem. Phys.* **113**, 7786 (2000).
- [93] P. W. Langhoff and M. Karplus, *J. Opt. Soc. Am.* **59**, 863 (1969).

- [94] R. H. Orcutt and R. H. Cole, *J. Chem. Phys.* **46**, 697 (1967).
- [95] W. Johnson, D. Kolb, and K.-N. Huang, *At. Data and Nucl. Data Tables* **28**, 333 (1983).
- [96] I. S. Lim, J. K. Laerdahl, and P. Schwerdtfeger, *J. Chem. Phys.* **116**, 172 (2002).
- [97] L. G. Gray, X. Sun, and K. B. MacAdam, *Phys. Rev. A* **38**, 4985 (1988).
- [98] U. Öpik, *Proceedings of the Physical Society* **92**, 566 (1967).
- [99] I. Johansson, *Ark. Fys.* **20**, 135 (1961).
- [100] I. S. Lim, J. K. Laerdahl, and P. Schwerdtfeger, *J. Phys. B* **33**, L91 (2000).
- [101] H. L. Zhou and D. W. Norcross, *Phys. Rev. A* **40**, 5048 (1989).
- [102] I. S. Lim and P. Schwerdtfeger, *Phys. Rev. A* **70**, 062501 (2004).
- [103] S. Chattopadhyay, B. K. Mani, and D. Angom, *Phys. Rev. A* **87**, 042520 (2013).
- [104] P. Beiersdorfer, *J. Phys. B* **43**, 074032 (2010).
- [105] A. Derevianko, V. A. Dzuba, and V. V. Flambaum, *Phys. Rev. Lett.* **109**, 180801 (2012).
- [106] B. K. Mani and D. Angom, ArXiv e-prints (2011), 1104.3473 .
- [107] D. A. Pigg, G. Hagen, H. Nam, and T. Papenbrock, *Phys. Rev. C* **86**, 014308 (2012).
- [108] S. Kvaal, *J. Chem. Phys.* **136**, 194109 (2012).

## Publications attached with the thesis

1. **Perturbed coupled-cluster theory to calculate dipole polarizabilities of closed-shell systems: Application to Ar, Kr, Xe, and Rn,**  
S. Chattopadhyay, B. K. Mani, and D. Angom,  
Phys. Rev. A, **86**, 062508 (2012).
2. **Electric dipole polarizabilities of doubly ionized alkaline Earth metal ions from perturbed relativistic coupled-cluster theory,**  
S. Chattopadhyay, B. K. Mani, and D. Angom,  
Phys. Rev. A **87** 062504 (2013).

# Perturbed coupled-cluster theory to calculate dipole polarizabilities of closed-shell systems: Application to Ar, Kr, Xe, and Rn

S. Chattopadhyay,<sup>1</sup> B. K. Mani,<sup>2</sup> and D. Angom<sup>1</sup><sup>1</sup>*Physical Research Laboratory, Ahmedabad 380009, Gujarat, India*<sup>2</sup>*Department of Physics, University of South Florida, Tampa, Florida 33620, USA*

(Received 23 October 2012; published 17 December 2012)

We use perturbed relativistic coupled-cluster (PRCC) theory to calculate the electric dipole polarizability of the noble-gas atoms Ar, Kr, Xe, and Rn. We also provide a detailed description of the nonlinear terms in the PRCC theory and consider the Dirac-Coulomb-Breit atomic Hamiltonian for the calculations. We find that the largest contribution from the Breit interaction to the electric dipole polarizability is 0.1%, in the case of Rn. As we go from Ar to Rn, based on the pattern in the random-phase-approximation effects, the contraction of the outermost  $p_{1/2}$  orbitals due to relativistic corrections is discernible without any ambiguity.

DOI: [10.1103/PhysRevA.86.062508](https://doi.org/10.1103/PhysRevA.86.062508)

PACS number(s): 31.15.bw, 31.15.ap, 31.15.ve

## I. INTRODUCTION

The electric dipole polarizability  $\alpha$  is the lowest-order linear-response property and relevant to a wide range of physical phenomena related to properties from the microscopic to the macroscopic. Among the macroscopic properties, the dielectric constant and refractive index of the gas are the important ones. In the case of microscopic properties, parity nonconservation in atoms [1], optical atomic clocks [2,3], and physics of the condensates of dilute atomic gases [4–6] are of current interest. For accurate theoretical calculation of  $\alpha$ , a precise treatment of the electron correlation effects is very important. In the past, a wide range of atomic many-body theories were used to calculate  $\alpha$ . The recent review by Mitroy *et al.* [7] gives a detailed overview of the atomic and ionic polarizabilities.

In the present work we use the perturbed relativistic coupled-cluster (PRCC) theory to calculate  $\alpha$  of the noble-gas atoms. It is a theory we have developed to incorporate a perturbation in the conventional relativistic coupled-cluster (RCC) theory. In general, the coupled-cluster theory (CCT) [8,9] is one of the most elegant many-body theories which incorporates the electron correlation to all orders. The details of the CCT and different variants are described in a recent review [10]. The theory has been widely used for atomic [11–14], molecular [15], nuclear [16], and condensed matter physics [17] calculations. The PRCC theory is different from the previous RCC-based theories in a number of ways. The most important one is the representation of the cluster operators in the PRCC theory. The cluster operator can be a rank-1 tensor operator and it has the advantage of incorporating multiple perturbations of different ranks in the electronic sector. One basic advantage of PRCC theory is that it does away with the summation over intermediate states in the first-order time-independent perturbation theory. The summation over all the possible intermediate states within the chosen basis set is subsumed in the perturbed cluster amplitudes.

For the calculations we use the no-virtual-pair Dirac-Coulomb-Breit Hamiltonian. However, to assess the importance of the Breit interaction we also carry out another series of calculations with the no-virtual-pair Dirac-Coulomb Hamiltonian. We isolate the changes arising from the Breit interaction by comparing the results from the two sets of

calculations. For the present work, we have chosen the noble-gas atoms to study as these systems are ideal for testing the closed-shell PRCC theory. In previous works,  $\alpha$  values for the noble-gas atoms were calculated in the framework of many-body perturbation theory [18], nonrelativistic coupled-cluster theory with single, double, and triple (CCSDT) excitations [19], and the RCCSDT approximation [20]. In the last work, using the RCCSDT, the third-order Douglas-Kroll method [21] was used. It is an alternative to the Foldy-Wouthuysen transformation and a quasirelativistic treatment. For the single-particle wave functions, we use kinetically balanced Gaussian-type Dirac-Hartree-Fock orbitals. The results from our PRCC theory calculations are in good agreement with the experimental data and consistent with previous calculations.

The paper is organized as follows. In Sec. II, for completeness and easy reference we briefly describe the RCC theory with the Breit interaction. In Sec. III we introduce the PRCC theory and provide a detailed description of the tensor structure of the PRCC operators. In Sec. III B we give the analytical structure of the PRCC equations. In Sec. III C we present a diagrammatic and algebraic description of the the nonlinear terms in the PRCC theory. In Sec. IV we introduce the formal expression of the dipole polarizability and its representation in the PRCC theory. In subsequent sections we describe the details of the methods of calculation and present the results and discussion. We then end with conclusions. All the results presented in this work and related calculations are in atomic units ( $\hbar = m_e = e = 4\pi\epsilon_0 = 1$ ). In this system of units the velocity of light is  $\alpha^{-1}$ , the inverse of the fine-structure constant, for which we use the value of  $\alpha^{-1} = 137.035\,999\,074$  [22].

## II. RCC THEORY

For high- $Z$  atoms and ions, the Dirac-Coulomb-Breit Hamiltonian, denoted by  $H^{\text{DCB}}$ , is an appropriate choice to include the relativistic effects. However, there are complications associated with the negative-energy continuum states of  $H^{\text{DCB}}$ . These lead to variational collapse and *continuum dissolution* [23]. A formal approach to avoid these complications is to use the no-virtual-pair approximation. In this approximation, for a

neutral atom of  $N$  electrons [24]

$$H^{\text{DCB}} = \Lambda_{++} \sum_{i=1}^N [c\alpha_i \cdot \mathbf{p}_i + (\beta_i - 1)c^2 - V_N(r_i)] + \sum_{i<j} \left[ \frac{1}{r_{ij}} + g^{\text{B}}(r_{ij}) \right] \Lambda_{++}, \quad (1)$$

where  $\alpha$  and  $\beta$  are the Dirac matrices,  $\Lambda_{++}$  is an operator which projects to the positive-energy solutions and  $V_N(r_i)$  is the nuclear potential. Sandwiching the Hamiltonian with  $\Lambda_{++}$  ensures that the effects of the negative-energy continuum states are neglected in the calculations. The last two terms  $1/r_{ij}$  and  $g^{\text{B}}(r_{ij})$  are the Coulomb and Breit interactions, respectively. The latter, Breit, interaction, represents the interelectron magnetic interactions and is given by

$$g^{\text{B}}(r_{12}) = -\frac{1}{2r_{12}} \left[ \alpha_1 \cdot \alpha_2 + \frac{(\alpha_1 \cdot \mathbf{r}_{12})(\alpha_2 \cdot \mathbf{r}_{12})}{r_{12}^2} \right]. \quad (2)$$

The Hamiltonian satisfies the eigenvalue equation

$$H^{\text{DCB}}|\Psi_i\rangle = E_i|\Psi_i\rangle, \quad (3)$$

where  $|\Psi_i\rangle$  is the exact atomic state and  $E_i$  is the energy of the atomic state. In CCT the exact atomic state is given by the ansatz

$$|\Psi_i\rangle = e^{T^{(0)}}|\Phi_i\rangle, \quad (4)$$

where  $|\Phi_i\rangle$  is the reference-state wave function and  $T^{(0)}$  is the unperturbed cluster operator. In the case of closed-shell atoms the model space of the ground state consists of a single Slater determinant  $|\Phi_0\rangle$ . For an  $N$ -electron closed-shell atom  $T^{(0)} = \sum_{i=1}^N T_i^{(0)}$ , where  $i$  is the order of excitation. In the coupled-cluster single and double (CCSD) approximation,

$$T^{(0)} = T_1^{(0)} + T_2^{(0)}. \quad (5)$$

The CCSD approximation is a good starting point for structure and property calculations of closed-shell atoms and ions. In the second quantized representation

$$T_1^{(0)} = \sum_{a,p} t_a^p a_p^\dagger a_a, \quad (6a)$$

$$T_2^{(0)} = \frac{1}{2!} \sum_{a,b,p,q} t_{ab}^{pq} a_p^\dagger a_q^\dagger a_b a_a, \quad (6b)$$

where  $t_{\dots}$  are cluster amplitudes,  $a_i^\dagger$  ( $a_i$ ) are single-particle creation (annihilation) operators, and  $abc\dots$  ( $pqr\dots$ ) represent core (virtual) single-particle states or orbitals. The eigenvalue equation of the closed-shell ground state in the CCT approximation is

$$H^{\text{DCB}}e^{T^{(0)}}|\Phi_0\rangle = E_0e^{T^{(0)}}|\Phi_0\rangle. \quad (7)$$

Following a similar procedure, the CC eigenvalue equation of closed-shell excited states may be defined as well.

### III. PRCC THEORY

To incorporate an additional interaction Hamiltonian  $H_{\text{int}}$  perturbatively, we introduce the perturbed coupled-cluster operator  $\mathbf{T}^{(1)}$ . This means that  $H_{\text{int}}$  is applied once and the residual Coulomb interaction is applied to all orders in all possible sequences. In general,  $\mathbf{T}^{(1)}$  is a tensor operator and

the multipole structure depends on the properties of  $H_{\text{int}}$ . With the perturbation, the modified eigenvalue equation is

$$(H^{\text{DCB}} + \lambda H_{\text{int}})|\tilde{\Psi}_i\rangle = \tilde{E}|\tilde{\Psi}_i\rangle, \quad (8)$$

where  $\lambda$  is the perturbation parameter. Consider the case where  $H_{\text{int}}$  represents the interaction with an external static electric field  $\mathbf{E}$ . The interaction Hamiltonian is then  $H_{\text{int}} = -\sum_i \mathbf{r}_i \cdot \mathbf{E} = \mathbf{D} \cdot \mathbf{E}$ , where  $\mathbf{D}$  is the many-electron electric dipole operator. The perturbed atomic state in PRCC theory is

$$|\tilde{\Psi}_i\rangle = e^{T^{(0)} + \lambda \mathbf{T}^{(1)} \cdot \mathbf{E}} |\Phi_0\rangle = e^{T^{(0)} [1 + \lambda \mathbf{T}^{(1)} \cdot \mathbf{E}]} |\Phi_0\rangle. \quad (9)$$

This approach has the advantage of taking into account the effect of multiple perturbations systematically. Other than  $\mathbf{E}$ ,  $H_{\text{int}}$  could be one of the interactions internal to the atom, such as the Breit interaction, hyperfine interaction, etc. For the present work, we examine  $\mathbf{T}^{(1)}$  arising from  $\mathbf{E}$ , which is parity odd and a vector operator in the electronic space.

#### A. Tensor structure of PRCC operator

For the present case, with  $\mathbf{E}$  as the perturbation, we can write the perturbed single-excitation cluster operator as

$$\mathbf{T}_1^{(1)} = \sum_{a,p} \tau_a^p \mathbf{C}_1(\hat{r}) a_p^\dagger a_a. \quad (10)$$

Note that  $\mathbf{T}_1^{(1)}$  is a vector operator in the electronic space and the  $\mathbf{C}$  tensor  $\mathbf{C}_1(\hat{r})$  represents the vector nature of  $\mathbf{T}^{(1)}$ . The key difference of  $\mathbf{T}_1^{(1)}$  from  $T_1^{(0)}$  is the parity condition, the total orbital parity must be odd; in other words  $(-1)^{l_a + l_p} = -1$ . Here,  $l_a$  ( $l_p$ ) is the orbital angular momentum of the core (virtual) orbital  $a$  ( $p$ ). Diagrammatically, the  $\mathbf{T}_1^{(1)}$  operator is represented as shown in Fig. 1(a). It is similar to the conventional representation of  $T_1^{(0)}$  but the interaction line is replaced by a wavy line.

The tensor structure of  $\mathbf{T}_2^{(1)}$ , on the other hand, has additional complications as it consists of two vertices. After due consideration of the  $H_{\text{int}}$  and  $T^{(0)}$  multipole structure, it is represented as

$$\mathbf{T}_2^{(1)} = \sum_{a,b,p,q} \sum_{l,k} \tau_{ab}^{pq}(l,k) \{ \mathbf{C}_l(\hat{r}_1) \mathbf{C}_k(\hat{r}_2) \}^1 a_p^\dagger a_q^\dagger a_b a_a. \quad (11)$$

As in  $\mathbf{T}_1^{(1)}$ ,  $\mathbf{C}_k$  are the  $\mathbf{C}$ -tensor operators and two  $\mathbf{C}$ -tensor operators of rank  $l$  and  $k$  are coupled to a rank-1 tensor operator  $\mathbf{T}_2^{(1)}$ . At the two vertices, the orbital angular momenta must satisfy the triangular conditions  $|j_a - j_p| \leq l \leq (j_a + j_p)$  and  $|j_b - j_q| \leq k \leq (j_b + j_q)$ . In addition, the two tensor operators must be such that  $|l - k| \leq 1 \leq (l + k)$ . These selection rules arise from the triangular conditions at the vertices. The other selection rule follows from the parity condition and  $H_{\text{int}}$  is parity odd; therefore  $(-1)^{(l_a + l_p)} = -(-1)^{(l_b + l_q)}$ . The

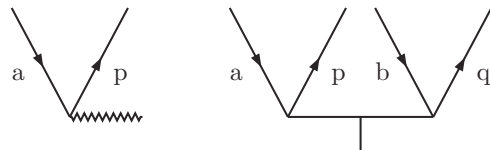


FIG. 1. Diagrammatic representation of  $\mathbf{T}_1^{(1)}$  and  $\mathbf{T}_2^{(1)}$ .

diagrammatic representation of  $\mathbf{T}_2^{(0)}$  is as shown in Fig. 1(b), where the vertical bar on the interaction line is to represent the rank of the operator. Furthermore, this representation, at a later stage, simplifies the angular integration using the diagrammatic technique.

### B. PRCC equations

The ground-state eigenvalue equation with  $H_{\text{int}}$  is

$$(H^{\text{DCB}} + \lambda H_{\text{int}})e^{[T^{(0)} + \lambda \mathbf{T}^{(1)} \cdot \mathbf{E}]|\Phi_0\rangle} = \tilde{E}_0 e^{[T^{(0)} + \lambda \mathbf{T}^{(1)} \cdot \mathbf{E}]|\Phi_0\rangle}. \quad (12)$$

When  $H_{\text{int}}$  is parity odd, as in the present case, there is no first-order perturbative correction to the energy so  $\tilde{E}_0 = E_0$ . In the CCSD approximation we define the perturbed cluster operator  $\mathbf{T}^{(1)}$  as

$$\mathbf{T}^{(1)} = \mathbf{T}_1^{(1)} + \mathbf{T}_2^{(1)}. \quad (13)$$

Using this, the PRCC equations are derived from Eq. (12). The derivation involves several operator contractions and these are more transparent with the normal-ordered Hamiltonian  $H_N^{\text{DCB}} = H^{\text{DCB}} - \langle \Phi_i | H^{\text{DCB}} | \Phi_i \rangle$ . The eigenvalue equation then assumes the form

$$[H_N^{\text{DCB}} + \lambda H_{\text{int}}]|\tilde{\Psi}_0\rangle = [E_0 - \langle \Phi_0 | H^{\text{DCB}} | \Phi_0 \rangle]|\tilde{\Psi}_0\rangle. \quad (14)$$

A more convenient form of the eigenvalue equation is

$$(H_N^{\text{DCB}} + \lambda H_{\text{int}})|\tilde{\Psi}_0\rangle = \Delta E_0 |\tilde{\Psi}_0\rangle, \quad (15)$$

where  $\Delta E_0 = E_0 - \langle \Phi_0 | H^{\text{DCB}} | \Phi_0 \rangle$  is the ground-state correlation energy. Following the definition in Eq. (13), the PRCC eigenvalue equation is

$$(H_N^{\text{DCB}} + \lambda H_{\text{int}})e^{T^{(0)} + \lambda \mathbf{T}^{(1)} \cdot \mathbf{E}}|\Phi_0\rangle = \Delta E_0 e^{T^{(0)} + \lambda \mathbf{T}^{(1)} \cdot \mathbf{E}}|\Phi_0\rangle. \quad (16)$$

Applying  $e^{-T^{(0)}}$  from the left, we get

$$[\tilde{H}_N^{\text{DCB}} + \lambda \tilde{H}_{\text{int}}]e^{\lambda \mathbf{T}^{(1)} \cdot \mathbf{E}}|\Phi_0\rangle = \Delta E_0 e^{\lambda \mathbf{T}^{(1)} \cdot \mathbf{E}}|\Phi_0\rangle, \quad (17)$$

where  $\tilde{H} = e^{-T^{(0)}} H e^{T^{(0)}}$  is the similarity-transformed Hamiltonian. Using the Campbell-Baker-Hausdorff expansion for the Dirac-Coulomb-Breit Hamiltonian

$$\begin{aligned} \tilde{H}^{\text{DCB}} &= H^{\text{DCB}} + [H^{\text{DCB}}, T^{(0)}] + \frac{1}{2!}[[H^{\text{DCB}}, T^{(0)}], T^{(0)}] \\ &+ \frac{1}{3!}[[[H^{\text{DCB}}, T^{(0)}], T^{(0)}], T^{(0)}] \\ &+ \frac{1}{4!}[[[[H^{\text{DCB}}, T^{(0)}], T^{(0)}], T^{(0)}], T^{(0)}]. \end{aligned} \quad (18)$$

The commutations represent contractions and as  $H^{\text{DCB}}$  consist of one- and two-body interactions, the expansion terminates at the fourth order. Multiplying Eq. (17) from the left by  $e^{-\lambda \mathbf{T}^{(1)}}$  and considering terms linear in  $\lambda$ , we get the PRCC equation

$$[\tilde{H}_N^{\text{DCB}}, \mathbf{T}^{(1)}] \cdot \mathbf{E} + \tilde{H}_{\text{int}}|\Phi_0\rangle = 0. \quad (19)$$

Here, the similarity-transformed interaction Hamiltonian  $\tilde{H}_{\text{int}}$  terminates at second order as  $H_{\text{int}}$  is a one-body interaction Hamiltonian.

Expanding  $\tilde{H}_{\text{int}}$ , the PRCC equation assumes the form

$$\begin{aligned} &([\tilde{H}_N^{\text{DCB}}, \mathbf{T}^{(1)}] + \dots) \cdot \mathbf{E}|\Phi_0\rangle \\ &= (\mathbf{D} + [\mathbf{D}, T^{(0)}] + \frac{1}{2}[[\mathbf{D}, T^{(0)}], T^{(0)}]) \cdot \mathbf{E}|\Phi_0\rangle. \end{aligned} \quad (20)$$

Hereafter, for simplicity, we drop  $\mathbf{E}$  from the equations and for compact notation, we use  $H_N$  to denote  $H_N^{\text{DCB}}$ . The cluster equations of  $\mathbf{T}_1^{(1)}$  are obtained after projecting the equation on singly excited states  $\langle \Phi_a^p |$ . These excited states, however, must be opposite in parity to  $|\Phi_0\rangle$ . Similarly, the  $\mathbf{T}_2^{(1)}$  equations are obtained after projecting on the doubly excited states  $\langle \Phi_{ab}^{pq} |$ . After the application of Wick's theorem, the  $\mathbf{T}^{(1)}$  equations are

$$\begin{aligned} &\langle \Phi_a^p | \left[ H_N + \overline{H_N \mathbf{T}^{(1)}} + \overline{H_N T^{(0)} \mathbf{T}^{(1)}} + \frac{1}{2!} \overline{H_N T^{(0)} T^{(0)} \mathbf{T}^{(1)}} \right] | \Phi_0 \rangle \\ &= \langle \Phi_a^p | \left[ \overline{\mathbf{D} T^{(0)}} + \frac{1}{2!} \overline{\mathbf{D} T^{(0)} T^{(0)}} \right] | \Phi_0 \rangle, \end{aligned} \quad (21)$$

$$\begin{aligned} &\langle \Phi_{ab}^{pq} | \left[ H_N + \overline{H_N \mathbf{T}^{(1)}} + \overline{H_N T^{(0)} \mathbf{T}^{(1)}} + \frac{1}{2!} \overline{H_N T^{(0)} T^{(0)} \mathbf{T}^{(1)}} \right. \\ &\left. + \dots \right] | \Phi_0 \rangle = \langle \Phi_{ab}^{pq} | \left[ \overline{\mathbf{D} T^{(0)}} + \frac{1}{2!} \overline{\mathbf{D} T^{(0)} T^{(0)}} \right] | \Phi_0 \rangle, \end{aligned} \quad (22)$$

where  $\overline{AB}$  represents all possible contractions between the two operators  $A$  and  $B$ . Equations (21) and (22) form a set of coupled nonlinear algebraic equations. However,  $T^{(0)}$  are solved for first as these are independent of  $\mathbf{T}^{(1)}$ ; the PRCC equations are then reduced to coupled linear algebraic equations. An approximation which incorporates all the important many-body effects like the random-phase approximation (RPA) is the linearized PRCC (LPRCC). In this approximation, only the terms linear in  $T$ , equivalent to retaining only  $\overline{H_N T^{(1)}}$  and  $\overline{\mathbf{D} T^{(0)}}$  in Eqs. (21) and (22), are considered in the equations. Hereafter we use  $T$  as the general representation of both the  $T^{(0)}$  and  $\mathbf{T}^{(1)}$  operators.

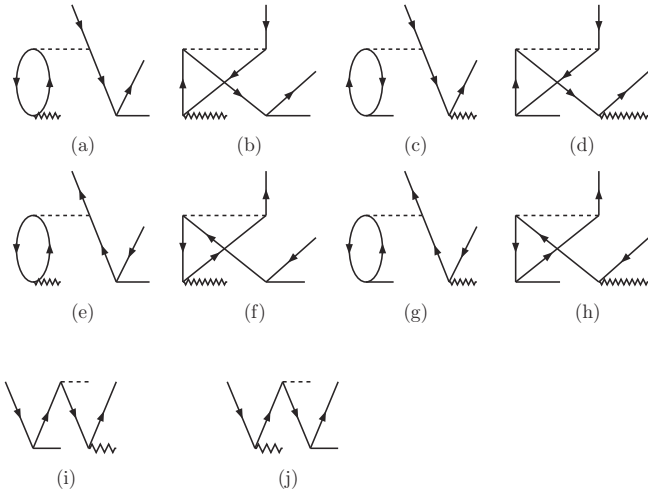
### C. Nonlinear terms in the PRCC

The calculation with the LPRCC approximation involves few many-body diagrams, and it is computationally less complex and hence faster. In our calculations, the LPRCC equations are solved first and we use the solutions as the initial guess to solve the PRCC equations. To describe the PRCC equations in detail, we examine each of the nonlinear terms. These involve more contractions and are larger in number than the linear terms. To begin with, consider the second term on the left-hand sides of Eqs. (21) and (22), second order in  $T$ . In the CCSD approximation it expands to

$$\begin{aligned} \overline{H_N T^{(0)} \mathbf{T}^{(1)}} &= \overline{H_N T_1^{(0)} \mathbf{T}_1^{(1)}} + \overline{H_N T_1^{(0)} \mathbf{T}_2^{(1)}} \\ &+ \overline{H_N T_2^{(0)} \mathbf{T}_1^{(1)}} + \overline{H_N T_2^{(0)} \mathbf{T}_2^{(1)}}. \end{aligned} \quad (23)$$

All the terms contribute to both  $\mathbf{T}_1^{(1)}$  and  $\mathbf{T}_2^{(1)}$ . Similarly, the third term on the left-hand sides of Eqs. (21) and (22), third order in  $T$ , expands to

$$\begin{aligned} \overline{H_N T^{(0)} T^{(0)} \mathbf{T}^{(1)}} &= \overline{H_N T_1^{(0)} T_1^{(0)} \mathbf{T}_1^{(1)}} + \overline{H_N T_1^{(0)} T_2^{(0)} \mathbf{T}_1^{(1)}} \\ &+ \overline{H_N T_1^{(0)} T_1^{(0)} \mathbf{T}_2^{(1)}} + \overline{H_N T_1^{(0)} T_2^{(0)} \mathbf{T}_2^{(1)}}. \end{aligned} \quad (24)$$

FIG. 2. Diagrams of  $\mathbf{T}_1^{(1)}$  arising from  $\overline{H_N T_1^{(0)}} \mathbf{T}_1^{(1)}$ .

In this equation, of the four terms, only the first one contributes to  $\mathbf{T}_1^{(1)}$ . But all the terms contribute to  $\mathbf{T}_2^{(1)}$ . At the fourth order there is only one term and it contributes to only  $\mathbf{T}_2^{(1)}$ . The terms on the right-hand sides of Eqs. (21) and (22) expand to

$$\overline{\mathbf{DT}}^{(0)} = \overline{\mathbf{DT}}_1^{(0)} + \overline{\mathbf{DT}}_2^{(0)}, \quad (25)$$

$$\overline{\mathbf{DT}}^{(0)} T^{(0)} = \overline{\mathbf{DT}}_1^{(0)} T_1^{(0)} + \overline{\mathbf{DT}}_1^{(0)} T_2^{(0)}. \quad (26)$$

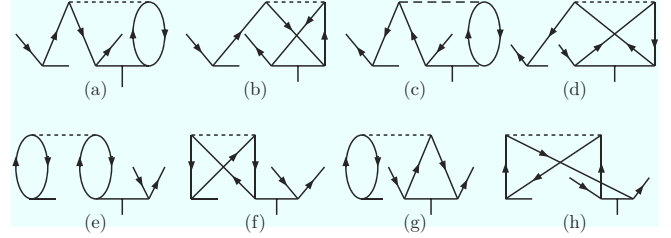
Here,  $\overline{\mathbf{DT}}_1^{(0)}$  and  $\overline{\mathbf{DT}}_1^{(0)} T_2^{(0)}$  are nonzero for only  $\mathbf{T}_1^{(1)}$  and  $\mathbf{T}_2^{(1)}$ , respectively. Each of the terms, after contraction, generates several topologically unique Goldstone diagrams. The diagrammatic treatment is the preferred mode of further analysis and calculation as it simplifies the calculations and is well suited to represent contractions between the operators. In the next few sections we discuss the  $\mathbf{T}_1^{(1)}$  and  $\mathbf{T}_2^{(1)}$  diagrams and their algebraic expressions.

### 1. $\mathbf{T}_1^{(1)}$ diagrams

In this section we describe the single-excitation diagrams arising from the nonlinear terms. The many-body diagrams or the Goldstone diagrams are drawn and evaluated as described in Ref. [25]. Consider the first term on the right-hand side of Eq. (23),  $\overline{H_N T_1^{(0)}} \mathbf{T}_1^{(1)}$ , it is equivalent to ten diagrams and these are shown in Fig. 2. Algebraically, we can write it as

$$\begin{aligned} \langle \overline{H_N T_1^{(0)}} \mathbf{T}_1^{(1)} \rangle_a^p &= \sum_{bcqa} \tilde{g}_{bcqa} (t_c^p \tau_b^q + t_b^q \tau_c^p) \\ &+ \sum_{bpqr} \tilde{g}_{bpqr} (t_a^r \tau_b^q + t_b^q \tau_a^r), \end{aligned}$$

where  $g_{ijkl} = \langle ij|1/r_{12} + g^B(r_{12})|kl \rangle$  is the matrix element of the electron-electron interactions and  $\tilde{g}_{ijkl} = g_{ijkl} - g_{ijlk}$  is the antisymmetrized matrix element. We have used  $\langle \dots \rangle_a^p$  to represent the matrix element  $\langle \Phi_a^p | \dots | \Phi_0 \rangle$ . The diagrams in Figs. 2(i) and 2(j), arising from the one-body part of  $H_N$ , evaluate to zero when the orbitals are calculated with the Dirac-Hartree-Fock potential. The next term,  $\overline{H_N T_1^{(0)}} \mathbf{T}_2^{(1)}$ , generates eight diagrams and these are shown in Fig. 3.

FIG. 3. Diagrams arising from the contraction  $\overline{H_N T_1^{(0)}} \mathbf{T}_2^{(1)}$ .

It is to be noted that here, contractions with only the  $g_{abpq}$  type of two-body interaction are nonzero. The algebraic expression of the diagrams is

$$\langle \overline{H_N T_1^{(0)}} \mathbf{T}_2^{(1)} \rangle_a^p = \sum_{bcqr} \tilde{g}_{cbrq} (t_a^r \tau_{pq}^{cb} + t_c^p \tau_{ab}^{rq} + t_c^r \tau_{ba}^{qp} + t_b^q \tau_{ac}^{rp}).$$

Among these terms, we next consider  $\overline{H_N T_2^{(0)}} \mathbf{T}_1^{(1)}$ , the last of the second-order terms. Like the previous term, after contraction it generates eight diagrams and these are shown in Fig. 4.

The topological structures of the diagrams are very similar to those of Fig. 3 and the algebraic expression of the diagrams is

$$\langle \overline{H_N T_2^{(0)}} \mathbf{T}_1^{(1)} \rangle_a^p = \sum_{bcqr} \tilde{g}_{bcqr} (t_{ba}^{qr} \tau_c^p + t_{bc}^{qp} \tau_a^r + t_{ab}^{pq} \tau_c^r + t_{ac}^{rp} \tau_b^q).$$

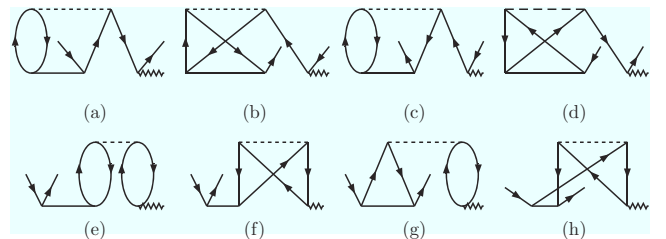
At the third order, as mentioned earlier, only  $\overline{H_N T_1^{(0)}} \mathbf{T}_1^{(0)} \mathbf{T}_1^{(1)}$  contributes to the  $\mathbf{T}_1^{(1)}$  diagrams. This term generates six Goldstone diagrams and these are shown in Fig. 5. The algebraic expression of the diagrams is

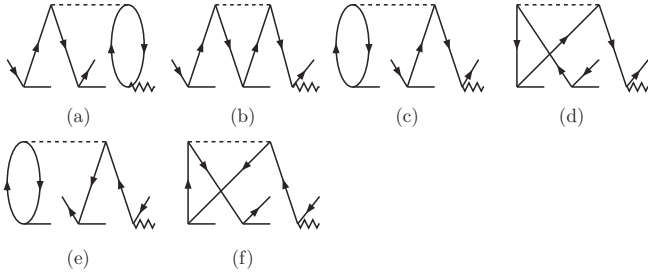
$$\langle \overline{H_N T_1^{(0)}} \mathbf{T}_1^{(0)} \mathbf{T}_1^{(1)} \rangle_a^p = \sum_{bcqr} \tilde{g}_{bcqr} (t_a^r t_c^p \tau_q^b + t_b^q t_a^r \tau_c^p + t_b^q t_c^p \tau_a^r).$$

In total, the nonlinear terms in the  $\mathbf{T}_1^{(1)}$  equation generate 30 Goldstone diagrams. Considering that  $T_2^{(0)}$  and  $\mathbf{T}_1^{(1)}$  are the dominant cluster operators, in terms of amplitudes, in the unperturbed RCC and PRCC approximations, respectively, we can expect the magnitude of  $\overline{H_N T_2^{(0)}} \mathbf{T}_1^{(1)}$  to be the largest.

### 2. $\mathbf{T}_2^{(1)}$ diagrams

In this section we discuss the Goldstone diagrams of  $\mathbf{T}_2^{(1)}$  arising from the nonlinear terms on the left-hand side of Eq. (22). Consider the second-order term; after expansion there are four terms as given in Eq. (23) and all have nonzero contributions to  $\mathbf{T}_2^{(1)}$ .

FIG. 4. Diagrams arising from the contraction  $\overline{H_N T_2^{(0)}} \mathbf{T}_1^{(1)}$ .


 FIG. 5. Diagrams arising from the contraction  $\overline{H_N T_1^{(0)} T_1^{(0)} T_1^{(1)}}$ .

The first term,  $\overline{H_N T_1^{(0)} T_1^{(1)}}$ , has six diagrams and these are shown in Fig. 6. The equivalent algebraic expression is

$$\langle \overline{H_N T_1^{(0)} T_1^{(1)}} \rangle_{ab}^{pq} = \sum_{rs} g_{pqrs} t_a^r t_b^s + \sum_{cd} g_{cdab} t_c^p t_d^q - \sum_{cr} g_{pcrb} \times [(t_a^r + t_b^r) t_c^q - t_c^q (t_a^r + t_b^r)],$$

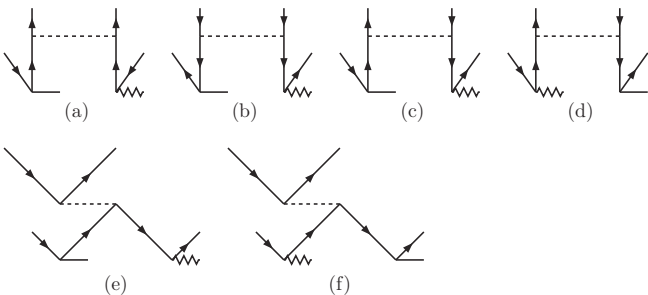
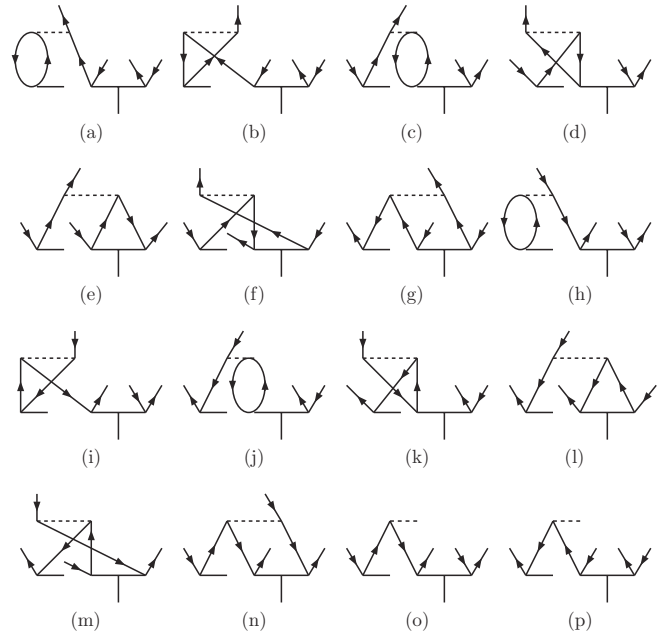
where we have used  $\langle \dots \rangle_{ab}^{pq}$  to represent the matrix element  $\langle \Phi_{ab}^{pq} | \dots | \Phi_0 \rangle$ . The next term,  $\overline{H_N T_1^{(0)} T_2^{(1)}}$ , has 16 diagrams and these are shown in Fig. 7.

However, the last two diagrams in Figs. 7(o) and 7(p) are zero when Dirac-Hartree-Fock-Breit orbitals are used, as in the present work. The equivalent algebraic expression is

$$\langle \overline{H_N T_1^{(0)} T_2^{(1)}} \rangle_{ab}^{pq} = \sum_{crs} g_{cqrs} (t_c^r t_{ba}^{sp} - t_c^s t_{ba}^{rp} + t_b^s \tilde{\tau}_{ca}^{rp} - t_b^r \tau_{ca}^{sp} - t_a^r \tau_{cb}^{ps} - t_c^p \tau_{ab}^{rs}) + \sum_{cdr} g_{cdrb} (-t_c^r \tau_{da}^{qp} + t_d^r \tau_{ca}^{qp} - t_d^q \tilde{\tau}_{ca}^{rp} + t_c^p \tau_{ad}^{rq} + t_a^r \tau_{cd}^{pq}),$$

where  $\tilde{\tau}_{ca}^{rp} = \tau_{ca}^{rp} - \tau_{ac}^{rp}$  is the antisymmetrized amplitude of  $T_2^{(1)}$ . Interchanging the order of excitations of the cluster operators, we get the next term  $\overline{H_N T_2^{(0)} T_1^{(1)}}$ . As in the previous term there are 16 diagrams; these are shown in Fig. 8 and the equivalent algebraic expression is

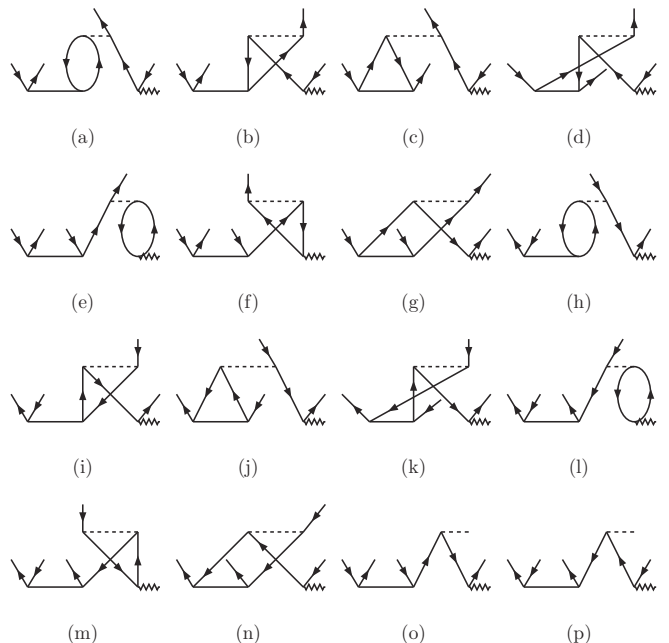
$$\langle \overline{H_N T_2^{(0)} T_1^{(1)}} \rangle_{ab}^{pq} = \sum_{crs} g_{cqrs} (\tilde{t}_{ac}^{pr} \tau_b^s - t_{ac}^{ps} \tau_b^r - t_{bc}^{sp} \tau_a^r + t_{ab}^{ps} \tau_c^r - t_{ab}^{pr} \tau_c^s - t_{ab}^{rs} \tau_c^p) + \sum_{cdr} g_{cdrb} (\tilde{t}_{ca}^{pr} \tau_d^q - t_{ad}^{pr} \tau_c^q + t_{da}^{qr} \tau_c^p - t_{ad}^{pq} \tau_c^r + t_{ac}^{pq} \tau_d^r + t_{cd}^{pq} \tau_a^r),$$


 FIG. 6. Diagrams arising from the contraction  $\overline{H_N T_1^{(0)} T_1^{(1)}}$ .

 FIG. 7. Diagrams arising from the contraction  $\overline{H_N T_1^{(0)} T_2^{(1)}}$ .

where  $\tilde{t}_{ac}^{pr} = t_{ac}^{pr} - t_{ac}^{rp}$  is the antisymmetrized amplitude of  $T_2^{(0)}$ . The last second-order term is  $\overline{H_N T_2^{(0)} T_2^{(1)}}$  and we can expect a large number of diagrams as both of the cluster operators are double excitation. There are 18 diagrams and these are shown in Fig. 9.

The algebraic expression for the diagrams is

$$\langle \overline{H_N T_2^{(0)} T_2^{(1)}} \rangle_{ab}^{pq} = \sum_{cdrs} g_{cdrs} (\tilde{t}_{ac}^{pr} \tilde{\tau}_{db}^{sq} - \tilde{t}_{ac}^{ps} \tau_{db}^{rq} + t_{ac}^{ps} \tau_{db}^{qr} + t_{ac}^{sq} \tau_{db}^{pr} - \tilde{t}_{ca}^{rs} \tau_{db}^{pq} - \tilde{t}_{cd}^{rp} \tau_{ab}^{sq} - t_{ab}^{ps} \tau_{dc}^{qr} + t_{ab}^{pr} \tau_{dc}^{qs} - t_{ac}^{pq} \tilde{\tau}_{bd}^{rs} + t_{ab}^{rs} \tau_{cd}^{pq} + t_{cd}^{pq} \tau_{ab}^{rs}).$$


 FIG. 8. Diagrams arising from the contraction  $\overline{H_N T_2^{(0)} T_1^{(1)}}$ .

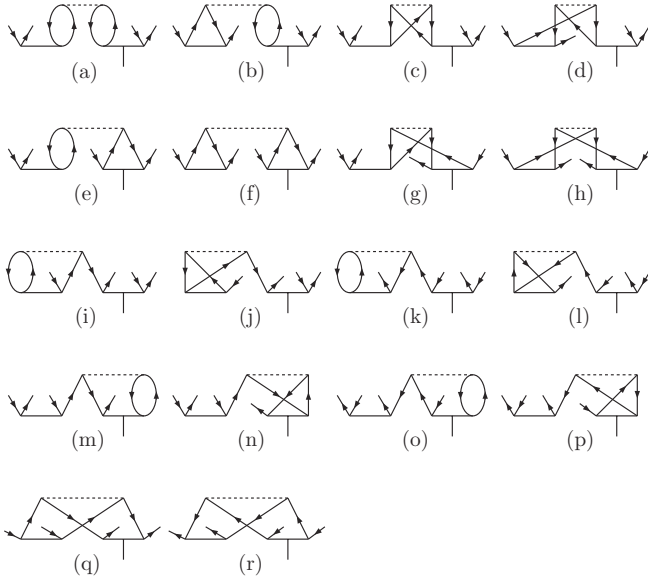


FIG. 9. Diagrams arising from the contraction  $\overline{H_N T_2^{(0)} T_2^{(1)}}$ .

Collecting all the diagrams which are second order in  $\mathbf{T}^{(1)}$ , there are 56 Goldstone diagrams in the  $\mathbf{T}_2^{(1)}$  equation after contraction of the cluster operators with  $H_N$ .

At the third order, all the terms in Eq. (24) have nonzero contributions to  $\mathbf{T}_2^{(1)}$ . There are six Goldstone diagrams from the first term  $\overline{H_N T_1^{(0)} T_1^{(0)} T_1^{(1)}}$  and these are shown in Fig. 10. The equivalent algebraic expression of the diagrams is

$$\begin{aligned} \langle \overline{H_N T_1^{(0)} T_1^{(0)} T_1^{(1)}} \rangle_{ab}^{pq} &= \sum_{crqs} g_{cqr} [ -t_a^r t_c^p \tau_b^s - (t_c^p \tau_a^r - t_a^r \tau_c^p) t_b^s ] \\ &+ \sum_{cdr} g_{cdr} [ t_a^r (t_c^p \tau_d^q + \tau_c^p t_d^q) + t_c^p \tau_a^r t_d^q ]. \end{aligned}$$

The overall contribution from these diagrams is expected to be small as these are quadratic in  $T_1^{(0)}$ . The next term,  $\overline{H_N T_1^{(0)} T_1^{(0)} T_2^{(1)}}$ , has ten Goldstone diagrams; these are shown in Fig. 11 and the equivalent algebraic expression of the diagrams is

$$\begin{aligned} \langle \overline{H_N T_1^{(0)} T_1^{(0)} T_2^{(1)}} \rangle_{ab}^{pq} &= \sum_{cdrs} g_{cdrs} [ t_a^r t_c^p \tilde{\tau}_{bd}^{sq} + t_a^r t_d^p \tau_{cb}^{sq} + t_a^r t_b^s \tau_{cd}^{pq} \\ &+ t_d^q (t_a^r \tau_{cb}^{ps} + t_c^p \tau_{ab}^{rs}) - (t_c^p t_a^s - t_c^s t_a^p) \tau_{db}^{pq} \\ &- (t_c^r t_d^p - t_d^r t_c^p) \tau_{ab}^{sq} ]. \end{aligned}$$

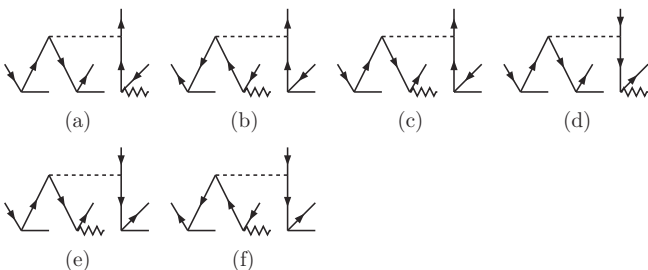


FIG. 10. Diagrams arising from the contraction  $\overline{H_N T_1^{(0)} T_1^{(0)} T_1^{(1)}}$ .

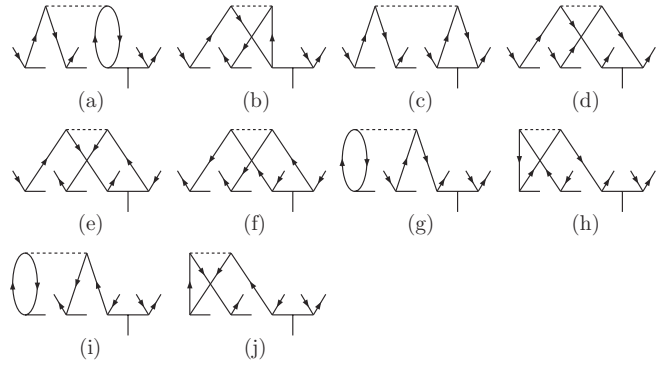


FIG. 11. Diagrams arising from the contraction  $\overline{H_N T_1^{(0)} T_1^{(0)} T_2^{(1)}}$ .

Contributions from these diagrams will be lower than  $\overline{H_N T_1^{(0)} T_1^{(0)} T_1^{(1)}}$  as these depend on  $\mathbf{T}_2^{(1)}$ , which is smaller in magnitude than  $\mathbf{T}_1^{(1)}$ . The contributions from the two terms are expected to be small as these are second order in  $T_1^{(0)}$ . The last third-order term  $\overline{H_N T_1^{(0)} T_2^{(0)} T_1^{(1)}}$  has 18 diagrams and these are shown in Fig. 12.

The algebraic equivalent of these diagrams is

$$\begin{aligned} \langle \overline{H_N T_1^{(0)} T_2^{(0)} T_1^{(1)}} \rangle_{ab}^{pq} &= \sum_{cdrs} g_{cdrs} [ (t_c^s t_{ab}^{pr} - t_c^r t_{ab}^{ps}) \tau_d^q - (t_c^r t_{ad}^{pq} \\ &- t_d^r t_{ac}^{pq}) \tau_b^s + t_a^r (t_{cb}^{ps} \tau_d^q - \tilde{t}_{db}^{sq} \tau_c^p + t_{cb}^{sq} \tau_d^p \\ &- t_{cb}^{pq} \tau_d^s + t_{db}^{pq} \tau_c^s + t_{cd}^{pq} \tau_b^s) + t_c^p (t_{ad}^{rq} \tau_b^s \\ &- \tilde{t}_{db}^{sq} \tau_a^r + t_{db}^{rq} \tau_a^s - t_{ab}^{rq} \tau_d^s + t_{ab}^{sq} \tau_d^r \\ &+ t_{ab}^{rs} \tau_d^q) ]. \end{aligned}$$

Among the third-order terms in the  $\mathbf{T}_2^{(1)}$  equation this will be the leading term as it depends on  $T_2^{(0)}$  and  $\mathbf{T}_1^{(1)}$ , the dominant cluster operators among the unperturbed and perturbed cluster operators, respectively. There are two Goldstone diagrams

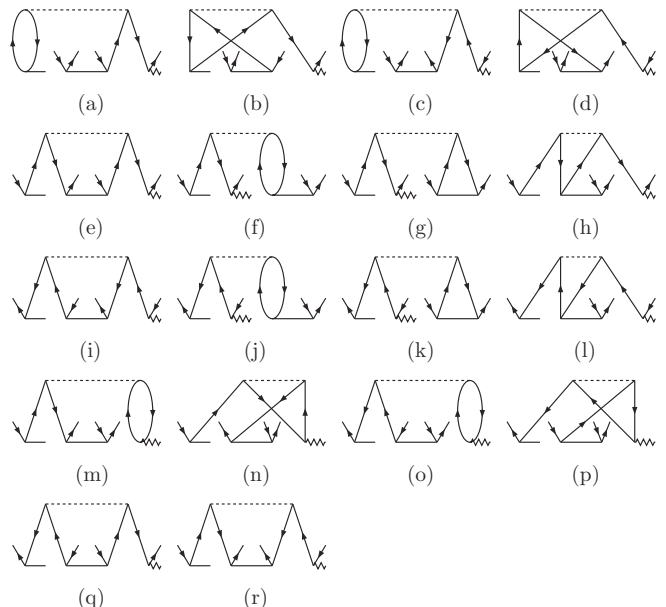
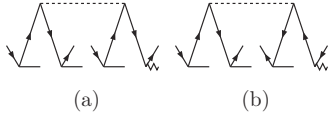


FIG. 12. Diagrams arising from the contraction  $\overline{H_N T_1^{(0)} T_2^{(0)} T_1^{(1)}}$ .


 FIG. 13. Diagrams arising from the contraction  $\overline{H_N T_1^{(0)} T_1^{(0)} T_1^{(0)} T_1^{(1)}}$ .

from the fourth-order term; these are shown in Fig. 13 and the algebraic expression is

$$\langle \overline{H_N T_1^{(0)} T_1^{(0)} T_1^{(0)} T_1^{(1)}} \rangle_{ab}^{pq} = \sum_{cdrs} g_{cdrs} t_d^r t_c^p (t_b^s \tau_d^q + t_d^q \tau_b^s).$$

Among all the diagrams considered so far these two diagrams will have the lowest contributions as these are third order in  $T_1^{(0)}$ . However, for completeness we include these in the calculations.

### 3. $\overline{\mathbf{D}T^{(0)}}$ and $\overline{\mathbf{D}T^{(0)}T^{(0)}}$ diagrams

Another group of PRCC diagrams arise from the contraction of  $\mathbf{D}$  and  $T^{(0)}$ ; these contribute to the right-hand side of Eqs. (21) and (22). In this group, there are five Goldstone diagrams of  $\mathbf{T}^{(1)}$  and these are shown in Fig. 14.

Among the diagrams only the last one is nonlinear in  $T^{(0)}$ . The algebraic expression of the diagrams is

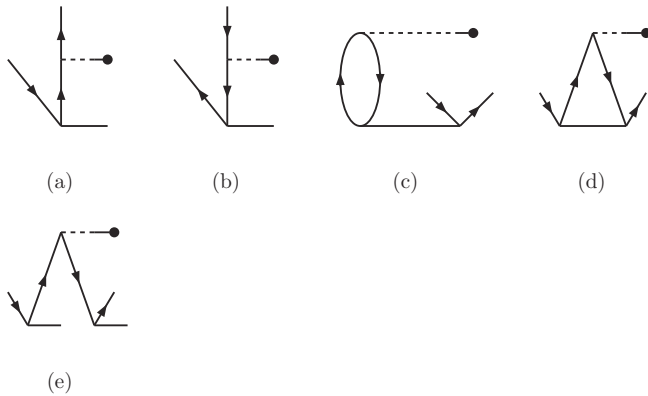
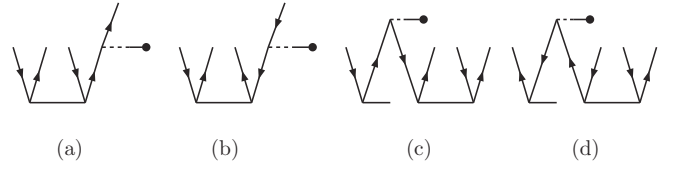
$$\begin{aligned} \langle \overline{\mathbf{D}T^{(0)}} \rangle_a^p + \langle \overline{\mathbf{D}T^{(0)}T^{(0)}} \rangle_a^p &= \sum_q \mathbf{r}_{pq} t_a^q - \sum_c \mathbf{r}_{ca} t_c^p \\ &\times \sum_{bq} \mathbf{r}_{bq} (t_{ba}^{qp} - t_{ab}^{qp} - t_a^q t_b^q), \end{aligned}$$

where  $\mathbf{r}_{ij} = \langle i | \mathbf{r} | j \rangle$  is the electronic part of the single-particle matrix element. For  $\mathbf{T}_2^{(1)}$ , there are four diagrams; these are shown in Fig. 15 and the last two are nonlinear in  $T^{(0)}$ .

The algebraic expression of the diagrams is

$$\begin{aligned} \langle \overline{\mathbf{D}T^{(0)}} \rangle_{ab}^{pq} + \langle \overline{\mathbf{D}T^{(0)}T^{(0)}} \rangle_{ab}^{pq} &= \sum_r \mathbf{r}_{qr} t_{ab}^{pr} - \sum_c \mathbf{r}_{cb} t_{ac}^{pq} \\ &\times \sum_{cr} \mathbf{r}_{cr} (-t_{a'cb}^{r pq} - t_c^p t_{ab}^{r q}). \end{aligned}$$

This completes the diagrammatic and algebraic analysis of the nonlinear terms in the  $\mathbf{T}^{(1)}$  equations. To obtain the linear


 FIG. 14. Singles diagrams arising from the contraction  $\overline{H_{\text{int}} T^{(0)} T^{(0)}}$ .

 FIG. 15. Doubles diagrams arising from the contraction  $\overline{H_{\text{int}} T^{(0)} T^{(0)}}$  and  $\overline{H_{\text{int}} T^{(0)} T^{(0)}}$ .

algebraic equations of the cluster amplitudes, each of the diagrams or terms in the algebraic expression requires further simplification to radial and angular components. The angular part is evaluated diagrammatically; however, the diagrams are different from the Goldstone diagrams.

## IV. DIPOLE POLARIZABILITY

From the second-order time-independent perturbation theory, the ground-state dipole polarizability of a closed-shell atom is

$$\alpha = -2 \sum_I \frac{\langle \Psi_0 | \mathbf{D} | \Psi_I \rangle \langle \Psi_I | \mathbf{D} | \Psi_0 \rangle}{E_0 - E_I}, \quad (27)$$

where  $|\Psi_I\rangle$  are the intermediate atomic states and  $E_I$  is the energy of the atomic state. As  $\mathbf{D}$  is an odd-parity operator,  $|\Psi_I\rangle$  must be opposite in parity to  $|\Psi_0\rangle$ . In the PRCC theory we can write

$$\alpha = - \frac{\langle \tilde{\Psi}_0 | \mathbf{D} | \tilde{\Psi}_0 \rangle}{\langle \tilde{\Psi}_0 | \tilde{\Psi}_0 \rangle}. \quad (28)$$

From the definition of  $|\tilde{\Psi}_0\rangle$  in Eq. (9) and based on the parity selection rules, only the terms linear in  $\lambda$  are nonzero. That is,

$$\alpha = - \frac{\langle \Phi_0 | \mathbf{T}^{(1)\dagger} \bar{\mathbf{D}} + \bar{\mathbf{D}} \mathbf{T}^{(1)} | \Phi_0 \rangle}{\langle \Psi_0 | \Psi_0 \rangle}, \quad (29)$$

where  $\bar{\mathbf{D}} = e^{T^{(0)\dagger}} \mathbf{D} e^{T^{(0)}}$  represents the unitary transformed electric dipole operator and  $\langle \Psi_0 | \Psi_0 \rangle$  is the normalization factor. From here on, it is implicit that expressions with more than one operator involve contraction and for compactness, we drop the notation representing operator contractions. Retaining the the leading-order terms, we obtain

$$\begin{aligned} \alpha \approx \frac{1}{\mathcal{N}} &\langle \Phi_0 | \mathbf{T}_1^{(1)\dagger} \mathbf{D} + \mathbf{D} \mathbf{T}_1^{(1)} + \mathbf{T}_1^{(1)\dagger} \mathbf{D} T_1^{(0)} + T_1^{(0)\dagger} \mathbf{D} \mathbf{T}_1^{(1)} \\ &+ \mathbf{T}_2^{(1)\dagger} \mathbf{D} T_1^{(0)} + T_1^{(0)\dagger} \mathbf{D} \mathbf{T}_2^{(1)} + \mathbf{T}_1^{(1)\dagger} \mathbf{D} T_2^{(0)} \\ &+ T_2^{(0)\dagger} \mathbf{D} \mathbf{T}_1^{(1)} + \mathbf{T}_2^{(1)\dagger} \mathbf{D} T_2^{(0)} + T_2^{(0)\dagger} \mathbf{D} \mathbf{T}_2^{(1)} | \Phi_0 \rangle, \end{aligned} \quad (30)$$

where  $\mathcal{N} = \langle \Phi_0 | \exp[T^{(0)\dagger}] \exp[T^{(0)}] | \Phi_0 \rangle$  is the normalization factor, which involves a nonterminating series of contractions between  $T^{(0)\dagger}$  and  $T^{(0)}$ . However, in the present work we use  $\mathcal{N} \approx \langle \Phi_0 | T_1^{(0)\dagger} T_1^{(0)} + T_2^{(0)\dagger} T_2^{(0)} | \Phi_0 \rangle$ . From the above expression for  $\alpha$ , an evident advantage of calculation using PRCC theory is the absence of summation over  $|\Psi_I\rangle$ . The summation is subsumed in the evaluation of  $\mathbf{T}^{(1)}$  in a natural way. This is one of the key advantages of using PRCC theory.

TABLE I. Comparison between GTO and GRASP92 results.

Atom	GTO	GRASP92
Ar	-528.6837	-528.6837
Kr	-2789.8605	-2788.8605
Xe	-7446.8976	-7446.8976
Rn	-23602.0202	-23602.0232

## V. CALCULATIONAL DETAILS

### A. Basis set and nuclear density

The first step of our calculations, which is also true of any atomic and molecular calculation, is to generate an orbital basis set. For the present work, we use the Dirac-Hartree-Fock Hamiltonian and even-tempered Gaussian-type orbitals (GTOs) [26]. The radial parts of the spin orbitals are linear combinations of the Gaussian-type functions

$$g_{\kappa p}^L(r) = C_{\kappa i}^L r^{n_{\kappa}} e^{-\alpha_p r^2}, \quad (31)$$

where  $p$  is the GTO index and  $C_{\kappa i}^L$  is the normalization constant. The exponent  $\alpha_p$  depends on two parameters  $\alpha_0$  and  $\beta$ ; these are related as  $\alpha_p = \alpha_0 \beta^{p-1}$ , where  $p = 0, 1, \dots, m$  and  $m$  is the number of Gaussian-type functions. The small components of the spin orbitals are linear combinations of  $g_{\kappa p}^S(r)$ , which are generated from  $g_{\kappa p}^L(r)$  through the kinetic balance condition [27]. We calculate the GTOs on a grid [28] and optimize the values of  $\alpha_0$  and  $\beta$  for individual atoms to match the spin-orbital energies and self-consistent-field (SCF) energy of GRASP92 [29], which solves Dirac-Hartree-Fock equations numerically. The comparison of the SCF energies is given in Table I. Except for Rn, there is excellent agreement between the SCF energies obtained from the GTOs and GRASP92. The symmetrywise values of the optimized  $\alpha_0$  and  $\beta$  are listed in Table II.

To optimize the basis set size, we examine the convergence of  $\alpha$  using the LPRCC theory. We start with a basis set of 50 GTOs and increase the basis set size in steps through a series of calculations. As an example, the results for the case of Kr are listed in Table III. The value of  $\alpha$  changes by only  $7 \times 10^{-4}$  when the number of basis states is increased from 117 to 131. So we can use the former for our calculations without compromising the desired accuracy.

In the present work we have considered a finite-size Fermi density distribution of the nucleus,

$$\rho_{\text{nuc}}(r) = \frac{\rho_0}{1 + e^{(r-c)/a}}, \quad (32)$$

TABLE II. The  $\alpha_0$  and  $\beta$  parameters of the even-tempered GTO basis used in the present calculations.

Atom	$s$		$p$		$d$	
	$\alpha_0$	$\beta$	$\alpha_0$	$\beta$	$\alpha_0$	$\beta$
Ar	0.00055	1.620	0.00515	2.405	0.00570	2.850
Kr	0.00015	2.015	0.00945	2.975	0.00635	2.845
Xe	0.00012	2.215	0.00495	2.995	0.00745	2.460
Rn	0.00010	2.280	0.00671	2.980	0.00715	2.720

TABLE III. Convergence pattern of  $\alpha(\text{Kr})$  as a function of the basis set size.

No. of orbitals	Basis size	$\alpha$
79	(15s, 9p, 9d, 7f, 7g)	16.8759
97	(17s, 11p, 11d, 9f, 9g)	16.7507
117	(21s, 13p, 13d, 11f, 11g)	16.7403
131	(25s, 15p, 14d, 13f, 11g)	16.7396
139	(25s, 16p, 15d, 13f, 13g)	16.7394
155	(29s, 17p, 16d, 15f, 15g)	16.7394

where  $a = t4 \ln(3)$ . The parameter  $c$  is the half charge radius so that  $\rho_{\text{nuc}}(c) = \rho_0/2$ , and  $t$  is the skin thickness. The PRCC equations are solved iteratively using the Jacobi method; we have chosen this method as it is easily parallelizable. The method, however, is slow to converge. So we use direct inversion in the iterated subspace [30] to accelerate the convergence.

### B. Breit interaction

There are two different but equivalent approaches, reported in previous works, to calculate the matrix elements of  $g^{\text{B}}(r_{12})$ . The first approach [31] is to couple the angular parts of the orbitals with Dirac matrices to give a linear combination of vector spherical harmonics. This is then combined with the angular part of  $1/r_{12}$  for integration. In the second approach [32],  $g^{\text{B}}(r_{12})$  is expanded as a linear combination of irreducible tensor operators. In the present work we use the latter and employ the expressions given in Ref. [33] to incorporate  $g^{\text{B}}(r_{12})$  in the GTO and RCC calculations. For the GTO calculation, Refs. [34,35] provide a very good description for inclusion of  $g^{\text{B}}(r_{12})$  in finite-basis-set calculations. To assess the relative importance of the Breit interaction, we calculate the first-order energy correction

$$\langle H^{\text{B}} \rangle_{\text{DF}} = \langle \Phi_0 | \sum_{i < j} g^{\text{B}}(r_{ij}) | \Phi_0 \rangle, \quad (33)$$

where  $|\Phi_0\rangle$  is the ground-state reference function generated from the Dirac-Hartree-Fock spin orbitals and  $H^{\text{B}} = \sum_{i < j} g^{\text{B}}(r_{ij})$  represents the many-particle form of the Breit interaction. The  $\langle H^{\text{B}} \rangle_{\text{DF}}$  values for the rare-gas atoms Ar, Kr, Xe, and Rn are listed in Table IV.

For each atom we calculated the SCF energy with  $H^{\text{DC}}$  and  $H^{\text{DCB}}$ ; these are  $E_{\text{SCF}}^{\text{DC}} = \langle \Phi_0 | H^{\text{DC}} | \Phi_0 \rangle$  and  $E_{\text{SCF}}^{\text{DCB}} = \langle \Phi_0 | H^{\text{DCB}} | \Phi_0 \rangle$ . Here,  $H^{\text{DC}} = H^{\text{DCB}} - H^{\text{B}}$  is the atomic Hamiltonian without the Breit interaction. From the table, it is evident that our results are in very good agreement with the previous results [36]. The largest deviation from the previous results is observed in Rn; our result for  $\langle H^{\text{B}} \rangle_{\text{DF}}$  is 0.8% lower than the previous result. However, as the Breit-interaction

TABLE IV. SCF energies for noble-gas atoms.

Atom	$E_{\text{SCF}}^{\text{DC}}$	$E_{\text{SCF}}^{\text{DCB}}$	$\langle H^{\text{B}} \rangle_{\text{DF}}$	Ref. [36]
Ar	-528.6837	-528.5511	0.1326	0.1324
Kr	-2788.8605	-2787.4310	1.4295	1.4268
Xe	-7446.8976	-7441.1248	5.7728	5.7753
Rn	-23602.0202	-23572.8480	29.1722	29.3968

contribution to  $E_{\text{SCF}}^{\text{DCB}}$  is a mere 0.12% in Rn, in absolute terms, the deviation is  $\approx 0.001\%$ . Our results are also in good agreement with the results of another previous study [37]. In the PRCC calculations, as described earlier, we treat  $H^{\text{B}}$  at par with the residual Coulomb interaction. However, to examine the relative importance of the Breit interaction, we calculate  $\alpha$  with and without  $H^{\text{B}}$ .

## VI. RESULTS AND DISCUSSION

The expression of  $\alpha$  in PRCC theory, as mentioned earlier, is a nonterminating series. However, the terms of order higher than quadratic in  $T$  have negligible contributions. For this reason, in the present work, we consider up to second order in the cluster operator. With the introduction of the Breit interaction in the total atomic Hamiltonian, the number of two-electron integrals becomes large and we need large memory to store these integrals. In first-order many-body perturbation theory (MBPT), which we use as the initial guess, there is an important change with the inclusion of  $H^{\text{B}}$ . With only the Coulomb interaction, at the first-order MBPT, the wave operator follows the parity selection rule and only selected multipoles of the Coulomb interaction contribute. However, with  $H^{\text{B}}$ , which has the opposite parity selection rule compared to the Coulomb interaction, all multipoles of the two-electron interaction which satisfy the triangular conditions are allowed. In Table V, we list the values of  $\alpha$  calculated using the LPRCC theory. For comparison we have also included the results from previous theoretical studies and experimental data. There are no discernible trends in the previous theoretical results and present work. For Kr and Xe, the results from the many-body perturbation theory [18] are higher than the experimental data, but with RCCSDT approximations [20], Ar and Kr have higher values. For Ar our result is 1% higher than the experimental data and this is consistent with the RCCSDT result reported in a previous work. It must, however, be mentioned that the previous work is based on the third-order Douglas-Kroll [21] method. Our result for Kr is in excellent agreement with the experimental data. This could be a coincidence arising from well-chosen basis set parameters and the inherent property of the PRCC theory to incorporate correlation effects more completely within a basis set.

In the case of Xe our result is 3.4% lower than the experimental data and 2.4% lower than the RCCSDT result. The latter difference from the the RCCSDT result can be partly attributed to the triple excitations. There is no experimental data for  $\alpha$  for Rn, the highest- $Z$  atom among the noble gases. In Ref. [20], the  $\alpha$  for Rn is computed using the RCCSDT approximation and their result is 6.2% lower than our result.

TABLE V. The static dipole polarizability  $\alpha$  (atomic units) from linearized PRCC calculations and comparison with previous results.

Method	Ar	Kr	Xe	Rn
RCCSDT [20]	11.22	16.80	27.06	33.18
CCSDT [19]	11.084	16.839	27.293	34.43
MBPT [18]	11.062	17.214	28.223	
This work	11.213	16.736	26.432	35.391
Expt. [38]	11.091	16.740	27.340	
Expt. [39]	11.081(5)	16.766(8)		

TABLE VI. Contribution to  $\alpha$  from different terms of the dressed dipole operator in the linearized PRCC theory.

Contributions from	Ar	Kr	Xe	Rn
$\mathbf{T}_1^{(1)\dagger}\mathbf{D} + \text{H.c.}$	12.191	18.613	30.855	41.641
$\mathbf{T}_1^{(1)\dagger}\mathbf{D}\mathbf{T}_2^{(0)} + \text{H.c.}$	-0.545	-0.888	-1.677	-2.328
$\mathbf{T}_2^{(1)\dagger}\mathbf{D}\mathbf{T}_2^{(0)} + \text{H.c.}$	0.510	0.748	1.352	1.862
$\mathbf{T}_1^{(1)\dagger}\mathbf{D}\mathbf{T}_1^{(0)} + \text{H.c.}$	-0.057	-0.118	-0.357	-0.301
$\mathbf{T}_2^{(1)\dagger}\mathbf{D}\mathbf{T}_1^{(0)} + \text{H.c.}$	0.022	0.038	0.092	0.073
Normalization	1.081	1.099	1.145	1.157
Total	11.213	16.736	26.432	35.391

To estimate the importance of the Breit interaction, we exclude  $H^{\text{B}}$  in the PRCC calculations and then calculate  $\alpha$ . The results are 11.202, 16.728, 26.404, and 35.266 for Ar, Kr, Xe, and Rn, respectively. These represent a decrease of 0.010, 0.012, 0.021, and 0.133 from the results with the inclusion of  $H^{\text{B}}$ . Except for Rn, the change in  $\alpha$  is below 0.1%. This implies that to obtain accurate results for Rn, it is desirable to include the Breit interaction in the calculations.

To examine the results in more detail, the contributions from the terms in the expression for  $\alpha$  given in Eq. (30) are listed in Table VI. It is evident that  $\mathbf{T}_1^{(1)\dagger}\mathbf{D}$  and its Hermitian conjugate are the leading-order terms. This is to be expected as these terms include the Dirac-Hartree-Fock-Breit contribution and RPA effects, which have the dominant contributions. In all the cases, the result from  $\mathbf{T}_1^{(1)\dagger}\mathbf{D}$  is larger than the total value of  $\alpha$  and shows dependence on  $Z$ : the results for Ar, Kr, Xe, and Rn from this term are 8.7%, 11.2%, 16.7%, and 17.7% higher than the total values of  $\alpha$ , respectively. The next-to-leading-order terms are  $\mathbf{T}_1^{(1)\dagger}\mathbf{D}\mathbf{T}_2^{(0)}$  and its Hermitian conjugate. Contributions from these terms are, approximately, a factor of 20 smaller than the leading-order terms and opposite in phase. On a closer inspection, it is natural that  $\mathbf{T}_1^{(1)\dagger}\mathbf{D}\mathbf{T}_2^{(0)}$  and its Hermitian conjugate are the next-to-leading-order terms. At the second order, these are the terms which have  $\mathbf{T}_1^{(1)}$  and  $\mathbf{T}_2^{(0)}$ , the dominant cluster amplitudes in the perturbed and unperturbed relativistic coupled-cluster theories. The results from  $\mathbf{T}_1^{(1)\dagger}\mathbf{D}\mathbf{T}_2^{(0)}$  have large cancellations with the term  $\mathbf{T}_2^{(1)\dagger}\mathbf{D}\mathbf{T}_2^{(0)}$ , which is almost the same in magnitude but opposite in sign. Interestingly, a similar pattern occurs with the  $\mathbf{T}_1^{(1)\dagger}\mathbf{D}\mathbf{T}_2^{(0)}$  terms. Namely, the results from  $\mathbf{T}_1^{(1)\dagger}\mathbf{D}\mathbf{T}_2^{(0)}$  are negative and opposite in sign to  $\mathbf{T}_2^{(1)\dagger}\mathbf{D}\mathbf{T}_2^{(0)}$ .

The results from the full PRCC, including the terms nonlinear in cluster amplitudes are given in Table VII. From

TABLE VII. Contribution to  $\alpha$  from different terms of the dressed dipole operator in the nonlinear PRCC theory.

Contributions from	Ar	Kr	Xe
$\mathbf{T}_1^{(1)\dagger}\mathbf{D} + \text{H.c.}$	12.950	18.622	33.108
$\mathbf{T}_1^{(1)\dagger}\mathbf{D}\mathbf{T}_2^{(0)} + \text{H.c.}$	-0.579	-0.899	-1.7964
$\mathbf{T}_2^{(1)\dagger}\mathbf{D}\mathbf{T}_2^{(0)} + \text{H.c.}$	0.488	0.769	1.278
$\mathbf{T}_1^{(1)\dagger}\mathbf{D}\mathbf{T}_1^{(0)} + \text{H.c.}$	-0.061	-0.096	-0.392
$\mathbf{T}_2^{(1)\dagger}\mathbf{D}\mathbf{T}_1^{(0)} + \text{H.c.}$	0.022	0.035	0.095
Normalization	1.081	1.099	1.145
Total	11.859	16.771	28.203

TABLE VIII. Core-orbital contribution from  $\mathbf{T}_1^{(1)\dagger}\mathbf{D} + \text{H.c.}$  to  $\alpha$ .

Ar	Kr	Xe	Rn
8.152 ( $3p_{3/2}$ )	12.872 ( $4p_{3/2}$ )	22.292 ( $5p_{3/2}$ )	34.524 ( $6p_{3/2}$ )
3.914 ( $3p_{1/2}$ )	5.572 ( $4p_{1/2}$ )	8.120 ( $5p_{1/2}$ )	6.502 ( $6p_{1/2}$ )
0.100 ( $3s_{1/2}$ )	0.058 ( $4s_{1/2}$ )	0.222 ( $4d_{5/2}$ )	0.382 ( $5d_{5/2}$ )
0.012 ( $2p_{3/2}$ )	0.056 ( $3d_{5/2}$ )	0.140 ( $4d_{3/2}$ )	0.214 ( $5d_{3/2}$ )

the table, it is clear that the nonlinear terms tend to increase the deviations from the experimental data. A similar trend was reported in our previous work on Ne [40]. For Ar, the nonlinear PRCC theory result is 5.4% larger than the result from linearized PRCC and it is 6.5% larger than the experimental result. Similarly, for Xe the nonlinear PRCC result is 6.3% larger than the linearized PRCC result. On the other hand for Kr, the nonlinear PRCC results are marginally larger than the linearized PRCC results. The larger values of  $\alpha$  in the nonlinear PRCC can almost entirely be attributed to the higher value of  $\mathbf{T}_1^{(1)\dagger}\mathbf{D}$  and its Hermitian conjugate. This means that the nonlinear terms tend to increase the RPA effects. This is an example where inclusion of higher-order terms enhances the uncertainty. It is possible that triple excitations, higher-order excitations not considered in the present work, may balance the deviations and bring the results closer to the experimental data.

For a more detailed analysis of the contributions from the RPA effects, we consider contributions from each of the core orbitals in  $\mathbf{T}_1^{(1)\dagger}\mathbf{D}$ . In terms of orbital indices the expression is

$$\mathbf{T}_1^{(1)\dagger}\mathbf{D} + \text{H.c.} = \sum_{ap} (\mathbf{r}_{ap}\tau_a^p + \tau_a^{p*}\mathbf{r}_{pa}), \quad (34)$$

where  $\mathbf{r}$  is the single-particle electric dipole operator. The values of the four leading core orbitals ( $a$ ) for each of the atoms are listed in Table VIII. In all the cases, the result from the outermost  $np_{3/2}$  valence orbitals are the largest. This is not surprising as these are the orbitals which have the largest spatial extent. In addition, as the matrix elements in the expression of  $\alpha$  have a quadratic dependence on radial distance, orbitals with larger radial extent have higher contributions. The next largest values arise from the  $np_{1/2}$  valence orbitals. Here we notice an interesting pattern in the results; with higher  $Z$  the ratio of the contribution from  $np_{3/2}$  to  $np_{1/2}$  increases. For Ar, Kr, and Xe the ratios are 2.1, 2.3, and 2.7, respectively. However, the ratio for Rn is much larger; it is 5.3. The reason for the trend in the ratios is the contraction of the  $np_{1/2}$  core orbitals due to relativistic corrections. Hence, the  $np_{1/2}$  valence orbitals of higher- $Z$  atoms show larger contraction and account for the higher ratio. The third largest contributions in Ar and Kr arise from the  $3s_{1/2}$  and  $4s_{1/2}$  orbitals, respectively. This is expected as these are the orbitals which are energetically just below the  $np$  orbitals, and spatially as well. On the contrary, for Xe and Rn, the third largest contributions should be from the  $5s_{1/2}$  and  $6s_{1/2}$  orbitals, respectively, but this is not case as these orbitals are contracted because of relativistic corrections. So the diffused  $nd_{5/2}$  orbitals have the third largest values. From the trends in the results of the RPA effects, it is obvious that the relativistic corrections are important for Xe and Rn.

TABLE IX. Core-orbital contributions from  $\mathbf{T}_1^{(1)\dagger}\mathbf{DT}_2^{(0)}$  to  $\alpha$  of argon and krypton.

Ar		Kr	
-0.124	( $3p_{3/2}, 3p_{1/2}$ )	-0.205	( $4p_{3/2}, 4p_{1/2}$ )
-0.118	( $3p_{3/2}, 3p_{3/2}$ )	-0.193	( $4p_{3/2}, 4p_{3/2}$ )
-0.027	( $3p_{1/2}, 3p_{1/2}$ )	-0.038	( $4p_{1/2}, 4p_{1/2}$ )
-0.006	( $3p_{3/2}, 3s_{1/2}$ )	-0.008	( $4p_{3/2}, 3d_{5/2}$ )

Next, we examine the pair-correlation effects, which are manifest through the next-to-leading-order term  $\mathbf{T}_1^{(1)\dagger}\mathbf{DT}_2^{(0)}$  and its Hermitian conjugate. In terms of orbital indices

$$\mathbf{T}_1^{(1)\dagger}\mathbf{DT}_2^{(0)} + \text{H.c.} = \sum_{abpq} [(\tau_a^{p*}\mathbf{r}_{bq} - \tau_a^{q*}\mathbf{r}_{bp})t_{ab}^{pq} + t_{ab}^{pq*}(\tau_a^p\mathbf{r}_{qb} - \tau_a^q\mathbf{r}_{pb})]. \quad (35)$$

The values of the four leading terms, listed in terms of the pairs of core orbitals ( $ab$ ), for Ar and Kr are given in Table IX. From the table we can identify ( $np_{3/2}, np_{1/2}$ ) as the most dominant pairing of the core orbitals among the double excitations. Considering that the pairing is between different orbitals, the number of cluster amplitudes is large and this explains the large contribution. The second and third dominant contributions, from the ( $np_{3/2}, np_{3/2}$ ) and ( $np_{1/2}, np_{1/2}$ ) pairs, are also on account of the number of cluster amplitudes. Since  $np_{3/2}$  and  $np_{1/2}$  accommodate four and two electrons each, respectively, the former has a larger number of cluster amplitudes. There is a small but important change in the results for Xe and Rn listed in Table X. The most dominant pair for these atoms is ( $np_{3/2}, np_{3/2}$ ) and the next dominant pair is ( $np_{3/2}, np_{1/2}$ ). This is in contrast to the sequence observed in Ar and Kr. The reason is that, although the latter pair has more cluster amplitudes, the  $np_{1/2}$  is contracted due to relativistic corrections. So the contribution to  $\alpha$  from  $T_2^{(0)}$  involving  $np_{1/2}$  is smaller. The difference between the results from the two pairs is even more dramatic in Rn. There are other changes in the case of Rn. The ( $6p_{3/2}, 5d_{5/2}$ ) pair, involving the diffused  $5d_{5/2}$  orbital, is now the third largest contribution, and the ( $6p_{1/2}, 6p_{1/2}$ ) pair, which has the contracted  $6p_{1/2}$  orbital, is the fourth largest contribution. This difference in the sequence of leading contributions for Rn arises from the larger relativistic corrections.

To estimate the uncertainty in our calculations, we have identified a few important sources of uncertainty. The first one is the truncation of the orbital basis sets. Although we start with nine symmetries for all the calculations, we increase the number of symmetries up to 13 in steps. The basis sets

TABLE X. Core-orbital contributions from  $\mathbf{T}_1^{(1)\dagger}\mathbf{DT}_2^{(0)}$  to  $\alpha$  of xenon and radon.

Xe		Rn	
-0.361	( $5p_{3/2}, 5p_{3/2}$ )	-0.591	( $6p_{3/2}, 6p_{3/2}$ )
-0.359	( $5p_{3/2}, 5p_{1/2}$ )	-0.387	( $6p_{3/2}, 6p_{1/2}$ )
-0.054	( $5p_{1/2}, 5p_{1/2}$ )	-0.071	( $6p_{3/2}, 5d_{5/2}$ )
-0.035	( $5p_{3/2}, 4d_{5/2}$ )	-0.036	( $6p_{1/2}, 6p_{1/2}$ )

chosen for the results given are taken after the value of  $\alpha$  converges to  $10^{-4}$ . So the uncertainty from the basis set truncation is negligible. The second source of uncertainty is the truncation of CC theory at the single and double excitations for both the unperturbed and perturbed RCC theories. Based on earlier studies, the contributions from the triple and quadruple excitations could be at the most  $\approx 3.3\%$ . This is also consistent with the deviations from the experimental data. Finally, the truncation of  $e^{T^{(1)\dagger}}\mathbf{D}e^{T^{(0)}} + e^{T^{(0)\dagger}}\mathbf{D}e^{T^{(1)}}$  is another source of uncertainty. From our earlier studies with an iterative method [41] to incorporate higher-order terms in the calculations of properties with CC theory, the contributions from the third or higher orders are negligibly small. Quantum electrodynamical corrections in this set of calculations are another source of uncertainty. However, they are expected to be smaller than the correction from the Breit interaction. As the largest Breit correction, in the case of Rn, is 0.1%, we can assume the corrections from QED effects to be at the most 0.1%. So, adding this, the maximum uncertainty in our calculations is 3.4%. However, it must be emphasized that, for Ar and Kr, the uncertainty is much smaller than this bound.

## VII. CONCLUSION

The PRCC theory is a general extension of the RCC method to incorporate an additional perturbation. The present work demonstrates that it is suitable for property calculations for closed-shell atoms. Although, in the present work we

have used the PRCC theory to calculate the electric dipole polarizability, the method can be extended to calculate other atomic properties as well.

The present study indicates, through a detailed analysis and identification of the dominant contributions, a discernible pattern in the relativistic corrections to  $\alpha$  arising from the contraction of the outermost  $p_{1/2}$  orbital. The notable impact of this is the larger fractional contribution from the outermost  $p_{3/2}$  orbitals to the terms which subsume RPA effects in the PRCC calculations,  $\mathbf{T}_1^{(1)\dagger}\mathbf{D}$  and its Hermitian conjugate, as we proceed from Ar to Rn. For Rn, the effect of relativistic corrections is also identifiable without any ambiguity in the pair-correlation effects; the  $(6p_{1/2}, 6p_{1/2})$  pair is below the  $(6p_{3/2}, 5d_{5/2})$  pair for the term  $\mathbf{T}_1^{(1)\dagger}\mathbf{D}\mathbf{T}_2^{(0)}$  in the PRCC calculations.

We have also examined the importance of the Breit interaction in the calculation of  $\alpha$ . The largest change of 0.1% is associated with Rn, the heaviest noble-gas atom. So, when the required uncertainty of the calculations is below 1%, the inclusion of the Breit interaction is desirable for higher- $Z$  closed-shell atoms like Rn.

## ACKNOWLEDGMENTS

We thank S. Gautam, Arko Roy, and Kuldeep Suthar for useful discussions. The results presented in the paper are based on computations using the 3TFLOP HPC Cluster at the Physical Research Laboratory, Ahmedabad.

- 
- [1] I. Khriplovich, *Parity Nonconservation in Atomic Phenomena* (Gordon and Breach Science Publishers, Philadelphia, 1991).
- [2] T. Udem, R. Holzwarth, and T. W. Hansch, *Nature (London)* **416**, 233 (2002).
- [3] S. A. Diddams, J. C. Bergquist, S. R. Jefferts, and C. W. Oates, *Science* **306**, 1318 (2004).
- [4] M. H. Anderson, J. R. Ensher, M. R. Matthews, C. E. Wieman, and E. A. Cornell, *Science* **269**, 198 (1995).
- [5] C. C. Bradley, C. A. Sackett, J. J. Tollett, and R. G. Hulet, *Phys. Rev. Lett.* **75**, 1687 (1995).
- [6] K. B. Davis, M. O. Mewes, M. R. Andrews, N. J. van Druten, D. S. Durfee, D. M. Kurn, and W. Ketterle, *Phys. Rev. Lett.* **75**, 3969 (1995).
- [7] J. Mitroy, M. S. Safronova, and C. W. Clark, *J. Phys. B* **43**, 202001 (2010).
- [8] F. Coester, *Nucl. Phys.* **7**, 421 (1958).
- [9] F. Coester and H. Kümmel, *Nucl. Phys.* **17**, 477 (1960).
- [10] R. J. Bartlett and M. Musiał, *Rev. Mod. Phys.* **79**, 291 (2007).
- [11] B. K. Mani, K. V. P. Latha, and D. Angom, *Phys. Rev. A* **80**, 062505 (2009).
- [12] H. S. Nataraj, B. K. Sahoo, B. P. Das, and D. Mukherjee, *Phys. Rev. Lett.* **101**, 033002 (2008).
- [13] R. Pal, M. S. Safronova, W. R. Johnson, A. Derevianko, and S. G. Porsev, *Phys. Rev. A* **75**, 042515 (2007).
- [14] G. Gopakumar, H. Merlitz, S. Majumder, R. K. Chaudhuri, B. P. Das, U. S. Mahapatra, and D. Mukherjee, *Phys. Rev. A* **64**, 032502 (2001).
- [15] T. A. Isaev, A. N. Petrov, N. S. Mosyagin, A. V. Titov, E. Eliav, and U. Kaldor, *Phys. Rev. A* **69**, 030501 (2004).
- [16] G. Hagen, T. Papenbrock, D. J. Dean, and M. Hjorth-Jensen, *Phys. Rev. Lett.* **101**, 092502 (2008).
- [17] R. F. Bishop, P. H. Y. Li, D. J. J. Farnell, and C. E. Campbell, *Phys. Rev. B* **79**, 174405 (2009).
- [18] A. J. Thakkar, H. Hettema, and P. E. S. Wormer, *J. Chem. Phys.* **97**, 3252 (1992).
- [19] P. Soldan, E. P. F. Lee, and T. G. Wright, *Phys. Chem. Chem. Phys.* **3**, 4661 (2001).
- [20] T. Nakajima and K. Hirao, *Chem. Lett.* **30**, 766 (2001).
- [21] T. Nakajima and K. Hirao, *J. Chem. Phys.* **113**, 7786 (2000).
- [22] P. J. Mohr, B. N. Taylor, and D. B. Newell, *Rev. Mod. Phys.* **84**, 1527 (2012).
- [23] G. E. Brown and D. G. Ravenhall, *Proc. R. Soc. London, A* **208**, 552 (1951).
- [24] J. Sucher, *Phys. Rev. A* **22**, 348 (1980).
- [25] I. Lindgren and J. Morrison, *Atomic Many-Body Theory*, 2nd ed. (Springer, New York, 1986).
- [26] A. K. Mohanty and E. Clementi, *J. Chem. Phys.* **93**, 1829 (1990).
- [27] R. E. Stanton and S. Havriliak, *J. Chem. Phys.* **81**, 1910 (1984).
- [28] R. K. Chaudhuri, P. K. Panda, and B. P. Das, *Phys. Rev. A* **59**, 1187 (1999).
- [29] F. A. Parpia, C. Froese Fischer, and I. P. Grant, *Comput. Phys. Commun.* **94**, 249 (1996).
- [30] P. Pulay, *Chem. Phys. Lett.* **73**, 393 (1980).

- [31] J. B. Mann and W. R. Johnson, *Phys. Rev. A* **4**, 41 (1971).
- [32] I. P. Grant and N. C. Pyper, *J. Phys. B* **9**, 761 (1976).
- [33] I. P. Grant and B. J. McKenzie, *J. Phys. B* **13**, 2671 (1980).
- [34] H. M. Quiney, in *Handbook of Molecular Physics and Quantum Chemistry*, edited by S. Wilson, P. P. Bernath, and R. McWeeny (John Wiley & Sons, Chichester, 2003), Vol. 2, pp. 444–483.
- [35] E. Clementi, *Modern Techniques in Computational Chemistry: MOTECC-91* (ESCOM Sci. Pub. B. V., Leiden, 1991).
- [36] F. A. Parpia, A. K. Mohanty, and E. Clementi, *J. Phys. B* **25**, 1 (1992).
- [37] Y. Ishikawa, H. M. Quiney, and G. L. Malli, *Phys. Rev. A* **43**, 3270 (1991).
- [38] P. W. Langhoff and M. Karplus, *J. Opt. Soc. Am.* **59**, 863 (1969).
- [39] R. H. Orcutt and R. H. Cole, *J. Chem. Phys.* **46**, 697 (1967).
- [40] S. Chattopadhyay, B. K. Mani, and D. Angom, *Phys. Rev. A* **86**, 022522 (2012).
- [41] B. K. Mani and D. Angom, *Phys. Rev. A* **81**, 042514 (2010).

# Electric dipole polarizabilities of doubly ionized alkaline-earth-metal ions from perturbed relativistic coupled-cluster theory

S. Chattopadhyay,<sup>1</sup> B. K. Mani,<sup>2</sup> and D. Angom<sup>1</sup><sup>1</sup>*Physical Research Laboratory, Ahmedabad 380009, Gujarat, India*<sup>2</sup>*Department of Physics, University of South Florida, Tampa, Florida 33620, USA*

(Received 21 May 2013; published 12 June 2013)

Using perturbed relativistic coupled-cluster (PRCC) theory we compute the ground-state electric dipole polarizability,  $\alpha$ , of doubly ionized alkaline earth metal ions  $\text{Mg}^{2+}$ ,  $\text{Ca}^{2+}$ ,  $\text{Sr}^{2+}$ ,  $\text{Ba}^{2+}$ , and  $\text{Ra}^{2+}$ . In the present work we use the Dirac-Coulomb-Breit atomic Hamiltonian and we also include the Uehling potential, which is the leading-order term in the vacuum polarization corrections. We examine the correction to the orbital energies arising from the Uehling potential in the self-consistent field calculations as well as perturbatively. Our results for  $\alpha$  are in very good agreement with the experimental data, and we observe a change in the nature of the orbital energy corrections arising from the vacuum polarization as we go from  $\text{Mg}^{2+}$  to  $\text{Ra}^{2+}$ .

DOI: [10.1103/PhysRevA.87.062504](https://doi.org/10.1103/PhysRevA.87.062504)

PACS number(s): 31.15.bw, 31.15.ap, 31.30.J-, 31.15.ve

## I. INTRODUCTION

The static electric dipole polarizability,  $\alpha$ , of an atom or ion is a measure of the first-order response to an external electric field. It is an essential parameter to determine any property associated with atom-field or ion-field interactions as well as atom-atom and atom-ion interactions. The properties include the refractive indexes, dielectric constants, ion mobility in gases, and van der Waal's constants [1] and  $\alpha$  has been measured using a wide variety of experimental techniques [2]. For closed-shell ions, like the doubly ionized alkaline-earth-metal ions,  $\alpha$  is a good representative of the core-polarization effects.

Theoretically,  $\alpha$  of the many electron atoms and ions have been calculated using different many-body methods. A recent review on atomic and ionic polarizabilities [3] provides a description of the theoretical methods used in the calculation of  $\alpha$ . However, among the various theoretical methods, the ones based on coupled-cluster theory (CCT) [4,5] are ideal for atoms and ions which are closed shell or with few valence electrons. The CCT is, among the many-body theories, one of the most reliable and powerful. It takes into account the electron correlation to all order. A detailed discussion on the CCT and different variants is given in a recent review [6], and very good descriptions of the application of nonrelativistic CCT to atomic and molecular systems are given in Refs. [7,8]. The CCT has been used with great success in atomic [9–14], molecular [15], nuclear [16], and condensed-matter physics [17] calculations. For the theoretical calculations of  $\alpha$ , the CCT-based methods which have given very precise results are the finite field [18], sum over states [19,20], and perturbed relativistic coupled-cluster (PRCC) theory [21–23].

In a previous work, the CCT-based finite-field method with the Douglas-Kroll Hamiltonian [24] was used to compute the  $\alpha$  of the alkaline-earth-metal ions [25]. In this work we compute the  $\alpha$  of doubly ionized alkaline-earth-metal ions using the PRCC theory. The method was used in our previous works to calculate the  $\alpha$  of noble gas atoms [21,22] and alkaline-earth metal ions [23]. The theory is the conventional relativistic coupled-cluster (RCC) theory with an additional perturbation. To account for the additional perturbation, we introduce a new set of cluster operators and accordingly define a second set

of cluster equations. The equations, however, are linear in the cluster operators and the new operators obey the same selection rules as the perturbation Hamiltonian. In the calculation of  $\alpha$  the perturbation is the external electric field  $\mathbf{E}$ . In the present work we use the Dirac-Coulomb-Breit atomic Hamiltonian along with the vacuum polarization (VP) potential. The VP potential is treated self-consistently as well as perturbatively.

The paper is organized as follows. In Sec. II we give a brief discussion on RCC and PRCC theory along with the VP correction. The theoretical formulation of  $\alpha$  in the framework of PRCC theory is discussed in Sec. III. In Sec. IV we give the details of our calculational methodology. Next we discuss about the VP correction to the orbital energies of doubly ionized alkaline-earth-metal ions. In the subsequent sections we give the results of static polarizability and discuss it in great detail. Then we end with the conclusion. All the results presented in this work and related calculations are in atomic units ( $\hbar = m_e = e = 4\pi\epsilon_0 = 1$ ). In this system of units the velocity of light is  $\alpha^{-1}$ , the inverse of fine structure constant, for which we use the value of  $\alpha^{-1} = 137.035\,999\,074$  [26].

## II. THEORETICAL METHODS

A detailed description of the RCC theory for closed-shell atoms is given in Ref. [13] and similarly a detailed account of PRCC theory is given in our previous works [21–23]. However, for completeness and easy reference we provide a brief overview in this section.

### A. RCC and PRCC theory

In the present work we use the Dirac-Coulomb-Breit non-virtual-pair Hamiltonian,  $H^{\text{DCB}}$ , to incorporate the relativistic effects and avoid the difficulties associated with the negative continuum states [27]. For a doubly ionized atom with  $N$  electrons [28]

$$H^{\text{DCB}} = \Lambda_{++} \sum_{i=1}^N [c\alpha_i \cdot \mathbf{p}_i + (\beta_i - 1)c^2 - V_{N+2}(r_i)] + \sum_{i < j}^{N,N} \left[ \frac{1}{r_{ij}} + g^{\text{B}}(r_{ij}) \right] \Lambda_{+++}, \quad (1)$$

where  $\alpha$  and  $\beta$  are the Dirac matrices,  $\Lambda_{++}$  is an operator which projects to the positive energy solutions, and  $V_{N+2}(r_i)$  is the nuclear potential arising from the  $Z = (N + 2)$  nucleus. Projecting the Hamiltonian with  $\Lambda_{++}$  ensures that the ill effects of the negative-energy continuum states are removed from the calculations. An elegant alternative to the projection operators, better suited for numerical computations, is to use the kinetically balanced finite basis sets [29–32]. This is the method adopted in the present work to generate the orbital basis sets. Returning to  $H^{\text{DCB}}$ , the last two terms,  $1/r_{ij}$  and  $g^{\text{B}}(r_{ij})$ , are the Coulomb and Breit interactions, respectively. The latter, Breit interaction, represents the transverse photon interaction and is given by

$$g^{\text{B}}(r_{12}) = -\frac{1}{2r_{12}} \left[ \alpha_1 \cdot \alpha_2 + \frac{(\alpha_1 \cdot \mathbf{r}_{12})(\alpha_2 \cdot \mathbf{r}_{12})}{r_{12}^2} \right]. \quad (2)$$

The general trends in the observables arising from the inclusion of Breit interaction in RCC and PRCC are discussed in our previous work on noble gas atoms [22]. For a closed-shell ion, the ground-state eigenvalue equation is

$$H^{\text{DCB}}|\Psi_0\rangle = E_0|\Psi_0\rangle, \quad (3)$$

where  $|\Psi_0\rangle$  is the ground state of the ion. In the presence of a perturbation Hamiltonian,  $H_{\text{int}}$ , the eigenvalue equation is modified to

$$(H^{\text{DCB}} + \lambda H_{\text{int}})|\tilde{\Psi}_0\rangle = \tilde{E}_0|\tilde{\Psi}_0\rangle, \quad (4)$$

where  $\lambda$  is the perturbation parameter,  $|\tilde{\Psi}_0\rangle$  is the perturbed ground state, and  $\tilde{E}_0$  is the corresponding eigenenergy. The origin of  $H_{\text{int}}$  could be internal to the ion, like the hyperfine interaction, or external, like the interaction with an external electromagnetic field  $\mathbf{E}$ .

In the RCC and PRCC theories, we define two sets of coupled-cluster operators  $T^{(0)}$  and  $\mathbf{T}^{(1)}$ , which we refer to as the unperturbed and perturbed coupled-cluster operators, respectively. The former is equivalent to the conventional cluster operators, and the latter is an additional set of cluster operators introduced in our recent works [21–23]. It accounts for the electron correlation effects arising from  $H_{\text{int}}$  and follows the same selection rules as  $H_{\text{int}}$ . To calculate  $\alpha$ , consider the interaction of the ion with an electrostatic electric field  $\mathbf{E}$ . The interaction Hamiltonian is then

$$H_{\text{int}} = -\sum_i \mathbf{r}_i \cdot \mathbf{E} = \mathbf{D} \cdot \mathbf{E}, \quad (5)$$

where  $\mathbf{D}$  is the many-electron electric dipole operator. The cluster operators  $\mathbf{T}^{(1)}$  are then rank one tensor operators in the electronic space and follows the same parity selection rule as  $H_{\text{int}}$ . Consequently, as  $H_{\text{int}}$  is parity odd, there is no first-order perturbative correction to the energy, so to first order in  $\lambda$  we get  $\tilde{E}_0 = E_0$ . Using the cluster operators  $T^{(0)}$  and  $\mathbf{T}^{(1)}$ , the atomic states of unperturbed and perturbed atomic Hamiltonians are

$$|\Psi_0\rangle = e^{T^{(0)}}|\Phi_0\rangle, \quad (6a)$$

$$|\tilde{\Psi}_0\rangle = e^{[T^{(0)} + \lambda \mathbf{T}^{(1)} \cdot \mathbf{E}]}\Phi_0, \quad (6b)$$

where  $|\Phi_0\rangle$  is the reference-state wave function. The cluster operators involve all possible excitations; however, a simplified but accurate representation is the coupled-cluster single and double (CCSD) excitation approximation. With this

approximation

$$T^{(0)} = T_1^{(0)} + T_2^{(0)}, \quad (7a)$$

$$\mathbf{T}^{(1)} = \mathbf{T}_1^{(1)} + \mathbf{T}_2^{(1)}, \quad (7b)$$

where the subscripts represent the level of excitation. In the second quantized notations

$$T_1^{(0)} = \sum_{a,p} t_a^p a_p^\dagger a_a, \quad (8a)$$

$$T_2^{(0)} = \frac{1}{2!} \sum_{a,b,p,q} t_{ab}^{pq} a_p^\dagger a_q^\dagger a_b a_a, \quad (8b)$$

where  $t_{\dots}$  are cluster amplitudes,  $a_i^\dagger$  ( $a_i$ ) are single-particle creation (annihilation) operators, and  $abc \dots$  ( $pqr \dots$ ) represent core (virtual) states. Similarly, the perturbed cluster operators are represented as

$$\mathbf{T}_1^{(1)} = \sum_{a,p} \tau_a^p \mathbf{C}_1(\hat{r}) a_p^\dagger a_a,$$

$$\mathbf{T}_2^{(1)} = \sum_{a,b,p,q} \sum_{l,k} \tau_{ab}^{pq}(l,k) \{\mathbf{C}_l(\hat{r}_1) \mathbf{C}_k(\hat{r}_2)\}^l a_p^\dagger a_q^\dagger a_b a_a.$$

Here,  $\mathbf{C}_1(\hat{r})$ , a  $\mathbf{C}$  tensor, is used to represent the vector nature of  $\mathbf{T}_1^{(1)}$ . On the other hand, two  $\mathbf{C}$  tensor operators of rank  $l$  and  $k$  are coupled together to form a rank one tensor operator,  $\mathbf{T}_2^{(1)}$ . For a more rigorous description of the tensor structure of the PRCC operators we refer to our previous work [22].

## B. Linearized PRCC theory

In this section we describe in brief the linearized form of the PRCC (LPRCC) theory. It is much simpler than the complete PRCC but encompasses all the important many-body effects. To derive the LPRCC equations, as discussed earlier, consider  $\mathbf{E}$  as the perturbation. The eigenvalue equation is then

$$(H^{\text{DCB}} + \lambda H_{\text{int}})e^{[T^{(0)} + \lambda \mathbf{T}^{(1)} \cdot \mathbf{E}]}\Phi_0 = \tilde{E}_0 e^{[T^{(0)} + \lambda \mathbf{T}^{(1)} \cdot \mathbf{E}]}\Phi_0. \quad (9)$$

By using the normal ordered form of the Hamiltonian, the eigenvalue equation may be written as

$$(H_{\text{N}}^{\text{DCB}} + \lambda H_{\text{int}})|\tilde{\Psi}_0\rangle = \Delta E_0|\tilde{\Psi}_0\rangle, \quad (10)$$

where  $\Delta E_0 = E_0 - \langle \Phi_0 | H^{\text{DCB}} | \Phi_0 \rangle$  is the ground-state correlation energy of the many-electron ion. Using the PRCC wavefunction in Eq. (6b), we write the ground state as

$$|\tilde{\Psi}_0\rangle \approx e^{T^{(0)}} [1 + \lambda \mathbf{T}^{(1)} \cdot \mathbf{E}]|\Phi_0\rangle. \quad (11)$$

Using this expression, the PRCC eigenvalue equation assumes the form

$$\begin{aligned} (H_{\text{N}}^{\text{DCB}} + \lambda H_{\text{int}}) e^{T^{(0)}} [(1 + \lambda \mathbf{T}^{(1)} \cdot \mathbf{E})]|\Phi_0\rangle \\ = \Delta E_0 e^{T^{(0)}} [(1 + \lambda \mathbf{T}^{(1)} \cdot \mathbf{E})]|\Phi_0\rangle. \end{aligned} \quad (12)$$

Following the standard coupled-cluster ansatz, as the initial step to derive the cluster amplitude equations, we apply  $e^{-T^{(0)}}$  from the left and get

$$[\tilde{H}_{\text{N}}^{\text{DCB}} + \lambda \tilde{H}_{\text{int}}] e^{\lambda \mathbf{T}^{(1)} \cdot \mathbf{E}}|\Phi_0\rangle = \Delta E_0 e^{\lambda \mathbf{T}^{(1)} \cdot \mathbf{E}}|\Phi_0\rangle, \quad (13)$$

where  $\bar{H} = e^{-T^{(0)}} H e^{T^{(0)}}$  is the similarity transformed Hamiltonian. After applying  $e^{-\lambda \mathbf{T}^{(1)}}$  from the left and considering the terms linear in  $\lambda$ , we obtain the PRCC equation

$$([\bar{H}_N^{\text{DC}}, \mathbf{T}^{(1)}] \cdot \mathbf{E} + \bar{H}_{\text{int}}) |\Phi_0\rangle = 0. \quad (14)$$

The linearized PRCC is the approximation where we take  $[\bar{H}_N^{\text{DC}}, \mathbf{T}^{(1)}] \approx [H_N^{\text{DC}}, \mathbf{T}^{(1)}]$  and  $\bar{H}_{\text{int}} \approx \mathbf{D} + [\mathbf{D}, T^{(0)}]$ . The eigenvalue equation is then reduced to

$$[H_N^{\text{DCB}}, \mathbf{T}^{(1)}] |\Phi_0\rangle = (\mathbf{D} + [\mathbf{D}, T^{(0)}]) |\Phi_0\rangle. \quad (15)$$

For simplicity, we have dropped  $\mathbf{E}$  from the equation. The equations of the cluster amplitudes  $\mathbf{T}_1^{(1)}$  and  $\mathbf{T}_2^{(1)}$  are obtained by projecting the above equation to singly and doubly excited states  $\langle \Phi_a^p |$  and  $\langle \Phi_{ab}^{pq} |$ , respectively. These states, however, must be opposite in parity to the reference state  $|\Phi_0\rangle$ . The equations so obtained form a set of linear algebraic equations and are solved using standard linear algebraic methods.

The other method of calculating  $\alpha$  which avoids summation over the intermediate states is the finite-field method [18]. The method, however, requires evaluation of the energy for different values of  $\mathbf{E}$  and this implies computing the cluster amplitudes multiple times. In the PRCC theory, however, the computations of the cluster amplitudes are limited to one time evaluation of  $T^{(0)}$  and  $\mathbf{T}^{(1)}$ . Although the equations of  $\mathbf{T}^{(1)}$  are linear, the tensor nature translates into angular factors consisting of a large number of  $6j$  symbols and  $9j$  symbols. So, for our present work we resort to a symmetry-adapted storing of these angular factors.

### C. Vacuum polarization

In the present work we incorporate the vacuum polarization (VP) corrections to the electron-nucleus interactions. It modifies the Coulomb potential between the nucleus and electrons. For a point nucleus, to the order of  $Z\alpha$ , it is given by the Uehling potential [33]

$$V_{\text{Ue}}(r) = -\frac{2\alpha Z}{3\pi r} \int_1^\infty dt \sqrt{t^2 - 1} \left( \frac{1}{t^2} + \frac{1}{2t^4} \right) \exp \left[ -\frac{2rt}{\alpha} \right],$$

where  $Z$  is the nuclear charge and  $\alpha$ , in this case, is the fine structure constant. The latter is not to be confused with the dipole polarizability. In heavy atoms a finite-size Fermi charge distribution model of the nucleus is more appropriate [34] and it is defined as

$$\rho_{\text{nuc}}(r) = \frac{\rho_0}{1 + e^{(r-c)/a}}, \quad (16)$$

where  $a = t4 \ln(3)$ . The parameter  $c$  is the half charge radius so that  $\rho_{\text{nuc}}(c) = \rho_0/2$  and  $t$  is the skin thickness. For a consistent treatment of the nucleus-electron electrostatic interaction,  $V_{\text{Ue}}(r)$  must be modified to account for the finite nuclear size. This is done by folding  $V_{\text{Ue}}(r)$  with the  $\rho_{\text{nuc}}(r)$  [35]. The modified form of the Uehling potential is [36]

$$V_{\text{Ue}}(r) = -\frac{2\alpha^2}{3r} \int_0^\infty dx x \rho(x) \int_1^\infty dt \sqrt{t^2 - 1} \\ \times \left( \frac{1}{t^3} + \frac{1}{2t^5} \right) (e^{-2ct|(r-x)} - e^{-2ct(r+x)}).$$

We add this to the electron-nucleus Coulomb interaction potential in the self-consistent field computations to generate the single-particle states. The Uehling potential is the leading order term in VP correction and it accounts for more than 90% of the VP correction in hydrogen-like ions, so we identify it as the VP correction in the subsequent sections.

### III. DIPOLE POLARIZABILITY

In the present calculation of  $\alpha$  we use the PRCC expression discussed and described in our previous works [21,22]. Accordingly, the  $\alpha$  of the ground state of a doubly ionized alkaline atom is

$$\alpha = -\frac{\langle \Phi_0 | \mathbf{T}^{(1)\dagger} \bar{\mathbf{D}} + \bar{\mathbf{D}} \mathbf{T}^{(1)} | \Phi_0 \rangle}{\langle \Psi_0 | \Psi_0 \rangle}, \quad (17)$$

where  $\bar{\mathbf{D}} = e^{T^{(0)\dagger}} \mathbf{D} e^{T^{(0)}}$  is a nonterminating series, we consider only the leading-order terms in this expression and we get

$$\alpha = -\frac{1}{\mathcal{N}} \langle \Phi_0 | \mathbf{T}_1^{(1)\dagger} \mathbf{D} + \mathbf{D} \mathbf{T}_1^{(1)} + \mathbf{T}_1^{(1)\dagger} \mathbf{D} T_2^{(0)} + T_2^{(0)\dagger} \mathbf{D} \mathbf{T}_1^{(1)} \\ + \mathbf{T}_1^{(1)\dagger} \mathbf{D} T_1^{(0)} + T_1^{(0)\dagger} \mathbf{D} \mathbf{T}_1^{(1)} + \mathbf{T}_2^{(1)\dagger} \mathbf{D} T_1^{(0)} \\ + T_1^{(0)\dagger} \mathbf{D} \mathbf{T}_2^{(1)} + \mathbf{T}_2^{(1)\dagger} \mathbf{D} T_2^{(0)} + T_2^{(0)\dagger} \mathbf{D} \mathbf{T}_2^{(1)} | \Phi_0 \rangle, \quad (18)$$

where  $\mathcal{N} = \langle \Phi_0 | \exp[T^{(0)\dagger}] \exp[T^{(0)}] | \Phi_0 \rangle$  is the normalization factor, which involves a nonterminating series of contractions between  $T^{(0)\dagger}$  and  $T^{(0)}$ . However, in the present work we use  $\mathcal{N} \approx \langle \Phi_0 | 1 + T_1^{(0)\dagger} T_1^{(0)} + T_2^{(0)\dagger} T_2^{(0)} | \Phi_0 \rangle$ . In the PRCC expression of  $\alpha$ , the summation over intermediate states is subsumed within  $\mathbf{T}^{(1)}$  in a natural way and eliminates the need for a complete set of intermediate states. This is, however, with the condition of solving an additional set of cluster equations.

### IV. CALCULATIONAL DETAILS

#### A. Basis set

To get accurate results the first step is to generate an appropriate basis set of orbitals. Here we use the Gaussian-type orbitals (GTO's), in which the orbitals are expressed as a linear combination of Gaussian-type functions [30]. In particular, the large component of the orbitals are the linear combination of the Gaussian-type functions of the form

$$g_{\kappa p}^L(r) = C_{\kappa i}^L r^{n_{\kappa}} e^{-\alpha_p r^2}, \quad (19)$$

where  $p = 0, 1, \dots, m$  is the GTO index and  $m$  is the number of Gaussian-type functions. The exponent  $\alpha_p = \alpha_0 \beta^{p-1}$ , where  $\alpha_0$  and  $\beta$  are two independent parameters. The small components are constructed from the large component through the kinetic balance condition [29–32]. The GTOs are calculated on a grid [37] and we optimize the values of  $\alpha_0$  and  $\beta$  for individual atoms to reproduce the orbital energies of the core orbitals and self-consistent field (SCF) energy from GRASP92 [38] code. The comparison of the SCF energies for the doubly ionized alkaline atoms are given in Table I.

From the table it is evident that the results of the SCF energies from the GTOs are in agreement with the GRASP92 results to the accuracy of at least  $10^{-3}$  hartree. The symmetry-wise values of the optimized  $\alpha_0$  and  $\beta$  are listed in Table II.

The number of Gaussian-type functions with the optimized basis set parameters is large and not all the GTOs generated

TABLE I. Comparison between the ground-state SCF energies obtained from the computations with GTO and GRASP92. The energies are in atomic units.

Atom	GTO	GRASP92
Mg <sup>2+</sup>	-199.1500	-199.1501
Ca <sup>2+</sup>	-679.1038	-679.1038
Sr <sup>2+</sup>	-3177.5211	-3177.5218
Ba <sup>2+</sup>	-8135.1404	-8135.1421
Ra <sup>2+</sup>	-26027.5632	-26027.5634

are important for the calculations. For the PRCC calculation we select the number of GTO's for each symmetry such that the electron correlation is accounted accurately. In order to investigate this, we examine the convergence pattern of the  $\alpha$  by varying the basis set size. Here we present the result for Sr<sup>2+</sup>. We start with a basis set size of 95 GTOs and increase it in steps up to 155 GTO's. For this the computations are done with the Dirac-Coulomb Hamiltonian and the results are listed in Table III. Based on the table the optimal basis size to get converged result accurate up to 10<sup>-3</sup> is 127.

To solve the PRCC equations for single and double excitations, we use the Jacobi method. We chose this method as it can be parallelized without any difficulty. However, there is a major drawback of the method or performance penalty: slow convergence. To accelerate the convergence we use direct inversion of the iterated subspace (DIIS) [39], and this improves the convergence significantly.

### B. VP corrections to the orbital energies

To study the VP corrections arising from  $V_{Ue}$ , we compute the orbital energy corrections in the self-consistent field (SCF) calculations. We also compute the first-order correction using the many-body perturbation theory. In the former case, SCF calculations, the VP potential is considered along with the Dirac-Hartree-Fock (DHF) potential,  $U_{DHF}$ . The orbital eigenvalue equation is then

$$[h_0 + V_{Ue}(r) + U_{DHF}(r)] |\psi'_i\rangle = \epsilon'_i |\psi'_i\rangle,$$

where  $h_0 = c\alpha \cdot \mathbf{p} + (\beta - 1)c^2 - V_{N-2}(r)$  is the single-particle part of Dirac-Coulomb Hamiltonian,  $U_{DHF}(r)$  is the DHF potential,  $|\psi'_i\rangle$  is a four-component orbital, and  $\epsilon'_i$  is the corresponding eigenvalue. Similarly, we use *unprimed* states,  $|\psi_i\rangle$ , to represent orbitals which are eigenfunctions of the DHF Hamiltonian, that is,

$$[h_0 + U_{DHF}(r)] |\psi_i\rangle = \epsilon_i |\psi_i\rangle,$$

TABLE II. The  $\alpha_0$  and  $\beta$  parameters of the even-tempered GTO basis for different ions used in the present calculations.

Atom	$s$		$p$		$d$	
	$\alpha_0$	$\beta$	$\alpha_0$	$\beta$	$\alpha_0$	$\beta$
Mg <sup>2+</sup>	0.00825	2.310	0.00715	2.365	0.00700	2.700
Ca <sup>2+</sup>	0.00895	2.110	0.00815	2.150	0.00750	2.500
Sr <sup>2+</sup>	0.00975	2.100	0.00915	2.010	0.00900	2.030
Ba <sup>2+</sup>	0.00985	2.150	0.00975	2.070	0.00995	2.010
Ra <sup>2+</sup>	0.00995	2.110	0.00925	2.090	0.00850	2.010

TABLE III. Convergence pattern of  $\alpha$  of Sr<sup>2+</sup> ion as a function of the basis set size. For this set of calculations we consider the Dirac-Coulomb Hamiltonian and result is in atomic units.

No. of orbitals	Basis size	$\alpha$
95	(15s, 11p, 11d, 9f, 9g)	5.762
113	(17s, 13p, 13d, 11f, 11g)	5.745
127	(19s, 15p, 15d, 13f, 11g)	5.743
137	(21s, 17p, 17d, 13f, 11g)	5.743
155	(23s, 19p, 19d, 15f, 13g)	5.743

where  $\epsilon_i$  is the DHF energy of the orbital. To quantify the VP effect we define

$$\Delta\epsilon_i = \epsilon'_i - \epsilon_i, \quad (20)$$

as the change in the orbital energy due to  $V_{Ue}(r)$ . Following the time-independent many-body perturbation theory, the first-order energy correction associated with  $V_{Ue}(r)$  is

$$\langle V_{Ue} \rangle_i = \langle \psi_i | V_{Ue}(r) | \psi_i \rangle.$$

Since the VP potential is attractive and short range in nature, it has larger effect on the orbitals which have finite-probability density within the nucleus. So, at the first order  $\langle V_{Ue} \rangle$  is negative for orbitals, but only the  $s_{1/2}$  orbitals have negative  $\Delta\epsilon$  for all the ions. A similar pattern is reported in Ref. [40] for the orbital energies of Cs<sup>+</sup>. For the Ra<sup>2+</sup> ion, in addition to  $s_{1/2}$  the  $p_{1/2}$  orbitals also have negative  $\Delta\epsilon$ . More details of the  $\Delta\epsilon_i$  and  $\langle V_{Ue} \rangle_i$  for the core orbitals of the Ca<sup>2+</sup>, Sr<sup>2+</sup>, Ba<sup>2+</sup>, and Ra<sup>2+</sup> are presented in the next section.

## V. RESULTS AND DISCUSSION

As mentioned earlier, the expression of the  $\alpha$  in PRCC theory is a nonterminating series of the cluster amplitudes. However, considering that the cluster operators  $T_2^{(0)}$  and  $T_1^{(1)}$  account for more than 95% of the many-body effects in RCC and PRCC, the terms considered in Eq. (18) give very accurate results. To verify, we have examined the leading terms which are third order in cluster amplitudes and find the contributions are  $\sim 10^{-4}$ . So, for the present work, as we consider  $\alpha$  up to the third decimal place, it is appropriate to neglect the contributions from terms which are third and higher order in cluster operators.

In Table IV we list the  $\alpha$  of alkaline-earth metal ions Mg<sup>2+</sup>, Ca<sup>2+</sup>, Sr<sup>2+</sup>, Ba<sup>2+</sup>, and Ra<sup>2+</sup> computed using Eq. (18). The results are based on two sets of calculations: One is based on the cluster amplitudes obtained from LPRCC and the other is based on PRCC. For a systematic comparison we also list the previous theoretical and experimental results. The results of  $\alpha$  along with the orbital energy corrections arising from  $V_{Ue}(r)$  for each of the ions are discussed in the subsequent sections.

### A. Mg<sup>2+</sup>

The  $\alpha$  of Mg<sup>2+</sup> computed with LPRCC is in excellent agreement with the experimental data. However, the PRCC result is 1.2% higher than the LPRCC result and experimental data. This may be due to a part of the additional many-body effects arising from the nonlinear terms in the cluster

TABLE IV. Static dipole polarizability of doubly ionized alkaline-earth-metal ions and the values are in atomic units.

Atom	This work	Method	Previous works	Method
$\text{Mg}^{2+}$	0.489	(LPRCC)	0.469 <sup>a</sup>	RRPA
	0.495	(PRCC)	0.489(5) <sup>b</sup>	Expt.
$\text{Ca}^{2+}$	3.284	(LPRCC)	3.262 <sup>c</sup>	RCCSDT
	3.387	(PRCC)	3.254 <sup>a</sup> 3.26(3) <sup>b</sup>	RRPA Expt.
$\text{Sr}^{2+}$	5.748	(LPRCC)	5.792 <sup>c</sup>	RCCSDT
	5.913	(PRCC)	5.813 <sup>a</sup>	RRPA
$\text{Ba}^{2+}$	10.043	(LPRCC)	10.491 <sup>c</sup>	RCCSDT
	10.426	(PRCC)	10.61 <sup>a</sup>	RRPA
$\text{Ra}^{2+}$	12.908	(LPRCC)	13.361 <sup>c</sup>	RCCSDT
	13.402	(PRCC)		

<sup>a</sup>Reference [41].<sup>b</sup>Reference [42].<sup>c</sup>Reference [25].

amplitude equations but which may ultimately cancel with the contributions from the cluster amplitudes of higher excitations like  $T_3^{(0)}$  and  $T_3^{(1)}$ . The RRPA result is 4.1% lower than the experimental data and it is also lower than both the LPRCC and PRCC results. It must be added that a similar trend is observed for the  $\text{Na}^+$  ion [23], which is isoelectronic with  $\text{Mg}^{2+}$ , and the RRPA result of  $\alpha$  is lower than the experimental data [41]. This trend may be on account of the inherent strength and limitation of RRPA, the potential to incorporate core-polarization effects very accurately, and the weakness to account for pair correlation effects.

To estimate the contribution from the Breit interaction we consider the Dirac-Coulomb Hamiltonian with the VP potential. The contribution from the Breit interaction can be safely neglected for this ion as the contribution is less than 0.02%. Not surprisingly, the orbital energy corrections  $\Delta\epsilon_i$  and  $\langle V_{\text{Ue}} \rangle_i$  are very small and can be neglected. For this reason we have not listed the values of  $\Delta\epsilon_i$  and  $\langle V_{\text{Ue}} \rangle_i$  for  $\text{Mg}^{2+}$ .

### B. $\text{Ca}^{2+}$

For  $\text{Ca}^{2+}$ , the LPRCC result of  $\alpha$  is within the experimental uncertainty and it is in good agreement with the result from a previous work, which is based on the RCCSDT theory. The PRCC result is 3.1% larger than the LPRCC result and deviates from the experimental data by 3.7%. On the other hand, the result from the RRPA [41], like in  $\text{Mg}^{2+}$ , is lower than the experimental data.

Based on another set of calculations with the Dirac-Coulomb Hamiltonian, the contribution from the Breit interaction is estimated to be 0.004, which is a mere  $\approx 0.1\%$  of the total value. Similarly, we calculate the VP correction to the orbital energy with a series of SCF calculations and results are listed in Table V. As is to be expected, the first-order correction  $\langle V_{\text{Ue}} \rangle$  is negative for all the core orbitals, but the values of  $\Delta\epsilon$  are negative only for the  $s_{1/2}$  orbitals. Another important observation is that for  $s_{1/2}$  orbitals  $\langle V_{\text{Ue}} \rangle_i$  and  $\Delta\epsilon_i$  are similar in value, but for the other orbitals, besides the change in sign, the values of  $\langle V_{\text{Ue}} \rangle_i$  and  $\Delta\epsilon_i$  are different by several orders of magnitude.

TABLE V. VP Corrections to the orbital energies of  $\text{Ca}^{2+}$ . Here  $[x]$  represents multiplication by  $10^x$ .

Orbital	$\Delta\epsilon$	$\langle V_{\text{Ue}} \rangle$
$1s_{1/2}$	-4.204[-3]	-4.435[-3]
$2s_{1/2}$	-3.531[-4]	-3.790[-4]
$2p_{1/2}$	4.884[-5]	-1.511[-6]
$2p_{3/2}$	4.938[-5]	-2.732[-7]
$3s_{1/2}$	-4.391[-5]	-4.500[-5]
$3p_{1/2}$	6.817[-6]	-1.619[-7]
$3p_{3/2}$	6.880[-6]	-2.931[-8]

### C. $\text{Sr}^{2+}$

For  $\text{Sr}^{2+}$  it is important to have accurate theoretical results as there are no experimental data of  $\alpha$ . From Table IV the LPRCC result of 5.748 is in very good agreement with the previous work using RCCSDT. And, like in the previous cases, the PRCC result of 5.913 is larger than the LPRCC result. Comparing the results from different theoretical methods, we observe the emergence of two important changes in the relative patterns when compared with the results of  $\text{Mg}^{2+}$  and  $\text{Ca}^{2+}$ . First, the RRPA result is higher than both the LPRCC and RCCSDT results, and second, the RCCSDT result is larger than the LPRCC result. This may be on account of the filled  $3d$  shell in  $\text{Sr}^{2+}$ . As it is of higher angular momentum, it has larger polarization effects as well as pair correlation effects. A method like RRPA incorporates the core-polarization effects very accurately but could potentially underestimate the pair correlation effects. Not surprisingly, the same trends are observed in the heavier ions  $\text{Ba}^{2+}$  and  $\text{Ra}^{2+}$  with filled  $d$  and  $f$  shells.

Based on a comparison with the calculations using the Dirac-Coulomb Hamiltonian, we estimate the Breit contribution as 0.005. This is negligibly small and similar in magnitude to the case of  $\text{Ca}^{2+}$ . The VP corrections to the orbital energies arising from  $V_{\text{Ue}}(r)$  are listed in Table VI. From the table it is evident that  $\Delta\epsilon_{1s_{1/2}}$  is an order of magnitude larger than in  $\text{Ca}^{2+}$ . In addition, we also observe a difference of four orders of magnitude between the  $\langle V_{\text{Ue}} \rangle_i$  and  $\Delta\epsilon_i$  of the  $3d$  orbitals. This is not surprising as the short-range  $V_{\text{Ue}}(r)$  have little

TABLE VI. VP Corrections to the orbital energies of  $\text{Sr}^{2+}$ . Here  $[x]$  represents multiplication by  $10^x$ .

Orbital	$\Delta\epsilon$	$\langle V_{\text{Ue}} \rangle$
$1s_{1/2}$	-5.721[-2]	-5.904[-2]
$2s_{1/2}$	-5.968[-3]	-6.231[-3]
$2p_{1/2}$	3.604[-4]	-1.144[-4]
$2p_{3/2}$	4.354[-4]	-1.636[-5]
$3s_{1/2}$	-1.003[-3]	-1.045[-3]
$3p_{1/2}$	8.281[-5]	-1.995[-5]
$3p_{3/2}$	9.664[-5]	-2.865[-6]
$3d_{3/2}$	8.145[-5]	-4.341[-9]
$3d_{5/2}$	8.048[-5]	-1.123[-9]
$4s_{1/2}$	-1.301[-4]	-1.320[-4]
$4p_{1/2}$	1.592[-5]	-2.086[-6]
$4p_{3/2}$	1.747[-5]	-2.984[-7]

TABLE VII. VP Corrections to the orbital energies of Ba<sup>2+</sup>. Here [x] represents multiplication by 10<sup>x</sup>.

Orbital	$\Delta\epsilon$	$\langle V_{Ue} \rangle$
1s <sub>1/2</sub>	-2.952[ -1]	-3.025[ -1]
2s <sub>1/2</sub>	-3.493[ -2]	-3.623[ -2]
2p <sub>1/2</sub>	5.074[ -4]	-1.669[ -3]
2p <sub>3/2</sub>	1.786[ -3]	-1.748[ -4]
3s <sub>1/2</sub>	-7.084[ -3]	-7.391[ -3]
3p <sub>1/2</sub>	1.984[ -4]	-3.725[ -4]
3p <sub>3/2</sub>	4.926[ -4]	-3.981[ -5]
3d <sub>3/2</sub>	4.856[ -4]	-2.047[ -7]
3d <sub>5/2</sub>	4.737[ -4]	-4.712[ -8]
4s <sub>1/2</sub>	-1.531[ -3]	-1.599[ -3]
4p <sub>1/2</sub>	8.513[ -5]	-7.689[ -5]
4p <sub>3/2</sub>	1.476[ -4]	-8.242[ -6]
4d <sub>3/2</sub>	1.272[ -4]	-4.004[ -8]
4d <sub>5/2</sub>	1.245[ -4]	-9.185[ -8]
5s <sub>1/2</sub>	-2.449[ -4]	-2.473[ -4]
5p <sub>1/2</sub>	2.295[ -5]	-1.071[ -5]
5p <sub>3/2</sub>	3.230[ -5]	-1.066[ -6]

effect on the electrons in the higher angular momentum orbitals like *d*.

#### D. Ba<sup>2+</sup>

Like in Sr<sup>2+</sup>, there are no experimental data of  $\alpha$  for Ba<sup>2+</sup>. Hence, it is important to have accurate theoretical results, and in this regard, it is pertinent to calculate  $\alpha$  with a reliable method like RCC. Here, computing with the relativistic version of coupled-cluster theory is essential as the high *Z* implies that the relativistic corrections are important. From Table IV, it is evident that our LPRCC result of 10.043 is 4.3% lower than the RCCSDT result. However, our PRCC result is in very good agreement with the RCCSDT result; it is just 0.6% less. Examining the results discussed so far, there is a discernible trend when we compare the PRCC and RCCSDT results. The difference between the two results narrows with increasing *Z*. This maybe due to the basic property of the CCT and which is to include selected electron correlation effects to all order. So, with higher *Z* the importance of the correlation effects grows and the two coupled-cluster-based methods incorporate the correlation effects to similar accuracy. The other theoretical result from the RPA theory is larger than the other results.

Following the computations described earlier, we estimate the Breit contribution as 0.007, which is similar to the previous cases. Coming to the orbital energy corrections arising from the VP, listed in Table VII, we find an important change in the pattern of  $\Delta\epsilon$ . The  $\Delta\epsilon$  of *p*<sub>1/2</sub> and *p*<sub>3/2</sub> continue to be positive, but  $\Delta\epsilon_{2p_{1/2}}$  is  $\approx 72\%$  smaller than  $\Delta\epsilon_{2p_{3/2}}$ . For the remaining *np*<sub>1/2</sub> and *np*<sub>3/2</sub>, although the difference is not so dramatic, the differences are still large.

#### E. Ra<sup>2+</sup>

Our PRCC result of  $\alpha$  for Ra<sup>2+</sup> is  $\approx 3.7\%$  larger than the LPRCC result. This trend is similar to the case of Ba<sup>2+</sup> and may be attributed to better accounting of correlation effects in PRCC. To be more precise, the importance of the correlation

TABLE VIII. VP Corrections to the orbital energies of Ra<sup>2+</sup>. Here [x] represents multiplication by 10<sup>x</sup>.

Orbital	$\Delta\epsilon$	$\langle V_{Ue} \rangle$
1s <sub>1/2</sub>	-2.560	-2.614
2s <sub>1/2</sub>	-3.881[ -1]	-3.999[ -1]
2p <sub>1/2</sub>	-3.802[ -2]	-5.753[ -2]
2p <sub>3/2</sub>	1.211[ -2]	-2.707[ -3]
3s <sub>1/2</sub>	-8.999[ -2]	-9.315[ -2]
3p <sub>1/2</sub>	-9.620[ -3]	-1.504[ -2]
3p <sub>3/2</sub>	3.728[ -3]	-7.545[ -4]
3d <sub>3/2</sub>	4.213[ -3]	-1.330[ -5]
3d <sub>5/2</sub>	3.953[ -3]	-2.385[ -6]
4s <sub>1/2</sub>	-2.362[ -2]	-2.451[ -2]
4p <sub>1/2</sub>	-2.238[ -3]	-3.938[ -3]
4p <sub>3/2</sub>	1.315[ -3]	-1.999[ -4]
4d <sub>3/2</sub>	1.350[ -3]	-3.943[ -6]
4d <sub>5/2</sub>	1.282[ -3]	-7.062[ -7]
4f <sub>5/2</sub>	1.015[ -3]	-1.647[ -9]
4f <sub>7/2</sub>	9.928[ -4]	-4.229[ -10]
5s <sub>1/2</sub>	-5.378[ -3]	-5.633[ -3]
5p <sub>1/2</sub>	-3.002[ -4]	-8.438[ -4]
5p <sub>3/2</sub>	4.845[ -4]	-4.200[ -5]
5d <sub>3/2</sub>	4.074[ -4]	-6.735[ -7]
5d <sub>5/2</sub>	3.859[ -4]	-1.187[ -7]
6s <sub>1/2</sub>	-9.883[ -4]	-9.951[ -4]
6p <sub>1/2</sub>	-1.613[ -5]	-1.290[ -4]
6p <sub>3/2</sub>	1.211[ -4]	-5.949[ -6]

effects grows with increasing number of electrons, but LPRCC theory is insufficient to incorporate the correlation effects as it considers only the linear terms. The PRCC theory, which includes the nonlinear terms, provides a better description of the electron correlations. This is borne by the fact that the PRCC results are in good agreement with the RCCSDT results; the difference between the two results is just  $\approx 0.3\%$ .

Like in the previous cases, the contribution from the Breit interaction is small and the value is 0.008. In regards to the orbital energy correction arising from VP, listed in Table VIII, there is a key difference from the other ions. The values of  $\Delta\epsilon_{np_{1/2}}$ , in addition to  $\Delta\epsilon_{ns_{1/2}}$  are negative.

#### F. Core-polarization and pair correlation effects

In the previous sections we discussed the comparison between the results from different theories, general trends, and orbital energy corrections from VP. To examine and investigate the contributions from various many-body effects, which are encapsulated in different terms of LPRCC and PRCC, we isolate the contributions from different terms through a series of computations. The results are listed in Table IX. From the table it is evident that the leading term in the LPRCC as well as PRCC theory is  $\{\mathbf{T}_1^{(1)\dagger} \mathbf{D} + \text{H.c.}\}$ . This is not surprising as it is the term which subsumes the DF contribution and the RPA effects. Now to understand and quantify the RPA effects in these systems, we separate the core orbital contribution to  $\alpha$ .

The four dominant contributions from the core orbitals to  $\{\mathbf{T}_1^{(1)\dagger} \mathbf{D} + \text{H.c.}\}$  are listed in Table X. For all the ions, the outermost *p*<sub>3/2</sub> orbital is the most dominant and this because of the larger radial extent of the *p*<sub>3/2</sub> orbitals. The

TABLE IX. Contribution to  $\alpha$  from different terms and their Hermitian conjugates in the LPRCC and PRCC theory.

Terms + H.c.	Mg <sup>2+</sup>	Ca <sup>2+</sup>	Sr <sup>2+</sup>	Ba <sup>2+</sup>	Ra <sup>2+</sup>
LPRCC results					
$\mathbf{T}_1^{(1)\dagger}\mathbf{D}$	0.496	3.594	6.400	11.708	15.160
$\mathbf{T}_1^{(1)\dagger}\mathbf{DT}_2^{(0)}$	-0.008	-0.180	-0.330	-0.676	-0.864
$\mathbf{T}_1^{(1)\dagger}\mathbf{DT}_1^{(0)}$	0.001	-0.022	-0.044	-0.114	-0.108
$\mathbf{T}_2^{(1)\dagger}\mathbf{DT}_1^{(0)}$	-0.0001	0.004	0.008	0.020	0.018
$\mathbf{T}_2^{(1)\dagger}\mathbf{DT}_2^{(0)}$	0.008	0.098	0.174	0.370	0.470
Normalization	1.019	1.064	1.080	1.126	1.137
Total	0.489	3.284	5.748	10.043	12.908
PRCC results					
$\mathbf{T}_1^{(1)\dagger}\mathbf{D}$	0.502	3.718	6.606	12.214	15.820
$\mathbf{T}_1^{(1)\dagger}\mathbf{DT}_2^{(0)}$	-0.008	-0.188	-0.344	-0.710	-0.908
$\mathbf{T}_2^{(1)\dagger}\mathbf{DT}_2^{(0)}$	0.002	-0.022	-0.046	-0.120	-0.114
$\mathbf{T}_1^{(1)\dagger}\mathbf{DT}_1^{(0)}$	-0.0001	-0.004	0.008	0.018	0.016
$\mathbf{T}_2^{(1)\dagger}\mathbf{DT}_1^{(0)}$	0.008	0.092	0.162	0.338	0.424
Normalization	1.019	1.064	1.080	1.126	1.137
Total	0.495	3.387	5.913	10.426	13.402

next important contribution arises from the outermost  $p_{1/2}$ . A prominent feature that we observe in the results is the ratio between the contribution from the outermost  $p_{3/2}$  to the  $p_{1/2}$  orbitals. The ratios are 2.03, 2.07, 2.24, 2.57, and 4.17 for Mg<sup>2+</sup>, Ca<sup>2+</sup>, Sr<sup>2+</sup>, Ba<sup>2+</sup>, and Ra<sup>2+</sup>, respectively. The ratio increase with increasing  $Z$  but for Ra<sup>2+</sup> it is 1.6 times higher than for Ba<sup>2+</sup>. This is an important feature arising from the contraction of  $p_{1/2}$  orbitals due to the relativistic effects, which are more prominent in the heavier atoms and ions. The third largest contribution arises from  $ns_{1/2}$  orbital in the cases of Mg<sup>2+</sup>, Ca<sup>2+</sup>, and Sr<sup>2+</sup>. This is because the  $ns_{1/2}$  orbital is energetically lower than the  $np_{1/2}$  and relativistic corrections are not large. However, for Ba<sup>2+</sup> and Ra<sup>2+</sup>, due to the relativistic contraction, the contribution from the outermost  $ns_{1/2}$  is suppressed. The third largest contribution arises from the more diffused outer  $nd_{5/2}$  orbital.

The next leading contribution arises from  $\{\mathbf{T}_1^{(1)\dagger}\mathbf{DT}_2^{(0)} + \text{H.c.}\}$ . The contribution from this term is much smaller and opposite in phase to the leading order term. A similar trend is observed in case of the noble gas atoms and was reported in one of our previous works [22]. Among the various terms

TABLE X. Four leading contributions to  $\{\mathbf{T}_1^{(1)\dagger}\mathbf{D} + \text{H.c.}\}$  to  $\alpha$  in terms of the core spin orbitals.

Mg <sup>2+</sup>	Ca <sup>2+</sup>	Sr <sup>2+</sup>
0.312 ( $2p_{3/2}$ )	2.378 ( $3p_{3/2}$ )	4.344 ( $4p_{3/2}$ )
0.154 ( $2p_{1/2}$ )	1.148 ( $3p_{1/2}$ )	1.940 ( $4p_{1/2}$ )
0.028 ( $2s_{1/2}$ )	0.056 ( $3s_{1/2}$ )	0.048 ( $4s_{1/2}$ )
0.0002 ( $1s_{1/2}$ )	0.006 ( $2p_{3/2}$ )	0.034 ( $3d_{5/2}$ )
Ba <sup>2+</sup> Ra <sup>2+</sup>		
8.182 ( $5p_{3/2}$ )	11.766 ( $6p_{3/2}$ )	
3.188 ( $5p_{1/2}$ )	2.822 ( $6p_{1/2}$ )	
0.162 ( $4d_{5/2}$ )	0.338 ( $5d_{5/2}$ )	
0.102 ( $4d_{3/2}$ )	0.192 ( $5d_{3/2}$ )	

TABLE XI. Core orbitals contribution from  $\mathbf{T}_1^{(1)\dagger}\mathbf{DT}_2^{(0)}$  to  $\alpha$  of Mg<sup>2+</sup> and Ca<sup>2+</sup>.

Mg <sup>2+</sup>	Ca <sup>2+</sup>
-0.002 ( $2p_{3/2}, 2p_{3/2}$ )	-0.038 ( $3p_{3/2}, 3p_{3/2}$ )
-0.001 ( $2p_{3/2}, 2p_{1/2}$ )	-0.022 ( $3p_{3/2}, 3p_{1/2}$ )
-0.001 ( $2p_{1/2}, 2p_{3/2}$ )	-0.022 ( $3p_{1/2}, 3p_{3/2}$ )
-0.0004 ( $2p_{1/2}, 2p_{1/2}$ )	-0.009 ( $3p_{1/2}, 3p_{1/2}$ )

the  $\{\mathbf{T}_1^{(1)\dagger}\mathbf{DT}_1^{(0)} + \text{H.c.}\}$  has the smallest contribution. This is because of the fact that  $T_1^{(0)}$  and  $T_2^{(1)}$  have smaller amplitudes in the RCC and PRCC theories, respectively. As can be seen from Table IX, the overall contribution from the second order terms are 0.0009, -0.100, -0.192, -0.400, and -0.484 for Mg<sup>2+</sup>, Ca<sup>2+</sup>, Sr<sup>2+</sup>, Ba<sup>2+</sup>, and Ra<sup>2+</sup>, respectively. Except for Mg<sup>2+</sup>, the higher order terms gives a negative contribution to the  $\alpha$ .

To study the pair-correlation effects we examine the next-to-leading-order term,  $\mathbf{T}_1^{(1)\dagger}\mathbf{DT}_2^{(0)}$ , in more detail. In Tables XI and XII we list the four leading-order core-orbital pairs which contribute to  $\alpha$ . The  $(np_{3/2}, np_{3/2})$  orbital pairing gives the most dominant contribution. The next leading-order contribution arises from the  $(np_{3/2}, np_{1/2})$  orbital pairing. The same pattern is observed for all the doubly charged ions. For Ra<sup>2+</sup> the fourth largest contribution arises from  $(6p_{3/2}, 5d_{5/2})$  orbital pairing, but for other ions it is from  $(np_{1/2}, np_{1/2})$  orbital pairing. This is because of the relativistic effects, which contract the outer  $s_{1/2}$  orbital in Ra<sup>2+</sup> more than the other ions. One important point to notice here is that the higher order terms do not translate to higher accuracy as observed in the cases of Mg<sup>2+</sup> and Ca<sup>2+</sup>.

### G. Theoretical uncertainty

We have isolated the following sources of uncertainty in the present calculations. The first is the truncation of the numerical basis set. We start our calculations with 9 symmetry and increase up to 13 symmetry. Along with this we also increase the number of orbitals per symmetry and we observe that our values of  $\alpha$  converge for all the doubly charged ions, so we can neglect this error safely. The second source of error is associated with the truncation of RCC theory at the single and double excitation in both the unperturbed and perturbed

TABLE XII. Core orbitals contribution from  $\mathbf{T}_1^{(1)\dagger}\mathbf{DT}_2^{(0)}$  to  $\alpha$  of Sr<sup>2+</sup>, Ba<sup>2+</sup>, and Ra<sup>2+</sup>.

Sr <sup>2+</sup>	Ba <sup>2+</sup>
-0.069 ( $4p_{3/2}, 4p_{3/2}$ )	-0.132 ( $5p_{3/2}, 5p_{3/2}$ )
-0.038 ( $4p_{3/2}, 4p_{1/2}$ )	-0.070 ( $5p_{3/2}, 5p_{1/2}$ )
-0.036 ( $4p_{1/2}, 4p_{3/2}$ )	-0.061 ( $5p_{1/2}, 5p_{3/2}$ )
-0.014 ( $4p_{1/2}, 4p_{1/2}$ )	-0.022 ( $5p_{1/2}, 5p_{1/2}$ )
Ra <sup>2+</sup>	
-0.186 ( $6p_{3/2}, 6p_{3/2}$ )	
-0.077 ( $6p_{3/2}, 6p_{1/2}$ )	
-0.052 ( $6p_{1/2}, 6p_{3/2}$ )	
-0.039 ( $6p_{3/2}, 5d_{5/2}$ )	

levels. Based on a series of test calculations, we estimate the contribution from triple excited cluster amplitudes to be less than 0.2% of the total value. So, we can consider the upper bound on the uncertainty from the truncation of the RCC and PRCC theories as 0.4% for the heavier ions  $\text{Sr}^{2+}$ ,  $\text{Ba}^{2+}$ , and  $\text{Ra}^{2+}$ . By examining the trend in the results of  $\text{Mg}^{2+}$  and  $\text{Ca}^{2+}$ , we conclude that the uncertainty is likely to be higher for the PRCC results of these ions, but the LPRCC results could have an uncertainty less than  $\approx 0.4\%$ . The third source of error is the truncation of the nonterminating series of  $\alpha$ . We terminate  $e^{\mathbf{T}^{(1)\dagger}} \mathbf{D} e^{\mathbf{T}^{(0)}} + e^{\mathbf{T}^{(0)\dagger}} \mathbf{D} e^{\mathbf{T}^{(1)}}$  at the second order in cluster operator. However, based on our earlier study [43], where we reported an iterative technique to calculate properties to all order, the contribution from the third and higher order terms is negligible. So, the uncertainty arising from the truncation in the expression of  $\alpha$  can be neglected. Quantum electrodynamic (QED) corrections is another source of uncertainty in the present calculation. We include the VP potential in the present work but the self-energy part of the radiative corrections is neglected. The self-energy correction is important for the heavy atoms [44]. We can, however, safely neglect it from the error estimates as the contribution is less than the correction from Breit interaction, which accounts for at the most 0.1% of the total value. So, considering all the sources, the upper bound on the uncertainty of the present calculations is  $\approx 0.4\%$  for the LPRCC results of  $\text{Mg}^{2+}$  and  $\text{Ca}^{2+}$  and PRCC results of  $\text{Sr}^{2+}$ ,  $\text{Ba}^{2+}$ , and  $\text{Ra}^{2+}$  ions.

## VI. CONCLUSION

The electric dipole polarizabilities of doubly ionized alkaline-earth-metal ions calculated using the PRCC theory are in very good agreement with the previous theoretical results and experimental data. An important observation is that for the lighter ions  $\text{Mg}^{2+}$  and  $\text{Sr}^{2+}$  the inclusion of nonlinear terms in PRCC does not translate to better agreement with the experimental data. However, for the heavier ions, the nonlinear terms are essential to obtain results which are in agreement with the other results based on relativistic coupled-cluster theory. The correction from the Breit interaction shows marginal increase with atomic number and this may be due to the radial dependence of the  $\alpha$ .

The changes in orbital energies, SCF, and first-order correction with the VP potential reflect the short-range nature of this potential. Furthermore, there is an important change in the SCF energy correction  $\Delta\epsilon$  with increasing  $Z$ . For lighter atoms only the  $\Delta\epsilon$  of the core  $ns_{1/2}$  are negative, but for  $\text{Ra}^{2+}$  in addition to the core  $ns_{1/2}$ , the core  $np_{1/2}$  orbitals also have negative  $\Delta\epsilon$ .

## ACKNOWLEDGMENTS

We thank A. Roy and K. Suthar for useful discussions. The results presented in the paper are based on the computations using the 3TFLOP HPC Cluster at Physical Research Laboratory, Ahmedabad, India.

- 
- [1] K. Bonin and V. Kresin, *Electric-Dipole Polarizabilities of Atoms, Molecules, and Clusters* (World Scientific, Singapore, 1997).
- [2] H. Gould and T. M. Miller, in *Advances in Atomic, Molecular, and Optical Physics*, Vol. 51, edited by H. Stroke (Elsevier Academic Press, San Diego, 2005), pp. 343–361.
- [3] J. Mitroy, M. S. Safronova, and C. W. Clark, *J. Phys. B* **43**, 202001 (2010).
- [4] F. Coester, *Nucl. Phys.* **7**, 421 (1958).
- [5] F. Coester and H. Kümmel, *Nucl. Phys.* **17**, 477 (1960).
- [6] R. J. Bartlett and M. Musiał, *Rev. Mod. Phys.* **79**, 291 (2007).
- [7] I. Lindgren and J. Morrison, *Atomic Many-Body Theory*, 2nd ed. (Springer, Berlin, 1986).
- [8] I. Shavitt and R. Bartlett, *Many-Body Methods in Chemistry and Physics: MBPT and Coupled-Cluster Theory* (Cambridge University Press, Cambridge, 2009).
- [9] E. Eliav, U. Kaldor, and Y. Ishikawa, *Phys. Rev. A* **49**, 1724 (1994).
- [10] G. Gopakumar, H. Merlitz, S. Majumder, R. K. Chaudhuri, B. P. Das, U. S. Mahapatra, and D. Mukherjee, *Phys. Rev. A* **64**, 032502 (2001).
- [11] R. Pal, M. S. Safronova, W. R. Johnson, A. Derevianko, and S. G. Porsev, *Phys. Rev. A* **75**, 042515 (2007).
- [12] H. S. Nataraj, B. K. Sahoo, B. P. Das, and D. Mukherjee, *Phys. Rev. Lett.* **101**, 033002 (2008).
- [13] B. K. Mani, K. V. P. Latha, and D. Angom, *Phys. Rev. A* **80**, 062505 (2009).
- [14] B. K. Mani and D. Angom, *Phys. Rev. A* **83**, 012501 (2011).
- [15] T. A. Isaev, A. N. Petrov, N. S. Mosyagin, A. V. Titov, E. Eliav, and U. Kaldor, *Phys. Rev. A* **69**, 030501 (2004).
- [16] G. Hagen, T. Papenbrock, D. J. Dean, and M. Hjorth-Jensen, *Phys. Rev. Lett.* **101**, 092502 (2008).
- [17] R. F. Bishop, P. H. Y. Li, D. J. J. Farnell, and C. E. Campbell, *Phys. Rev. B* **79**, 174405 (2009).
- [18] H. D. Cohen and C. C. J. Roothaan, *J. Chem. Phys.* **43**, S34 (1965).
- [19] M. S. Safronova, W. R. Johnson, and A. Derevianko, *Phys. Rev. A* **60**, 4476 (1999).
- [20] A. Derevianko, W. R. Johnson, M. S. Safronova, and J. F. Babb, *Phys. Rev. Lett.* **82**, 3589 (1999).
- [21] S. Chattopadhyay, B. K. Mani, and D. Angom, *Phys. Rev. A* **86**, 022522 (2012).
- [22] S. Chattopadhyay, B. K. Mani, and D. Angom, *Phys. Rev. A* **86**, 062508 (2012).
- [23] S. Chattopadhyay, B. K. Mani, and D. Angom, *Phys. Rev. A* **87**, 042520 (2013).
- [24] M. Douglas and N. M. Kroll, *Ann. Phys.* **82**, 89 (1974).
- [25] I. S. Lim and P. Schwerdtfeger, *Phys. Rev. A* **70**, 062501 (2004).
- [26] P. J. Mohr, B. N. Taylor, and D. B. Newell, *Rev. Mod. Phys.* **84**, 1527 (2012).
- [27] G. E. Brown and D. G. Ravenhall, *Proc. R. Soc. London A* **208**, 552 (1951).
- [28] J. Sucher, *Phys. Rev. A* **22**, 348 (1980).
- [29] R. E. Stanton and S. Havriliak, *J. Chem. Phys.* **81**, 1910 (1984).
- [30] A. K. Mohanty and E. Clementi, *J. Chem. Phys.* **93**, 1829 (1990).

- [31] I. Grant, in *Springer Handbook of Atomic, Molecular, and Optical Physics*, edited by G. Drake (Springer, New York, 2006), pp. 325–357.
- [32] I. P. Grant, *Relativistic Quantum Theory of Atoms and Molecules: Theory and Computation* (Springer, New York, 2010).
- [33] E. A. Uehling, *Phys. Rev.* **48**, 55 (1935).
- [34] F. A. Parpia and A. K. Mohanty, *Phys. Rev. A* **46**, 3735 (1992).
- [35] L. W. Fullerton and G. A. Rinker, *Phys. Rev. A* **13**, 1283 (1976).
- [36] W. R. Johnson, I. Bednyakov, and G. Soff, *Phys. Rev. Lett.* **87**, 233001 (2001).
- [37] R. K. Chaudhuri, P. K. Panda, and B. P. Das, *Phys. Rev. A* **59**, 1187 (1999).
- [38] F. A. Parpia, C. Froese Fischer, and I. P. Grant, *Comput. Phys. Commun.* **94**, 249 (1996).
- [39] P. Pulay, *Chem. Phys. Lett.* **73**, 393 (1980).
- [40] A. Derevianko, B. Ravaine, and W. R. Johnson, *Phys. Rev. A* **69**, 054502 (2004).
- [41] W. Johnson, D. Kolb, and K.-N. Huang, *At. Data Nucl. Data Tables* **28**, 333 (1983).
- [42] U. Öpik, *Proc. Phys. Soc., London* **92**, 566 (1967).
- [43] B. K. Mani and D. Angom, *Phys. Rev. A* **81**, 042514 (2010).
- [44] P. J. Mohr, G. Plunien, and G. Soff, *Phys. Rep.* **293**, 227 (1998).